UNIVERSITÀ DEGLI STUDI DI MILANO

DOTTORATO DI RICERCA IN SCIENZE FARMACEUTICHE

CICLO XXXIV

NOVEL SMART DEVICES FOR THE ADMINISTRATION OF DRUGS INTO HOLLOW MUSCULAR ORGANS

SETTORE CHIM/09 FARMACEUTICO TECNOLOGICO APPLICATIVO

Dott. MARCO UBOLDI

Matricola: R12179

Tutor: Prof.ssa LUCIA ZEMA

Coordinatore del dottorato: Chiar.mo Prof. GIANCARLO ALDINI

ANNO ACCADEMICO
2020/2021

Table of contents

Preface

Limited adherence to prescribed pharmacological treatments may severely compromise patients' outcome and ultimately increase relevant mortality [1-3]. Indeed, approximately half of people undergoing therapies do not take their medications as indicated and this phenomenon was demonstrated to have repercussions on risk-to-benefit *ratio* and overall healthcare costs. A range of factors may contribute to poor medication adherence: those relevant to patients, *e.g.* age as well as living conditions, suboptimal health literacy, lack of involvement in the treatment decision-making process, and those that are related to physicians, such as ineffective communication (*e.g.* of information about adverse effects) or provision of care by multiple physicians [4].

High dosing frequency was often identified as a key factor in the reduction of subject compliance, especially in the case of chronic diseases entailing uncomfortable modes as well as routes of administration and the use of multiple medications through the day [5]. Therefore, limiting the complexity of dosing schedules would be of utmost importance for therapy success. In such a scenario, prolonged-release drug delivery systems (DDSs) able to make the active molecule slowly available for absorption over an extended period of time have drawn a renewed interest [6]. Indeed, researchers are pushing the boundaries of controlled release, looking for DDSs capable to give rise to ultra-long release performances ranging from more than 24 h to many months [7-12]. Their ultimate goal would be counteracting drug elimination, especially in the case of short half-life molecules, which would result in repeated administrations at closed intervals.

The lengthening of release times also entailed the need for extended residence of the device at the site of action or absorption, leading to the attainment of the so-called retentive DDSs. These involve a complex approach relying on formulation, design as well as manufacturing strategies aiming at slowing down the release rate of the drug conveyed, irrespective of the physiological variables (*e.g.* volume, pH, ionic strength, composition and hydrodynamics of the medium, presence of enzymes, mucus), while maintaining the device in the targeted area for a sufficient period of time. This approach may become particularly effective when dealing with hollow muscular organs, in view of their peculiar

characteristics. By way of example, the treatment of local illnesses affecting the urinary bladder and the stomach could especially benefit from the availability of retentive prolonged-release DDSs [5,13-16]. Moreover, by making use of gastroretentive systems, the oral bioavailability of drugs that are preferably absorbed from the upper gastrointestinal tract could be increased.

Hollow muscular organs entail an inner cavity surrounded by overlaid layers of tissues, in which a biological fluid varying in volume and composition could be found [5]. This cavity is connected to the outer environment through different ducts that fulfil diverse physiological functions and whose opening could be regulated by the contraction of the relevant sphincters. Because the physiological activity of these organs relies on filling and emptying cycles, administration of immediate-release dosage forms may fail in ensuring effective concentrations during long time frame. As a result, frequent dosing is required to overcome the drug loss due to continuous washout.

DDSs intended for prolonged retention and release into hollow muscular organs should be characterized by different sizes, one for safe entry through the relevant ducts and the other for effective retention within the cavity. In fact, a sufficiently small-size is essential for enabling convenient and comfortable administration inside the cavity, while expansions leading to a larger spatial encumbrance would be strategic to avoid rapid emptying of the systems in spite of smooth muscle contractions. A range of other requirements, mainly associated with safety issues, have to be fulfil when dealing with retentive DDSs. For instance, possible hazards associated with their long-term maintenance in the specific body district has to be ruled out. In addition, spontaneous elimination of the device from the targeted organ at the end of release (*e.g.* by dissolving, disintegrating, undergoing chemical degradation or collapsing) would be highly beneficial. Indeed, this would allow to avoid painful and uncomfortable removal procedures. Focusing on the working mechanism of these systems, the expansion phenomena targeted to ensure relevant retention may be a result of swelling, water uptake or attained upon recovery of a bulkier shape. The latter could occur *i)* by unfolding,

thanks to an elastic behavior upon removal of an external compressive force, and *ii)* due to the shape memory effect of the materials selected for the fabrication of the DDSs, often referred to as smart.

Smart materials, and in particular shape-memory materials, including both alloys and polymers, are known and have been already employed in many industrial fields [17-22]. They are capable to respond and adapt themselves to an external non-mechanical *stimulus*, thus performing their functions according to the changes undergone. More into detail, they can be forced, by application of an external stress, to take on a temporary shape, starting from the original one they were processed into. The temporary shape is kept after the stress removal and until the material is exposed to the specific triggering *stimulus* (*e.g.* direct heating, indirect heating through the application of electromagnetic fields, contact with water, change in the pH or composition of the medium), which is able to induce the recovery of the original shape (*i.e.* shape memory effect). The possibility of taking advantage of these smart materials in pharmaceutics is currently at the forefront of research and has opened up new frontiers. Their application in the field of retentive DDSs for intravesical and intragastric administration of drugs was therefore the main topic of this thesis. Moreover, the combined use of smart materials and novel additive manufacturing technologies (*i.e.* 3D printing) have further widened the range of application potential of smart materials, by also providing the tool for 4D printing [23-27]. This term refers to the fabrication, *via* different 3D printing techniques and using smart materials as feedstock, of items showing self-transformation at a specific time after production, in response to an external *stimulus* of non-mechanical nature. This is often represented by a change in temperature, light, pH, by the contact with water and even by a modification in the composition of the fluids the object is in contact with. The main changes triggered by such *stimuli* would occur in item size and shape and would also make possible to modify the relevant performance and to achieve new functionalities.

The shape memory effect is driven by the unique chemical structure of smart materials. In the case of shape memory polymers, they are characterized by the presence of hard and

soft domains, which entail the possibility for the polymeric network to be dynamic enough to react to the appropriate *stimulus* with a controlled evolution of the macroscopic conformation over time. Over years, various studies have been focused on fine-tuning the properties of a range of purposely synthetized polymers with the final goal to tailor their overall characteristics to the intended application. These included not only thermo-mechanical properties but also those related to the shape memory effect, such as type and intensity of the triggering *stimulus* to be applied, time needed to induce the response and overall time frame during which the shape evolution sought needs to take place. Conversely, common elastic materials are just characterized by a passive behavior, as they are simply able to modify their shape as a result of either application or removal of an external constraint (*i.e.* mechanical *stimulus*). By way of example, they can be forced into a different, eventually smaller, shape, and, once the external stress is removed, they instantly come back to the stress-free configuration, regardless of any control. For these reasons, smart materials are often defined as "active" and their appropriate application generally require a deep understanding of their structure-behavior correlation.

Because the topic appeared from the very beginning as particularly innovative and challenging, the development of an in-depth background in this respect was deemed essential (Part I). The applications proposed so far in the scientific literature and focused on the use of shape memory materials in the development of DDSs were thus reviewed. A classification based on the objective pursued through the recovery of the original shape was proposed. In addition, studies aimed at investigating the shape memory behavior of different materials for sole characterization purposes were also considered.

Based on the knowledge acquired and working in collaboration with engineers from the Universities of Pavia and Brescia and from the Politecnico di Milano, a few original retentive systems were developed, either for intravesical and intragastric applications (Part II and Part III). Hot-processing techniques, particularly hot melt extrusion and fused deposition modeling 3D printing, were the manufacturing technologies employed in this project. These techniques were selected based on the experience already gained by

the research group within which I carried out my Ph.D. and because they are well-known to yield high versatile geometries, details and sizes of products. A further differentiation from the few works already available in the literature on this topic, was the idea of using an already approved material for human administration. Indeed, pharmaceutical-grade poly(vinyl alcohol) (PVA), a hydrophilic swellable/soluble polymer available in different molecular weights, was chosen in view of its suitability for hot-processing and on preliminary results pointing out its shape memory effect. Specimens having diverse original shapes and compositions were successfully extruded and printed. Prototypes were conceived in an original shape (*e.g.* U-, S- and helix like) with such a spatial encumbrance that their rapid emptying from either the bladder or the stomach could be prevented, thus ensuring long-lasting residence and release. The systems attained were fully studied in terms of physico-technological characteristics. Moreover, after programming of the temporary shape, they were able to recover the original configuration, following interaction with aqueous fluids at body temperature. This phenomenon was considered particularly advantageous in the prospect of achieving prompt retention of the final system immediately after arrival in the targeted organ. Notably, the temporary shape was chosen to be compatible for administration either inside a catheter (*e.g.* I-shape) for intravesical applications, or within a commercially available capsule (*e.g.* supercoiled helix- and paper clip shape) in the case of intragastric ones. The softening upon glass-rubber transition of the polymer would also impart favorable hardness characteristics to the device, such that limited mechanical impact on the targeted organ. The systems were characterized by a modified release consistent with the nature of the starting polymer before complete dissolution, which would ensure safe and non-invasive removal of the device. Thus, multi-functionality of the PVA-based prototypes investigated was highlighted, entailing shape memory effect, controlled release and erosion/dissolution in biological fluids. Although preliminary, the work demonstrated the viability of the strategy based on FDM 3D printing of pharmaceutical-

grade polymers having shape memory response in the manufacturing of retentive DDSs, opening up new possibilities toward the application of 4D printing in pharmaceutics.
Ultimately, a couple of additional steps forward were pursued to refine the research carried out. A comprehensive experimental campaign and computer-aided simulation modelling was performed to ease design and development stages of shape memory gastroretentive DDSs fabricated by hot-processing (Part III, Chapter II). A deep thermal, mechanical and shape memory characterization under various testing conditions was performed on PVA-based samples having different geometries. The data collected enabled calibration and validation of the numerical predictions provided by a thermo-viscoelastic constitutive model, implemented within a finite element framework. Simulation results were compared with those obtained from the shape memory experiments carried out on a selected prototype having original S-shape. Finally, in order to improve the mechanical properties and release duration of the DDSs proposed, without affecting the shape memory effect, the possibility to film-coat PVA-based prototypes with different polymeric liquid formulations was evaluated (Part III, Chapter III). In view of the peculiar characteristics of these prototypes (*i.e.* complex asymmetrical shapes with edges and folds, thermal and mechanical properties and need for thermal programming of the temporary shape), the development of dedicated coating processes was approached. Feasibility of a lab-scale, versatile and easy to set up equipment was demonstrated, the latter consisting in two assemblies for both spraying the coating formulation and implementing the rotation of samples. Set up of the coating conditions was performed using both a ethanolic solution of Eudragit® RS and RL and a ready-to-use aqueous suspension of Eudragit® NE. Moreover, integrity and thickness of the applied layer and relevant impact on shape memory and release behavior of samples was investigated.

All the results reported in the thesis have been already disclosed, *i.e.* published, submitted for publication or presented in the form of communications to international conferences.

ARTICLES

- A. Melocchi, N. Inverardi, M. Uboldi, F. Baldi, A. Maroni, S. Pandini, F. Briatico-Vangosa, L. Zema, A. Gazzaniga, Retentive device for intravesical drug delivery based on water-induced shape memory response of poly(vinyl alcohol): design concept and 4D printing feasibility, Int. J. Pharm., 559 (2019) 299-311.
- A. Melocchi, M. Uboldi, N. Inverardi, F. Briatico-Vangosa, F. Baldi, S. Pandini, G. Scalet, F. Auricchio, M. Cerea, A. Foppoli, A. Maroni, L. Zema, A. Gazzaniga, Expandable drug delivery system for gastric retention based on shape memory polymers: Development via 4D printing and extrusion, Int. J. Pharm., 571 (2019) 118700.
- A. Melocchi, M. Uboldi, M. Cerea, A. Foppoli, A. Maroni, S. Moutaharrik, L. Palugan, L. Zema, A. Gazzaniga, Shape memory materials and 4D printing in pharmaceutics, Adv. Drug. Deliv. Rev., 173 (2021) 216-237.
- N. Inverardi, G. Scalet, A. Melocchi, M. Uboldi, A. Maroni, L. Zema, A. Gazzaniga, F. Auricchio, F. Briatico-Vangosa, F. Baldi, S. Pandini, Experimental and computational analysis of a pharmaceutical-grade shape memory polymer applied to the development of gastroretentive drug delivery systems, J. Mech. Behav. Biomed., 124 (2021) 104814.
- M. Uboldi, A. Melocchi, S. Moutaharrik, M. Cerea, A. Gazzaniga, L. Zema, Dataset on a small-scale film-coating process developed for self-expanding 4D printed devices, Coatings submitted for publication (2021).

COMMUNICATIONS

- A. Melocchi, M. Uboldi, F. Baldi, F. Briatico-Vangosa, N. Inverardi, S. Pandini, A. Maroni, L. Zema, A. Gazzaniga, Study of shape memory response of poly(vinyl alcohol) for development of retentive intravesical drug delivery systems via hot melt extrusion and 4D printing, Annual Workshop of the Italian Chapter of the CRS, Padova, October 18-20, 2018.
- A. Melocchi, M. Uboldi, F. Baldi, F. Briatico-Vangosa, N. Inverardi, S. Pandini, M. Cerea, A. Maroni, L. Zema, A. Gazzaniga 4D printing for fabrication of retentive intravesical drug delivery systems based on poly(vinyl alcohol), AAPS Annual meeting and exposition, Washington, November 4-7, 2018.
- A. Melocchi, M. Uboldi, N. Inverardi, S. Pandini, F. Baldi, F. Briatico-Vangos3, S. Palea, A. Maroni, L. Zema, A. Gazzaniga, 4D printing in the development of an indwelling delivery device for intravesical administration of drugs, 3rd European Conference on Pharmaceutics, Bologna, March 25-26, 2019.
- A. Melocchi, M. Uboldi, N. Inverardi, F. Briatico-Vangosa, F. Baldi, S. Pandini, G. Scalet, F. Auricchio, A. Maroni, L. Zema, A. Gazzaniga, Self-expandable drug delivery systems for gastric retention, 13th A.It.U.N. Meeting, Castelraimondo, June 13-14, 2019.
- A. Melocchi, M. Uboldi, N. Inverardi, F. Baldi, A. Maroni, S. Pandini, F. Briatico-Vangosa, G. Scalet, L. Zema, A. Gazzaniga, Expandable gastroretentive drug delivery system based on shape memory poly(vinyl alcohol) fabricated by hot-melt extrusion and fused deposition modeling: design and 4D printing concept, CRS Annual Meeting, Valencia, July 21-24, 2019.
- M. Uboldi, A. Melocchi, L. Zema, A. Gazzaniga, Development, via hot melt extrusion and 4D printing, of a self-expandable drug delivery system for gastric retention, 19th Advanced School in Pharmaceutical Technology, Soverato, September, 9-12, 2019.

- A. Melocchi, M. Uboldi, N. Inverardi, F. Briatico-Vangosa, F. Baldi, S. Pandini, G. Scalet, F. Auricchio, M. Cerea, A. Maroni, L. Zema, A. Gazzaniga, Shape memory expandable gastroretentive drug delivery system manufactured by 4D printing, AAPS Annual Meeting & Exposition, San Antonio, November 3-6, 2019.
- M. Uboldi, A. Melocchi, A. Maroni, L. Zema, A. Gazzaniga, Coating of retentive drug delivery systems based on shape-memory poly(vinyl alcohol) for improved release performance, Oral presentation, Annual Workshop of the Italian Chapter of the CRS, Catania, November 7-10, 2019.
- A. Gazzaniga, F. Baldi, F. Briatico-Vangosa, N. Inverardi, A. Maroni, A. Melocchi, S. Pandini, M. Uboldi, L. Zema, Coated expandable drug delivery systems for gastric retention based on shape memory poly(vinyl alcohol), CRS Virtual Annual Meeting, Online, June 29- July 2, 2020.
- G. Scalet, N. Inverardi, A. Melocchi, M. Uboldi, F. Auricchio, F. Baldi, S. Pandini, F. Briatico-Vangosa, M. Cerea, A. Foppoli, A. Maroni, L. Zema, A. Gazzaniga, Computational approach for the analysis of 4D gastroretentive drug delivery systems, 14th World Congress on Computational Mechanics ECCOMAS Congress, Paris, July 19-24, 2020.
- M. Uboldi, A. Melocchi, S. Moutaharrik, A. Maroni, L. Zema, A. Gazzaniga, Eudragit® RL/RS-coated drug delivery systems based on shape memory poly(vinyl alcohol) for gastric or vesical retention, 12th World Meeting on Pharmaceutics, Biopharmaceutics and Pharmaceutical Technology, Online, May 11-14, 2021.
- N. Inverardi, C. Pasini, A. Melocchi, M. Uboldi, G. Scalet, A. Maroni, L. Zema, A. Gazzaniga, F. Briatico-Vangosa, F. Auricchio, F. Baldi, S. Pandini, Optimization of a shape memory-based platform for drug delivery, 31st Conference of the European society for biomaterials, Online, September 5-9, 2021.

References

1. L. R. Martin, S. L. Williams, K. B. Haskard, M. R. DiMatteo, The challenge of patient adherence, Ther. Clin. Risk Manag. 3 (2005) 189-199.
2. K. S. Ingersoll, J. Cohen, The impact of medication regimen factors on adherence to chronic treatment: a review of literature, J. Behav. Med. 31 (2008) 213-224.
3. A. M. Paquin, K. M. Zimmerman, T. R. Kostas, L. Pelletier, A. Hwang, M. Simone, L. M. Skarf, J.L. Rudolph, Complexity perplexity: a systematic review to describe the measurement of medication regimen complexity, Expert. Opin. Drug Saf. 12 (2013) 829-840.
4. M. T. Brown, J. K. Bussell, Medication Adherence: WHO Cares?, Mayo Clin. Proc. 86 (2011) 304-314.
5. A. Maroni, A. Melocchi, L. Zema, A. Foppoli, A. Gazzaniga, Retentive drug delivery systems based on shape memory materials, J. Appl. Polym. Sci. 137 (2020) 48798
6. M. J. Cima, H. Lee, K. Daniel, L. M. Tanenbaum, A. Mantzavinou, K. C. Spencer, Q. Ong, J. C. Sy, J. Santini, C. M. Schoellhammer, D. Blankschtein; R. Langer, Single compartment drug delivery, J. Control. Release 190 (2014) 157-171
7. S. Babaee, S. Pajovic, A. R. Kirtane, J. Shi, E. Caffarel-Salvador, K. Hess, J. E. Collins, S. Tamang, A. V. Wahane, A. M. Hayward, H. Mazdiyasni, R. Langer, G. Traverso, Temperature-responsive biometamaterials for gastrointestinal applications, Sci. Trans. Med. 11 (2019) eaau8581
8. A. Abramson, E. Caffarel-Salvador, M. Khang, D. Dellal, D. Silverstein, Y. Gao, M. R. Frederiksen, A. Vegge, F. Hubálek, J. J. Water, A. V. Friderichsen, J. Fels, R. K. Kirk, C. Cleveland, J. Collins, S. Tamang, A. Hayward, T. Landh, S. T. Buckley, N. Roxhed, U. Rahbek, R. Langer, G. Traverso, An ingestible self-orienting system for oral delivery of macromolecules, Sci. 363 (2019) 611-615
9. M. Verma, K. Vishwanath, F. Eweje, N. Roxhed, T. Grant, M. Castaneda, C. Steiger, H. Mazdiyasni, T. Bensel, D. Minahan, V. Soares, J. A.F. Salama, A. Lopes, K. Hess, C. Cleveland, D. J. Fulop, A. Hayward, J. Collins, S. M. Tamang, T. Hua, C. Ikeanyi,

G. Zeidman, E. Mule, S. Boominathan, E. Popova, J. B. Miller, A. M. Bellinger, D. Collins, D. Leibowitz, S. Batra, S. Ahuja, M. Bajiya, S. Batra, R. Sarin, U. Agarwal, S. D. Khaparde, N. K. Gupta, D. Gupta, A. K. Bhatnagar, K. K. Chopra, N. Sharma, A. Khanna, J. Chowdhury, R. Stoner, A. H. Slocum, M. J. Cima, J. Furin, R. Langer, G. Traverso, A gastric resident drug delivery system for prolonged gram-level dosing of tuberculosis treatment, Sci. Transl. Med. 11 (2019) eaau6267

10. D. H. Altreuter, A. R. Kirtane, T. Grant, C. Kruger, G. Traverso, A. M. Bellinger, Changing the pill: developments toward the promise of an ultra-long-acting gastroretentive dosage form, Expert Opin. Drug Deliv. 15 (2018) 1189-1198
11. A. R. Kirtane, O. Abouzid, D. Minahan, T. Bensel, A. L. Hill, C. Selinger, A. Bershteyn, M. Craig, S. S. Mo, H. Mazdiyasni, C. Cleveland, J. Rogner, Y. A. L. Lee, L. Booth, F. Javid, S. J. Wu, T. Grant, A. M. Bellinger, B. Nikolic, A. Hayward, L. Wood, P. A. Eckhoff, M. A. Nowak, R. Langer, G. Traverso, Development of an oral once-weekly drug delivery system for HIV antiretroviral therapy, Nat. Commun. 9 (2018) 2
12. O. C. Farokhzad, J. D. Dimitrakov, J. M. Karp, A. Khademhosseini, M. R. Freeman, R. Langer, Drug delivery systems in urology - getting “smarter”, Urol. 68 (2006) 463-469.
13. H. Lee, M J. Cima, An intravesical device for the sustained delivery of lidocaine to the bladder, J. Control. Release 149 (2011) 133-139.
14. S. H. Lee, Y. B. Choy, Implantable devices for sustained, intravesical drug delivery, Int. Neurourol. J. 20 (2016) 101-106.
15. E. A. Klausner, E. Lavy, M. Friedman, A. Hoffman, Expandable gastroretentive dosage forms, J. Control. Release 90 (2003) 143-162.
16. J. C. Nickel, P. Jain, N. Shore, J. Anderson, D. Giesing, H. Lee, G. Kim, K. Daniel, S. White, C. Larrivee-Elkins, J. Lekstrom-Himes, M. Cima, Continuous intravesical lidocaine treatment for interstitial cystitis/bladder pain syndrome: safety and efficacy of a new drug delivery device, Sci. Transl. Med. 4 (2012) 1-11.

17. W. M. Huang, Z. Ding, C. C. Wang, J. Wei, Y. Zhao, H. Purnawali, Shape memory materials, Mater. Today 13 (2010) 54-61.
18. W. M. Huang, C. L. Song, Y. Q. Fu, C. C. Wang, Y. Zhao, H. Purnawali, H. B. Lu, C. Tang, Z. Ding, J. L. Zhang, Shaping tissue with shape memory materials, Adv. Drug Deliv. Rev. 65 (2013) 515–535.
19. W. Zhao, L. Liu, F. Zhang, J. Leng, Y. Liu, Shape memory polymers and their composites in biomedical applications, Mater. Sci. Eng. C., 97 (2019) 864-883.
20. D. C. Lagoudas Ed., Shape memory alloys – Modeling and engineering applications, Springer (2013), New York, US-NY.
21. A. Lendlein Ed., Shape-memory polymers, Springer (2010), New York, US-NY.
22. S. Kamila, Introduction, classification and applications of smart materials: an overview, Am. J. Appl. Sci. 10 (2013) 876–880.
23. Y. S. Lui, W. T. Sow, L. P. Tan, Y. Wu, Y. Lai, H. Li, 4D printing and stimuli-responsive materials in biomedical aspects, Acta Biomater. 92 (2019) 19-36.
24. I. Lukin, S. Musquiz, I. Erezuma, T. H. Al-Tel, N. Golafshan, A. Dolatshahi-Pirouz, G. Orive, Can 4D bioprinting revolutionize drug development?, Expert Opin. Drug Discov. 14 (2019) 953–956.
25. S. J. Trenfield, A. Awad, C. M. Madla, G. B. Hatton, J. Firth, A. Goyanes, S. Gaisford, A. W. Basit, Shaping the future: recent advances of 3D printing in drug delivery and healthcare, Expert Opin. Drug Deliv. 16 (2019) 1081–1094.
26. X. Li, J. Shang, Z. Wang, Intelligent materials: A review of applications in 4D printing, Assem. Autom. 37 (2017) 170–185.
27. Z. Zhang, K. G. Demir, G. X. Gu, Developments in 4D-printing: a review on current smart materials, technologies, and applications, Int. J. Smart Nano Mater. 10 (2019) 205–224.

Part I

The content of Part I has already been published in: Adv. Drug Deliv. Rev. 173 (2021) 216-237.

SHAPE MEMORY MATERIALS AND 4D PRINTING IN PHARMACEUTICS

Abstract

Shape memory materials (SMMs), including alloys and polymers, can be programmed into a temporary configuration and then recover the original shape in which they were processed in response to a triggering external *stimulus* (*e.g.* change in temperature or pH, contact with water). For this behavior, SMMs are currently raising a lot of attention in the pharmaceutical field where they could bring about important innovations in the current treatments. 4D printing involves processing of SMMs by 3D printing, thus adding shape evolution over time to the already numerous customization possibilities of this new manufacturing technology. SMM-based drug delivery systems (DDSs) proposed in the scientific literature were here reviewed and classified according to the target pursued through the shape recovery process. Administration route, therapeutic goal, temporary and original shape, triggering *stimulus,* main innovation features and possible room for improvement of the DDSs were especially highlighted.

Keywords: shape memory alloys, shape memory polymers, shape memory effect, 3D printing, 4D printing, drug delivery systems, controlled release.

1. Introduction and aim of the review

Versatility currently represents a key concept for R&D in many industrial fields and increasing attention is driven towards materials showing advanced functionalities that make them suitable for a range of applications [1-2]. In this respect, shape memory materials (SMMs), generally referred to as smart or intelligent materials, started to raise a lot of interest in different areas [3-5]. They are supposed to dynamically respond and adapt themselves to an external *stimulus* - typically a variation in the environment - thus performing their functions according to the changes undergone [6-8]. The actual ability to control the modifications undertaken is a key factor in the definition of smart materials. In particular, SMMs are able to change their shape in a predefined way upon appropriate stimulation. They can be forced, by application of an external stress, to take on a secondary/temporary shape, starting from the permanent/original one they were processed into. This is called programming step or shape-memory creation process. The temporary shape is maintained, even after the stress removal, until the material is exposed to the specific non-mechanical *stimulus* (*e.g.* direct heating, indirect heating through the application of electromagnetic fields or light, contact with water, change in the pH or ion composition of the liquid environment) able to induce the so-called shape memory behavior or effect, *i.e.* the recovery of the original shape. In other words, SMMs have the ability to temporarily store the mechanical stress applied during programming and undergo, only upon application of a suitable trigger, the pre-defined mechanical actuation. Notably, the movement occurring during recovery reverses the mechanical deformation that has led to the temporary shape. For these peculiar characteristics, literature refers to SMMs as materials able to remember the memorized shape.

Although the identification and the first knowledge of SMMs can be traced back to the 1940s, their diffusion and the strongest impetus for their use came at the end of the 1990s [9]. In view of their broad applicability potential and of the possibility of using them for targets hardly achievable in other ways, SMMs started to be employed in automotive, packaging, electronic and textile industries. Indeed, product design phase was

revolutionized by SMMs, giving to designers the possibility of working on two different geometries of the same product at the same time and on how the transition from the former to the latter would happen [10]. Later on, SMMs spread out also towards more sophisticated fields such aerospace and biomedicine [1,5,11]. As a consequence, the market associated with these materials and the relevant application is expected to reach $ 1.84 B by the end of year 2026, with a growth of approximately 25% *per* year from 2019 to 2026 and with the Asia-Pacific region highlighting the fastest rate [12,13].

Only more recently, SMMs were also considered in the pharmaceutical area, particularly at the research level, given their potential for innovating current therapeutic strategies. The aim of the present review is to critically discuss the applications proposed so far in the primary scientific literature describing the use of SMMs in this new field. More into detail, articles focused on drug products, mainly drug delivery systems (DDSs), were considered. Conversely, drug-free items showing shape memory response, such as medical devices and scaffolds, were deliberately excluded. Due to the complexity of the subject investigated, the research articles here reviewed often represented a joint work from experts of different fields, such as chemical and mechanical engineering, chemistry, biology, medicine and pharmaceutical technology.

Applications relying on both shape memory alloys (SMAs) and shape memory polymers (SMPs) were analyzed, and a classification based on the objective pursued through the recovery of the original shape was proposed. Particularly, shape recovery was employed to *i)* reach the site of drug delivery, *ii)* enable prolonged retention *in situ* after minimally invasive administration, *iii)* ensure removal from the target site, and *iv)* trigger drug release. Considering the real novelty of such applications, studies mainly aimed at in-depth investigating the shape memory behavior for sole characterization purposes were also reviewed. With reference to the definition of smart materials, in this manuscript only DDSs based on SMPs and SMAs were reviewed, for which well-defined and recognizable original and temporary shapes were described, the latter obtained following a specific programming step. On the contrary, the numerous smart applications based on hydrogels

involving a generic gel-sol transition, which was not associated with well-defined temporary and original shapes and relied on a non-programmed shape shifting, have been purposely ruled out.

1.1 Shape memory alloys (SMAs)

In 1951, the shape memory effect of an alloy based on gold and cadmium was observed for the first time by Chang and Read [6,14]. In 1963, Buehler and colleagues described the same phenomenon for nitinol, an equiatomic nickel and titanium alloy. Subsequently, other SMAs were studied, such Cu-Zn-Al and Fe-Mn-Si based materials. However, nitinol probably remains the main SMA investigated in the biomedical field for its unique characteristics, such as superelasticity, good combination of high strength and low elastic module, high corrosion resistance as well as biocompatibility and non-ferromagnetic properties, which provide a clear image during magnetic resonance and make it particularly suitable for biomedical applications [15,16]. Recently, a few attempts have also been proposed to attain surface modifications of nitinol-based materials thus mitigating the risks associated with the presence of a potentially toxic, allergenic and carcinogenic component, *i.e.* nickel [17-20].

Starting from nitinol as such or in combination with other materials, various shapes and sizes can be fabricated: thin films, fibers, particles and porous matrices. Nitinol based-ternary alloys have also been proposed to meet particular needs, such as to provide the material with intrinsic antibacterial activity (*e.g.* Ni-Ti-Cu, Ni-Ti-Ag) [15,21,22]. However, the associated fluctuations in the nitinol stoichiometry were shown to have strong impact on the properties of the resulting SMA, such as changing the relevant activation temperature [6].

1.1.1 Mechanism of shape recovery

From the structural point of view, SMAs and particularly nitinol occur in two solid phases, each with a different crystal structure and peculiar properties [3,6,23-28]. The

austenite phase, predominant at higher temperatures, generally exhibits a cubic crystal structure, while the martensite phase is characterized by tetragonal, orthorhombic or monoclinic crystal structure, depending on the alloy composition. Moreover, each martensitic crystal can exhibit a different orientation, called a variant, so that a twinned martensite, composed of a combination of self-accommodated martensitic variants, and a detwinned martensite, in which a specific variant is dominant, can be recognized. The transformation from one crystal structure to the other (referred to as martensitic transformation) is the basis for the shape memory effect. More into detail, austenite, under no load conditions and upon cooling, begins to transform into twinned martensite at the martensitic start temperature (M_s) and complete the transformation at the martensitic finish temperature (M_f). During heating, the reverse transformation takes place, initiating at the austenitic start temperature (A_s) and ending at the austenitic finish temperature (A_f). If a mechanical stress (σ) is applied to the material in the twinned martensitic phase at low temperatures, a detwinning phenomenon occurs with the reorientation of a certain number of variants. Such a process results in a macroscopic shape change and the configuration attained upon deformation can be retained also when the load is removed. This behavior makes it possible to program the SMA temporary shape. Upon heating above A_f, the detwinned martensite will go back to austenite phase, thus leading to complete shape recovery. Cooling back to a temperature below M_f will result in the formation of twinned martensite with no associated shape change. The minimum stress required for starting the detwinning process is named detwinning start stress (σ_s), while the stress level corresponding to complete detwinning of martensite is recognized as the detwinning finish stress (σ_f). When the material in the austenitic phase is cooled upon a mechanical stress greater than σ_s, the phase transformation can cause the direct formation of detwinned martensite, thus producing a shape change. On the other hand, reheating the material would determine the relevant shape recovery while the load is still applied. Overall, the transformation temperatures increase with an increase in the stress magnitude. Stress-free cooling of austenite below the M_s and M_f results in the

formation of twinned martensite. When the latter is subjected to an applied stress that exceeds σ_s, a reorientation process is initiated, with the growing of favorably oriented martensitic variants. The detwinning process is completed at σ_f and is maintained also in the absence of stress. Upon heating with no stress, from A_s to A_f the shape recovery occurs and only the parent austenitic phase remains. Subsequent cooling to martensite will result in the formation of self-accommodated twinned martensitic variants with no associated shape change, and the whole cycle of the shape memory could be repeated. To summarize, a SMA exhibits the shape memory effect when it is deformed in the twinned martensitic phase and then unloaded while at a temperature below A_s (Figure 1). Upon heating above A_f, it will recover its original shape, by going back to the parent austenitic phase.

The phase transformation of SMAs can be triggered not only by temperature (*i.e.* shape memory effect) but also by applying a sufficiently high mechanical load to the material in its austenitic phase, leading from austenite to fully detwinned martensite. When the stress is released at temperatures above A_f, the crystal form returns to the austenite phase and the material regains the more stable initial micro-/macroscopic configuration. This phenomenon is known as superelasticity, and it leads to an immediate shape change on unloading, which cannot be controlled nor programmed. In the case of nitinol, such a phenomenon typically occurs at room temperature.

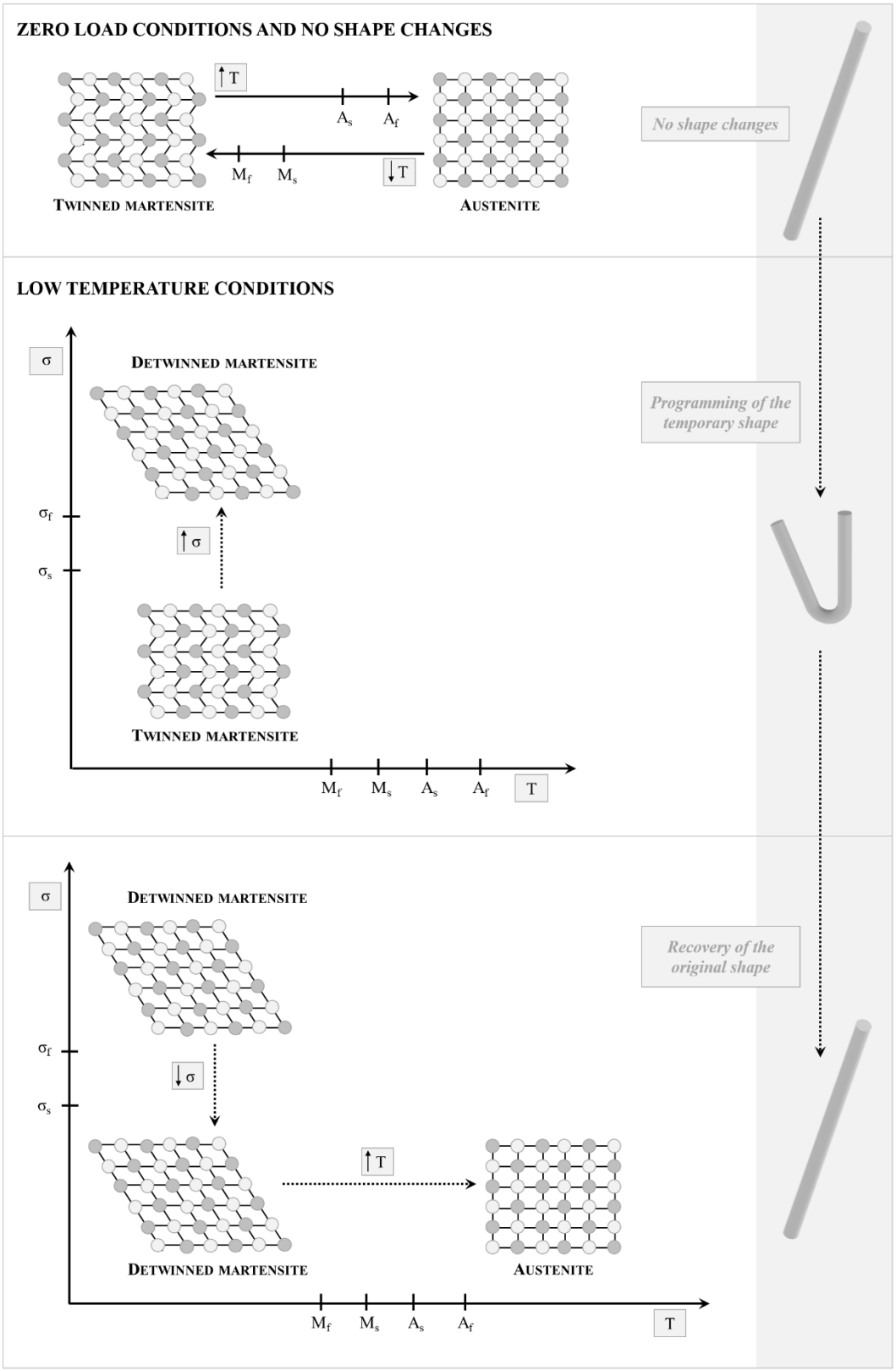

Figure 1: Outline of the typical transformations of SMAs involved in the shape memory effect (adapted from [6]).

1.1.2 Main applications and characterization studies

Since its discovery, many commercial applications of nitinol were proposed, but only in the 1990s this material made its commercial breakthrough in the biomedical field [26,29]. In this respect, various devices have been designed, such as archwires, drills for root canal surgery, spinal vertebra spacers, artificial bone implants, tools for microsurgery such as a cardiovascular atrial septal occlusion device, filters for removing blood clots, and the so-called self-expanding stents [30-33]. The latter have been investigated for allowing expansion of esophagus, biliary duct, trachea, bronchi, ureters and urethra. However, their blockbuster is probably represented by the vascular application. Traditionally, vascular stents were made of stainless steel. They were inserted in the human body through a catheter and were expanded *in situ* to the size of the artery by an inflatable balloon. The use of self-expanding superelastic nitinol stents allowed to overcome the limitations typical of stainless steel stents, such as the partial fit loose associated with the elastic unloading and damages of vessels resulting from over-expansion, while improving adaptability to different anatomical characteristics. After being constrained, the stent is introduced into the body where the temperature exceeds A_s. When the external constriction of the catheter is removed, the stent expands to adapt itself to the larger diameter of the vessel due to the above mentioned superelasticity and gently pushes outward on the walls.

When dealing with the applications in the pharmaceutical field, nitinol still turned out to be the main material investigated. Different targets for using its shape recovery capability were identified and will be discussed in Chapter 2. In this respect, DDSs only relying on the superelastic behavior of nitinol were deemed out of the scope of the present review, although they may show similar functionality. In fact, some of these systems would be able to attain therapeutic objectives close to those of the DDSs exploiting just the shape memory effect of the SMA [34-37]. Besides drug-containing stents showing self-expansion, two of the most significant applications of nitinol superelasticity are the Lidocaine-releasing intravesical system named LiRIS and a gastroretentive device for

long-term tuberculosis treatment developed by Verma and coauthors [34,38]. The LiRIS system is an osmotic pump in which a nitinol wire is inserted into a silicon tube also housing a drug containing formulation (*e.g.* powder, mini-tablets). The nitinol wire has a pretzel-like shape which allows the system to assume a bulky configuration that prevents its emptying from the bladder. However, to accommodate the system inside a catheter for intravesical administration, the nitinol wire was mechanically forced into an elongated shape which was maintained by the constraint. When the stress was released at body temperature, the crystal nitinol returned to the austenite phase and regained the coiled shape in which it was produced.

The gastroretentive systems devised by Verma and colleagues for long-term doxycycline hyclate and isoniazid treatment relied on an analogous working mechanism. It entailed a superelastic nitinol wire, in which pierced drug-containing matrices were inserted, ending with a retainer and a magnet. To increase drug loading and duration of therapy, the length of the wire and the formulation of matrices could be modified. After reaching the stomach through a nasogastric tube, in which the system was forced to assume an elongated configuration, the nitinol wire curled back to the cylindrical coil shape, thus preventing the relevant emptying through the pylorus.

Given the wide diffusion of SMAs, ASTM (American Society for Testing and Materials) International has published standard test methods to guide experimentation efforts towards the definition of their behavior, especially for R&D [6,23,27]. These may involve differential scanning calorimetry (DSC), thermomechanical testing and the bend test to draw indications about austenite-related temperatures. DSC analyses can be used for highlighting solid phase transformations in SMAs under zero stress and for estimating the key transformation temperatures. Thermomechanical testing performed on wires, dumbbell specimens and hollow cylinders mainly involve uniaxial and compressive tests as well as multiaxial loading. The bend test is performed to gain qualitative information about austenite-related temperatures. In fact, at the beginning of the test, the specimen, in the shape of wire, tube, or strip is deformed at temperature lower than A_s, causing

formation of the detwinned martensite. The temporary shape would then be kept also when the stress is released as the temperature is below A_s. The sample is then slowly heated, monitoring its geometric configuration. The temperature at which the sample begins to recover its original shape would be approximately A_s, and that at which the recovery process is completed is taken as A_f.

1.2 Shape memory polymers (SMPs)

SMPs, also known as actively moving polymers, exhibit many advantageous features with respect to SMAs, such as being lightweight (density in the 1.13-1.25 g cm^{-3} range *versus* 6.4–6.5 g cm^{-3} for nitinol) and allowing larger deformation in the programming step (up to 400%). [7,8,39-40]. Moreover, they can be combined with specific adjuvants (*e.g.* nanotubes, carbon fibers, magnetic nanoparticles and dyes) in formulations showing new properties [41]. The shape recovery of SMPs can be triggered by a range of external *stimuli* (*e.g.* increase in temperature, application of a magnetic field, irradiation, pH change, contact with water), which could also be applied remotely or wirelessly [7,42-45]. SMPs are generally characterized by a greater shape recovery capability with respect to alloys and they can turn out compatible with a variety of cost-effective manufacturing processes, which have recently started to be considered for their potential in the pharmaceutical field (*e.g.* hot melt extrusion, injection molding, 3D printing) [46-55]. For these reasons, they could be tailored to specific applications.

Polynorbornene developed by CdF Chimie Company in 1984 was the first SMP, commercialized under the trade name of Norsorex by the Nippon Zeon Company [6,56]. In the following years, Kurare TP-301 by Kurare Corporation, Asmer by Asahi Company and polyurethane-based SMP developed by Mitsubishi Heavy Industries became available on the market. Initially, SMPs were employed for the fabrication of a range of medical devices, such as self-knotting sutures, scaffolds for tissue engineering and relevant repair, orthodontics, stents, clot removal and aneurysm occlusion devices, systems for cardiac valve repair and occludes for congenital heart diseases [5,40,57]. Later on, they were

proposed also in the drug delivery field. In particular, thermo- and chemo-responsive SMPs as well as those based on supramolecular interactions were mainly tested, while applications involving the use of light-responsive polymer are still minor [58-60].

1.2.1 Mechanism of shape recovery

The shape recovery behavior of SMPs requires suitable architecture and morphology of the polymeric network, combined with tailored processing and programming steps [56,57,61,62] (Figure 2).

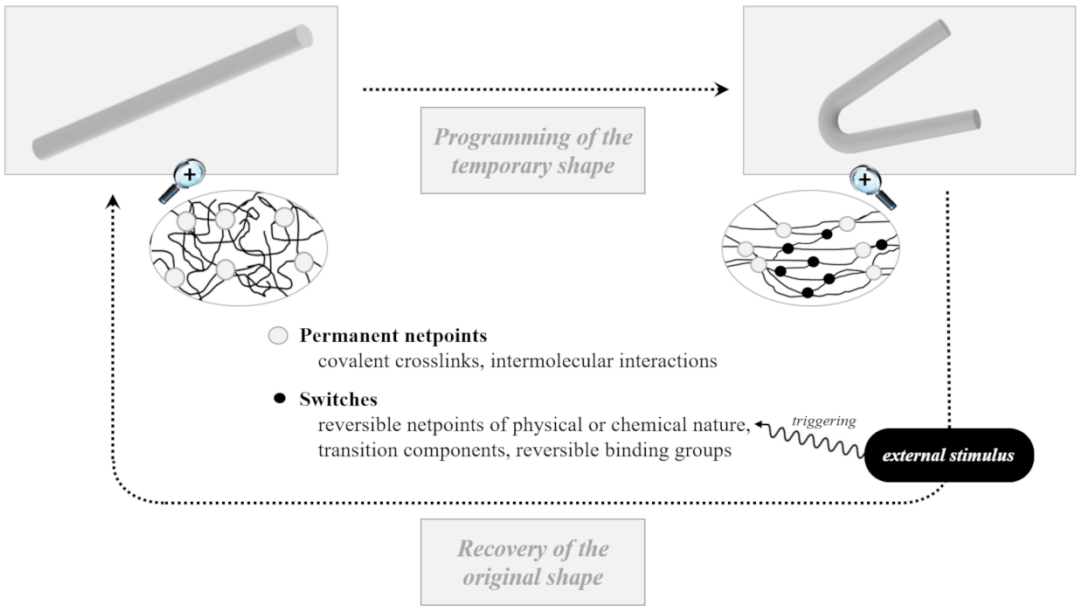

Figure 2: Outline of the structural components of SMPs involved in the shape memory effect (adapted from [7]).

The typical SMP network is characterized by the presence of permanent netpoints connected by chain segments, which can interact forming switches sensitive to an external *stimulus* [7,8,62-64]. These netpoints are responsible for memorizing the original shape. Indeed, they are not affected by deformation of the material after production (*e.g.* programming step) and for this reason are generally named as permanent. On the other hand, the chain segments would retain a certain conformational freedom, leading to

deformability, which generally increases with length and flexibility of such chains. In particular, flexibility is essential for programming the temporary shape. Therefore, while the secondary shape is stabilized by the temporary fixation of the conformation of chain segments in the deformed shape, the recovery of the original shape is enabled by the entropy-driven recoiling of these segments, as the randomly coiled state represents the most favorable state from the entropic point of view. Such a reversible fixation can be attained either by solidification of the so-called switching domains, which are formed by the switching segments, or by formation of further covalent crosslinks that should be reversible (*i.e.* reversible netpoints), which means that can be formed and cleaved when needed.

Netpoints responsible for the original shape are generally of chemical (*i.e.* covalent crosslinks) or physical (*i.e.* intermolecular interactions) nature. Chemical crosslinks can be created either directly during the synthesis of the SMP or by post-processing methods, adding a radical initiator to the starting materials and inducing relevant crosslinking by radiation (*e.g.* γ-radiation, UV light, neutrons). On the other hand, physical interactions are typical of polymers consisting of at least two segregated domains, such as a crystalline and an amorphous phase. In this structure, the domains related to the highest thermal transition temperature (*i.e.* T_{perm}) are named hard domains and generally show a glass transition temperature (T_g) or a melting temperature (T_m) much higher than the temperature of use, thus acting as physical netpoints in their typical operating conditions. Conversely, the chain segments with the second highest thermal transition (*i.e.* T_{trans}), which means a lower T_g or T_m with respect to that previously mentioned, represent the switching domains. These are responsible for fixing the temporary shape. Fixing can also be promoted by the formation of additional reversible netpoints either of physical or chemical nature. In the former case, the additional netpoints are obtained by solidification of switching domains (*e.g.* vitrification, crystallization) following cooling. The consequent reduction in molecular mobility allows macroscopic shape fixation. Such netpoints are considered reversible because, by increasing the temperature, the crystals could melt and

the glassy domains return to the liquid state. On the other side, reversible chemical crosslinks are generally obtained upon reaction of two functional groups and the resulting chemical bond can be cleaved on demand by exposure to an appropriate *stimulus* (*e.g.* cinnamic acid and cinnamyliden acid groups that can undergo a photoreversible reaction when irradiated with light of suitable wavelengths). In this respect, T_{trans} enabling the reversible solidification of the switching domain can be a melting transition, a liquid crystalline transition and also a glass transition. Notably, chain segments providing the switching domains for the temporary shape and netpoints determining the permanent shape do not need to be covalently connected with each other, as in the case of polymer blends. Chemically crosslinked SMPs, in which the temporary shape is fixed by one switching domain, would show marked decrease in the mechanical properties when the temperature exceeds T_{trans}. In the same conditions thermoplastic SMPs (*i.e.* polymers characterized by physical crosslinks) do not show such a drastic change as the crystalline domains, providing the physical cross-links for the original shape, would cooperate with the amorphous switching domains in stiffening the polymer. Moreover, although covalent polymeric networks generally exhibit greater capability to fix the temporary shape and recover the original one, thermoplastic SMPs, when actuated, are able to develop much higher stresses. Moreover, they could be subjected to hot processing.

For thermo-responsive SMPs, the temporary shape can generally be programmed by heating the device at a temperature above T_{trans} but below T_{perm} while applying an external stress. The temporary shape is then fixed by cooling the item below T_{trans}. Subsequently, the shape recovery will be triggered only when the temperature will be higher than T_{trans} thanks to either a direct or indirect heating process. Besides using a heat source directly in contact with the SMP object, which may also occur on administration at body temperature, indirect heating was attained using laser light, alternating magnetic fields, near-infrared illumination and ultrasound treatment. However, this strategy often requires appropriate formulation, for instance adding to the SMP suitable absorbing dyes, magnetic nanoparticles and other functional excipients.

In the case of chemo-responsive SMPs, the programming step is essentially analogous to that previously described for thermo-responsive polymers [65-67]. However, instead of heating above the switching temperature to start the shape recovery process, the latter is activated by reducing the interaction among macromolecules. This can be attained by softening, swelling or dissolving the so-called transition component (*i.e.* the part of the polymer able to alter its mobility in response to the triggering external *stimulus*), thus promoting a reduction in the transition temperature. Focusing on the softening-induced shape memory effect, the recovery of the original shape is driven by the diffusion of solvent molecules into the polymer network. Indeed, the absorbed molecules would act as a plasticizer and decrease the interaction force among macromolecules while promoting the mobility of the polymer chains. Overall, this leads to a reduction in the switching temperature with the recovery of the original shape occurring under isothermal conditions and potentially at room temperature. Such an approach may be applied to fine-tune the transition temperatures of a given polymer network without changing the relevant chemical composition. Moreover, it represents the basis of the water-induced shape memory effect. In pharmaceutical applications, this has the main advantage to reduce the risks of damaging the surrounding tissue due to an excessive increase in temperature needed to trigger the shape switching. Swelling-induced shape memory behavior is typical of hydrogels. The polymer network, upon immersion into an appropriate medium, may progressively hydrate and swell, thus resulting in the formation of a gel. The latter is able to undergo a large deformation, which can be translated in a volume expansion until an equilibrium state for a given environment is reached. At the same time, a reduction in the transition temperature of the polymer could be attained activating the shape recovery process.

More recently, supramolecular interactions have also emerged as an interesting strategy for the development of novel SMPs with properties not always achievable by the conventional triggering approaches [59,65,68]. These materials are based on the incorporation of reversible binding groups into the polymer network, serving as either

permanent or temporary netpoints. Indeed, a reversible binding group is a kind of molecular sticker that associates to form dynamic linkages. Depending on the type of sticker, the equilibrium concentration of disassociated groups and the rate of bond exchange can be altered upon appropriate stimulation. For this reason, an ideal reversible binding group should be more stable in the associated state, with slow exchange to establish long-lived netpoints, while exhibiting good reversibility when exposed to the trigger. Reversible binding groups could be either noncovalent or covalent. By way of example, they include hydrogen bonds, ionic interactions, metal coordination, hydrophobic interactions, transesterification and reversible addition-fragmentation reactions, as well as disulfide bonds. By using reversible binding groups different goals could be attained, such as decoupling the shape memory effect from the mechanical behavior of the polymer and enabling alternative shape memory triggering strategies (*e.g.* non-thermal switching mechanisms relying on the changes in chemical environment). This way, multiple and tunable shape memory effects could be combined in a single polymer network. Indeed, the relevant shape memory effect can be triggered, step by step, by heating, by contact with a specific solvent and by varying the chemical composition of the fluid in which the material has to perform its function.

1.2.2 Main applications and characterization studies

A few decades after the advent of SMPs in the biomedical field, the research interest is currently aimed at *i)* testing unusual *stimuli* to induce the shape-memory effect (*e.g.* biological *stimuli* such as interaction with enzymes), *ii)* achieving more complex shape changes, involving for instance multiple shifts between several temporary shapes, and *iii)* combining the shape memory behavior with other functions (*e.g.* biodegradability, electrical conduction, magnetism), to develop so-called multifunctional materials [62,64,69-72].

The level of in-depth knowledge acquired on SMPs over the years has allowed the modification of structural parameters of their molecular architecture, resulting for

instance in the modulation of the switching temperature between temporary and original shape [7,8,57,71]. This turned out useful for the development of materials specifically tailored to a desired application. Besides the reversible fixation of the temporary shape, the phase transition of the switching domains would determine changes in diffusivity, transparency and mechanical properties of the SMPs. Indeed, the knowledge-based development of new polymers was made possible by appropriate characterization methods employed to study the network on the macroscopic and molecular scale. Also morphological analyses were carried out by fabricating prototypes, mainly by casting.

On the macroscopic scale, the extent to which a deformation can be fixed to give a temporary shape and the recoverability of the permanent shape are of utmost importance and depend on many parameters, such as temperature, environment, kinetics, and type of mechanical deformation in addition to the intrinsic properties of the polymer under investigation [7,73]. For this reason, cyclic thermomechanical experiments, carried out using a tensile tester equipped with a thermal chamber, were employed to determine the capability of the switching segment to maintain the programmed shape (*i.e.* shape fixity ratio) and of the material to memorize and recover the original shape (*i.e.* shape recovery ratio). The tests involved the programming of the temporary shape, carried out under stress-controlled or strain-controlled conditions, and the recovery of the original one, generally occurring under stress-free conditions. By way of example, a cycle may consist in heating the sample to a temperature higher than T_{trans}, but lower than T_{perm}, and stretching it to the desired strain. Then the specimen is cooled down below T_{trans} under the imposed constant strain, thus fixing the temporary shape. After heating the sample up to T_{trans}, shape recovery would occur and the cycle can be repeated. By performing multiple cycles, the effect of processing and storage could also be understood. Also bending tests were in some cases performed, during which the sample heated above T_{trans} was bent to a desired curvature and then cooled down to fix the temporary shape. To trigger the shape recovery, the items was then re-heated above T_{trans}, and the changes in the deformation curvature were monitored over time. Such tests can be carried out either

in air or in contact with suitable aqueous media, depending on the final intended application of the system.

The polymer architecture, intended as netpoints determining the permanent shape and reversible domains determining the temporary one, were in-depth characterized on the molecular/morphological level. Complete testing procedures can be followed to evaluate many different aspects, such as chemical composition and structure, segment lengths, network geometry and relevant morphology, crosslinking density and functionality or physical netpoints, thermal transitions as well as the mechanisms for closure and cleaving of reversible chemical netpoints. In the scientific literature currently available various techniques were proposed: swelling experiments and nuclear magnetic resonance spectroscopy to evaluate crosslink density, differential scanning calorimetry and dynamic mechanical thermal analysis to study the thermal characteristics, transmission or scanning electron microscopy, polarized optical microscopy and scattering methods to investigate the morphology.

Considering the application of SMPs in the pharmaceutical field, various research works were focused on the chemical structure of the polymer and how to engineer it, for instance to develop multifunctional materials [64,71,74-79]. Indeed, the polymer structure would affect not only the device performance, *e.g.* in terms of shape memory, dissolution/biodegradation and capability of controlling the release, but also the way the material can be processed to the desired original shape and therefore the compatibility with different drugs to be loaded. The drug itself would represent another key element to take into account. If it is embedded into the SMP matrix, also the loading procedure may have an effect on the overall behavior of the system. Finally, even the characteristics of the physiological environment in which the device is expected to perform (*e.g.* temperature, pH, presence of ions and proteins) may impact on the SMP behavior. In this respect, an ideal SMP, depending on the functions it has to fulfill in the final DDS, would allow independent tailoring of each of the features it should be provided with [7].

In a great number of publications, newly synthetized materials for the manufacturing of implantable devices were described, which involved the need for sterilization [7,8,56,63]. The method for sterilizing the product can affect the biocompatibility and performance of the DDSs, for instance by altering the thermomechanical properties of SMPs. Steam sterilization would be risky due to the high temperatures required (121-132 °C), which can potentially melt or change the intrinsic structure of the material. Although ethylene oxide and low temperature plasma sterilization are carried out at lower operating temperatures, the former involves proper aeration of the device, as the gas is inherently toxic, and the latter may affect the surface chemistry and toxicity of the DDS due to vapor residuals and hydroxyl radicals associated with the plasma phase. On the other hand, γ-rays and e-beam irradiation can be associated with changes in the molecular weight of the SMP and either crosslinking or scission of its chains. Therefore, irradiation could affect not only biocompatibility of a selected polymer but also the degradation rate in the case of materials designed to be biodegradable. Notably, any sterilization method operates at temperatures above body temperature. Considering that many of the systems described were fine-tuned to show shape recovery at body temperature, sterilization may result in premature deployment if the device is sterilized in its temporary shape. To overcome such an issue, some researchers have proposed to make use of the water uptake process that occurs *in vivo*, having the water working as a plasticizer and decreasing the SMP activation temperature. This would foster stability of the device at higher temperature during sterilization without affecting its shape memory capability in biological fluids (*i.e.* at body temperature in contact with water). On the other hand, *in vivo* water uptake may proceed slowly and this could be an issue with regards to the kinetics of the activation process. In addition, the mechanical properties of the device may be negatively modified over time with the water uptake. Indeed, the presence of water would increase the polymer free volume and promote chain flexibility at a given temperature. Also, hydrogen bonds between water molecules and possible hydrogen-bond acceptors in the polymer chain may weaken the polymer-polymer interaction and further contribute to the increased

chain flexibility. Due to all the above-mentioned criticalities, despite the increase in the costs of manufacturing, asepsis production methods could turn out mandatory. However, challenges still remain about how to prevent early activation of the shape memory device during storage and shipping. Use of packaging constraints, as done for alloys, may prevent the device from deploying in the case of undesired temperature increase. However, the same constraints may determine further challenges for sterilization. In addition, if the device is built to be activated at body temperature, there would be a narrow gap between storage temperature, typically room temperature, and activation temperature, which may cause its premature activation. For this reason, researchers have also considered other triggers, such as electromagnetic field and ultrasound, to enable an increase in temperature for the DDS only once administered. This strategy would allow to set a higher activation temperature for the device as the source of indirect heating would be limited to affect the device. This approach would need extra equipment and has anyway the potential to overheat the surrounding tissues with relevant damages. At the same time, *in vitro* and *in vivo* studies should be performed to understand compatibility and toxicity of the resulting item, taking in mind that these characteristics are dependent on the tissue in which the system is intended to perform [7,8,39,64,71]. The time during which the system is to be maintained in a specific tissue plays a pivotal role, and thus material biodegradability should be considered. Biodegradation is mainly caused by hydrolytic bond cleavage, the rate of which is in turn affected by diffusion processes. In the case of slow diffusion into the polymer matrix, this could lead to a degradation gradient from the surface to the core of the device, with a high degradation rate at the surface. As a result, the system appears reduced in size, but it may maintain its integrity and behavior at the core level. By contrast, when diffusion is faster than hydrolysis, degradation takes place all over the polymer matrix, thus resulting in bulk degradation. During this time, mechanical properties of the device should be so as to avoid damage to the tissue or acute inflammation would occur.

1.2.3 4D printing

Considering SMPs processing into the original shape, the advent of 3D printing technologies has further widened the range of applications of these materials by providing the tool for 4D printing [79-85]. This term was used for the first time in 2013 by Tibbits during a TED talk to highlight time as a new dimension for the development of 3D objects. In this respect, 4D printing was described to entail either materials that can change from one programmed shape to another or multi-material prints with the capability to transform over time, thus overcoming the concept of 3D printed objects as static structures. Afterwards, being employed by different other researchers, the meaning of this term was expanded to indicate any targeted evolution of 3D printed structures, in terms of shape, properties and functionality. Over time, 4D printing has taken on a main meaning by referring to the fabrication, *via* different 3D printing techniques and using smart materials as feedstocks, of items showing self-transformation ability, after production and in response to an external *stimulus* [26,86-90]. Although the main changes occur in size and shape of the object, these make also possible to modify the relevant performance and to achieve new functionalities.

Morphological changes in the end-product when exposed to a certain *stimulus* might depend on the use of smart materials as such and in combination, on the fine-tuning of the design and on the printing orientation as well as composition of layers. In this respect, in addition to the x, y and z axis for the definition of a shape, 4D printing takes into account also how these coordinates change over time during the transformation. The basic principle of 4D printing is to create precisely controlled localized internal stress within a printed structure, which upon subsequent release of this stress can undergo further 3D shape shifting in a predictable manner [81,86,90-93]. In this respect, deformation mismatch and shape memory effect are the main ways to attain 4D printing. A deformation mismatch is typical of multi-material objects and may be induced by the relevant differences in physical properties, such as thermal expansion coefficient and swelling ratio. By way of example, 4D printed structures investigated so far were

purposely designed to entail rigid polymeric structures and hydrogels. The diffusion of water into the hydrogel network would cause a specific and localized swelling, thus ensuring an evolution of the overall item shape in a controlled way. Alternatively, 4D printing could rely on the use of SMPs even for single composition items. These are the applications we found relevant in this review. In those cases, 4D printing also involved a so-called smart design phase, which has to take account of the original shape, the temporary shape, the transformations undergone by the object to shift from one another and relevant mechanisms.

3D printing technology has found main application in the pharmaceutical field for the development of personalized medicines, thanks to the versatility in composition, geometry and performance of drug products it can bring about [47,51,55,94-97]. In this respect, 4D printing holds even greater potential in tailoring to the needs of a specific patient, being able to define at the same time not only the characteristics the DDSs would have during administration but also those acquired at the target site prior, during or after the release of the drug. This would be particularly interesting in the case of implants that should be placed in a specific body area and whose shape should be adapted to the characteristics of the subject to be treated. As 4D printing involves the use of technologies still relatively little known in the pharmaceutical field, where formulation and process parameters are heavily conditioned by the need to comply with stringent quality and safety requirements, the number of applications proposed so far in the scientific literature are very limited and there is no full awareness of the potential of this technology yet. However, they are expected to largely grow in the next years, bringing a deeper understanding of 4D printing technique from the material, manufacturing and transformation over time points of view.

2. DDSs based on SMMs

Gene therapy and precision dosing, as well as the research for more effective and efficient production models, especially in view of the reduction in manufacturing scale associated with personalized medicine, seem to represent the new frontiers for the pharmaceutical field [48,98-107]. These applications would take advantage of new fabrication methods and drug delivery strategies, which SMMs could enable. Indeed, the use of such materials might represent a promising strategy to broaden the boundaries of traditional drug delivery and for the development of the so-called smart DDSs. As a part of a very innovative research topic, putting therapeutic needs before patient compliance has been already demonstrated to impact on adherence to the treatment, with important economic and epidemiological consequences, and this should not be disregarded [108-110]. In this respect the development of DDSs relying on SMMs may provide significant improvements: *i)* new ways to trigger drug release besides time-, rate- and site-dependent approaches and *ii)* increased freedom to design systems able to settle, adapt or remain and then release the conveyed drug, in the target districts or move away from them. These goals could even be attained overcoming the limitations associated with the conditions of administration, such as frequency, invasiveness and need for hospitalization.

Before the advent of smart DDSs, SMMs were already widely studied for biomedical applications, in particular for the production of drug-free stents and scaffolds. As a natural evolution, since the mid-2000s, a research line was launched aiming at exploring the feasibility of new materials to be used for the development of implantable DDSs. These polymers were intended to combine shape-memory effect at body temperature, to enable administration *via* minimally invasive implantation, biodegradability, to avoid a second surgery for removal, and controlled release of drugs, to pursue a range of therapeutic benefits [77-79,111-113]. With the idea of broadening the range of available multifunctional materials - *i.e.* polymers showing different independent functionalities - and to tailor them to the desired application, new polymers were purposely synthetized [64,72,74-76,79,113-121]. In this respect, a fine tuning of various molecular parameters

was carried out during the synthetic process. By way of examples, polyurethane-poly lactide-co-glycolide and polyurethane-poly-L-lactide/polyethylene glycol [114], polyestermethacrylate copolymers [79], copolyester urethanes [75,115], AB-polymer networks having cooligoester and poly(n-butyl acrylate) segments [114], polydiolcitrate polyester elastomers [74], poly(L-lactide-co-glycolide-co-trimethylene carbonate) [116] and poly(ε-caprolactone)/trisilanolphenylpolyhedraloligomericsilsequioxan networks [72,76,118] were proposed. Overall, temperature-sensitive multifunctional materials were mainly proposed with a few examples of shape memory polymers based on supramolecular interaction. The research works were thus focused on the design and the application of a characterization strategy involving the evaluation of *i)* polymer network architectures (*e.g.* crosslinking density, molecular weight), *ii)* polymer biocompatibility, biodegradability, thermo-mechanical and shape memory properties, even in an aqueous environment as water may act as a plasticizer, *iii)* feasibility of drug incorporation in the polymeric network, either before the relevant synthesis or in the resulting material by soaking, *iii)* influence of drug properties (*e.g.* solubility, hydrophilic-lipophilic balance, molecular weight), loaded amount and incorporation method on the thermo-mechanical and shape memory properties of the material, and release performance as well as biodegradability of the system. On the other hand, what has not yet been addressed in these research works was the design concept of the DDSs, *i.e.* the shape and dimension in which they were manufactured and that would be recovered *in vivo*, the site of administration and the target area for the release of drugs, the molecule conveyed and the therapeutic use. Only well-defined DDSs relying on the use of SMAs and SMPs have been considered in detail and are presented in the following 2.1-2.4 Sections, being classified according to the objective for which the recovery of the original shape was exploited. Particularly, the temporary administered shape, the original recovered one and the *stimulus* employed for activation of the shape memory effect were highlighted. The most common triggering mechanism used was that of body temperature and was indicated as direct heating. SMPs proposed for the development of DDSs were most frequently

represented by purposely synthetized and in-house crosslinked polymers to obtain the network enabling the desired shape recovery effect, in terms of triggering conditions (*e.g.* temperature, supramolecular composition), efficiency of recovery (*e.g.* shape fixity and shape recovery ratio) and mechanical characteristics of the device. This could pose a major limitation since biocompatibility, quality and safety of the DDSs need to be demonstrated. Only in few cases, commercially available starting materials were employed as such.

Overall, systems at an early development stage were presented. In this respect, the research works reviewed mainly involved use of tracers or model drug molecules, simple study of model original and temporary shapes, rare adoption of industrially scalable manufacturing techniques, with preference to manual fabrication processes, *in vitro* studies of the shape memory behavior and release performance, few *ex* and *in vivo* data obtained in animal models or cadavers. Therefore, an effort was made to describe and summarize in the following Tables the research level achieved for the systems described in the reviewed articles, the innovation features and the possible room for improvement identified by the authors themselves.

2.1 Shape recovery for reaching the target area

In one main application, the shape recovery of nitinol provided a DDS with the ability to deliver drugs into the eustachian tube after being administered through the nasal cavity [122]. This approach would in principle allow to treat sudden hearing loss with no need for invasive insertion in the middle ear and overcoming the limits of movement in the nasopharyngeal cavity imposed by the nasal vestibule. The main features of this system are summarized in Table 1.

Tendon-driven manipulators with a size in the range of mm are generally used for transnasal administration. The availability of an actuator based on the nitinol shape memory effect can be considered particularly interesting as this material is characterized by excellent strength to weight ratio, thus enabling device miniaturization without losing

performance. This way, a good distal control of the device is maintained even in very tortuous administration paths, thus making the drug administration safer. Conversely to other active DDSs, no expensive microelectromechanical systems (MEMS) technology would be required for providing heating to trigger the shape recovery. In fact, the actuation would be obtained by Joule heating of the alloy, connected to an external direct current power supply through copper wires to overcome battery life limitations.

Table 1: DDSs for which the shape recovery effect allowed to reach the target area.

Reference	[122]
SMM	Commercial nitinol
Brief description of the system	Nitinol wire enclosed in a stainless steel ribbon spring, working antagonistically to the wire. A flexible tube acting as a drug reservoir inserted into the wire-ribbon assembly and connected to an external syringe for pumping the drug.
Administration route	Insertion in the middle ear through the nasopharyngeal cavity
Temporary (administered) shape	Curved shape 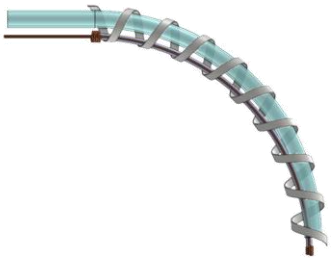
Triggering *stimulus*	Indirect Joule heating *via* an external direct current power supply
Original (recovered) shape	Straight shape 
Time frame of shape recovery	2-10 seconds
Target area for drug release	Eustachian tube (middle ear)
Therapeutic goal	Treatment of sudden hearing loss
Loaded drug/tracer	A dye solution
Main advantages / Innovation features	Capability of the system to navigate through tortuous paths characterized by wide range of dimensions High distal control Passive activation leading to cost reduction
Research level	Design concept and preliminary *in vitro* studies (arranging a set of loosely placed rings based on the anatomy of the middle ear) and *ex vivo* studies (on a cadaver head) with a tracer
Room for improvement identified by the authors	Relatively high activation temperature

2.2 Shape recovery for enabling retention in the target area

The ability of SMMs to take on a shape, different from that in which they were administered, bulkier or otherwise suitable for being retained in a specific body region, was applied for the design of implants/scaffolds, stents and systems specifically devised either for being maintained within hollow organs (*e.g.* stomach, bladder or vagina) or for wound treatment. By extending the residence time of DDSs, inherently designed to control rate or time of release, complex release performance and new therapeutic targets became accessible.

These DDSs were conceived with a temporary shape such as to ease the conditions of administration when these involved sites inside the human body that are rather difficult to reach, without impacting the ability of the systems to remain in the target areas and release their content. In fact, the latter objectives were fulfilled by the recovered original shape. On the other hand, the temporary shape could, for example, allow to insert the DDS into a catheter, make it injectable through syringes, swallowable and even implantable by minimally invasive surgery.

In the following Tables 2-5 the main features of the systems proposed so far in the literature, which were subdivided on the basis of the route, mode or objective of administration, were summarized. In particular, the SMMs employed and main characteristics of the DDSs were briefly described including the site of administration/release, the therapeutic goal pursued, the administered temporary shape as well as the recovered original one, and the triggering *stimulus*.

2.2.1 Implants/Scaffolds

SMMs have found an interesting use in the pharmaceutical field in response to the strong clinical trend towards minimally invasive surgery (Table 2). Indeed, implantation of initially small objects, that only *in situ* may gain a bulkier configuration with the desired shape and functionality, would be highly advantageous [113,123]. Only a few systems were proposed for specific administration sites, such as bones and cartilage, while the

great majority of the applications reviewed were mainly focused on general tissue and vascular regeneration, on the release of anti-bacterial and anti-inflammatory drugs to prevent implant failure and on promoting wound healing [124,125].

In the field of tissue engineering, SMMs have also enabled evolution of scaffolds, *i.e.* from devices having poorly versatile and editable physical/chemical properties, to implants designed for the growth of cells and the release of drugs intended, for instance, to promote repair or regeneration of tissues. In consideration of the high cost and limited bio-security of scaffolds containing *in vitro*-grown cells, cell-free shape-memory scaffolds were then proposed [123]. Porosity, which affects the formation of blood vessels through the scaffold, and biodegradation, required to occur in a specific period of time in order to make space for the grown tissue to take over, are of crucial importance in the development of scaffolds [126-128]. In this respect, hydrogels showing shape memory effect were widely employed in cell culture and tissue engineering as their internal structure easily allowed to provide enough support for cell growth using a limited amount of material. However, there was no effective ways to control the internal structure of the resulting systems. To overcome such a challenge, 4D printing relying on gel extrusion 3D printing was successfully tested for the fabrication of scaffolds based on shape memory hydrogels characterized by a good control of the internal mesh structure [129]. Notably, in such a system the shape memory effect was triggered by supramolecular interactions (*i.e.* removal of calcium ions). This strategy was used to avoid temperature triggering, but still lacks the identification of a suitable procedure to activate the shape recovery *in vivo*.

In most of the manuscripts considered, temperature-responsive SMMs were investigated to fulfill the need for administering implants through minimally invasive surgery [123,124]. Besides being biodegradable and characterized by suitable mechanical properties they should also enable the control of drug release in terms of time, rate and site. Not only typical polymeric prolonged-release matrices were proposed, but also multiple-unit systems based on bonded microspheres [42,124]. Such systems were

produced, programmed and administered as a single whole unit, but showed the ability to maintain the independent release performance of the subunits.

With respect to the *stimulus* triggering the shape recovery behavior, direct heating was often used *in vitro* but the relevant application *in vivo* remains an open question, especially in view of the relatively high temperatures required. Thus, indirect heating sources were investigated. By way of example, high intensity focused ultrasound (HIFU) was tested as an interesting triggering *stimulus* because the beam can be collimated into a tight focal spot of about 3 mm and can show a prominent selective heating effect [42,44]. SMPs can absorb the mechanical energy generated by viscous shearing oscillation exerted by focused ultrasound and subsequently relax, releasing the energy in the form of heat. Besides being well-known for the ability to penetrate much deeper into the body with respect for instance to light, HIFU could also be involved in controlling drug release. In the systems investigated, ultrasound waves were demonstrated able to trigger drug release *via* thermal and cavitation effects. Indeed, the temperature rise would determine swelling of the polymeric network and increase in the relevant permeability. On the other hand, ultrasound waves passing through a liquid determine the creation of microbubbles that grow and collapse in a few microseconds, thus generating high speed microstream and shock waves on the surface of the polymer matrix. These would promote the penetration of water into the polymeric network leading to drug dissolution and diffusion outside. In addition, HIFU was proved able to selectively heat the devices, even at high temperatures, without warming in a risky mode the surrounding environment and causing possible tissue damage. Such a localized heating could also be exploited to trigger shape recovery only in pre-defined areas of the DDS. However, the use of an indirect heating source would require an extra equipment to have the system perform correctly, thus increasing the cost of therapy.

Many of the proposed systems were in a preliminary stage of development, entailing prototypes having model shapes (*e.g.* I, U or cylindrical shapes), and were not provided with a geometry specially designed for the final application. Since they consisted of

polymers/copolymers either purposely synthesized or crosslinked to give rise to the shape memory effect, biocompatibility and biodegradability, the latter being particularly challenging for implant removal at the end of their performance, have started to be approached but would benefit from further investigation, especially after identifying a specific therapeutic goal/target area for each system.

Table 2: DDSs for which the shape recovery effect allowed prolonged retention in the target area: implants/scaffolds.

Reference	[44]	[42]	[125]	[124]	[129]	[123]
SMM	Purposely synthetized crosslinked poly(butyl methacrylate -co-methyl methacrylate) copolymers	Commercial poly(lactic-co-glycolic) acid and chitosan	Purposely synthetized 2-vinyl-4,6-diamino-1,3,5-triazine, 1-vinylimidazole and polyethylene glycol diacrylate copolymer	Commercial poly(lactic-co-glycolic) acid	Purposely crosslinked commercial alginate and pluronic F127	Purposely synthetized crosslinked poly(glycerol sebacate) and poly(1,3-propylene sebacate) copolymer
Brief description of the system	Drug-containing polymeric matrix	Bonded polymer-based microspheres containing the drug	Terpolymer hydrogels coordinating ionic drugs	Bonded polymer-based microspheres containing the drug	3D printed hydrogels (gel extrusion) containing the drug	Drug-containing polymeric matrix
Administration route	Implantation	Implantation	Implantation	Implantation	Implantation	Implantation
Temporary (administered) shape	I shape 	V shape 	Tetrahedron, pentahedron, cube, cylindrical and multiwalled-tube shapes 	I, U shape 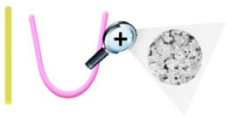	Folded shape 	Compressed cylindrical shape (smaller height); kissi-like, bear-like, quadripod-like, chair-like and drone-like shapes 

Triggering *stimulus*	Indirect heating *via* HIFU	Indirect heating *via* HIFU	Removal of zinc	Direct heating	Removal of calcium	Direct heating
Original (recovered) shape	M shape 	I shape 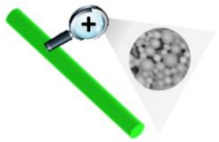	Triangular, four-angular, cruciform and rectangular shaped films 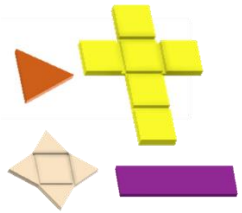	I, J, N, U shapes 	Planar shape 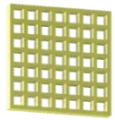	Cylindrical and sunflower-like shapes 
Time frame of shape recovery	60 seconds	120 seconds	Few hours	10-26 minutes	10-30 minutes	Less than 30 minutes
Target area for drug release	General	General/Bones	Subcutis	Bones	General	Cartilage
Therapeutic goal	Tissue and vascular regeneration	Tissue regeneration	Anti-bacterial and anti-inflammatory activity to prevent implant failure and promote wound healing	Tissue regeneration and prevention of relevant infections	Tissue regeneration	Tissue regeneration
Loaded drug/tracer	Copper sulfate	Fluorescein isothiocyanate-labeled lysozime	Zinc	Vancomycin and vancomycon-rhodamine B	Methotrexate	Kartogenin
Main advantages /	Use of localized	Shape recovery also triggers drug release	Fine-tuning of the mechanical, shape	Release performance of the system different from	Suitable for short term implantation	High porosity

Innovation features	heating to promote shape recovery of selected parts (switch on-off behavior with fine-control) Shape recovery also triggers drug release	Modulation of shape recovery extent and drug release (pulsatile release) obtained by varying the HIFU output power Biodegradability	memory and release controlling capabilities Biocompatibility	that of single microsphere components Biodegradability	4D printing Biocompatibility Biodegradability	Shape memory effect also considering complex configurations Biocompatibility Biodegradability
Research level	Design concept and preliminary *in vitro* studies	Design concept and preliminary *in vitro* studies with a tracer	Design concept and preliminary *in vitro* and *in vivo* (rats) studies	Design concept and preliminary *in vitro* studies	Design concept and preliminary *in vitro* studies	Design concept and preliminary *in vitro* and *in vivo* (rats) studies
Room for improvement identified by the authors	-	-	Poorly investigated coordination capabilities	Relatively long degradation time Relatively high activation temperature	Relatively long time needed for complete recovery	-

2.2.2 Stents

Stents are tubular structures widely used in surgery to prevent the closure of vessels or ducts (*e.g.* esophagus, urethra, bronchi) [32,33,130,131]. According to the insertion procedure and expected duration, various metal stents have been proposed over time, intended to fulfill a series of physical, mechanical and chemical requirements. Already in 2006 approximately half of the stents produced worldwide were made of SMAs, and of nitinol in particular, taking advantage of the relevant superelastic behavior [29,31,132]. Particularly, vascular self-expanding stents represent the most successful biomedical application of SMAs, both in terms of therapeutic goals achieved and impact on the market. The main limitation showed by these products was restenosis observed about 6 months after implantation, so that a subsequent invasive intervention was needed to remove the old stent and place a new one [133]. Moreover, cell proliferation and thrombus formation often occurred, leading to stent failure. To counteract such issues, strategies based on coating the stent surface with noble materials (*e.g.* gold), biocompatible polymers as well as heparin were pursued [134,135]. The research has then moved towards SMPs as these enabled the production of biodegradable (not inducing restenosis) and biocompatible (reducing the risks of thrombus formation) stents, which were also implantable through minimally invasive surgery [136-138]. In fact, stents could be manufactured with the desired final diameter and then programmed with a smaller diameter so as to facilitate the correct positioning *in situ*, prevent early elastic recoil as well as negative vessel remodeling, and avoid any auxiliary devices for triggering the shape modification (*e.g.* balloons). Moreover, the use of thermoplastic SMPs could enable the manufacturing of stents *via* cost-effective hot-processing techniques and possibly by 3D printing, making them suitable for customization.

More recently, shape memory polymeric stents were also implemented for the controlled release of drugs (*i.e.* drug-eluting stents) (Table 3). These turned out to be mainly intended for vascular application. In fact, besides the primary structural function of maintaining the vessels open, they were enforced to ensure delivery of drugs to locally

reduce inflammation, restenosis rate and risk of thrombus formation (*e.g.* antiproliferative and antiplatelet drugs), and of immunosuppressants to prevent rejection [136-138]. Chemo-responsive and temperature-triggered SMPs were generally employed for the manufacturing of helix-shaped prototypes because this design would offer better mechanical resistance [137]. Indeed, in addition to biocompatibility, biodegradation, release performance, which were features studied for many other applications, platelet adhesion and mechanical properties of the stents as well as their ability to maintain the vessels open during their whole life were considered fundamental. In preliminary studies, these properties were evaluated at least by using high pressure vessel models. However, type and duration of stressful conditions as well as the impact of the biodegradation process on the mechanical resistance of stents should also be considered, taking the characteristics of the blood district actually involved into special account [134,137,138,139].

Table 3: DDSs for which the shape recovery effect allowed prolonged retention in the target area: stents.

Reference	[133]	[134,135]	[139]	[137]	[136]	[138]
SMM	Commercial polyurethane	Purposely crosslinked commercial chitosan	Purposely synthetized poly(ester-urethanes)	Purposely synthetized crosslinked polyethylene glycol and poly(ε-caprolactone) block copolymers	Commercial poly-lactic acid and poly (lactic-co-glycolide)	Commercial poly (ε-caprolactone) and poly(propylene carbonate)
Brief description of the system	Polymer matrix containing the drug	Uncoated and heparin-coated polymer matrix containing the drug	Polymer matrix containing the drug	Coated polymer matrix containing drugs in the core structure and in the coating film	Polymer matrix containing the drug	Polymer matrix containing the drug
Administration route	Implantation	Implantation	Implantation	Implantation	Implantation	Implantation
Temporary (administered) shape	Elongated-tube shape 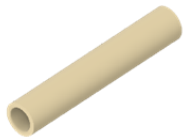	Crimped-helix shape 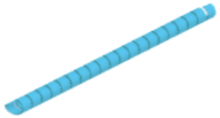	Supercoiled helix shape of smaller diameter 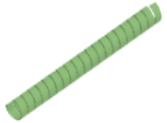	Straight shape 	Supercoiled helix shape of smaller diameter 	Straight shape 
Triggering *stimulus*	Direct heating	Hydration	Direct heating	Direct heating	Direct heating	Direct heating

	Tube shape	Helix shape	Helix shape	Helix shape	Helix shape	Helix shape
Original (recovered) shape	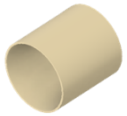		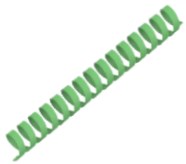			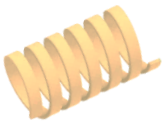
Time frame of shape recovery	2 minutes	80-160 seconds	Less than 1 minute	10 seconds	5 minutes	15 seconds
Target area for drug release	Blood vessels in the cardiac area	Blood vessels	Blood vessels	Blood vessels	Blood vessels	Blood vessels
Therapeutic goal	Reduce the risk of restenosis, thrombus formation, inflammation and vascular disfunction	Decrease neointimal hyperplasia	Decrease neointimal hyperplasia	Reduce platelet adhesion and hyperproliferation (antiproliferative and anticoagulant action)	Reduce platelet adhesion	Reduce the risk of restenosis, thrombus formation, inflammation and vascular disfunction
Loaded drug/tracer	Not disclosed drugs	Sirolimus, Heparin	Paclitaxel	Mitomycin C, Curcumin	Tacrolimus	Metoprolol tartrate
Main advantages / Innovation features	Versatility in terms of target organs (urethra, esophagus, trachea)	Ability to decrease the risk of thrombus formation, improve the hemocompatibility and modify the drug	Quick shape recovery Possibility of fine-tuning the stent performance based on the chemical	Combined release of two-different drugs Possibility of fine-tuning the stent performance based	Quick shape recovery Possibility of fine-tuning the stent performance based	Quick shape recovery Possibility of fine-tuning the stent performance based

		release performance (reduction of the burst phase and rate of release) by adding a heparin coating Possibility of fine-tuning the stent performance based on the preparation method (crosslinking degree) Biodegradability Biocompatibility	structure of the polymer Prolonged drug release Suitable mechanical resistance for *in vivo* application Biodegradability Biocompatibility	on the chemical structure of the polymer Suitable mechanical resistance for *in vivo* application Biodegradability Biocompatibility	on the weight ratio of the polymers Biodegradability Biocompatibility No increase in bacterial adhesion	on the weight ratio of the polymers Biodegradability Biocompatibility No pro-coagulant and inflammatory activities
Research level	Design concept and preliminary *in vitro* studies with tracers	Design concept and preliminary *in vitro* and *in vivo* (rabbits) studies	Design concept and preliminary *in vitro* studies	Design concept and preliminary *in vitro* studies	Design concept and preliminary *in vitro* and *ex vivo* (goat vessels) studies	Design concept and preliminary *in vitro* studies
Room for improvement identified by the authors	-	Potential for long-term application still needs to be established	-	Relatively high activation temperature	-	-

2.2.3 Intra-organ systems

Prolonged-release of drugs in a target site is mainly pursued for the purpose of reducing the frequency of administration, the drug strength and the side effects of a therapy, improving efficacy and patient compliance [140]. In hollow muscular organs such as the stomach and urinary bladder, such a release mode, should be accompanied by the easy insertion of the DDSs into the target area and the relevant retention as long as necessary. This, in the case of chronic treatments, could even last for months. Non-invasive removal/elimination from the organ at the end of the performance would also be an advantageous additional feature. Taking these premises into account, SMPs were used to develop DDSs with original shapes and mechanical properties suitable for the retention into the selected hollow organs, to be fixed into temporary shapes enabling comfortable and minimally invasive administration (Table 4). The latter turned out to be of suitable spatial encumbrance for being inserted into a urethral or vaginal catheter, or conveyed inside a commercial hard capsule for oral administration. Since these were DDSs designed for indwelling within specific sites, not only their mechanical characteristics and release performance, but also their design has been considered within the analysis already carried out in the preliminary studies. With respect to the SMPs employed, poly(vinyl alcohol) offering the advantage of a long-established use in the formulation of drug products and safety profile, exhibited water-induced shape memory response and good hot-processability [141-144]. Different devices suitable for retention in the stomach and in the bladder were fabricated by hot melt extrusion and fused deposition modeling 3D printing. In the latter case, this resulted in one of the first application of 4D printing for the development of DDSs using commercially available pharmaceutical-grade polymers with no need for any chemical modification and employing the fused deposition modeling technique. The matrix systems proposed showed prolonged release, further fine-tuned by applying external coatings with different permeability, and dissolution/erosion behavior enabling safe elimination from the target organs with no need for invasive removal procedures. Also a commercial shape memory polyurethane

was employed for the manufacturing of an intravaginal device including a flux controlled pump, in which the release control function was decoupled from the shape memory effect [145].

Table 4: DDSs for which the shape recovery effect allowed prolonged retention in the target area: gastroretentive, intravaginal and intravesical systems.

Reference	[145]	[143]	[144]
SMM	Commercial polyether urethane	Commercial poly(vinyl alcohol)	Commercial poly(vinyl alcohol)
Brief description of the system	Flux controlled pump, composed of a rigid polymer envelop having orifices for fluid influx and efflux, filled with a drug containing tablet and coupled with a shape memory retainer	Polymer matrix containing the drug	Polymer matrix containing the drug
Administration route	Intravaginal (by catheterization)	Intravesical (by catheterization)	Oral (by swallowing into commercial hard capsules)
Temporary (administered) shape	Compressed ellipsoidal shape 	I shape 	Supercoiled and paper clip shapes 
Triggering *stimulus*	Direct heating	Direct heating and contact with water	Direct heating and contact with water

Original (recovered) shape	Ellipsoidal shape 	U and helix shapes 	Cylindrical and conical helices, S- and atom-like shapes 
Time frame of shape recovery	-	25-150 minutes	2-10 minutes
Target area for drug release	Vagina	Bladder	Stomach
Therapeutic goal	Prolonged release of macromolecules for the treatment of sexually transmitted infections, endometriosis and uterine fibroids	Prolonged release of drugs in the bladder for treatment of local diseases overcomimg failures and discomfort connected with repeated instillations through catheters	Prolonged release of drugs having an absorption window in the upper gastrointestinal tract, lower solubility in the intestinal environment or employed to treat local pathologies
Loaded drug/tracer	10 kDa rhodamine B dextran, 5-(and-6)-carboxytetramethyl rhodamine labelled insulin	Caffeine	Allopurinol
Main advantages / Innovation features	No irritation or immune cell infiltration Flexibility of the release performance	4D printing Biocompatibility Biodegradability	4D printing Biocompatibility Biodegradability
Research level	Design concept and preliminary *in vitro* and *in vivo* (rabbits) studies with tracers	Design concept and preliminary *in vitro* studies with a tracer	Design concept and preliminary *in vitro* studies
Room for improvement identified by the authors	-	Variation of mechanical properties upon interaction with biological fluids Duration of release	Variation of mechanical properties upon interaction with biological fluids Duration of release

2.2.4 Systems for wound treatment

Injuries are typically treated by the application of wound dressing in order to foster relevant healing [146]. This is a challenging process involving both proliferation and migration of cells, leading to tissue regeneration. Also the use of surgical sutures to reconnect tissues and restore their structure as well as function could be included in the wound treatment category [147,148]. This application remains challenging especially in the case of minimally invasive surgeries, during which knotting a suture is hindered by the confined space and possible site infections.

Systems devised for wound treatment have to fulfill a series of requirements related to their structural function and to the desired release performance as well. In fact, they should provide a suitable microenvironment for cell growth, for instance being semi-permeable and highly porous to ensure sufficient gas and nutrient exchange. Moreover, as the main objective to be attained through their application is to avoid the re-opening of the treated injuries, they should be characterized by specific mechanical properties (*e.g.* good stretching ability, suitable mechanical strength, appropriate adhesion to the substrate). On the other side, besides the need for being sterile the capability to prevent possible bacterial infection is considered a plus. In this respect, a relatively high water vapor transmission ratio, enabling appropriate wound drying, would be highly advantageous.

In the field of application just described, SMMs were shown to provide the DDSs with smart performance, such as shape fixation-assisted easy application and shape recovery-assisted closure of wounds [146]. Wet and electrospinning processes turned out to be the most investigated techniques for the fabrication of prototypes conceived in the form of polymeric matrices and layered structures [147-149]. In the case of treatments requiring anastomosis, rings surgically applied following resection of bowel segments to enable accurate joining of two viable ends without any tension represent one of the most commonly employed systems [150]. In this respect, hydrogels having shape memory effect were proved effective in ensuring efficient reconnection. In addition, the original

shape could even be rather slowly recovered, thus allowing gradual release of the applied pressure. Indeed, this behavior helped attain a better intestinal healing. Finally, the shape memory effect was also exploited to promote perfect seal of sutures even when applied loosely as a consequence of difficult procedures, especially in the case of limited room in the area affected by surgery [147].

The use of SMMs in the development of systems for wound treatment ultimately provided easy application and enhanced comfort, while speeding up the wound closure process. Overall, the devices reviewed were mainly characterized by anti-inflammatory/antibacterial activity, thanks to the presence of specific drugs, also of natural source. Notably, a few of these systems showed rapid clotting due to the presence of thrombogenic materials in the formulation and the high surface area of the entire device, associated with the peculiar microstructure [146]. In this respect, the use of nanofibers typically prepared through electrospinning technology was especially successful [146-149]. Moreover, shape memory foams were devised for bleeding control, even in stressful conditions, such as in the battlefield and in high temperature environment [151]. Polyurethane currently represents a frequently used commercially available material for the development of embolic foams, but in this specific case it was purposely synthetized to also show the desired shape recovery behavior. Indeed, these DDSs were characterized by an expanded original shape and a compressed temporary one and showed an extremely quick shape memory effect once exposed to blood at body temperature. Besides surface area, porosity was found of utmost importance for the intended application and turned out not to be affected by the programming of the temporary shape and recovery of the original one.

Considering the application of the devices belonging to this category to particularly sensitive areas and the use of direct heating as the main triggering *stimulus*, biocompatibility studies carried out on cell cultures of common fibroblasts still seem too preliminary, while more in depth *in vivo* evaluation should be envisaged.

Table 5: DDSs for which the shape recovery effect allowed prolonged retention in the target area: systems for wound treatment.

References	[146]	[150]	[151]	[147,148]	[149]
SMM	Purposely-synthetized polyurethane	Purposely-crosslinked poly(vinyl alcohol)/gelatin copolymer	Purposely-synthetized polyurethane	Purposely-synthetized polyurethane	Purposely-synthetized polyurethane
Brief description of the system	Nanofibrous material composed of gelatin, chitosan and shape memory polyurethane, containing the drug	Hydrogel-based ring containing the drug	Polymeric foam containing the drug	Polymer-based nanofibers containing the drug	Three-layer polymer-based nanofibers with two external placebo layers and the internal one containing the drug
Administration route	Topical application	Implantation	Injection	Implantation	Topical application
Temporary (administered) shape	Elongated rectangular shape 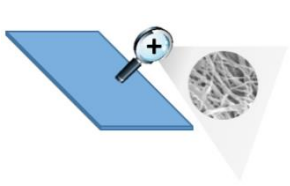	Compressed ring shape 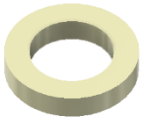	Cylindrical shape with smaller diameter 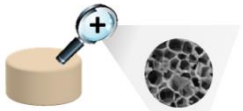	Elongated cylindrical fibers 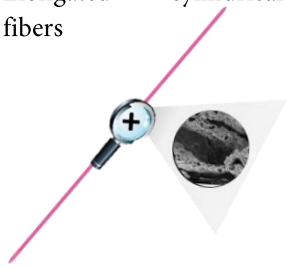	Elongated rectangular shape 
Triggering *stimulus*	Direct heating	Contact with water	Direct heating and contact with water	Direct heating	Direct heating

	Rectangular shape	Ring shape	Cylindrical shape	Cylindrical fibers	Rectangular shape
Original (recovered) shape	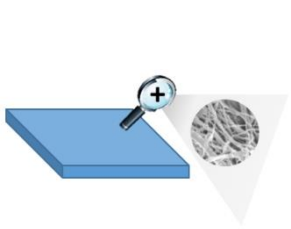	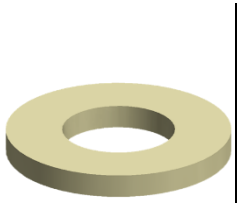	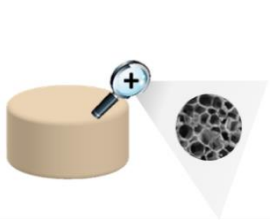	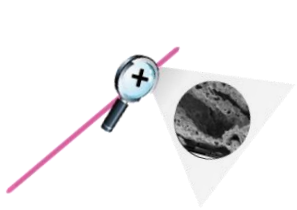	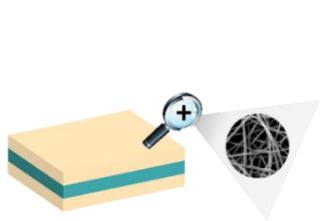
Time frame of shape recovery	-	7 days	1-5 minutes	-	-
Target area for drug release	Wounds	Bowel wounds	Wounds	Wounds	Wounds
Therapeutic goal	Promote healing of open wounds reducing the risks of bleeding, infections and inflammation	Create anastomosis while reducing the inflammation	Stop bleeding and promote blood clotting, while reducing the risks of infections	Suture wounds while reducing the risks of infections and inflammation	Promote healing of open wounds reducing the risks of infections and inflammation
Loaded drug/tracer	Silver nitrate	Acetylsalicylic acid	Cinnamic acid	Berberine hydrochloride	Berberine hydrochloride
Main advantages / Innovation features	High porosity Stretching ability Biocompatibility Potential as hemostatic (improvement of clotting rate)	Biocompatibility Time for shape recovery and mechanical properties compatible with the therapeutic site/goal Possible sterilization	Stability at relatively high temperature and quick shape recovery enabling suitability for the battlefield High porosity Biocompatibility Possibility of fine-tuning the foam	High porosity Biocompatibility Shape memory effect also influences the release kinetics One-step production process, easy to be scaled up	High porosity Biocompatibility Prolonged drug release obtained with the multilayer design One-step production process, easy to be scaled up

			performance based on the chemical structure of the polymer		
Research level	Design concept and preliminary *in vitro* studies	Design concept and preliminary *in vitro* studies	Design concept and preliminary *in vitro* studies	Design concept and preliminary *in vitro* and *in vivo* (mice) studies	Design concept and preliminary *in vitro* studies
Room for improvement identified by the authors	-	-	-	-	-

2.3 Shape recovery for ensuring removal from the target area

Release of active ingredients in specific sites within the gastrointestinal tract has largely been pursued for the treatment of local pathologies, such as gastric ulcers or inflammatory bowel disease that affects the colonic region [152-160]. However, the possibility of increasing the DDS residence time and prolonging the release of the loaded drug in the upper gastrointestinal tract, even in the esophagus, would also be beneficial. This release mode would be particularly advantageous for active molecules *i)* strongly affected by pre-systemic metabolization, *ii)* with specific absorption windows or *iii)* poorly soluble as well as stable in the intestinal environment. In this respect, Babaee and co-workers took advantage of the combination of elastic elements and nitinol for the development of an esophageal flower-like DDS showing a unique performance. The system, conceived as a complex structure composed of different units, was intended to be orally administered within a commercially available hard capsule [161]. It entailed separated arms connected to a central core by means of elastic recoil elements. These enabled *i)* assembly of the system, *ii)* relevant folding into the collapsed/closed configuration to be conveyed within the capsule and *iii)* mechanical reopening of the device inside the esophagus. More specifically, the flower deployment would occur upon the elastic recoil elements relieving the elastic energy trapped during system folding. This elastic expansion would allow retention in the target area while drug-containing microneedles, attached on the external surface of the arms, would penetrate the esophageal mucosa without causing relevant perforation, thus promoting anchoring of the system and enabling drug delivery. The device also included temperature-responsive nitinol-based springs connecting each arm to the central core. Their shape memory effect, triggered upon administration of warm liquids (*i.e.* in the 55-65 °C temperature range), would be responsible for effective closure of the exhausted device at the end of the performance. This way, safe removal from the target area and passage of the closed system in the stomach would be ensured.

Notably, the administration of warm liquids was demonstrated to generally provide the users with a satisfactory feeling, without causing either burning or harmful effects.

The DDSs proposed was rather complex and the fabrication process required a number of subsequent steps, including a prototyping phase *via* fused deposition modeling 3D printing followed by compression molding and other manual tasks such as welding, drilling and final assembling. The ability of the system to be retained and then eliminated *in vivo* was only preliminarily tested on sedated animals, using endoscopic guidance for placing it into the proximal esophagus.

Table 6: DDSs for which the shape recovery effect allowed the elimination from the target area.

References	[161]
SMM	Commercial nitinol
Brief description of the system	4 arms, equipped with polymeric microneedles containing the drug at their distal ends, connected to a central core through elastic L-beam-shaped recoil elements and nitinol springs
Administration route	Oral
Temporary (administered) shape	Open flower-like shape 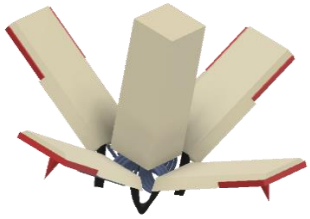
Triggering *stimulus*	Direct heating attained by administration of warm liquids (55 - 65 °C)
Original (recovered) shape	Closed flower-like shape 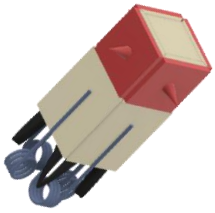
Time frame of shape recovery	Few seconds
Target area for drug release	Esophagus
Therapeutic goal	Prolonged release of drugs in the upper gastrointestinal tract
Loaded drug/tracer	70-kDa dextran labeled with texas red and budesonide
Main advantages / Innovation features	Release in an area hard to target Ultra-responsive system
Research level	Design concept and preliminary *in vitro*, *ex vivo* (pig esophagus samples) and *in vivo* (pigs) studies with tracer and drug
Room for improvement identified by the authors	Fabrication process requiring multiple steps currently done manually

2.4 Shape recovery for triggering drug release

Since their appearance on the pharmaceutical market, DDSs were intended to ensure an appropriate concentration of specific drugs to be attained at the site of interest when needed [162]. As a consequence, they would in principle allow to overcome limitations and avoid side effects associated with the systemic administration through different routes (*e.g.* ensuring high local concentrations of drugs or amounts that can be tuned for specific patient needs, enable multiple release kinetics, avoid first-pass effect). Conversely to traditional passive DDSs mainly employed so far, the use of SMMs gave the opportunity to develop innovative DDSs able to actively enable the achievement of the same objectives and the identification of new, even more challenging, targets, without resorting to other expensive active technologies such as micro electro mechanical systems [45,163]. In particular, systems for which the release performance was controlled by the shape memory effect were proposed, not only in terms of rate and site but also allowing for subsequent pulses of release. Such pulses turned out even more flexible as they could be started and ended on demand by the controlled application of the triggering *stimulus*. In addition, the recovery-based triggering mechanism could in some cases be remotely controlled (*e.g.* upon application of a radio-controlled electromagnetic field) [45,163,164]. The working principle of such devices potentially offers not only quite high precision drug dosing but also increased safety as the system only responds to an external suitably tuned non-mechanical *stimulus* [165]. To enhance the system flexibility, additional release controlling mechanisms to be coupled with the shape memory effect were also tested, for instance relying on the application of functional coatings and on the variation of the viscosity of the drug containing formulation when in contact with aqueous fluids at body temperature [164].

Triggering of drug release was more often accomplished through the use of micropumps, mainly activated by the shape memory effect of purposely-developed actuators based on SMMs [45,163]. For this reason, the devices were conceived in the form of containers (*e.g.* capsules, chips) hosting a more or less complex pumping system and drug-loaded

reservoirs, the latter connected to the external environment through holes and valves (*e.g.* two-way, passive-check or thermoactive valves) [165,166]. In some cases, these DDSs were envisaged so that the removal of the *stimulus* allowed the interruption of the release. As a consequence, fine tuning of the drug delivered (even up to picometric amounts) and on demand pulsatile-release performance could be achieved, leading to good potential for customization [164,165]. Endoscopic capsules were also proposed, entailing a tracking mechanism to monitor the position of the device in the human body after oral administration and ensure drug release at the right site [166].

These applications are probably among the more complex here reviewed. They seemed to be suited for quite innovative therapeutic approaches, but highlighted the need for sophisticated manufacturing methods, complex actuation and controls, whose feasibility upon administration still need to be deepened to establish their true application potential. Indeed, the DDSs proposed were generally characterized by a high level of engineering, already recognizable in the design of the device, often combined with innovative fabrication techniques for the pharmaceutical field, such as photolithography- or lithography-based processing, microfabrication and micromachining technology, and shared the need for using biocompatible materials, which unfortunately was not always accomplished. At the same time, dyes, water and solutions with specific pHs were used to assess the controlled release capability of the devices investigated, instead of active molecules and drug tracers. Even if the proof of concept for fabrication and working mechanism of these systems was preliminary achieved, most of them still need to find a solution for many limitations, such as the control of temperature (as the increase needed for operating the device could be an issue both for stability of the drug and for the surrounding tissue), miniaturization of the components and refilling of the drug-containing reservoirs.

Table 7: DDSs for which the shape recovery effect allowed triggering of drug release.

References	[166]	[163]	[165]	[45]	[164]
SMM	Commercial nitinol	Commercial nitinol	Purposely prepared Ni-Mn-Ga alloy	Commercial polyurethanes	Purposely-synthesized poly(ε-caprolactone) and oligo(ε-caprolactone) copolymers
Brief description of the system	Acrylic capsule equipped with a two-way valve, housing a drug-containing reservoir and a wood piston relying on a nitinol spring actuator	Polyimide case with a hole on the top equipped with a two-way valve, housing a drug-containing reservoir and a microfluidic pump driven by a nitinol actuator	3D printed case with holes housing a drug-containing reservoir and pumping mechanisms based on two flat plates connected with tubes and a cylindrical rotating magnet	Drug-containing reservoir in a polymethylmethacrylate sheet closed with a lid entailing a planar inductor capacitor circuit composed of a copper-clad/polyimide planar film, laminated on a shape memory polymer flat actuator	Tube-shaped container made of a shape-memory polymer, eventually blended with a near-infrared dye, filled with a drug-containing thermosensitive hydrogel. The tube sides were sealed by coating
Administration route	Oral	Implantation	Implantation	Implantation	Implantation
Temporary (administered) shape	Compressed spring	Rectangular spiral-coil shape with one longitudinal end lifted up	Flat shape with shrinkage in specific areas	Cylindrical planar shape	Elongated tube shape
		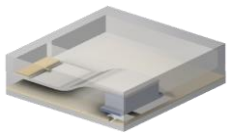	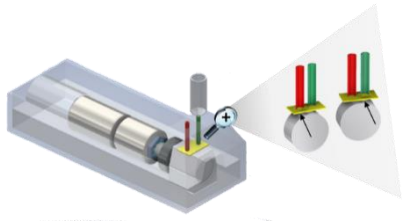	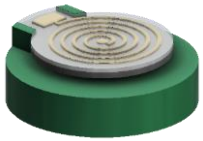	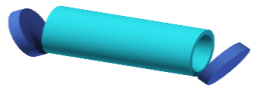

Triggering *stimulus*	Indirect heating *via* current application	Indirect heating *via* application of radio-frequency electromagnetic fields	Magnetic field	Indirect Joule heating attained *via* an external radio controlled electromagnetic field	Direct and indirect heating *via* near infrared light absorption
Original (recovered) shape	Elongated spring 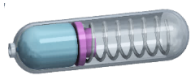	Flat rectangular spiral-coil shape 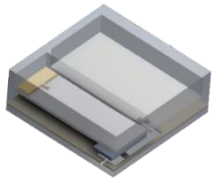	Flat shape 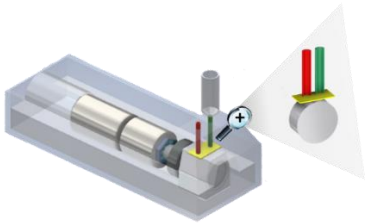	Cylindrical lifted shape 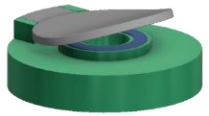	Tube shape + 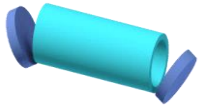
Time frame of shape recovery	-	-	-	-	2-40 seconds
Target area for drug release	Any area of the gastrointestinal tract	Bones	Animal brain	General (no identification of a specific area of implantation)	Regeneration of tissues involved in surgical operations
Therapeutic goal	Local administration of drus in specific areas of the gastrointestinal tract by tracking the position of the system in real-time	Local treatment of osteoporosis with parathyroid hormone fragments	Delivery of drugs to specific areas into the brain	Not defined	Local administration of proteins (*e.g.* growth factors) for tissue regeneration and on demand administration of drug proteins based on the analysis of clinical biomarkers
Loaded drug/tracer	Water	Dyes and test agents	Ketamine and tetrodotoxin	Dyes and pH 2 buffer solution	Bovine serum albumin, lysozyme, ovalbumin,

					immunoglobulin G, stromal cell-derived factor 1α
Main advantages / Innovation features	Wireless triggering of release Possibility of conveying multiple reservoirs containing different drugs	Ensure high drug loading, and refilling over time Passive activation, leading to a cost reduction	When employed for testing purposes enable *in vivo* experiments in freely moving animals Simplicity of the structure and easy scale-up Fine tuning of the dose delivered by modification of the magnetic field applied	Capability to perform consistently, in terms of opening displacement and volume released, during 500 cycles of actuation	Possibility of attaining complex release kinetics by changing the design and composition of the device Possibility of conveying the indirect heating just towards the device
Research level	Design concept and preliminary *in vitro* studies with a tracer	Design concept and preliminary *in vitro* studies with tracers	Design concept and preliminary *in vitro* and *in vivo* (rats) studies	Design concept and preliminary *in vitro* studies with tracers	Design concept and preliminary *in vitro* studies with tracers and drugs
Room for improvement identified by the authors	-	Need for thermally insulating the system (drug stability and tissue damage) Backflow of the drug in the pump chamber	-	Need for miniaturization Selection of biocompatible SMPs with lower glass transition temperature Need for improving the release control ability	Need for high temperature to trigger the shape recovery process Need for photoinitiators to induce the thermal response mediated by irradiation whose safety and tolerability still have to be determined

3. Conclusions

In the last few decades, materials science and engineering has witnessed incredible progress, which has positively influenced all sectors of industry. In this respect, SMMs, with their ability to dynamically respond to specific environmental *stimuli* by modifying the relevant shape over time, have just begun to show their application potential in the biomedical and pharmaceutical fields. Moreover, the use of these intelligent materials together with the recent development of 3D printing technologies will provide a tool for 4D printing implementation, leading to further benefits in terms of personalization of therapy.

Within this review, we considered the overall applications of SMPs and SMAs in pharmaceutics and more specifically their use in DDS design, trying to highlight the state of the art in the field of shape memory-based and 4D printed drug products. The systems reviewed turned out to be at a rather limited degree of development, in terms of actual production (*e.g.* manual manufacturing, lab-scale synthesis of materials) and relevant scalability, as well as in the identification of specific therapeutic objectives, also including feasibility of administration and relevant safety. However, based on a shape memory effect well-refined and tailored through an advanced design concept, such DDSs seemed very promising, which means in principle able to provide innovative performance and to overcome many limitations of the current therapeutic strategies (*e.g.* poor patient compliance or adherence, ability to ensure therapeutic drug levels at the site of action for a prolonged period of time, fine tuning and customization of the performance in terms of time and site of release). The evolution of the shape over time has been sought to adapt to different needs, such as reaching, enabling retention into and ensuring removal from the target area or triggering the release of the active molecule itself. Shape memory-based DDSs were proposed for oral administration, injection or implantation, topical application and intra-organ (*e.g.* into the bladder and vagina) insertion. Their feasibility and further development have taken advantage of and will further benefit from the remarkable technological advances we are currently experiencing in many fields, which

have led to the spread of 3D printing, electrospinning and complex microfabrication techniques.

The main challenge for the next years remains that of their introduction into the clinical practice, especially considering that most of the materials employed are new and purposely synthetized. In this respect, the adoption of shape memory-based DDSs might be strongly supported by the growing interest in precision dosing, but the development of materials and production processes allowing stringent quality and safety requirements to be met would need to be pursued.

References

1. H. J. Huang, Y. L. Tsai, S. H. Lin, S. H. Hsu, Smart polymers for cell therapy and precision medicine, J. Biomed. Sci. 26 (2019) 1-11.
2. A. Jain, S. P. Ong, G. Hautier, W. Chen, W. D. Richards, S. Dacek, D. Gunter, D. Skinner, G. Ceder, K. A. Persson, A. Jain, P. Ong, G. Hautier, W. Chen, D. Gunter, D. Skinner, G. Ceder, K. A. Persson, The Materials project: a materials genome approach to accelerating materials innovation, APL Materials. 1 (2013) 011002.
3. W. M. Huang, Z. Ding, C. C. Wang, J. Wei, Y. Zhao, H. Purnawali, Shape memory materials, Mater. Today. 13 (2010) 54-61.
4. W. M. Huang, C. L. Song, Y. Q. Fu, C. C. Wang, Y. Zhao, H. Purnawali, H. B. Lu, C. Tang, Z. Ding, J.L. Zhang, Shaping tissue with shape memory materials, Adv. Drug Deliv. Rev. 65 (2013) 515-535.
5. W. Zhao, L. Liu, F. Zhang, J. Leng, Y. Liu, Shape memory polymers and their composites in biomedical applications, Mater. Sci. Eng. C. 97 (2019) 864-883.
6. D. C. Lagoudas, Shape memory alloys – Modeling and engineering applications, Springer Ed. (2013), New York, US-NY.
7. A. Lendlein Ed., Shape-memory polymers, Springer (2010), New York, US-NY.
8. A. Lendlein, R. Langer, Biodegradable, elastic shape-memory polymers for potential biomedical applications, Science. 296 (2002) 1673–1676.
9. V. L. Junior, V. Ste, M. A. Savi, Dynamics of smart systems and structures, Springer Eds. (2010), New York, US-NY.
10. S. Kamila, Introduction, classification and applications of smart materials: an overview, Am. J. Appl. Sci. 10 (2013) 876-880.
11. R. Dhanasekaran, S. R. S, G. K. B, A. S. Anirudh, Shape memory materials for bio-medical and aerospace applications, Mater. Today Proc. 5 (2018) 21427–21435.
12. https://www.acumenresearchandconsulting.com/shape-memory-polymer-market, last access on December 4, 2020.

13. https://www.globenewswire.com/news-release/2019/06/13/1868119/0/en/Shape-Memory-Polymers-Market-Size-Worth-USD-1-84-bn-by-2026.html, last access on December 4, 2020.
14. T. Omori, R. Kainuma, Alloys with long memories, Nature. 502 (2013) 42–44.
15. Z. G. Wei, R. Sandstroröm, Shape-memory materials and hybrid composites for smart systems Part I Shape-memory materials, J. Mater. Sci. 3 (1998) 3743–3762.
16. L. Petrini, F. Migliavacca, Biomedical applications of shape memory alloys, J. Metall. (2011) 501483.
17. A. Biesiekierski, J. Wang, M. Abdel-Hady Gepreel, C. Wen, A new look at biomedical Ti-based shape memory alloys, Acta Biomater. 8 (2012) 1661-1669.
18. R. Chakraborty, M. S. Raza, S. Datta, P. Saha, Synthesis and characterization of nickel free titanium–hydroxyapatite composite coating over nitinol surface through in-situ laser cladding and alloying, Surf. Coat. Technol. 358 (2019) 539-550.
19. S. Shabalovskya, J. Van Humbeeck, Biocompatibility of Nitinol for biomedical applications, Chapter 9, pagg. 194-233, in: T. Yoneyama, S. Miyazaki Eds., Woodhead Publishing Series in Biomaterials (2009). Cambridge, UK.
20. E. O. Nasakina, M. A. Sudarchikova, K. V Sergienko, S. V. Konushkin, M. A. Sevost, Ion release and surface characterization of nanostructured nitinol during long-term testing, Nanomater. 9 (2019) 1569.
21. A. Biscarini, G. Mazzolai, A. Tuissi, Enhanced nitinol properties for biomedical applications, Recent Pat. Biomed. Eng. (2008) 180-196.
22. H. F. Li, K. J. Qiu, F. Y. Zhou, L. Li, Y. F. Zheng, Design and development of novel antibacterial Ti-Ni-Cu shape memory alloys for biomedical application, Sci. Rep. 6 (2016) 1-11.
23. I. M. Ihálcz, Fundamental characteristics and design method for nickel-titanium shape memory alloy, Periodica Polytechnica Ser. Mech. Eng. 45 (2001) 75–86.

24. S. Miyazaki, Martensitic transformation in TiNi alloys. Chapter 3, pagg. 73-87 in: S. Miyazaki, F. Shuichi, Y. Qing, H. Wei Min Eds., Thin film shape memory alloys - Fundamentals and device applications. (2010).
25. C. Naresh, P. S. C. Bose, C. S. P. Rao, Shape memory alloys: a state of art review, IOP Conf. Ser. Mater. Sci. Eng. 149 (2016) 012054.
26. N. Sabahi, W. Chen, C. Wang, J. J. Kruzic, X. Li, A Review on additive manufacturing of shape-memory materials for biomedical applications, JOM. 72 (2020) 1229-1253.
27. L. Sun, W. M. Huang, Nature of the multistage transformation in shape memory alloys upon heating, Met. Sci. Heat. Treat. 51 (2009) 573-578.
28. C. M. Wells, M. Harris, L. Choi, V. P. Murali, F. D. Guerra, J. A. Jennings, Stimuli-responsive drug release from smart polymers, J. Funct. Biomater. 10 (2019) 34.
29. F. Auricchio, E. Boatti, M. Conti, SMA Biomedical Applications. Chapter 11, pagg. 307-341, in: Shape memory alloy engineering for aerospace, structural and biomedical applications, L. Lecce, A. Concilio Eds. Elsevier, (2015), Oxford, UK.
30. G. Rees Douglas, Design of stent expansion mechanism, Master thesis in applied science, 2012.
31. A. F. Saleeb, B. Dhakal, J. S. Owusu-Danquah, On the role of SMA modeling in simulating NiTinol self-expanding stenting surgeries to assess the performance characteristics of mechanical and thermal activation schemes, J. Mech. Behav. Biomed. Mater. 49 (2015) 43-60.
32. T. Schmidt, J. Abbott, Coronary Stents: History, Design, and Construction, J. Clin. Med. 7 (2018) 126.
33. M. Shaikh, G. Kichenadasse, N. R. Choudhury, R. Butler, S. Garg, Non-vascular drug eluting stents as localized controlled drug delivery platform: Preclinical and clinical experience, J. Control. Release 172 (2013) 105-117.
34. H. Lee, M. J. Cima, An intravesical device for the sustained delivery of lidocaine to the bladder, J. Control. Release 149 (2011) 133-139.

35. M. Reeves, B. Katz, J. Canela, M. Hathaway, M. Tal, Initial evaluation of a novel nitinol, low-dose-copper intrauterine contraceptive, Contraception 90 (2014) 315.

36. D. K. Turok, A. L. Nelson, C. Dart, C. A. Schreiber, K. Peters, M. J. Schreifels, B. Katz, Efficacy, Safety, and Tolerability of a New Low-Dose Copper and Nitinol Intrauterine Device: Phase 2 Data to 36 Months, Obstet. Gynecol. 135 (2020) 840–847.

37. D. K. Turok, L. M. Gawron, S. Lawson, New developments in long-acting reversible contraception: the promise of intrauterine devices and implants to improve family planning services, Fertil. Steril. 106 (2016) 1273-1281.

38. M. Verma, K. Vishwanath, F. Eweje, N. Roxhed, T. Grant, M. Castaneda, C. Steiger, H. Mazdiyasni, T. Bensel, D. Minahan, V. Soares, J. A. F. Salama, A. Lopes, K. Hess, C. Cleveland, D. J. Fulop, A. Hayward, J. Collins, S. M. Tamang, T. Hua, C. Ikeanyi, G. Zeidman, E. Mule, S. Boominathan, E. Popova, J. B. Miller, A. M. Bellinger, D. Collins, D. Leibowitz, S. Batra, S. Ahuja, M. Bajiya, S. Batra, R. Sarin, U. Agarwal, S. D. Khaparde, N. K. Gupta, D. Gupta, A. K. Bhatnagar, K. K. Chopra, N. Sharma, A. Khanna, J. Chowdhury, R. Stoner, A. H. Slocum, M. J. Cima, J. Furin, R. Langer, G. Traverso, A gastric resident drug delivery system for prolonged gram-level dosing of tuberculosis treatment, Sci. Transl. Med. 11 (2019) eaau6267.

39. G. I. Peterson, A. V. Dobrynin, M. L. Becker, Biodegradable shape memory polymers in medicine, Adv. Healthc. Mater. 6 (2017) 1-16.

40. W. Sokolowski, A. Metcalfe, S. Hayashi, L. Yahia, J. Raymond, Medical applications of shape memory polymers, Biomed. Mater. 2 (2007) S23-S27.

41. H. Meng, G. Li, A review of stimuli-responsive shape memory polymer composites, Polymer 54 (2013) 2199–2221.

42. M. Bao, Q. Zhou, W. Dong, X. Lou, Y. Zhang, Ultrasound-modulated shape memory and payload release effects in a biodegradable cylindrical rod made of chitosan-functionalized PLGA microspheres, Biomacromolecules 14 (2013) 1971-1979.

43. M. Behl, M. Y. Razzaq, A. Lendlein, Multifunctional shape-memory polymers, Adv. Mater. 22 (2010) 3388-3410.

44. G. Li, G. Fei, H. Xia, J. Han, Y. Zhao, Spatial and temporal control of shape memory polymers and simultaneous drug release using high intensity focused ultrasound, J. Mater. Chem. 22 (2012) 7692-7696.

45. M. A. Zainal, A. Ahmad, M. S. Mohamed Ali, Frequency-controlled wireless shape memory polymer microactuator for drug delivery application, Biomed. Microdevices 19 (2017) 1-10.

46. A. W. Basit, S. Gaisford, 3D Printing of pharmaceuticals, Springer Eds. (2018), Cham CH.

47. W. Jamróz, J. Szafraniec, M. Kurek, R. Jachowicz, 3D Printing in pharmaceutical and medical applications – recent achievements and challenges, Pharm. Res. 35 (2018) 176.

48. V. R. Kallakunta, S. Sarabu, S. Bandari, H. Patil, M. A. Repka, An update on the contribution of hot-melt extrusion technology to novel drug delivery in the twenty-first century: part I, Expert Opin. Drug Deliv. 16 (2019) 539-550.

49. A. Melocchi, M. Uboldi, M. Cerea, A. Foppoli, A. Maroni, S. Moutaharrik, L. Palugan, L. Zema, A. Gazzaniga, A graphical review on the escalation of fused deposition modeling (FDM) 3D printing in the pharmaceutical field, J. Pharm. Sci. 109 (2020) 2943–2957.

50. A. Melocchi, F. Briatico-vangosa, M. Uboldi, M. Turchi, D. Von Zeppelin, A. Maroni, A. Gazzaniga, A. Zidan, Quality considerations on the pharmaceutical applications of fused deposition modeling 3D printing, Int. J. Pharm. (2020) 119901.

51. A. Melocchi, M. Uboldi, A. Maroni, A. Foppoli, L. Palugan, L. Zema, A. Gazzaniga, 3D printing by fused deposition modeling of single- and multi-compartment hollow systems for oral delivery – A review, Int. J. Pharm. 579 (2020) 119155.

52. S. Sarabu, S. Bandari, V. R. Kallakunta, H. Patil, M. A. Repka, An update on the contribution of hot-melt extrusion technology to novel drug delivery in the twenty-first century: part II, Expert Opin. Drug Deliv. 16 (2019) 567–582.
53. G. Loreti, A. Maroni, M. D. Del Curto, A. Melocchi, A. Gazzaniga, L. Zema, Evaluation of hot-melt extrusion technique in the preparation of HPC matrices for prolonged release, Eur. J. Pharm. Sci. 52 (2014) 77-85.
54. L. Zema, G. Loreti, A. Melocchi, A. Maroni, A. Gazzaniga, Injection Molding and its application to drug delivery, J. Control. Release 159 (2012) 324-331.
55. L. Zema, A. Melocchi, A. Maroni, A. Gazzaniga, Three-dimensional printing of medicinal products and the challenge of personalized therapy, J. Pharm. Sci. 106 (2017) 1697-1705.
56. A. Lendlein, S. Kelch, Shape-Memory Polymers A, Angew. Chem. Int. Ed. Engl. 41 (2002) 2034-2057.
57. M. C. Serrano, G. A. Ameer, Recent insights into the biomedical applications of shape-memory polymers, Macromol. Biosci. 12 (2012) 1156-1171.
58. W. M. Huang, Y. Zhao, C. C. Wang, Z. Ding, Thermo/chemo-responsive shape memory effect in polymers: a sketch of working mechanisms, fundamentals and optimization, J Polym. Res. 19 (2012) 9952.
59. Z. Jiang, Y. Xiao, Y. Kang, M. Pan, B. Li, S. Zhang, Shape memory polymers based on supramolecular interactions, CS Appl. Mater. Interfaces 9 (2017) 20276-20293.
60. Y. Xia, Y. He, F. Zhang, Y. Liu, J. Leng, A review of shape memory polymers and composites: mechanisms, Adv. Mater. (2020) 2000713.
61. M. Balk, M. Behl, C. Wischke, J. Zotzmann, A. Lendlein, Recent advances in degradable lactide-based shape-memory polymers, Adv. Drug Deliv. Rev. 107 (2016) 136-152.
62. M. D. Hager, S. Bode, C. Weber, U. S. Schubert, Shape memory polymers: Past, present and future developments, Prog. Polym. Sci. 49-50 (2015) 30-33.

63. A. Lendlein, M. Behl, B. Hiebl, C. Wischke, Shape-memory polymers as a technology platform for biomedical applications, Expert Rev. Med. Devices. 7 (2010) 357-379.

64. C. Wischke, A. Lendlein, Shape-memory polymers as drug carriers-a multifunctional system, Pharm. Res. 27 (2010) 527-529.

65. R. Liang, L. Wang, H. Yu, A. Khan, B. Ul Amin, R. U. Khan, Molecular design, synthesis and biomedical applications of stimuli-responsive shape memory hydrogels, Eur. Polym. J. 114 (2019) 380-396.

66. H. Lu, J. Leng, S. Du, A phenomenological approach for the chemo- responsive shape memory effect in amorphous polymers, Soft Matter 9 (2013) 3851-3858.

67. H. Lu, W. M. Huang, Chemo-responsive shape-memory polymers for biomedical applications, Chapter 6, pagg. 99-132, in: L. Yahia Ed., Shape memory polymers for biomedical applications, Woodhead Publishing Series in Biomaterials, Elsevier (2015), Cambridge, UK.

68. C. L. Lewis, E. M. Dell, A review of shape memory polymers bearing reversible binding groups, J. Polym. Sci. B Polym. Phys. 54 (2016) 1340-1364.

69. S. L. Buffington, J. E. Paul, M. M. Ali, M. M. Macios, P. T. Mather, J. H. Henderson, Enzymatically triggered shape memory polymers, Acta Biomater. 84 (2019) 88-89.

70. B. Q. Y. Chan, Z. W. K. Low, S. J. W. Heng, S. Y. Chan, C. Owh, X. J. Loh, Recent advances in shape memory soft materials for biomedical applications, ACS Appl. Mater. Interfaces 8 (2016) 10070–10087.

71. C. Wischke, M. Behl, A. Lendlein, Drug-releasing shape-memory polymers-the role of morphology, processing effects, and matrix degradation, Expert Opin. Drug Deliv. 10 (2013) 1193-1205.

72. Y. Wu, L. Wang, X. Zhao, S. Hou, B. Guo, P. X. Ma, Self-healing supramolecular bioelastomers with shape memory property as a multifunctional platform for biomedical applications via modular assembly, Biomaterials 104 (2016) 18–31.

73. D. L. Safranski, K. E. Smith, K. Gall, Mechanical requirements of shape-memory polymers in biomedical devices, Polym. Rev. 53 (2013) 76–91.

74. M. C. Serrano, L. Carbajal, G. A. Ameer, Novel biodegradable shape-memory elastomers with drug-releasing capabilities, Adv. Mater. 23 (2011) 2211–2215.

75. Y. Feng, S. Zhang, H. Wang, H. Zhao, J. Lu, J. Guo, M, Behl, A. Lendlein, Drug release from biodegradable polyesterurethanes with shape-memory effect. J. Control. Release 152 (2011) e20-21.

76. M. Kashif, B. M. Yun, K. S. Lee, Y. W. Chang, Biodegradable shape-memory poly(ε-caprolactone)/polyhedral oligomeric silsequioxane nanocomposites: Sustained drug release and hydrolytic degradation, Mater. Lett. 166 (2016) 125-128.

77. A. T. Neffe, B. D. Hanh, S. Steuer, A. Lendlein, Polymer networks combining controlled drug release, biodegradation, and shape memory capability, Adv. Mater. 21 (2009) 3394–3398.

78. A. Neffe, H. Bui, S. Steuer, C. Wischke, A. Lendlein, Thermoemechanical properties and shape-memory capability of drug loaded semi- crystalline polyestermethacrylate networks, Mater. Res. Soc. Symp. Proc. 1144 (2009) 1144-LL16-04.

79. C. Wischke, A. T. Neffe, S. Steuer, A. Lendlein, Comparing techniques for drug loading of shape-memory polymer networks - effect on their functionalities, Eur. J. Pharm. Sci. 41 (2010) 136-147.

80. C. de Marco, C. C. J. Alcântara, S. Kim, F. Briatico, A. Kadioglu, G. de Bernardis, X. Chen, C. Marano, B. J. Nelson, S. Pané, Indirect 3D and 4D Printing of Soft Robotic Microstructures, Adv. Mater. Technol. 4 (2019) 1-7.

81. J. Firth, S. Gaisford, A. W. Basit, A new dimension: 4D printing opportunities in pharmaceutics, AAPS Adv. Pharm. Sci. Ser. 31 (2018) 153-162.

82. Y. S. Lui, W. T. Sow, L. P. Tan, Y. Wu, Y. Lai, H. Li, 4D printing and stimuli-responsive materials in biomedical aspects, Acta Biomater. 92 (2019) 19-36.

83. I. Lukin, S. Musquiz, I. Erezuma, T.H. Al-Tel, N. Golafshan, A. Dolatshahi-Pirouz, G. Orive, Can 4D bioprinting revolutionize drug development?, Expert Opin. Drug Discov. 14 (2019) 953–956.
84. S. Tibbits, 4D Printing, Archit. Des. 84 (2014) 116–121.
85. S. J. Trenfield, A. Awad, C. M. Madla, G. B. Hatton, J. Firth, A. Goyanes, S. Gaisford, A. W. Basit, Shaping the future: recent advances of 3D printing in drug delivery and healthcare, Expert Opin. Drug Deliv. 16 (2019) 1081-1094.
86. L. Ionov, 4D Biofabrication: Materials, Methods, and Applications, Adv. Healthc. Mater. 7 (2018) 1-14.
87. X. Li, J. Shang, Z. Wang, Intelligent materials: A review of applications in 4D printing, Assem. Autom. 37 (2017) 170–185.
88. G. H. Yang, M. Yeo, Y. W. Koo, G. H. Kim, 4D Bioprinting: technological advances in biofabrication, Macromol. Biosci. 19 (2019) 1-10.
89. Z. Zhang, K. G. Demir, G. X. Gu, Developments in 4D-printing: a review on current smart materials, technologies, and applications, Int. J. Smart Nano Mater. 10 (2019) 205–224.
90. Y. Zhou, W. M. Huang, S. F. Kang, X. L. Wu, H. B. Lu, J. Fu, H. Cui, From 3D to 4D printing: approaches and typical applications, J. Mech. Sci. Technol. 29 (2015) 4281-4288.
91. B. Gao, Q. Yang, X. Zhao, G. Jin, Y. Ma, F. Xu, 4D Bioprinting for Biomedical Applications, Trends Biotechnol. 34 (2016) 746–756.
92. J. J. Wu, L. M. Huang, Q. Zhao, T. Xie, 4D Printing: History and Recent Progress, Chinese J. Polym. Sci. - English Ed. 36 (2018) 563–575.
93. M. Zafar, H. Zhao, 4D Printing: future insight in additive manufacturing, Met. Mater. Int. 26 (2020) 564–585.
94. M. A. Alhnan, T. C. Okwuosa, M. Sadia, K. Wan, W. Ahmed, Emergence of 3D printed dosage forms: opportunities and challenges, Pharm. Res. 33 (2016) 1817-1832.

95. A. Awad, S. J. Trenfield, A. Goyanes, S. Gaisford, A.W. Basit, Reshaping drug development using 3D printing, Drug Discov. Today 23 (2018) 1547-1555.

96. A. Melocchi, M. Uboldi, F. Parietti, M. Cerea, A. Foppoli, L. Palugan, A. Gazzaniga, A. Maroni, L. Zema, Lego-Inspired Capsular Devices for the Development of Personalized Dietary Supplements: Proof of Concept With Multimodal Release of Caffeine, J. Pharm. Sci. 109 (2020) 1990-1999.

97. L. K. Prasad, H. Smyth, L. K. Prasad, H. Smyth, 3D Printing Technologies for Drug Delivery: A Review, Drug Discov. Today 9045 (2015) 1019-1031.

98. G. R., Gameiro, V. Sinkunas, G. L. Liguori, J. O-Ccauler-Junior. Precision Medicine: changing the way we think about healthcare. Clinics 73 (2018) e723.

99. G. S. Ginsburg, K. A. Phillips, Precision medicine: from science to value, Value. Health Affairs 37 (2018) 694-701.

100. L. H. Goetz, N. J. Schork, Personalized medicine: motivation, challenges, and progress. Fertil. Steril. 109 (2018) 952-963.

101. D. Ho, S. R. Quake, E. R. B. McCabe, W. J. Chng, E. K. Chow, X. Ding, B. D. Gelb, G. S. Ginsburg, J. Hassenstab, C. M. Ho, W. C. Mobley, G. P. Nolan, S. T. Rosen, P. Tan, Y. Yen, A. Zarrinpar, Enabling Technologies for Personalized and Precision Medicine, Trends Biotechnol. 38 (2020) 497-518.

102. W. K. Redekop, D. Mladsi, The faces of personalized medicine: a framework for understanding its meaning and scope. Value Health. 16 (2013) S4-9.

103. C. Sarisozen, G. Salzano, V. P. Torchilin, Recent advances in siRNA delivery, Biomol. Concepts. 6 (2015) 321-341.

104. A. A. Seyhan, C. Carini, Are innovation and new technologies in precision medicine paving a new era in patients centric care?, J. Transl. Med. 17 (2019) 1-28.

105. A. Subhan, V. P. Torchilin, siRNA based drug design, quality, delivery and clinical translation, Nanomedicine. 29 (2020) 102239.

106. R. Tang, Z. Xu, Gene therapy: a double-edged sword with great powers, Mol. Cell. Biochem. 474 (2020) 73-81.

107. X. Wu, T. Wu, J. Liu, B. Ding, Gene Therapy Based on Nucleic Acid Nanostructure, Adv. Healthc. Mater. 9 (2020) 1-10.

108. J. Lin, G. E. Sklar, V. M. Sen Oh, S. C. Li, Factors affecting therapeutic compliance: A review from the patient's perspective, Ther. Clin. Risk Manag. 4 (2008) 269-286.

109. B. Steward, Compliance, Adherence and Concordance: A Review of Engaging Patients in their Treatment, Br. J. Hand Ther. 9 (2004) 88-95.

110. T. Walters-Salas, The challenge of patient adherence, Bariatr. Nurs. Surg. Patient Care. 7 (2012) 186.

111. S. Kelch, S. Steuer, A. M. Schmidt, A. Lendlein, Shape-memory polymer networks from oligo[(ε-hydroxycaproate)-co-glycolate]dimethacrylates and butyl acrylate with adjustable hydrolic degradation rate, Biomacromolecules. 8 (2007) 1018-1027.

112. K. Nagahama, Y. Ueda, T. Ouchi, Y. Ohya, Biodegradable shape-memory polymers exhibiting sharp thermal transitions and controlled drug release, Biomacromolecules 10 (2009) 1789-1794.

113. C. Wischke, A. T. Neffe, S. Steuer, A. Lendlein, Evaluation of a degradable shape-memory polymer network as matrix for controlled drug release, J. Control. Release 138 (2009) 243-250.

114. C. Wischke, A. T. Neffe, S. Steuer, E. Engelhardt, A. Lendlein, AB-polymer networks with cooligoester and poly(n-butyl acrylate) segments as a multifunctional matrix for controlled drug release, Macromol. Biosci. 10 (2010) 1063-1072.

115. M. Bil, E. Kijeńska-Gawrońska, E. Głodkowska-Mrówka, A. Manda-Handzlik, P. Mrówka, Design and in vitro evaluation of electrospun shape memory polyurethanes for self-fitting tissue engineering grafts and drug delivery systems, Mater. Sci. Eng. C. 110 (2020) 110675.

116. Y. K. Feng, S. F. Zhang, L. Zhang, J. T. Guo, Y. S. Xu, Release of Aspirin from Biodegradable Polyesterurethane Networks, Adv. Mater. Res. 79-82 (2009) 1431-1434.

117. J. Jaworska, K. Jelonek, M. Sobota, J. Kasperczyk, P. Dobrzynski, M. Musial-Kulik, A. Smola-Dmochowska, H. Janeczek, B. Jarzabek, Shape-memory bioresorbable terpolymer composite with antirestenotic drug, J. Appl. Polym. Sci. 132 (2015) 1-8.
118. X. Li, X. Peng, R. Li, Y. Zhang, Z. Liu, Y. Huang, S. Long, H. Li, Multiple hydrogen bonds–reinforced hydrogels with high strength, shape memory, and adsorption anti-inflammatory molecules, Macromol. Rapid Commun. 41 (2020) 1-10.
119. K. S. Lee, Y. W. Chang, Thermal and mechanical properties of poly(ε-caprolactone)/polyhedral oligomeric silsesquioxane nanocomposites, Polym. Int. 62 (2013) 64-70.
120. Y. Xu, H. Yang, H. Zhu, L. Jiang, H. Yang, Self-healing gelatin-based shape memory hydrogels via quadruple hydrogen bonding and coordination crosslinking for controlled delivery of 5-fluorouracil, J. Biomater. Sci. Polym. Ed. 31 (2020) 712-728.
121. R. Zamani Alavijeh, P. Shokrollahi, J. Barzin, A thermally and water activated shape memory gelatin physical hydrogel, with a gel point above the physiological temperature, for biomedical applications, J. Mater. Chem. B 5 (2017) 2302-2314.
122. M. Sivaperuman Kalairaj, B. S. Yeow, C. M. Lim, H. Ren, Nitinol actuated soft structures towards transnasal drug delivery: a pilot cadaver study, Med. Biol. Eng. Comput. 58 (2020) 611-623.
123. H. Xuan, H. Hu, C. Geng, J. Song, Y. Shen, D. Lei, Q. Guan, S. Zhao, Z. You, Biofunctionalized chondrogenic shape-memory ternary scaffolds for efficient cell-free cartilage regeneration, Acta Biomater. 105 (2020) 97-110.
124. L. Du, S. Yang, W. Li, H. Li, S. Feng, R. Zeng, B. Yu, L. Xiao, H. Y. Nie, M. Tu, Scaffold composed of porous vancomycin-loaded poly(lactide-co-glycolide) microspheres: A controlled-release drug delivery system with shape-memory effect, Mater. Sci. Eng. C 78 (2017) 1172-1178.
125. B. Xu, Y. Li, F. Gao, X. Zhai, M. Sun, W. Lu, Z. Cao, W. Liu, High strength multifunctional multiwalled hydrogel tubes: ion-triggered shape memory,

antibacterial, and anti-inflammatory efficacies, ACS Appl. Mater. Interfaces. 7 (2015) 16865-16872.

126. R. Dimatteo, N. J. Darling, T. Segura, In situ forming injectable hydrogels for drug delivery and wound repair, Adv. Drug Deliv. Rev. 127 (2018) 167-184.
127. W. He, M. Reaume, M. Hennenfent, B. P. Lee, R. Rajachar, Biomimetic hydrogels with spatial- and temporal-controlled chemical cues for tissue engineering, Biomater. Sci. 8 (2020) 3248-3269.
128. H. Jo, M. Yoon, M. Gajendiran, K. Kim, Recent strategies in fabrication of gradient hydrogels for tissue engineering applications, Macromol. Biosci. 20 (2020) 1-11.
129. Y. Wang, Y. Miao, J. Zhang, J. P. Wu, T. B. Kirk, J. Xu, D. Ma, W. Xue, Three-dimensional printing of shape memory hydrogels with internal structure for drug delivery, Mater. Sci. Eng. C 84 (2018) 44-51.
130. M. G. Mennuni, P. A. Pagnotta, G. G. Stefanini. Coronary Stents: the impact of technological advances on clinical outcomes. Ann Biomed Eng. 44 (2016):488-496.
131. S. M. Shamimi-Noori, T. W. I. Clark, Venous stents: current status and future directions, Tech. Vasc. Interv. Radiol. 21 (2018) 113-116.
132. J. Mohd Jani, M. Leary, A. Subic, M. A. Gibson, A review of shape memory alloy research, applications and opportunities, Mater. Des. 56 (2014) 1078-1113.
133. H. M. Wache, D. J. Tartakowska, A. Hentrich, M. H. Wagner, Development of a polymer stent with shape memory effect as a drug delivery system, J. Mater. Sci. Mater. Med. 14 (2003) 109-112.
134. M. C. Chen, H. W. Tsai, Y. Chang, W. Y. Lai, F. L. Mi, C. T. Liu, H. S. Wong, H. W. Sung, Rapidly self-expandable polymeric stents with a shape-memory property, Biomacromolecules 8 (2007) 2774-2780.
135. M. C. Chen, Y. Chang, C. T. Liu, W. Y. Lai, S. F. Peng, Y. W. Hung, H. W. Tsai, H. W. Sung. The characteristics and in vivo suppression of neointimal formation with sirolimus-eluting polymeric stents. Biomaterials 30 (2009) 79-88.

136. V. C. Sonawane, M. P. More, A. P. Pandey, P. O. Patil, P. K. Deshmukh, Fabrication and characterization of shape memory polymers based bioabsorbable biomedical drug eluting stent, Artif. Cells Nanomed. Biotechnol. 45 (2017) 1740-1750.
137. C. S. Yang, H. C. Wu, J. S. Sun, H. M. Hsiao, T. W. Wang, Thermo-induced shape-memory PEG-PCL copolymer as a dual-drug-eluting biodegradable stent, ACS Appl. Mater. Interfaces 5 (2013) 10985–10994.
138. Y. Zheng, Y. Li, X. Hu, J. Shen, S. Guo, Biocompatible shape memory blend for self-expandable stents with potential biomedical applications, ACS Appl. Mater. Interfaces 9 (2017) 13988-13998.
139. L. Xue, S. Dai, Z. Li, Synthesis and characterization of elastic star shape-memory polymers as self-expandable drug-eluting stents, J. Mater. Chem. 22 (2012) 7403-7411.
140. A. Maroni, A. Melocchi, L. Zema, A. Foppoli, A. Gazzaniga, Retentive drug delivery systems based on shape memory materials, J. Appl. Polym. Sci. 137 (2020).
141. A. Melocchi, G. Loreti, M. D. Del Curto, A. Maroni, A. Gazzaniga, L. Zema, evaluation of hot-melt extrusion and injection molding for continuous manufacturing of immediate-release tablets, J. Pharm. Sci. 104 (2015) 1971-1980.
142. A. Melocchi, F. Parietti, A. Maroni, A. Foppoli, A. Gazzaniga, L. Zema, Hot-melt extruded filaments based on pharmaceutical grade polymers for 3D printing by fused deposition modeling, Int. J. Pharm. 509 (2016) 255-263.
143. A. Melocchi, N. Inverardi, M. Uboldi, F. Baldi, A. Maroni, S. Pandini, F. Briatico-Vangosa, L. Zema, A. Gazzaniga, Retentive device for intravesical drug delivery based on water-induced shape memory response of poly(vinyl alcohol): design concept and 4D printing feasibility, Int. J. Pharm. 559 (2019) 299-311.
144. A. Melocchi, M. Uboldi, N. Inverardi, F. Briatico-Vangosa, F. Baldi, S. Pandini, G. Scalet, F. Auricchio, M. Cerea, A. Foppoli, A. Maroni, L. Zema, A. Gazzaniga, Expandable drug delivery system for gastric retention based on shape memory

polymers: Development via 4D printing and extrusion, Int. J. Pharm. 571 (2019) 118700.

145. R. S. Teller, R. Rastogi, T. J. Johnson, M. J. Blair, R. W. Hitchcock, P. F. Kiser, Intravaginal flux controlled pump for sustained release of macromolecules, Pharm. Res. 31 (2014) 2344-2353.
146. L. Tan, J. Hu, H. Huang, J. Han, H. Hu, Study of multi-functional electrospun composite nanofibrous mats for smart wound healing, Int. J. Biol. Macromol. 79 (2015) 469-476.
147. J. Tang, R. Zhao, X. Yin, Y. Wen, Y. Shi, P. Zhu, Z. Chen, R. Zeng, L. Tan, Programmable release of berberine chloride hydrate from shape memory fibers prepared from core-sheath wet-spinning technology. J. Biomed. Nanotechnol. 15 (2019) 1432-1442.
148. W. C. Zhou, P. F. Tan, X. H. Chen, Y. Cen, C. You, L. Tan, H. Li, M. Tian, Berberine-incorporated shape memory fiber applied as a novel surgical suture, Front. Pharmacol. 10 (2020) 1-13.
149. X. Yin, P. Tan, H. Luo, J. Lan, Y. Shi, Y. Zhang, H. Fan, L. Tan, Study on the release behaviors of berberine hydrochloride based on sandwich nanostructure and shape memory effect, Mater. Sci. Eng. C 109 (2020) 110541.
150. S. Paonessa, N. Barbani, E. C. Rocchietti, C. Giachino, C. Cristallini, Design and development of a hybrid bioartificial water-induced shape memory polymeric material as an integral component for the anastomosis of human hollow organs, Mater. Sci. Eng. C 75 (2017) 1427-1434.
151. M. B. B. Monroe, A. D. Easley, K. Grant, G. K. Fletcher, C. Boyer, D. J. Maitland, Multifunctional shape-memory polymer foams with bio-inspired antimicrobials, ChemPhysChem. 19 (2018) 1999-2008.
152. P. L. Bardonnet, V. Faivre, W. J. Pugh, J. C. Piffaretti, F. Falson, Gastroretentive dosage forms: Overview and special case of Helicobacter pylori, J. Control. Release 111 (2006) 1-18.

153. M. Cerea, A. Maroni, L. Palugan, M. Bellini, A. Foppoli, A. Melocchi, L. Zema, A. Gazzaniga. Novel hydrophilic matrix system with non-uniform drug distribution for zero-order release kinetics. J Control Release 287 (2018) 247-256.

154. A. Foppoli, A. Maroni, S. Moutaharrik, A. Melocchi, L. Zema, L. Palugan, M. Cerea, A. Gazzaniga, In vitro and human pharmacoscintigraphic evaluation of an oral 5-ASA delivery system for colonic release, Int. J. Pharm. 572 (2019) 118723.

155. A. Maroni, L. Zema, M. Cerea, A. Foppoli, L. Palugan, A. Gazzaniga, Erodible drug delivery systems for time-controlled release into the gastrointestinal tract, J. Drug Deliv. Sci.Technol. 32 Part B (2016)229-235.

156. J. F. Pinto, Site-specific drug delivery systems within the gastro-intestinal tract: from the mouth to the colon, Int. J. Pharm. 395 (2010) 44-52.

157. C. M. Lopes, C. Bettencourt, A. Rossi, F. Buttini, P. Barata, Overview on gastroretentive drug delivery systems for improving drug bioavailability, Int. J. Pharm. 510 (2016) 144-158.

158. R. Arévalo-Pérez, C. Maderuelo, J. M. Lanao, Recent advances in colon drug delivery systems, J. Control. Release 327 (2020) 703-724.

159. N. Rouge, P. Buri, E. Doelker, Drug absorption sites in the gastrointestinal tract and dosage forms for site-specific delivery, Int. J. Pharm. 136 (1996) 117-139.

160. A. H. Teruel, I. Gonzalez-Alvarez, M. Bermejo, V. Merino, M. D. Marcos, F. Sancenon, M. Gonzalez-Alvarez, R. Martinez-Mañez, New insights of oral colonic drug delivery systems for inflammatory bowel disease therapy, Int. J. Mol. Sci. 21 (2020) 1-30.

161. S. Babaee, S. Pajovic, A. R. Kirtane, J. Shi, E. Caffarel-Salvador, K. Hess, J. E. Collins, S. Tamang, A. V. Wahane, A. M. Hayward, H. Mazdiyasni, R. Langer, G. Traverso, Temperature-responsive biometamaterials for gastrointestinal applications, Sci. Transl. Med. 11 (2019). eaau8581.

162. K. Park, Drug delivery research: the invention cycle, Mol. Pharm. 13 (2016) 2143-2147.

163. J. Fong, Z. Xiao, K. Takahata, Wireless implantable chip with integrated nitinol-based pump for radio-controlled local drug delivery, Lab Chip 15 (2015) 1050-1058.

164. D. C. Tuncaboylu, F. Friess, C. Wischke, A. Lendlein, A multifunctional multimaterial system for on-demand protein release, J. Control. Release 284 (2018) 240-247.

165. S. Barker, E. Rhoads, P. Lindquist, M. Vreugdenhil, P. Müllner, Magnetic shape memory micropump for submicroliter intracranial drug delivery in rats, J. Med. Devices, Trans. ASME 10 (2016) 1-6.

166. S. Murad, J. Murad, H. Khan, A smarter SMA technology for the realization of drug delivering endoscopic capsule, Rawal Med. J. 38 (2013) 66-74.

Part II

The content of Chapter II has already been published in: Int. J. Pharm. 559 (2019) 299-311.

RETENTIVE DEVICE FOR INTRAVESICAL DRUG DELIVERY BASED ON WATER-INDUCED SHAPE MEMORY RESPONSE OF POLY(VINYL ALCOHOL): DESIGN CONCEPT AND 4D PRINTING FEASIBILITY

Abstract

The use of shape memory polymers exhibiting water-induced shape recovery at body temperature and water solubility was proposed for the development of indwelling devices for intravesical drug delivery. These could be administered *via* catheter in a suitable temporary shape, retained in the bladder for a programmed period of time by recovery of the original shape and eliminated with urine following dissolution/erosion. Hot melt extrusion and fused deposition modeling 3D printing were employed as the manufacturing techniques, the latter resulting in 4D printing because of the shape modifications undergone by the printed item over time. Pharmaceutical-grade poly(vinyl alcohol) was selected based on its hot-processability, availability in different molecular weights and on preliminary data showing water-induced shape memory behavior. Specimens having various original and temporary geometries as well as compositions, successfully obtained, were characterized by differential scanning calorimetry and dynamic-mechanical thermal analysis as well as for fluid uptake, mass loss, shape recovery and release behavior. The samples exhibited the desired ability to recover the original shape, consistent in kinetics with the relevant thermo-mechanical properties, and concomitant prolonged release of a tracer. Although preliminary in scope, this study indicated the viability of the proposed approach to the design of retentive intravesical delivery systems.

Keywords: shape memory polymer, poly(vinyl alcohol), hot melt extrusion, fused deposition modeling, 3D printing, 4D printing, intravesical delivery.

1. Introduction

The bladder is a muscle-epithelial sac responsible for the collection of waste substances from the systemic circulation, coming from the kidneys, and their elimination as urinary fluids [1-3]. Considering its pivotal role in the homeostasis of the human body, any change in its functionality, even caused by the natural aging process or brought about by the onset of diseases, is necessarily associated with inconveniences of different extent. Vesical diseases, such as atonic and hyperactive bladder, interstitial cystitis and cancer, are widespread in individuals of different age and gender. However, their incidence increases in elderly people, who represent the population segment of developed countries in continuous growth and whose therapeutic treatments have great impact on healthcare expenses. The pharmacological therapy of such pathologies involves both systemic administration, mainly by the oral route, and *in situ* transurethral instillation of different active ingredients. Topical administration of drugs offers several advantages, *e.g.* to reduce the systemic side effects and avoid possible presystemic elimination mainly by the liver (first-pass effect), thus also allowing lower drug strengths to be used. Currently, solutions, suspensions or emulsions containing one or more drugs are instilled into the bladder through a catheter, inserted directly into the urethra of the patient and then clamped off for a pre-determined time period (from few minutes up to at least 1 h for chemotherapy), before being drained or normally excreted after withdrawal of the catheter. In this case the latter is removed immediately after instillation and the patient is asked to keep the solution in the bladder for the longest possible time, the maximum residence time of drugs within the bladder hardly exceeds 2 h, even when fluid intake is avoided. With the aim of counteracting the drug washout, repeated instillations are thus required, and this may entail other complications, such as primarily the onset of infections.

In order to maintain effective concentrations of the bioactive molecules within the bladder, various strategies have been pursued such as the use of bioadhesive liposome- or thermosensitive hydrogel-based formulations [4-7]. One of the most innovative

approaches to intravesical delivery is represented by indwelling systems administered transurethrally *via* catheter, that are designed to remain in the bladder for longer time periods (*e.g.* weeks). This resembles the concept of expandable gastroretentive dosage forms, the original size of which is reduced, *e.g.* by folding, into a carrier system such as a capsule: after administration, the carrier dissolves or opens up in stomach and the unit conveyed recovers a significantly larger spatial encumbrance due to swelling or unfolding processes that prolong its gastric retention time [8]. Analogously, bladder retention was obtained through either an increase in the size of the devices (*e.g.* UROS, Situs Corporation) or a change in the relevant geometry after being positioned into the organ (*e.g.* LiRIS, TARIS Biomedical). The success of the indwelling drug delivery systems described so far is still limited due to their poor tolerability, mainly associated with relatively large dimensions, density higher than that of urine and need for a removal procedure at the end of the treatment [9-11]. The idea of a biodegradable indwelling system that would not involve subsequent removal was preliminarily proposed [12]. However, the mechanism of retention (*e.g.* based on size increase or on geometry variation) was not clearly defined.

Over the last few years, shape memory polymers (SMPs) have drawn great interest in the area of advanced systems intended for biomedical applications [13-19]. They belong to smart materials capable of *i)* memorizing a permanent/original shape, *ii)* being fixed, under appropriate temperature conditions and mechanical stress, to a temporary shape and *iii)* being triggered, by an external *stimulus* such as a change in temperature, light, moisture, magnetic field or electrical current, to spontaneously recover the memorized stress-free permanent shape [20-22]. Microstructural changes of the polymer are responsible for shape fixing and shape recovery, the latter relaxation step being associated with elastic deformation stored during previous manipulation.

In this respect, much attention has been focused on SMP-based devices in which shape changes could be obtained at body temperature. Once introduced into the human body, these would be able to modify their shape thanks to exposure to 37 °C, thus performing

their function. Interestingly, in a particular class of SMPs, shape modifications can be triggered not only by heating but also through contact with water (*i.e.* water-induced shape memory effect). Such SMPs are hydrophilic polymers for which water taken up acts as a plasticizer and reduces the temperature required to activate the shape memory response [23]. In addition, SMPs characterized by water-induced shape memory behavior and suitable thermoplastic properties could be subjected to hot-processing *via* forming manufacturing techniques, such as hot melt extrusion (HME), injection molding and fused deposition modeling (FDM) 3D printing, which are well-known to yield high versatile geometries, details and sizes of products. Notably, the combined use of 3D printing technologies and SMPs has recently led to the new concept of 4D printing, intended as fabrication *via* 3D printing of items capable of self-transforming after production in terms of morphology, and thus possibly of functionality, in response to an external *stimulus* [24-27]. As compared with 3D printing, 4D printing involves the use of smart materials and also an advanced design, which has to take account of the original shape, the temporary shape, the transformations undergone by the object to shift from one another and relevant mechanisms. The time frame in which the original shape is recovered represents the 4^{th} dimension. In spite of the huge potential held, major applications of 4D printing in the development of drug delivery systems are yet to come. Based on such premises, the aim of the present work was to study the possible water-induced shape memory response of specimens fabricated from poly(vinyl alcohol) (PVA) of pharmaceutical grade by means of hot-processing techniques, namely HME and FDM. In particular, PVA was chosen in view of its known suitability for hot-processing and on preliminary results pointing out its water-induced shape memory behavior. Indeed, such a property could advantageously be exploited for the development of intravesical retentive systems, *i.e.* devices suitable for administration *via* catheter in the programmed/temporary shape and for bladder retention following spontaneous recovery of the permanent/original shape. Thanks to its slow interaction with aqueous fluids and related dissolution, it was deemed to hold potential as the main component of an

indwelling drug delivery system for prolonged release, with no need for being removed thanks to its erosion/dissolution over time. Moreover, the release rate could interestingly be tuned by selecting the polymer molecular weight. The feasibility of 4D printing in the manufacturing of such a device was preliminarily evaluated by characterizing the specimens obtained for thermo-mechanical properties, water-induced shape recovery, fluid uptake, mass loss as well as release behavior, using samples containing an analytical tracer.

2. Materials and Methods

2.1 Materials

PVA of different grades (Gohsenol™ EG 05P and Gohsenol™ EG 18P, Nippon Gohsei, J) (PVA05 and PVA18); glycerol, GLY (Pharmagel, I); caffeine, CFF (A.c.e.f, I, melting point 238 °C).

2.2. Methods

2.2.1 Preparation of PVA-based formulations

Plasticized PVA formulations containing 15% by weight of GLY calculated on the dry polymer, indicated as PVA05GLY and PVA18GLY, were prepared by kneading. PVA powder, previously dried in an oven (40 °C for 24 h), was placed in a mortar and the liquid plasticizer was added dropwise under continuous mixing. The resulting mixture was oven dried at 40 °C for 8 h. Afterwards, aggregates were ground by means of a blade mill and the < 250 μm powder fraction was recovered.

A tracer-containing formulation, indicated as PVA05GLY-CFF, was prepared immediately before processing by mixing in a mortar CFF powder, previously desiccated at 40 °C in an oven for 24 h, with PVA05GLY in a 1:9 weight ratio.

2.2.2 Manufacturing of PVA-based samples

Specimens having different geometries were prepared by HME and FDM. Virtual models of the straight bar (I-shape), U-shaped and helix items designed are reported in Figure 1.

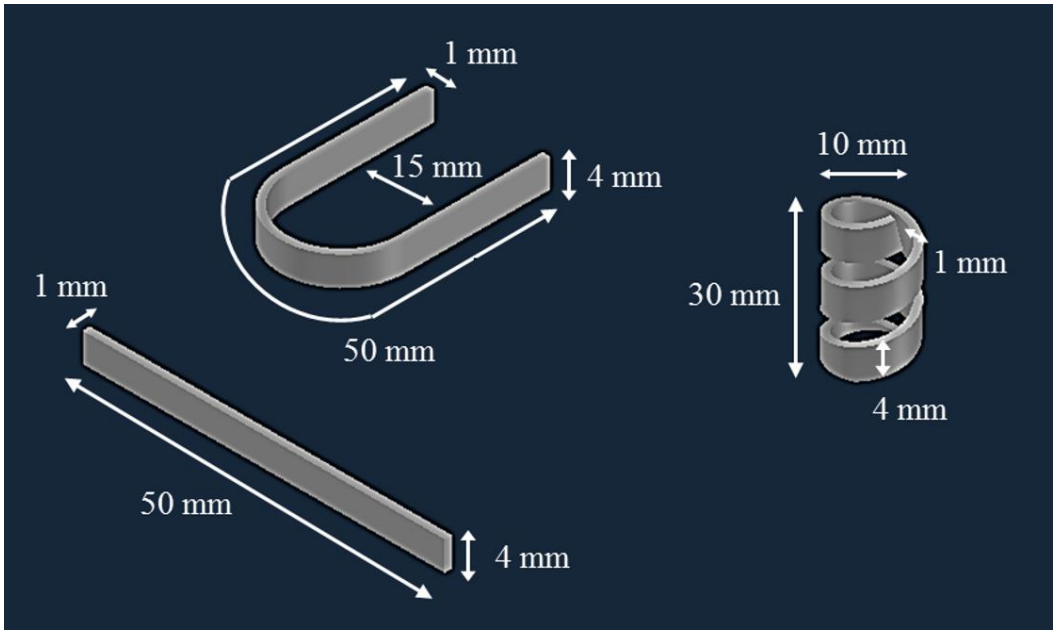

Figure 1: Virtual models with dimensional details of items having original I-, U- and helix-shapes.

2.2.2.1 Extrusion

HME was performed by a twin-screw extruder (Haake™ MiniLab II, Thermo Scientific, US-WI) equipped with counter-rotating screws. The material was extruded through a rectangular cross-section die (4 x 1 mm). In Table 1, the polymeric formulations and processing conditions are reported. Both were selected through a preliminary setup based on evaluation of the product quality (*e.g.* aspect, homogeneity, compliance with previously set size specifications and reproducibility), taking advantage of the experience previously acquired on hot-processing of PVA [28,29]. Particularly, GLY was chosen as the plasticizer based on its widely reported use with PVA [30-32].

I-shaped samples of 50 mm in length were obtained by cutting. U- and helix-shape items required manual post-processing. In the former case, the material coming out of the

extruder was bent around a stainless steel tool (ø = 15 mm) and then removed after 2 min of cooling. In the latter case, the extruded material was wrapped around a stainless steel tool (ø = 6 mm), purposely developed with a groove of the helix to be obtained (distance between adjacent turns = 5 mm), and then removed after the same cooling time. Immediately after production, I-, U- and helix-shaped samples were packed in heat seal alufoil moisture barrier bags.

Filaments for FDM were prepared under analogous process conditions by extruding the same polymeric formulations through a custom-made aluminum circular die (ø = 1.80 mm), as reported in [29]. Extruded rods were manually pulled and forced to pass through a caliper connected with the extruder and set at 1.80 mm. This was required to counteract possible swelling phenomena of the extruded rods and calibrate the relevant diameter, thus enhancing the yield of final product compliant with the specifications set, *i.e.* 1.75 ± 0.05 mm. After production and cooling, filament diameter was verified every 5 cm in length, and portions out of specifications were discarded. Indeed, filaments with diameter greater than 1.80 mm were unsuitable for printing.

2.2.2.2 3D printing

FDM was performed by a Kloner3D 240® Twin (Kloner3D, I) printer equipped with 0.4 mm nozzle (infill = 100%, layer height = 0.10 mm, printing speed = 23 mm/s, separation gap for raft and supports = 0.5 mm), using computer-aided design (CAD) files purposely developed. Items were designed using Autodesk® Autocad® 2016 software version 14.0 (Autodesk Inc., US-CA), saved in .stl format and imported to the 3D printer software (Simplify 3D, I). A further software (Netfab, I) was employed when the mesh number of the digital model needed to be increased, *i.e.* in the case of samples comprising curvatures. Portions 25 cm long of the in-house prepared filaments were used. Printing temperature was set as reported in Table 1.

Table 1: HME and FDM process conditions.

Material	HME			FDM
	T (°C)	Screw speed (rpm)	Torque (N·cm)	T (°C)
PVA05	200	100	190	200
PVA05GLY	170	100	100	180
PVA18GLY	200	100	220	n.d.*
PVA05GLY-CFF	175	100	120	185

*n.d. = not determined because of unfeasible manufacturing

2.2.3 Thermo-mechanical characterization

Samples cut from I-shaped items fabricated by HME and FDM, were subjected to differential scanning calorimetry (DSC) and dynamic-mechanical thermal analysis (DMTA).

DSC analyses were performed by DSC Q100 (TA Instruments, US-DE; n = 1), using nitrogen as a purge gas (70 mL/min). Indium was used as a calibration standard. Samples of about 10 mg were heated in aluminum crucibles from -50 °C to 240 °C, maintained at this temperature for 1 min, cooled down to -50 °C and reheated up to 240 °C. Both heating and cooling steps were run at 10 °C/min. Additional DSC tests were carried out with wet samples, maintained in distilled water for 30 min, and equilibrated under ambient conditions overnight (final water content of about 8-10% evaluated by thermogravimetric analysis).

DMTA tests were performed by a Q800 TA Instruments analyzer (TA Instruments, US-DE; n = 1), in displacement-controlled tensile mode, on ≈ 15 mm long specimens. The experiments were carried out at 1 Hz, with an applied displacement amplitude of 10 μm, from -50 °C to a maximum temperature equal to 100 °C / 120 °C, at a heating rate of 3 °C/min.

2.2.4 Water-induced shape memory experiments

The shape memory test consisted of two different phases, *i)* programming of the temporary shape and *ii)* recovery of the original shape (Figure 2). The programming step was performed as follows.

- Heating of the sample up to the deformation temperature ($T_{def} \approx T_g + 35$ °C, where T_g indicates the material glass transition temperature measured by DSC).

- Deformation, by means of specially designed tools, of the sample maintained at T_{def}. Samples having original U- or helix-shape were deformed to take on programmed temporary I-shape. Conversely, I-shaped samples were deformed to take on programmed temporary U-shape.

- Cooling of the sample in the fixed temporary shape below T_g. In case of plasticized PVAs, showing relatively low T_g, after deformation the samples were kept in a freezer at -20 °C in order to avoid early recovery.

Recovery of the original shape was obtained following immersion of the deformed samples into 100 mL of unstirred distilled water. The experiment was carried out both at room temperature and at 37 ± 0.5 °C, by using a thermoregulated bath. The recovery process was monitored using digital cameras (n = 1, Nikon D700 18-105 VR Kit, AF-S DX NIKKOR 18-105 mm f/3.5-5.6G ED VR, J and GoPro Hero Session, US-CA).

In case of originally I- or U- shaped samples, photographs acquired were processed by means of a specific software (ImageJ, US-MD) to measure the variation of the angle between the two arms (α) occurring during the recovery. Recovery index (RI) versus time curves were then built, with RI calculated as follows:

- for specimens with original I-shape

$$RI = \frac{\alpha - \alpha_p}{\pi - \alpha_p} \qquad \text{(Eq. 1)}$$

- for specimens with original U-shape

$$RI = 1 - \frac{\alpha}{\alpha_p} \qquad \text{(Eq. 2)}$$

where α_p is the angle obtained in the programming phase (angles in rad).

The time ($t_{RIfinal}$) to reach final RI (RI_{final}), *i.e.* the RI value calculated based on measurement after which no more changes in α were observed, was also recorded.

For specimens with original helix-shape, only the RI_{final} was considered, being calculated as follows:

$$RI_{final} = \frac{N_{fin}}{N_0} \qquad \text{(Eq. 3)}$$

where N_{final} and N_0 represent the number of windings at the end of recovery and before programming, respectively.

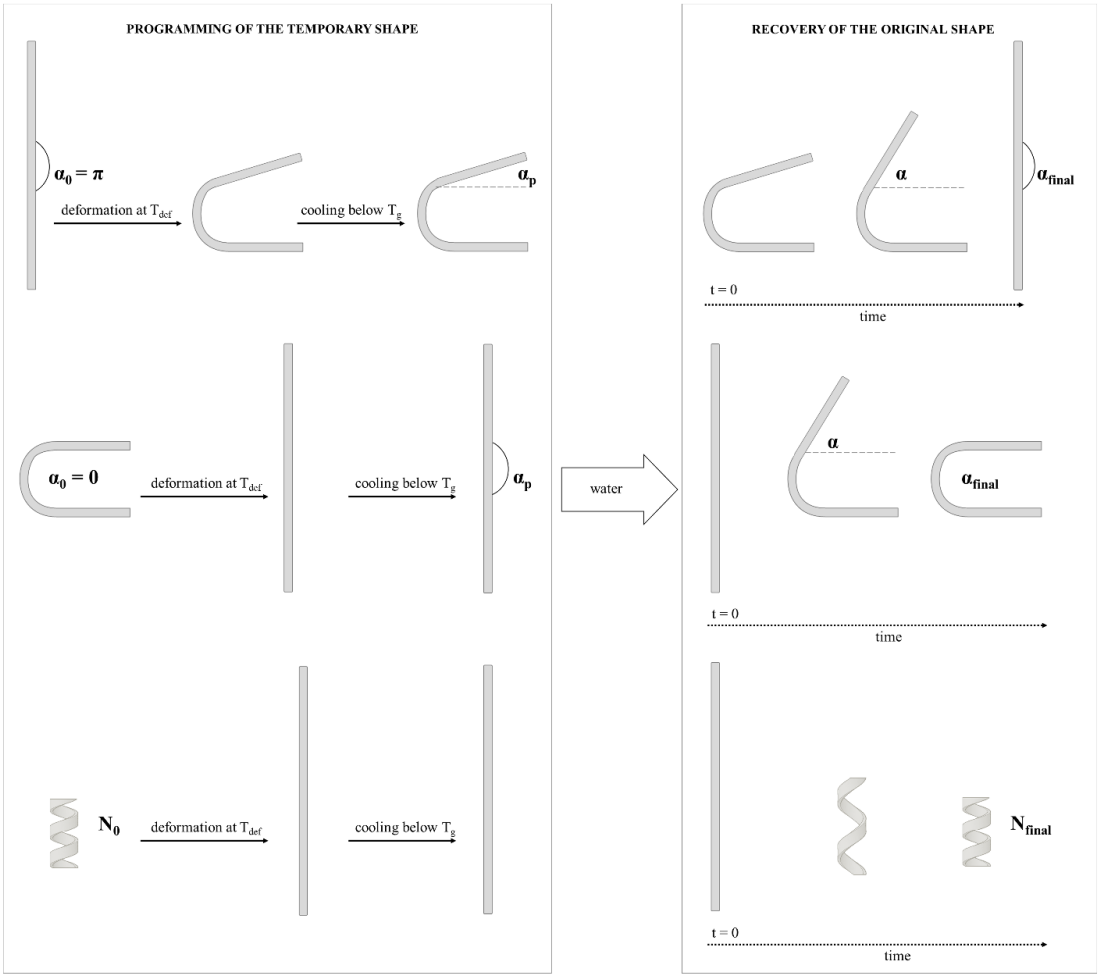

Figure 2: Outline of the experiments performed to evaluate the water-induced shape memory response.

2.2.5 Evaluation of fluid uptake and residual dry mass

Extruded and printed samples having original I-shape (n = 3) were characterized in terms of fluid uptake and residual dry mass over 4 h of immersion in unstirred simulated urine fluid (400 mL) kept at 37 ± 0.5 °C prepared as indicated in [33]. Each specimen was laid on a stainless steel net (w = 2.5 cm, h = 7 cm, mesh = 1.5 mm) before immersion and then withdrawn after predetermined time periods, gently blotted and weighed. Final dry masses were also determined after maintaining samples in an oven at 40 °C for 24 h. Two parameters were calculated, the percentage fluid uptake (FU) and the percentage residual dry mass (RDM), according to the following equations:

$$FU(\%) = \left[\frac{(W_m - W_d)}{W_m}\right] \times 100 \qquad \text{(Eq. 4)}$$

where W_m is the mass of the wet sample on withdrawal and W_d is the mass of the sample after drying;

$$RDM(\%) = 1 - \left[\frac{(W_i - W_d)}{W_i}\right] \times 100 \qquad \text{(Eq. 5)}$$

where W_i is the initial mass of the sample.

2.2.6 Evaluation of release performance

Tracer-containing extruded and printed samples were tested for release using a USP38 dissolution apparatus 2 (10 rpm, 37 ± 0.5 °C; Distek, CH; n = 3). 400 mL of simulated urinary fluid were used as the dissolution medium. Fluid samples were withdrawn at specific time points and assayed spectrophotometrically (λ = 206 nm). By linear interpolation of the release data immediately before and after the time point of interest, times to 10% and 90% release ($t_{10\%}$ and $t_{90\%}$, respectively) were calculated.

During the release test, photographs of samples were taken every 5 s (GoPro Hero Session, US-CA).

3. Results and Discussion

The temporary shape of a retentive intravesical delivery system should be such as to allow administration through a catheter without any constraints (*e.g.* straight bars with limited diameter and indefinite length). On the other hand, recovery of the original shape, designed to promote retention within the bladder for a pre-determined period of time (from few hours up to several days) without damaging its walls, should spontaneously take place *in situ* as a result of interaction with biological fluids. If water soluble SMPs are chosen as main components of the delivery system, no invasive procedure would ultimately be needed for the relevant removal.

3.1 Design and fabrication of specimens

The experimental work was aimed at attaining specimens showing water-induced shape shifting phenomena representative of each stage of performance for the retentive intravesical delivery platform proposed. For this purpose, hot-processing techniques, namely HME and FDM, were employed. FDM has recently been demonstrated to be a versatile manufacturing process for fabrication of drug delivery systems having complex geometries and composition, such as orally administered dosage forms (*e.g.* tablets, matrices, capsules, hollow and multilayer systems), implants and inserts [34-43]. In the particular field of intravesical delivery, which FDM has not been applied to so far, this 3D printing technique would grant the possibility of personalizing the pharmacological therapy in terms of type and dose of conveyed drugs, possible co-administration scheme (fixed drug combinations or extemporary compositions), and achievable release kinetics. With regard to HME, not only would it be viable for the device fabrication, but also is necessarily associated with FDM processing as it provides the filaments required for printer feeding.

Among polymers exhibiting water-induced shape memory response and good hot-processability, swellable/erodible ones, able to interact with aqueous fluids ultimately dissolving/eroding, appeared especially advantageous as main components for the

delivery system. Indeed, such materials undergo a glass-rubber transition when in contact with biological fluids with formation of a gel, the dissolution/erosion behavior of which depends on the relevant viscosity and, therefore, on the polymer molecular weight. Particularly, PVA was selected based on both the experience gained on relevant processing *via* HME and FDM as well as the review of preliminary literature findings on the exhibited water-driven shape memory ability, which relies on its semi-crystalline nature or may be obtained by crosslinking [28,29,44-46]. With respect to SMPs already proposed for drug delivery purposes, mainly including newly synthetized crosslinked polymers wanting regulatory approval, the PVA selected offers the advantage of a long-established use and safety profile [47-50]. In addition, being available in different molecular weights, it was expected to be a versatile material that would allow for a range of diversified release rates of the active ingredient conveyed and bladder retention times of the system.

Different molecular weights of PVAs, either unplasticized or in admixture with a plasticizer and/or tracer, were used. In order to broaden the scope of information achievable in terms of process and performance, the specimens based on these formulations were conceived in three geometries, having different extent of complexity, either mimicking the original (*i.e.* enabling bladder retention) or the temporary (*i.e.* enabling administration) shape of the device: a U-shaped item, a helix, as a possible evolution of the U-shape, and a simple straight bar (I-shape). The latter shape was chosen as a prototypical screening tool on account of the expected ease of fabrication, while the helix shape was considered of particular interest in view of intravesical application as it combines several advantages and a rather simple design. As compared with the U-shape, helical geometry could not only take on a temporary bar-like shape suitable for administration and then recover the original retentive configuration, but also be expected to have improved bladder retention, thanks to their numerous windings, and enhanced patient compliance. Indeed, a helix might behave like a spring that undergoes compression from resting position and shortens its natural length, thereby withstanding

possible mechanical stresses, deriving from muscle contraction during urination, and limiting discomfort. If further improvement of the helical geometry were pursued, the presence of any sharp tip might be overcome to reduce the potential for damaging the urothelium.

Originally I-, U- and helix-shaped samples were fabricated by FDM starting from in-house extruded filaments. Specimens having such designs were also fabricated by HME for comparison purposes and were thus used as a reference to design the virtual models for FDM. By way of example, Figure 3 shows photographs of the extruded and printed samples based on plasticized PVA05. Notably, materials being extruded have to undergo bending and coiling before cooling to reach final original shapes other than straight ones, thus involving purposely-developed tools and attentive process design. Conversely, items having relatively complex geometries (*e.g.* U- and helix-shape) could directly be fabricated by 3D printing. Revision of CAD files was needed to counteract possible expansion phenomena encountered with the polymeric formulations in use following preliminary printing trials. Indeed, by calculating a correction coefficient, as described in [38], printed items matching the dimensions of those prepared by HME were obtained. In addition, for samples comprising curvatures (*i.e.* originally U-shaped and helix-shaped specimens), the mesh number, *i.e.* a collection of vertices, edges and faces used to describe the shape of a tridimensional object, had to be increased in the virtual model in order to improve the resolution thus obtaining a smoother surface. FDM was performed by means of a 3D printer characterized by two arms working independently, which enabled contemporaneous fabrication of different parts thus reducing the overall printing time. The presence of a fixed build plate allowed to overcome manual calibration issues and also limited the exposure of the object in fabrication to uncontrolled airflow, known to hinder uniform cooling thereby impacting on product mechanical properties (*e.g.* reduced stiffness, layer detachment in the area subjected to greater cooling). Items were fabricated in the presence of a raft, because this turned out to increase adhesion of first printed layers to the build plate. Printing of helix-shaped items also required the use of

supports between each winding to avoid collapsing during vertical growth. A separation gap of 0.5 mm was set between the object and the raft as well as supports to make them easily removable without damage. Printing speed was kept low (23 mm/s) to enhance accuracy and avoid dragging of latest layered material, which may cause detachment of the item in fabrication from the build plate. Under these conditions, PVA05-based formulations were successfully printed without technical issues at temperatures established on the basis of their thermal behavior. As expected, the presence of the plasticizer resulted in improved printing and reduced number of failures. Notably, the obtained helical-samples, subjected to manual compression, were shown to behave like a spring, *i.e.* shorten in length when stressed and then return to the initial position after stress removal. In spite of the overall actions taken to make the process feasible, it was not possible to print any item starting from PVA18, either unplasticized or in admixture with GLY. Indeed, because the pressure needed for material extrusion during the 3D process is only exerted by the mass of the filament being loaded, the melt viscosity of such polymer was too high to enable its flow through the available nozzle. While increasing the printing temperature was expected to reduce the polymer viscosity, such an adjustment turned out not to be viable as browning of the material was observed. On the other hand, HME was successfully carried out with all the PVA formulations under investigation, except for PVA18 in the absence of plasticizer because torque values exceeding the maximum allowed by the equipment in use would have been needed.

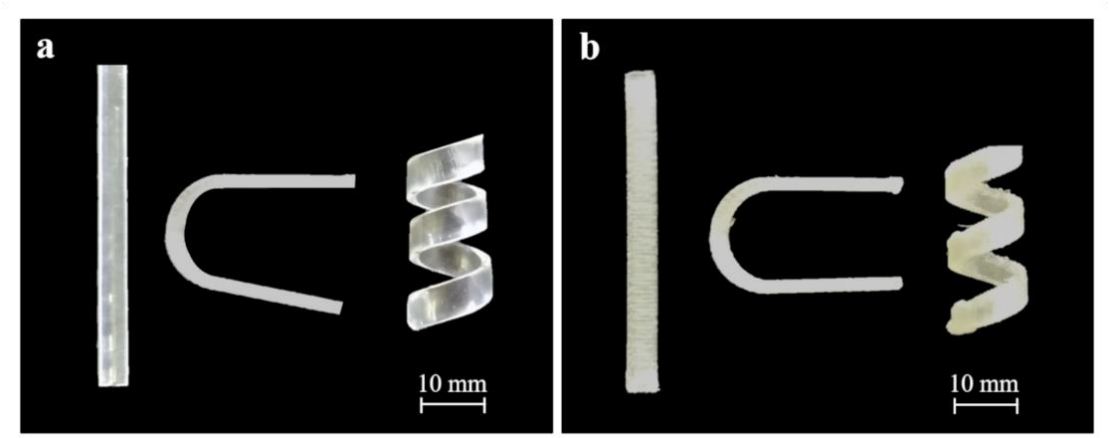

Figure 3: Photographs of originally I-, U- and helix-shaped specimens based on PVA05GLY obtained by a) HME and b) FDM.

3.2 Shape memory response

A basic experimental screening was carried out on I-shaped specimens obtained by HME and FDM in order to determine how the thermo-mechanical properties of samples may lead to their shape memory. In particular, as the temperature required to activate the shape transformation strictly depends on the material glass transition temperature, DSC analyses were initially performed. Indeed, shape shifting phenomena depend on amorphous regions of the polymer gaining mobility when T_g is reached, while permanent shape could be supported by crystalline domains, which would undergo melting at a higher temperature thus acting as net points [45]. Therefore, evaluating how T_g is affected by the polymer grade, the presence of plasticizer and the interaction with water is of utmost importance because the temporary shape *i)* must be programmed at $T_{def} > T_g$ (in the present case $T_{def} \approx T_g + 35$ °C), *ii)* can be preserved keeping the material at $T < T_g$ and *iii)* is reversed to the original shape at $T > T_g$. In this specific case, shape recovery phenomena should take place at 37 °C. Because shape recovery is activated at temperatures above T_g, any change in such a property is expected to be highlighted in the shape memory experiments. By DMTA, the evolution of material stiffness was described, and in particular storage modulus was measured below room temperature (T_{room}) and at T_{def}, corresponding to sample stiffness before and after recovery, respectively.

3.2.1 DSC experiments

DSC thermograms are reported in Figure 4, choosing the second scan since it provided T_g values similar to those of the first one but easier to read. These curves displayed a regular shape, *i.e.* a well-defined inflection point corresponding to the material T_g, and no other exo-/endo-thermal signals. T_g values obtained from these thermograms are reported in Table 2: minor differences in T_g measured for extruded and printed specimens were observed.

The plasticization effect of GLY turned out evident for PVA05, as a decrease of 37 °C and 46 °C in T_g was noticed with PVA05GLY-based samples obtained by HME and FDM, respectively. Such an effect was attributed to the ability of the plasticizer to modify the 3D organization of the polymer matrix [32]. In fact, due to its low-molecular weight and hydroxyl groups, GLY is known to lead to the formation of polymer-plasticizer hydrogen bonds to the detriment of interactions among polymer chains, thus reducing the intermolecular attraction forces and increasing the macromolecule mobility at temperatures below those at which the neat polymer undergoes transition.

In the case of wet samples, it was evident that also water taken up acted as a plasticizer for PVA, reasonably by weakening intra- and inter-molecular hydrogen bonds and increasing mobility of macromolecular chains (Figure 4a, Table 2). Indeed, progressive water absorption is known to concomitantly induce a decrease in the polymer T_g below room temperature until an equilibrium is reached. Particularly, the most marked decrease was recorded in the case of the wet as compared with dry PVA05 sample. The observed plasticization effect of water, allowing macromolecules to gain mobility, would enable activation of the shape shifting process at room temperature and below, which is the basis for the water-induced shape memory response.

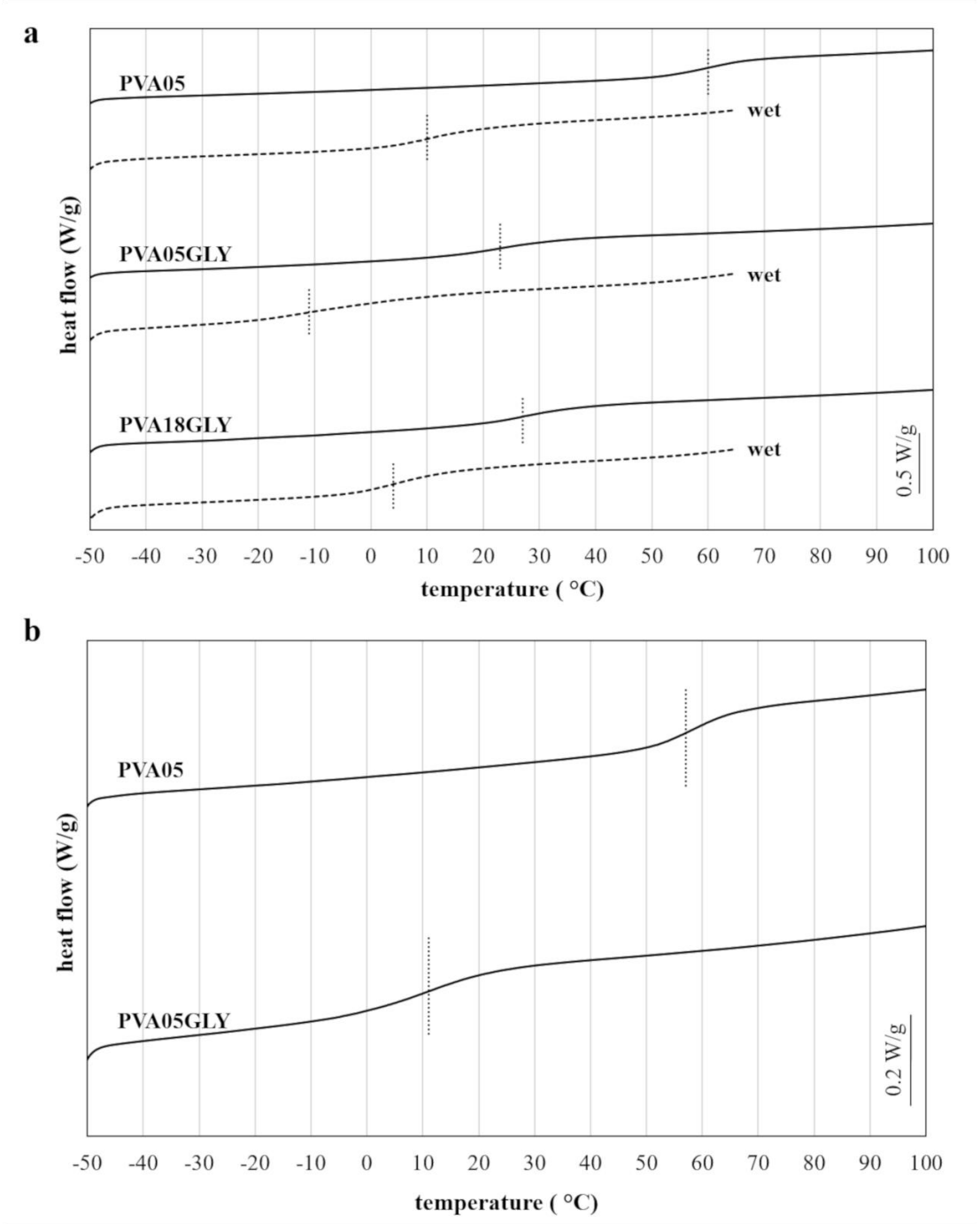

Figure 4: DSC thermograms (in the T_g region) from originally I-shaped specimens obtained by a) HME and b) FDM. Dotted vertical bars indicate T_g.

Table 2: T_g from DSC analyses, for originally I-shaped specimens obtained by HME and FDM. Data in brackets refer to wet samples.

	T_g (°C)	
	HME	**FDM**
PVA05	60 (10)	57
PVA05GLY	23 (-11)	11
PVA18GLY	27 (4)	n.a.*

* n.a. = non-available sample because of unfeasible manufacturing

3.2.2 DMTA experiments

Figure 5 shows the storage modulus (E') *vs* temperature curves obtained from extruded and printed specimens subjected to DMTA.

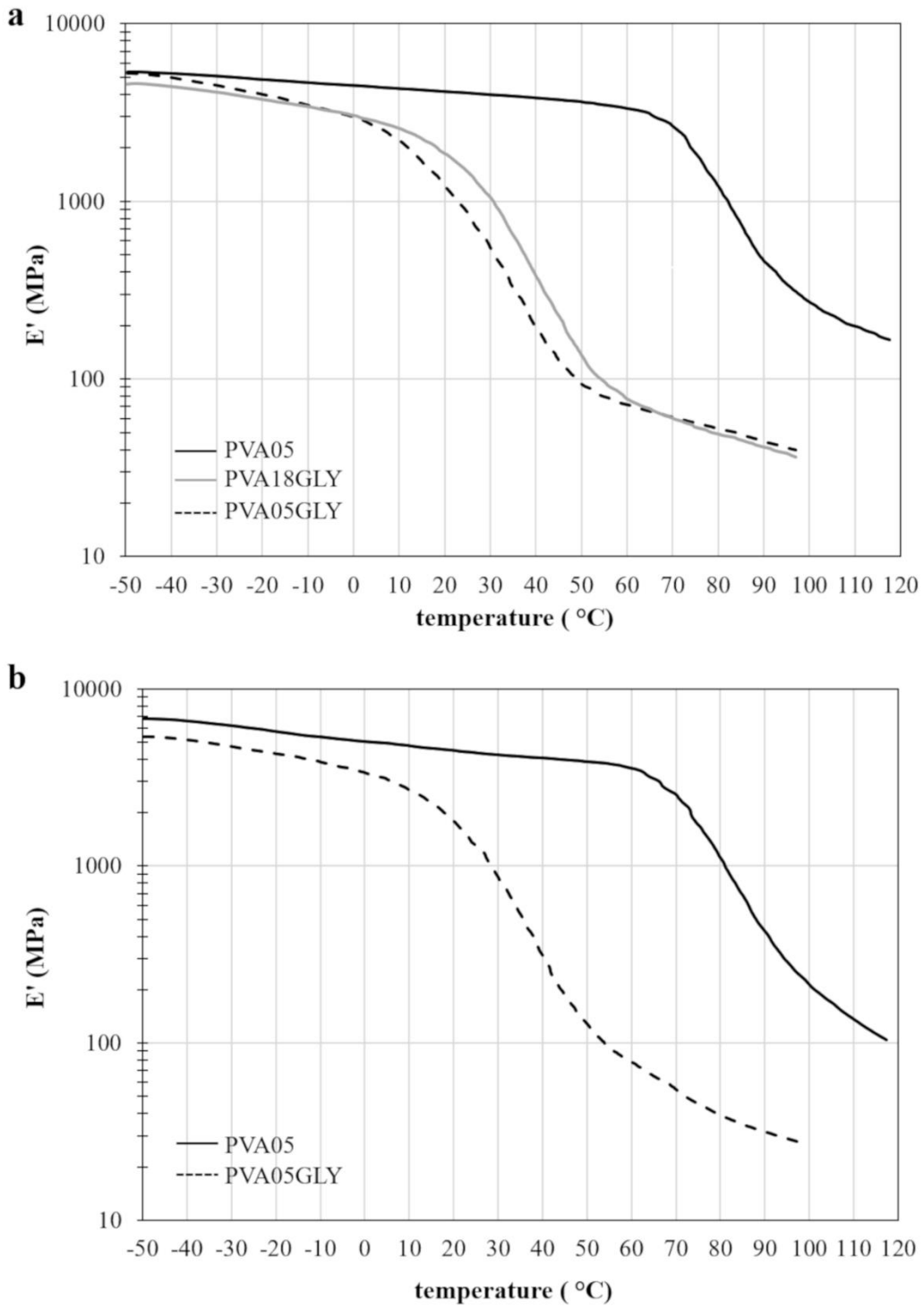

Figure 5: E' *vs* temperature curves from originally I-shaped specimens obtained by a) HME and b) FDM.

The plasticization effect induced by GLY, previously observed in DSC thermograms, was confirmed by DMTA data. Indeed, the reduced extent of interaction among PVA chains brought about by the addition of plasticizer resulted in a decrease in the sample stiffness, irrespective of the manufacturing technique considered. A decrease in T_g for GLY-containing specimens was confirmed by shifting of E' curves towards lower temperatures. E' traces also provided an indication of the stiffness of the material below and across the transition region. Table 3 reports E' values determined both at room temperature (E'_{Troom}) and at T_{def} (E'_{Tdef}), at which the material showed a rubbery behavior, as well as the relevant percentage difference ($\Delta E'$), defined as:

$$\Delta E'(\%) = \frac{E'_{Troom} - E'_{Tdef}}{E'_{Troom}} \times 100 \qquad \text{(Eq. 6)}$$

These values were chosen since E'_{Troom} would be representative of the stiffness of samples in their original shape, E'_{Tdef} would be an estimation of such a characteristic right after the shape memory transition, while $\Delta E'$ would represent the overall stiffness change during the transition. E'_{Tdef} and $\Delta E'$ may overestimate and underestimate, respectively, stiffness and overall change in stiffness, since it is known that water absorption, and eventually polymer dissolution, would lead to a relevant decrease.

Table 3: E'_{Troom}, E'_{Tdef} and $\Delta E'$ from originally I-shaped specimens obtained by HME and FDM.

	E'_{Troom} (MPa)		E'_{Tdef} (MPa)		$\Delta E'$ (%)	
	HME	**FDM**	**HME**	**FDM**	**HME**	**FDM**
PVA05	4060	4330	440	410	89	90
PVA05GLY	830	2750	70	120	92	96
PVA18GLY	1420	n.a.*	80	n.a.*	94	n.a.*

* n.a. = non-available sample because of unfeasible manufacturing

Irrespective of the manufacturing technique employed, PVA05 specimens displayed a stiff behavior at T_{room}, the storage modulus decreasing of one order of magnitude at T_{def}

with an overall stiffness change of about 90%. Not only the PVA05GLY but also PVA18GLY samples exhibited, because of the presence of GLY, lower E'_{Troom} and E'_{Tdef}, and a slightly higher overall variation (92-96%). The higher stiffness shown at T_{room} by printed specimens with respect to extruded ones might be ascribed to processing.

In general, the drop of E' indicates the occurrence of a relaxation process that, for these materials, could be ascribed to glass transition of PVA [51]. In support of the DSC data, T_g was also evaluated by DMTA, confirming minor differences, associated with the technique employed for sample manufacturing, as observed by DSC. Indeed, for a given material and specimen preparation method, a difference between transition temperatures determined by DSC and by DMTA, with the latter being systematically higher than the former, is expected and intrinsically related to the differences between the two experimental techniques and corresponding testing parameters, such as heating rate and frequency. Because transition temperatures coming from DMTA exhibit testing frequency dependence, T_g values obtained by DSC were used for assessment of T_{def} in the shape memory experiments.

3.2.3 Shape recovery experiments

The water-induced shape recovery process was studied in unstirred distilled water at room temperature, by monitoring evolution of the shape of extruded and printed samples from the temporary one. By analyzing photographs taken at successive time points, RI was calculated to describe the shape recovery process. By way of example, images of printed PVA05GLY specimens having different original shapes are collected in Table 4.

Table 4: Photographs acquired during shape recovery experiments (room temperature) of PVA05GLY specimens having original I- and U-shape obtained by FDM. A solid line is superimposed to highlight the recovery process.

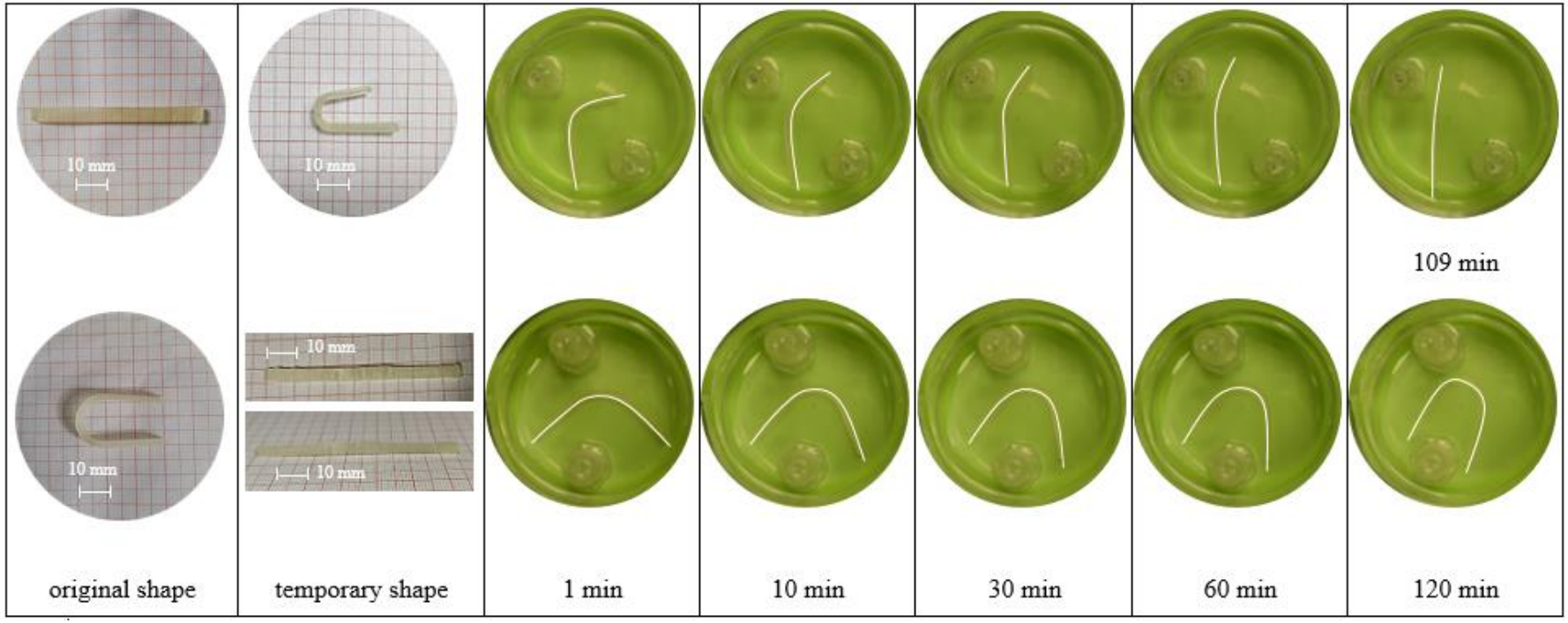

The recovery ability observed for a very simple original shape (*i.e.* I-shaped specimen programmed to take on temporary U-shape) was also shown by samples having an original U-shape (programmed to take on temporary I-shape) and comparable recovery times were found in both cases, irrespective of geometry. A shape-shifting effect similar to that exhibited by printed PVA05GLY samples was observed for the other formulations examined. An almost full recovery of the original shape was obtained from specimens having all geometries under investigation. The recovery process was also monitored over time and α was measured at successive time points to calculate the corresponding RI values. Recovery curves from selected extruded and printed samples with different original shapes are reported in Figure 6. With PVA05 samples, determination of RI in the final stage of the recovery process was impaired by concurrent polymer dissolution causing distortion of the specimens, which impaired the assessment of their shape evolution. In such cases, measurements had to be interrupted, and this was highlighted in the curves by marking the last RI value acquired.

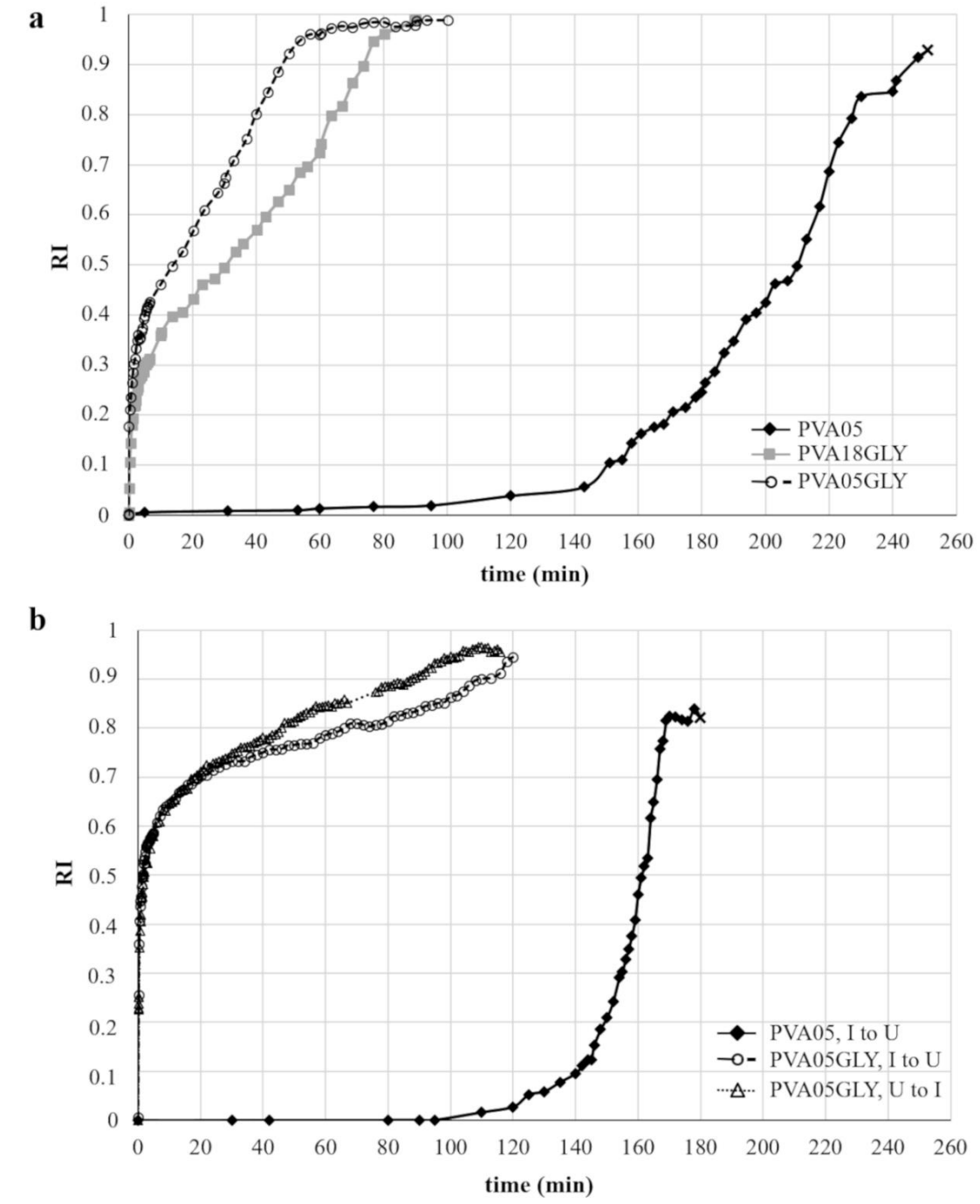

Figure 6: RI *vs* time curves from a) Originally I-shaped specimens of all compositions obtained by HME and b) Originally I- and U-shaped PVA05-based specimens obtained by FDM, tested at room temperature (x indicates the last datum acquired before measurements were impaired by the polymer dissolving).

For samples manufactured by HME, the addition of GLY to PVA05 modified the recovery process kinetics (Figure 6a). This is consistent with previous reports showing the effect of plasticizer on the shape memory response of semi-crystalline polymers [52]. With unplasticized PVA05, recovery showed an initial induction phase followed by a high rate phase (about 120 min long). By contrast, with PVA05GLY the process started with a high rate without any induction phase and the overall duration of recovery was reduced. These differences may be related to the fact that for PVA05GLY, having T_g below the recovery test temperature, the recovery process would be a combination of water- and temperature-induced shape memory effects, whereas for the unplasticized polymer, having T_g above the test temperature of approximately 30 ° C, recovery would result from water-induced shape memory only. Moreover, because of the greater free volume associated with the lower T_g, water diffusion phenomenon may be faster with the plasticized polymer, thus resulting in a faster activation of the shape memory effect. As regards PVA18, HME was feasible with the formulation containing GLY only, and the resulting sample exhibited a similar recovery pattern as compared with the PVA05GLY one, although the rate of the process was lower after the first few minutes of testing. The influence of molecular weight of the polymer on the relevant shape shifting phenomena would deserve further investigation, also considering literature findings mainly focused on its impact on recovery index [53,54].

In Figure 6b, it can be observed that the recovery curve of the printed PVA05 specimen showed an analogous induction phase, of approximately 2 h, with respect to the extruded sample having the same composition. However, the recovery rate in the subsequent phase turned out higher for the specimen obtained by FDM. The printed *vs* extruded PVA05GLY specimens were characterized by much faster initial recovery followed by a decrease in the process rate after some minutes from the beginning of the test, regardless of their original shape. Such differences in the initial recovery rate might be related to the different surface porosity/roughness of specimens fabricated by HME and FDM. Although specimens of comparable dimensions were prepared by the two techniques, the effective surface/volume ratio that governs water absorption kinetics is likely to be higher

for printed than extruded specimens due to a more porous structure resulting from the additive manufacturing process. The subsequent decrease in recovery rate of printed items, together with a less marked difference in the time needed for complete recovery observed with plasticized *vs* unplasticized samples, may be suggestive of the inherent layered nature, which would be brought out by the contact with water. It could be hypothesized that the various layers may not swell jointly following progressive water penetration. By contrast, extruded items would most likely be expected to behave as a continuous matrix. However, such an aspect is little known and is worth being explored, because in-depth studies comparing the water-induced shape memory response of extruded and printed items have not been reported in the scientific literature. An investigation into the possible differences in the temperature-induced shape memory behavior of items obtained starting from poly(ethylene-co-methacrylic acid) either by FDM or compression molding, a technique well-known for producing non-porous items, has so far been reported [55].

Recovery studies were also carried out under body temperature conditions. Table 5 summarizes RI_{final} values obtained and corresponding $t_{RIfinal}$, collected at room temperature and 37 °C from extruded and printed specimens having original I-shape.

Table 5: RI_{final} values and corresponding $t_{RIfinal}$ from specimens having original I-shape tested at room temperature and 37 °C.

		Room temperature		**37 °C**	
		RI_{final}	**$t_{RIfinal}$ (min)**	**RI_{final}**	**$t_{RIfinal}$ (min)**
HME	**PVA05**	0.93[a]	251[a]	0.97	146
	PVA05GLY	0.99	100	0.86	28
	PVA18GLY	0.99[a]	90[a]	0.92[a]	55[a]
FDM	**PVA05**	0.82[a]	180[a]	n.d.	n.d.
	PVA05GLY	0.97	109	0.88[a]	26[a]

[a] determination hindered by dissolving of the polymer with possible distortion of the specimen

n.d. = not determined because of pronounced distortion of the specimen

Generally high RI_{final} was shown by both extruded and printed specimens, with lower values for PVA05-based formulations. Because shape recovery and polymer dissolution occur concomitantly, RI_{final} could hardly be determined when the rate of shape recovery was lower than that of dissolution, thus leading to considerably reduced size or changes in consistency of the sample. In the case of the printed PVA05 specimen, it was not even possible to determine RI_{final} because of dissolution-driven distortion that was ascribed to the reduced gel viscosity and sample stiffness due to the high extent of hydration reached, close to the dissolution threshold. At both temperatures, the presence of GLY accelerated the recovery process, with up to a four-fold decrease in $t_{RIfinal}$ at 37 °C for PVA05GLY specimens. Because the T_g was by far lower than the test temperature, such a marked acceleration of recovery may have resulted from a combination of water- and temperature-induced shape memory effects. A reduction of $t_{RIfinal}$ was observed for all formulations tested at 37 °C as compared with room temperature, with extent of reduction of $t_{RIfinal}$ consistent with that of T_g values, as could be expected based on the increased mobility of the amorphous PVA domains. In the case of extruded specimens containing plasticizer (PVA05GLY and PVA18GLY), the time needed for recovery turned out to be affected by the polymer molecular weight at 37 °C.

The overall results confirmed that the use of originally straight bar-shaped samples as a screening tool could be appropriate, and the information gathered may profitably be exploited in the design of devices with more complex geometries

3.3 Fluid uptake and residual dry mass

Because thermo-mechanical properties and recovery of the original shape of samples was demonstrated to be affected not only by temperature but also by their exposure to aqueous media, it was deemed interesting to investigate the kinetics of biological fluid uptake. Concomitantly, the mass loss behavior of the same specimens was studied over time. Indeed, the overall bladder retention time of the device, the onset and time frame of shape shifting phenomena as well as its ability to control the release of the conveyed drug would

be related to the rate and extent of hydration and erosion/dissolution of the polymeric formulation.

Extruded and printed specimens having original I-shape were thus evaluated for FU and RDM, employing simulated urinary fluid kept at 37 ± 0.5 °C to mimic the environment in which the system was supposed to perform.

From FU and RDM profiles, reported in Figure 7, it turned out evident that the rate of fluid uptake was by far higher than that of mass loss. Indeed, approximately 40% of fluid taken up was reached within the first 15 min of testing, irrespective of the formulation and manufacturing technique considered. In the case of extruded items, the rate of mass loss of PVA05GLY was greater than that of PVA18GLY specimens. This could be explained on the basis of the different molecular weights of the employed polymer, which is known to be associated with viscosity of the hydrated matrix thus affecting the relevant rate of erosion/dissolution. The addition of GLY to PVA05 slightly accelerated the initial fluid uptake, which was evident especially in the case of extruded samples reasonably due to their less porous structure that could have hindered penetration of the aqueous medium. Because of pronounced hygroscopicity, the plasticizer may have increased water affinity of specimens, thus favoring absorption of the aqueous fluid [32]. Indeed, the hydroxyl groups of GLY would be able to establish hydrogen bonds with both water and polymer, thus increasing the molecular mobility of the latter and the free volume in the samples. In the case of PVA05, the threshold absorbed amount of aqueous medium needed for sufficient mobility of the polymer chains to be acquired and dissolution to take place was therefore higher than with the plasticized formulation.

Interestingly, the fluid uptake behavior of the specimens was consistent with the shape recovery previously discussed. As expected, activation of shape shifting phenomena in GLY-containing samples was especially rapid because the polymer T_g was not only decreased by the presence of plasticizer but also by the relatively high extent of fluid taken up in the first minutes of testing.

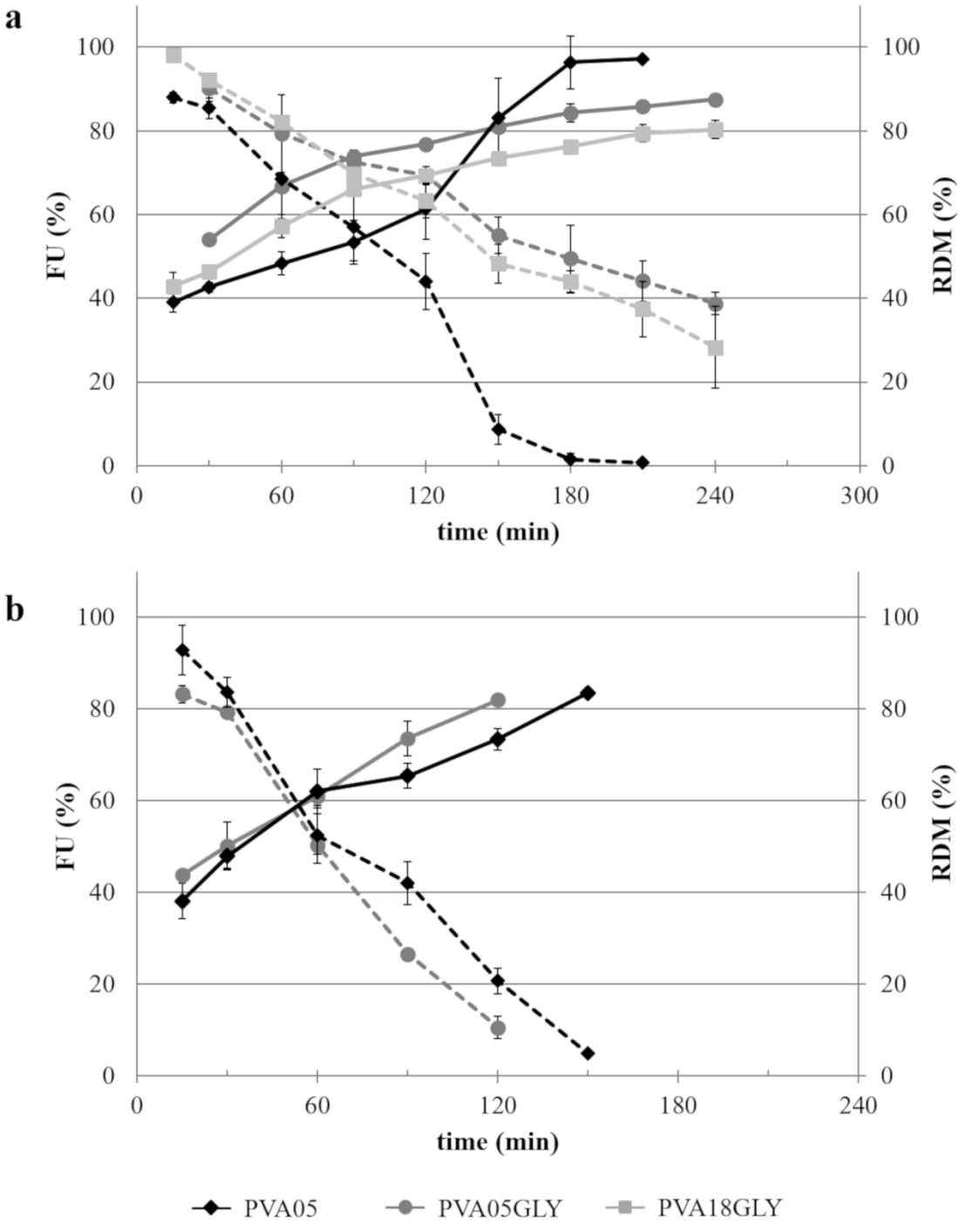

Figure 7: Average FU (solid lines) and RDM (dashed lines) curves from originally I-shaped specimens obtained by a) HME and b) FDM.

3.4 Evaluation of tracer-containing specimens

The potential of the PVA-based formulations under investigation for slowly releasing an active ingredient while undergoing prompt shape modifications was preliminarily evaluated using specimens containing CFF as an analytical tracer. Specimens having original I-shape were initially characterized for thermo-mechanical properties. A further decrease in T_g was found with respect to the corresponding samples devoid of CFF (T_g = 1 °C *vs* T_g = -3 °C for extruded *vs* printed items), which was already observed with a different thermoplastic polymer [56]. Moreover, the printed and extruded tracer-containing specimens showed comparable stiffness at T_{room} while higher values of E'_{Tdef}, thus resulting in an overall stiffness reduction of about 70% (E'_{Troom} = 1110 MPa *vs* E'_{Troom} = 1010 MPa and E'_{Tdef} = 340 *vs* E'_{Tdef} = 280 MPa for extruded *vs* printed items).

Samples having different original shapes, fabricated *via* both techniques, showed the ability to undergo shape recovery induced by water at room temperature and 37 °C, regardless of the presence of CFF (Table 6 and 7). With originally I-shaped samples, recovery turned out faster with respect to the previously tested ones, which was consistent with the T_g values relevant to the PVA05GLY-CFF formulation. In spite of a comparable extent of recovery, $t_{RIfinal}$ was nearly doubled for the extruded specimen as compared with the printed one. This was in agreement with the findings obtained from tracer-free specimens and is not surprising on account of the layered nature of items attained by additive manufacturing.

Table 6: RI_{final} values and corresponding $t_{RIfinal}$ from specimens having original I- and helix-shape tested at room temperature.

	Original shape	**RI_{final}**	**$t_{RIfinal}$ (min)**
HME	I-shape	0.94	40
	helix-shape	0.75	26
FDM	I-shape	0.76[a]	12[a]
	helix-shape	0.71	12

[a] determination hindered by dissolving of the polymer with possible distortion of the specimen

Table 7: Photographs acquired during shape recovery experiments (37 °C) of PVA05GLY-CFF specimens having original helix shape, obtained by HME and FDM, programmed to take on a temporary I-shape. A solid line is superimposed to highlight the recovery process.

HME	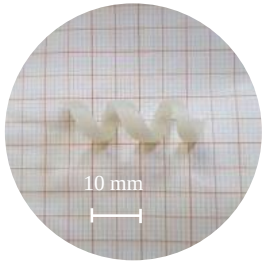					
FDM	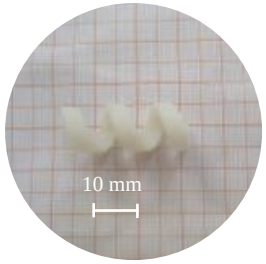					
	original shape	1 min	5 min	10 min	15 min	30 min

Release of the tracer from extruded and printed samples having original I-shape was studied after programming and fixing of the temporary U-shape, in order to evaluate the performance during recovery (Figure 8a). For this purpose, photographs of specimens were collected throughout the release test, and selected images relevant to printed items are reported in Figure 8b by way of example.

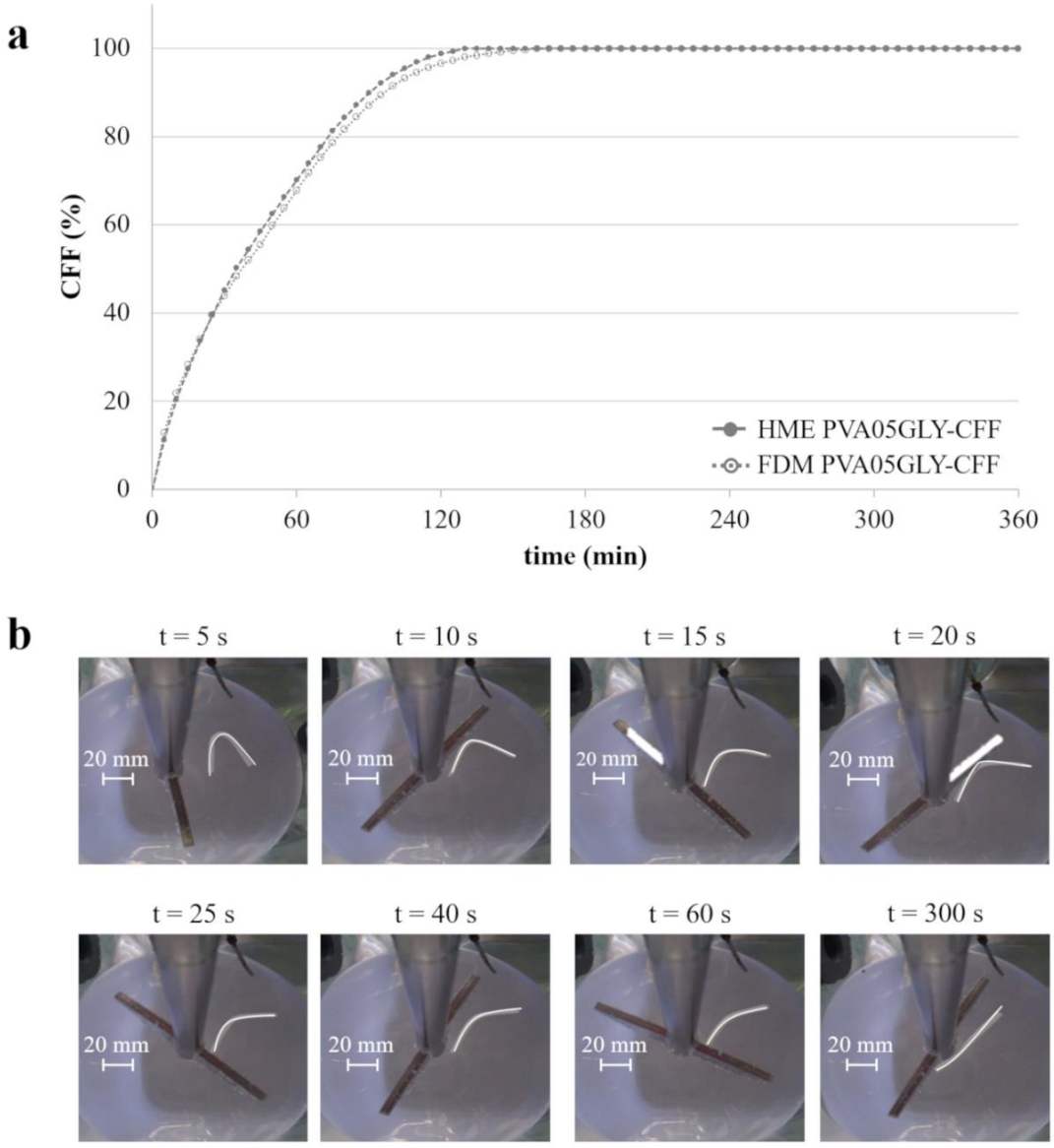

Figure 8: a) Release profiles from originally I-shaped PVA05GLY-CFF specimens obtained by HME and FDM following programming and fixing of the temporary U-shape and b) Photographs of the printed specimen at successive time points during the test. A solid line is superimposed to highlight the recovery process.

Release curves from extruded and printed specimens were almost superimposed. The release started without any lag phase and was completed within 2 h. Notably, with both extruded and printed specimens, the original straight shape was almost fully recovered before $t_{10\%}$, the most marked changes occurring within 60 s.

Conclusions

Indwelling drug delivery systems could be highly beneficial in the treatment of bladder diseases by increasing the intravesical residence time of drugs and compensating for the relevant washout. Such systems would thereby overcome failures and discomfort connected with repeated instillations through catheters. Moreover, they would allow different release kinetics to be established. The use of SMPs, in view of their ability to take on a programmed/temporary shape and recover the permanent/original one in the presence of an external *stimulus*, was regarded as an innovative strategy to develop retentive drug delivery systems with convenient administration mode. Among swellable/erodible SMPs characterized by water-induced shape memory response and good melt-processability, PVA of pharmaceutical-grade was selected for design and fabrication *via* hot-processing techniques, namely FDM 3D printing and HME, of an indwelling device for intravesical drug administration involving no removal procedure. In this respect, application of a 3D printing technique to an SMP would notably provide the basis for 4D printing because of the programmed changes in shape of the printed item occurring over time.

Starting from formulations based on PVA of different molecular weights, specimens having diverse original shapes and compositions were successfully extruded and printed. After programming and fixing of a temporary shape, these exhibited the desired ability to recover the original one following interaction with aqueous fluids, and the overall recovery as well as its rate were consistent with those expected according to the thermo-mechanical properties of the investigated materials. The recovery process was relatively fast, particularly at 37 °C, which was considered potentially advantageous in the prospect

of achieving prompt retention of the final system immediately after insertion into the bladder. The softening upon glass-rubber transition of the polymer would impart favorable hardness characteristics to the device, such that limited mechanical impact on the bladder epithelium could be ensured. Purposely fabricated samples containing an analytical tracer turned out able to modify the release of the latter before complete dissolution, yielding prolonged release patterns consistent with the molecular weight of PVA employed. Thus, multi-functionality of the PVA-based materials investigated was highlighted, entailing water-induced shape shifting, controlled release of a tracer and erosion/dissolution in biological fluids. More extended and varied release profiles, associated with diversified retention times, could be pursued by appropriate formulation and processing choices, such as selection and combination of polymers having higher molecular weights, modulation of the amount of plasticizer, addition of release modifiers and improvement of the equipment to ease processing.

Although preliminary in scope, this study pointed out the viability of the proposed approach based on hot-processing of a pharmaceutical-grade polymer having water-induced shape memory response in the manufacturing of retentive intravesical delivery systems, opening up new perspectives in application of 4D printing to the pharmaceutical field.

References

1. S. GuhaSarkar, R. Banerjee, Intravesical drug delivery: challenges, current status, opportunities and novel strategies, J. Control. Release 148 (2010) 147-159.
2. C.-C. Hsu, Y.-C. Chuang, M. B. Chancellor, Intravesical drug delivery for dysfunctional bladder, Int. J. Urol. 20 (2013) 552-562.
3. M. M. Zacchè, S. Srikrishna, L. Cardozo, Novel targeted bladder drug-delivery systems: a review, Res. Rep. Urol. 7 (2015) 169-178.
4. M. J. Cima, H. Lee, K. Daniel, L. M. Tanenbauma, A. Mantzavinou, K. C. Spencer, Q. Ong, J. C. Sy, J. Jr. Santini, C. M. Schoellhammer, D. Blankschtein, R. S. Langer, Single compartment drug delivery, J. Control. Release 190 (2014) 157-171.
5. O. C. Farokhzad, J. D. Dimitrakov, J. M. Karp, A. Khademhosseini, M. R. Freeman, R. Langer, Drug delivery systems in urology - getting "smarter", Urol. 68 (2006) 463-469.
6. J. Nirmal, Y.-C. Chuang, P. Tyagi, M. B. Chancellor, Intravesical therapy for lower urinary tract symptoms, Urol. Sci. 23 (2010) 70-77.
7. P. Tyagi, M. Kashyap, H. Hensley, N. Yoshimura, Advances in intravesical therapy for urinary tract disorders, Expert Opin. Drug Deliv. 13 (2016) 71-84.
8. E. A. Klausner, E. Lavy, M. Friedman, A. Hoffman, Expandable gastroretentive dosage forms, J. Control. Release 90 (2003) 143-162.
9. S. H. Lee, Y. B. Choy, Implantable devices for sustained, intravesical drug delivery, Int. Neurourol. J. 20 (2016) 101-106.
10. H. Lee, M. J. Cima, An intravesical device for the sustained delivery of lidocaine to the bladder, J. Control. Release 149 (2011) 133-139.
11. J. C. Nickel, P. Jain, N. Shore, J. Anderson, D. Giesing, H. Lee, G. Kim, K. Daniel, S. White, C. Larrivee-Elkins, J. Lekstrom-Himes, M. Cima, Continuous intravesical lidocaine treatment for interstitial cystitis/bladder pain syndrome: safety and efficacy of a new drug delivery device, Sci. Transl. Med. 4 (2012) 1-11.

12. I. S. Tobias, H. Lee, G. C. Jr. Engelmayr, D. Macaya, C. J. Bettinger, M. J. Cima, Zero-order controlled release of ciprofloxacin-HCl from a reservoir-based, bioresorbable and elastomeric device, J. Control. Release 146 (2010) 356-362.
13. M. Behl, A. Lendlein Shape memory polymers, Mater. Today 10 (2007) 20-28.
14. B. Q. Y. Chan, Z. W. K. Low, S. J. W. Heng, S. Y. Chan, C. Owh, X. J. Loh, Recent advances in shape memory soft materials for biomedical applications, ACS Appl. Mater. Interfaces 8 (2016) 10070-10087.
15. E. F. El Feninat, G. Laroche, M. Fiset, D. Mantovani, Shape memory materials for biomedical applications, Adv. Eng. Mater. 4 (2002) 91-104.
16. A. Lendlein, R. Langer, Biodegradable, elastic shape-memory polymers for potential biomedical applications, Sci. 296 (2002) 1673-1676.
17. A. Lendlein, M. Behl, B. Hiebl, C. Wischke. Shape-memory polymers as a technology platform for biomedical applications, Expert Rev. Med. Devices 7 (2010) 357-379.
18. W. Sokolowski, A. Metcalfe, S. Hayashi, L. Yahia, J. Raymond, Medical applications of shape memory polymers, Biomed. Mater. 2 (2007) S23-S27.
19. L. Yahia, Shape memory polymers for biomedical applications, Woodhead Publishing (2015) London, UK.
20. C. Liu, H. Qin, P. T. Mather, Review of progress in shape-memory polymers, J. Mater. Chem. 17 (2007) 1543-1558.
21. M. D. Hager, S. Bode, C. Weber, U S. Schubert, Shape memory polymers: Past, present and future developments, Prog. Polym. Sci. 49-50 (2015) 3-33.
22. W. M. Huang, Z. Ding, C. C. Wang, J. Wei, Y. Zhao, H. Purnawali, Shape memory materials, Mater. Today 13 (2010) 54-61.
23. B. Yang, W. M. Huang, C. Li, C. M. Lee, L. Li, On the effects of moisture in a polyurethane shape memory polymer, Smart Mater. Struct. 13 (2004) 191-195.
24. Z. Ding, C. Yuan, X. Peng, T. Wang, H. J. Qi, M. L. Dunn, Direct 4D printing via active composite materials, Sciences Adv. 3 (2017) e1602890-e1602896.

25. B. Gao, Q. Yang, X. Zhao, G. Jin, Y. Ma, F. Xu, 4D bioprinting for biomedical applications, Trends Biotechnol. 34 (2016) 746-756.
26. A. Y. Lee, J. An, C. K. Chua, Two-way 4D printing: a review on the reversibility of 3D-printed shape memory materials, Eng. 3 (2017) 663-674.
27. M. Maniruzzamann, 3D and 4D printing in biomedical applications: process engineering and additive manufacturing, Weinheim Ed., Wiley VCH (2018) Weinheim, D.
28. A. Melocchi, G. Loreti, M. D. Del Curto, A. Maroni, A. Gazzaniga, L. Zema, Evaluation of hot- melt extrusion and injection molding for continuous manufacturing of immediate-release tablets, J. Pharm. Sci. 104 (2015) 1971-1980.
29. A. Melocchi, F. Parietti, A. Maroni, A. Foppoli, A. Gazzaniga, L. Zema, Hot-melt extruded filaments based on pharma-grade polymers for 3D printing by fused deposition modeling, Int. J. Pharm. 509 (2016) 255-263.
30. J. Jang, D. K. Lee, Plasticizer effect on the melting and crystallization behavior of polyvinyl alcohol, Polymer 44 (2003) 8139-8146.
31. C.-A. Lin, T.-H. Ku, Shear and elongational flow properties of thermoplastic polyvinyl alcohol melts with different plasticizer contents and degrees of polymerization, J. Mater. Process Technol. 200 (2008) 331-338.
32. M. Mohsin, A Hossin, Y. Haik, Thermal and mechanical properties of poly(vinyl alcohol) plasticized with glycerol, J. Appl. Polym. Sci. 122 (2011) 3102-3109.
33. A. Y. Sherif, G. M. Mahrou, F. K. Alanazi, Novel in-situ gel for intravesical administration of ketorolac, Saudi Pharm. J. 26 (2018) 845-851.
34. N. Genina, J. P. Boetker, S. Colombo, N. Harmankaya, J. Rantanen, A. Bohr, Anti-tuberculosis drug combination for controlled oral delivery using 3D printed compartmental dosage forms: from drug product design to in vivo testing, J. Control. Release 268 (2017) 40-48.
35. J. Goole, K. Amighi, 3D printing in pharmaceutics: A new tool for designing customized drug delivery systems, Int. J. Pharm. 499 (2016) 376-394.

36. A. Goyanes, J. Wang, A. Buanz, R. Martínez-Pacheco, R. Telford, S. Gaisford, A. W. Basit, 3D Printing of medicines: engineering novel oral devices with unique design and drug release characteristics, Mol. Pharm. 12 (2015) 4077-4084.
37. A. Maroni, A. Melocchi, F. Parietti, A. Foppoli, L. Zema, A. Gazzaniga, 3D printed multi-compartment capsular devices for two-pulse oral drug delivery, J. Control. Release 268 (2017) 10-18.
38. A. Melocchi, F. Parietti, G. Loreti, A. Maroni, A. Gazzaniga, L. Zema, 3D printing by fused deposition modeling (FDM) of a swellable/erodible capsular device for oral pulsatile release of drugs, J, Drug Deliv. Sci. Technol. 30 Part B (2015) 360-367.
39. A. Melocchi, F. Parietti, S. Maccagnan, M. A. Ortenzi, S. Antenucci, F. Briatico-Vangosa, A. Maroni, A. Gazzaniga, L. Zema, Industrial development of a 3D-printed nutraceutical delivery platform in the form of a multicompartment HPC capsule, AAPS PharmSciTech. (2018).
40. T. C. Okwuosa, B. C. Pereira, B. Arafat, M. Cieszynska, A. Isreb, M. A. Alhnan, Fabricating a shell-core delayed release tablet using dual FDM 3D printing for patient-centred therapy, Pharm. Res. 34 (2017) 427-437.
41. N. Sandler, M. Preis, Printed drug-delivery systems for improved patient treatment, Trends Pharmacol. Sci. 37 (2016) 1070-1080.
42. T. Tagami, N. Nagata, N. Hayashi, E. Ogawa, K. Fukushige, N. Sakai, T. Ozeki, Defined drug release from 3D-printed composite tablets consisting of drug loaded polyvinylalcohol and a water-soluble or water-insoluble polymer filler, Int. J. Pharm. 543 (2018) 361-367.
43. L. Zema, A. Melocchi, A. Maroni, A. Gazzaniga, 3D printing of medicinal products and the challenge of personalized medicine, J. Pharm. Sci. 106 (2016) 1697-1705.
44. W. De Jaeghere, T. De Beer, J. Van Bocxlaer, J. P. Remon, C. Vervaet, Hot- melt extrusion of polyvinyl alcohol for oral immediate release applications, Int. J. Pharm. 492 (2015) 1-9.

45. Z. Q. Fang, Y. D. Kuang, P. P. Zhou, S. Y. Ming, P. H. Zhu, Y. Liu, H. L. Ning, G. Chen, Programmable shape recovery process of water-responsive shape memory poly(vinyl alcohol) by wettability contrast strategy, ACS Appl. Mater. Interfaces 9 (2017) 5495-5502.
46. X. D. Qi, X. L. Yao, S. Deng, T. N. Zhou, Q. Fu, Water-induced shape memory effect of graphene oxide reinforced polyvinyl alcohol nanocomposites, J. Mater. Chem. A Mater. 2 (2014) 2240-2249.
47. K. Nagahama, Y. Ueda, T. Ouchi, Y. Ohya, Biodegradable shape-memory polymers exhibiting sharp thermal transitions and controlled drug release, Biomacromolecules 10 (2009) 1789-1794.
48. A. T. Neffe, B. D. Hanh, S. Steuer, A. Lendlein, Polymer networks combining controlled drug release, biodegradation, and shape memory capability, Adv. Mater. 21 (2009) 3394-3398.
49. C. Wischke, T. A. Neffe, S. Steuer, A. Lendlein, Evaluation of a degradable shape-memory polymer network as matrix for controlled drug release, J. Control. Release 138 (2009) 246-250.
50. C. Wischke, A. Lendlein, Shape-memory polymers as drug carriers -a multifunctional system, Pharm. Res. 27 (2010) 527-529.
51. R. P. Chartoff, J. D. Menczel, S. H. Dillman, Dynamic Mechanical Analysis (DMA), in: J.D. Menczel, R.B. Prime, Thermal Analysis of Polymers: fundamentals and applications, Hoboken Eds., John Wiley & Sons (2009), Hoboken, US-NJ.
52. S. Cai, Y.-C. Sun, J. Ren, H. E. Naguib, Toward the low actuation temperature of flexible shape memory polymer composites with room temperature deformability via induced plasticizing effect, J. Mater. Chem. B 5 (2017) 8845-8853.
53. S. Chen, J. Hu, Y. Liu, H. Liem, Y. Zhu, Q. Meng, Effect of molecular weight on shape memory behavior in polyurethane films, Polym. Int. 56 (2007) 1128-1134.
54. S. Petisco-Ferrero, J. Fernández, M. M. Fernández San Martín, P. A. Santamaría Ibarburu, J. R. Sarasua Oiz, The relevance of molecular weight in the design of

amorphous biodegradable polymers with optimized shape memory effect, J. Mech. Behav. Biomed. Mater. 61 (2016) 541-553.

55. Z. Zhao, F. Peng, K. A. Cavicchi, M. Cakmak, R. A. Weiss, B. D. Vogt, Three-dimensional printed shape memory objects based on an olefin ionomer of zinc-neutralized poly(ethylene-co-methacrylic acid), ACS Appl. Mater. Interfaces. 9 (2017) 27239-27249.

56. S. K. Burgess, J. S. Lee, C. R. Mubarak, R. M. Kriegel, W. J. Koros, Caffeine antiplasticization of amorphous poly(ethylene terephthalate): Effects on gas transport, thermal, and mechanical properties, Polymer 65 (2015) 34-44.

Part III

Chapter I

The content of Part III, Chapter II has already been published in: Int. J. Pharm. 571 (2019) 118700.

EXPANDABLE DRUG DELIVERY SYSTEM FOR GASTRIC RETENTION BASED ON SHAPE MEMORY POLYMERS: DEVELOPMENT VIA 4D PRINTING AND EXTRUSION

Abstract

Several diseases would benefit from prolonged drug release provided by systems retained in the stomach for extended time periods. Expandable gastroretentive devices are administered in a collapsed configuration enabling swallowing and regain *in situ* their native shape having larger spatial encumbrance, thus hindering voidance through the wide open pylorus. An expandable system for gastric retention was here proposed relying on the shape memory behavior of pharmaceutical-grade poly(vinyl alcohol). Different original configurations to be recovered upon exposure to aqueous fluids at 37 °C, potentially enabling gastric retention, were conceived. Prototypes containing allopurinol were directly manufactured by fused deposition modeling or shaped by purposely-designed templates from hot melt extruded rods immediately after production. Various temporary shapes, in principle suitable for administration, were programmed by manual deformation of samples by means of specific templates, under defined temperature conditions. In 0.1N hydrochloric solution at 37 °C, the prototypes recovered their original shape, reaching the desired spatial encumbrance within few minutes. Release from the samples, although of relatively short duration, was independent of the original shape and processing undergone, and was noticeably slowed down by application of Eudragit® RS/RL-based coatings.

Keywords: poly(vinyl alcohol), shape memory polymer, hot melt extrusion, fused deposition modeling, 4D printing, gastroretentive drug delivery system.

1. Introduction

Recently, the use of the water-induced shape memory response of swellable soluble polymers was demonstrated to be a viable strategy for the development of an indwelling delivery system for intravesical administration of drugs [1]. The system, based on poly(vinyl alcohol) (PVA) of pharmaceutical grade, was fabricated via hot melt extrusion (HME) and 3D printing by fused deposition modeling (FDM) in a permanent bulky shape enabling retention within the bladder. Its ability to *i)* be fixed to a temporary shape suitable for administration, *ii)* recover the stress-free permanent shape following interaction with simulated urine at body temperature and *iii)* dissolve/erode while releasing a drug tracer was demonstrated. Moreover, it was the first 4D printing attempt of a drug delivery system (DDS) using pharmaceutical-grade polymers. A similar approach could be advantageously applied to the development of drug delivery systems to be retained in another hollow organ, such as the stomach, wherein sustained concentrations of drugs are needed in a number of disease conditions.

Gastric retention has long been pursued to enhance the bioavailability of drugs having either an absorption window in the upper gastrointestinal tract (*e.g.* metformin hydrochloride, baclofen) or lower solubility in the intestinal environment (*e.g.* captopril, metronidazole, ranitidine hydrochloride), and would also be desirable for the local treatment of gastric or duodenal ulcers, esophagitis and eradication of *Helicobacter pylori* [2-6] The use of prolonged-release gastroretentive drug delivery systems (GRDDSs) would also increase patient compliance by reducing the dosing frequency. Moreover, it would improve the therapy efficacy by limiting fluctuations in the drug concentration. Therefore, it would be highly advantageous in poor-adherence populations (*e.g.* children, elderly people and patients with cognitive/mental disorders) and in the therapy of chronic diseases (*e.g.* diabetes, HIV) that currently require drug administration via injection or other invasive procedures. In the latter case, major benefits would be obtained by prolonging drug release over days/weeks/months. However, gastric retention represents a quite challenging goal due to anatomical, mechanical, hydrodynamic and chemical

issues involved, such as peristaltic contractions and housekeeper waves, variable fluid volume, propulsive and retropulsive jets of gastric fluid, enzymatic processes, acidic pH. Inter-individual variables, *e.g.* gender, age, diet, alcohol consumption, physical activity, comorbidities and medications, may also play a critical role.

In order to enable gastric retention, a variety of approaches have been proposed in the scientific literature over the years, basically relying on *i)* density modifications, leading to devices undergoing high-density sedimentation or low-density floatation, *ii)* adhesion to the gastric mucosa, *iii)* magnetic localization and/or *iv)* size increase preventing passage through the pylorus [2].

Size-increasing GRDDSs, also known as expandable gastroretentive systems, were initially developed for veterinary application and currently represent one of the most promising strategies [5-11]. Few of them have already received FDA approval or are in phase III clinical trials (*e.g.* Depomed's Acuform® technology, IntecPharma's Accordion Pill™) [2,9]. For safety and efficacy purposes, these systems have to fulfill a number of requirements including *i)* convenient and well-tolerated administration mode, *ii)* prompt achievement of the bulky configuration only upon entry into the gastric environment, *iii)* retention for a programmed period of time without damaging the stomach walls or interfering with the relevant motility, *iv)* mechanical resistance to counteract muscle contraction, *v)* controlled release of the drug conveyed irrespective of diverse physiological conditions (*e.g.* pH fluctuations, presence of food and liquid content), and *vi)* elimination following reduction in size. In particular, the latter process should take place in such a way as not interfere with physiological stomach emptying and be completed before the administration of a subsequent dose, thus circumventing the risk of accumulation of multiple devices.

Expandable GRDDSs can be distinguished based on the ability to either take on a bulky configuration in the stomach by swelling, or go back to the bulky shape in which they were fabricated. In the latter case, the system is forced after production to a collapsed configuration which enables easy swallowing, typically within a carrier dosage form (*e.g.*

a capsule), for instance by folding. Once in the stomach, the system regains its native configuration with larger spatial encumbrance, preventing passage through the wide open pylorus that has diameter ranging between 5.6 mm and 22.1 mm, more commonly reported to be of 11-13 mm [2].

Pioneering research in the field of expandable GRDDSs was recently performed at Massachusetts Institute of Technology (MIT), leading to innovative systems based on either swelling or unfolding [12-15]. In both cases, great attention was focused on the mechanism of voidance of the devices. Particularly, gastric emptying of the exhausted system was ensured by a decrease in its size, either brought about by exposure to specific substances administered orally when appropriate, or associated with weakening/breaking of purposely designed portions due to diminished resistance to gastric contractions.

Based on these premises, the aim of the present work was to evaluate the feasibility of an expandable GRDDS able to self-modify its configuration upon external *stimuli* relying on the water-induced shape memory response of pharmaceutical-grade poly(vinyl alcohol) (PVA). The proposed system would thus spontaneously shift from a temporary collapsed configuration, imposed to allow administration, to a bulky original one enabling retention. Unlike previously described expandable GRDDSs based on unfolding, such a shifting would be programmed to occur in a time-dependent mode upon interaction with gastric fluid at body temperature rather than upon removal of a mechanical constraint (*e.g.* dissolution of the capsule). Therefore, the proposed device would result in a shape-memory expandable GRDDS (SMX GRDDS). Taking advantage of the experience gained in the use of FDM and HME, these techniques were selected for manufacturing of the device in view of the versatility in geometry they are well known to provide, which is of utmost importance due to the critical role played by shape for gastric retention [16-25]. Dealing with FDM, because recovery of the original shape of the 3D printed device is expected to take place over a set period of time, time itself would be considered as the fourth dimension, thus resulting in 4D printing [26-29]. This concept refers to production, *via* different 3D printing techniques, of objects based on smart materials such

as shape-memory polymers, intended for self-transformation when exposed to proper external *stimuli* other than mechanical ones [30-32]. Interestingly, the approach to gastric retention here pursued has not been used before or reported in the scientific literature, and would also benefit from regulatory acceptability on account of the safety profile of the polymer employed [1,25]. Thanks to the solubility of PVA, this system could also be subject to elimination from the stomach because of modification in its steric hindrance and mechanical properties over time, by gradually softening, dissolving and/or eroding when hydrated.

The feasibility of the SMX GRDDS was evaluated by *i)* designing original shapes in principle enabling gastric retention and setting up appropriate process conditions for manufacturing, *ii)* identifying temporary shapes compatible with oral administration into capsules and methods for their programming and *iii)* characterizing the obtained prototypes for water-induced shape recovery and release performance. At first, fabrication of systems by FDM was attempted. Subsequently, HME was used, and a systematic work was performed with extruded samples, including study of different shapes, quantitative evaluation of shape recovery and preliminary coating experiments.

2. Materials and Methods

2.1 Materials

PVA of different molecular weights (PVA05 and PVA18; Gohsenol™ EG 05P and Gohsenol® EG 18P, Nippon Gohsei, J); glycerol (GLY; Pharmagel, I); methacrylic acid copolymer Eudragit® RL100 and Eudragit® RS100 (Evonik, D); triethyl citrate (Sigma Aldrich, D) allopurinol (ALP; FarmaQuimica sur S.L., ES; boiling point 250.36 °C, melting point > 300 °C) [33]; carbonium nylon filament (ø = 1.75 mm, TreeDFilaments, I); hard-gelatin Coni-snap® capsule size 00el (capacity 1.02 mL, body external diameter 8.18 ± 0.06 mm, overall closed length 25.3 mm ± 0.03) and DB caps® size AA (capacity

0.80 mL, internal diameter 9.39 ± 0.06 mm, overall closed length 17.5 ± 0.03 mm) (Capsugel, I).

2.2. Methods

2.2.1 Preparation of PVA-based materials

Plasticized polymeric formulations containing 15% by weight of GLY calculated on the dry polymer were prepared starting from PVA05 and PVA18 (PVA05GLY and PVA18GLY). PVA powder, previously kept in an oven at 40 °C for 24 h, was placed in a mortar and GLY was added dropwise under continuous mixing. The resulting mixture was dried at 40 °C for 8 h and possible aggregates were then ground by a blade mill. The < 250 μm powder fraction was collected and used. Drug-containing materials were prepared immediately before processing by mixing in a mortar ALP powder, previously oven-dried at 40 °C for 24 h, with PVA05GLY or PVA18GLY in a 1:9 weight ratio (PVA05GLY-ALP and PVA18GLY-ALP, respectively).

2.2.2 Fabrication of SMX GRDDS prototypes

SMX GRDDS prototypes entailed an original shape resulting from fabrication and a temporary shape attained by programming (Figure 1). Preparation steps were different according to whether FDM or HME was used.

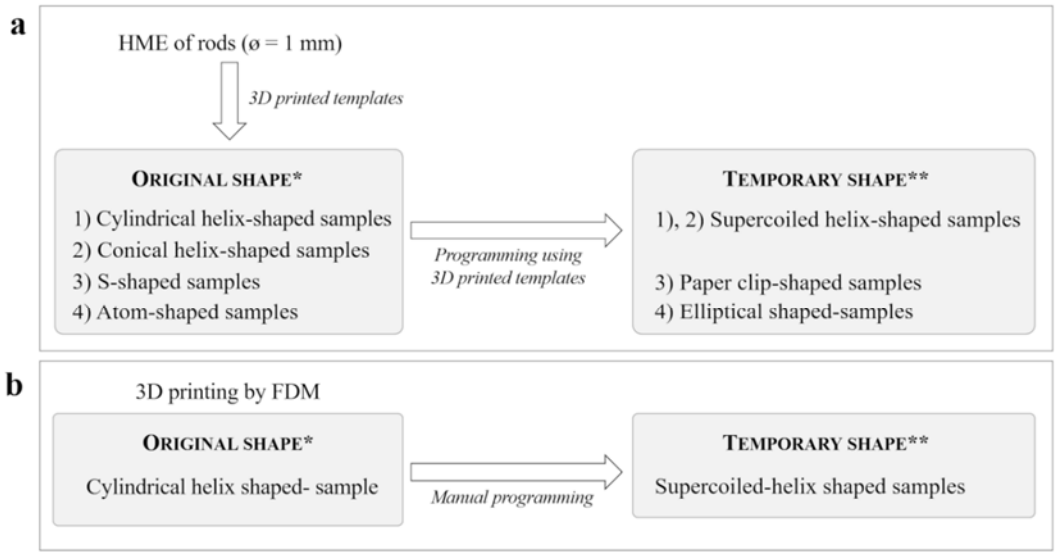

Figure 1: Preparation steps of SMX GRDDS prototypes by (a) HME and (b) FDM.

2.2.2.1 Hot melt extrusion

Extrusion was performed by a twin-screw extruder (Haake™ MiniLab II, Thermo Scientific, US-WI) equipped with counter-rotating screws and different dies under the conditions reported in Table 1.

Table 1: HME process conditions and maximum torque values recorded.

Material	**HME**		
	T (°C)	**Screw speed (rpm)**	**Torque (N·cm)**
PVA05GLY	170	20	100
PVA05GLY-ALP	175	20	120
PVA18GLY	200	20	190
PVA18GLY-ALP	200	20	210

HME was both employed to fabricate filaments for FDM and rods to be shaped into SMX GRDDS prototypes in their original shape.

Filaments were fabricated from PVA05GLY-based materials by extrusion through a custom-made aluminum circular die (ø = 1.80 mm), as previously described [1,34]. In order to counteract possible swelling phenomena and enhance the yield for filament compliant with the pre-established diameter specifications (1.75 ± 0.05 mm), the material coming out of the extruder was manually pulled to pass through a caliper connected with the equipment and set at 1.80 mm. After production and cooling, filament diameter was verified every 5 cm in length, and portions out of specifications were discarded.

Rods were fabricated from PVA18GLY-based materials by extrusion through a custom-made aluminum circular die (ø = 1.00 mm). While still hot, the rod was wrapped around purposely-developed templates, as described in the Results and Discussion section, and removed after 2 min of cooling under pressurized air. Samples having different original shapes, *i.e.* conical and cylindrical helices, S-shaped and atom-shaped samples, were thereby obtained. The resulting prototypes were packed in heat-sealed alufoil moisture barrier bags before being employed.

Samples of cylindrical helix shape were manually coated up to 60% weight gain with a 14% w/w ethanolic solution of Eudragit® RS/Eudragit® RL (1/1 w/w) plasticized with 15% w/w of triethyl citrate on the dry polymers. Coating was performed at ambient conditions inside an isolated room equipped with an air intake system, a spraying system with a 0.8 mm nozzle (pump speed 10 rpm, atomizer 0.75 atm, pattern 1 atm), and a rotating gear (2.3 rpm) enabling planetary movements. Coated samples were cured in a ventilated oven at 40 °C for 2 h.

2.2.2.2 3D printing

FDM was performed by a Kloner3D 240® Twin (Kloner3D, I) printer equipped with 0.5 mm nozzle. Computer-aided design (CAD) files were purposely developed as described in the Results and Discussion section using Autodesk® Autocad® 2016 software version 14.0 (Autodesk Inc., US-CA) and Netfab (I), specifically employed to increase the mesh number of virtual models. Designs were saved in .stl format and imported to the printer

software (Simplify 3D, I). FDM 3D printing was both employed to directly fabricate prototypes of SMX GRDDSs in their original shape and templates. Such templates were in turn employed for manual post-processing of extruded rods, to achieve the desired original shape of prototypes, and for programming of their temporary shape.

Prototypes of SMX GRDDSs in their original shape were printed using 25 cm-long portions of the in-house prepared PVA05GLY-ALP filament (printing temperature = 200 °C, infill = 100%, layer height = 0.10 mm, printing speed = 23 mm/s, separation gap for raft and supports = 0.5 mm).

Templates were printed from commercial carbonium nylon filament used as received (printing temperature = 230 °C, infill = 100%, layer height = 0.10 mm, printing speed = 50 mm/s).

2.2.2.3 Programming of the temporary shape

Programming of the temporary shape was performed by heating samples up to the deformation temperature ≈ T_g + 35 °C (where T_g is the material glass transition temperature measured by DSC), and manually deforming them with or without using templates, as described in the Results and Discussion section. The temporary shape was then fixed by cooling the deformed samples at -20 °C (well below T_g). The deformed specimens were maintained under this temperature for at least 1 h before testing.

2.2.3 Evaluation of SMX GRDDS prototypes

2.2.3.1 Shape recovery

Recovery of the original shape was studied upon immersion of the deformed samples into a crystallization vessel, filled with 250 mL of unstirred HCl 0.1 N and kept at 37 ± 0.5 °C by means of a thermoregulated bath. When the samples in their temporary shape were inserted into a capsule, the latter was glued to a microscope slide placed into the crystallization vessel to avoid floating. The recovery process was monitored using digital cameras positioned above (distance 13 cm) and in front of (distance 10 cm) the specimen

(GoPro Hero Session, US-CA; n = 3). The photographs acquired were processed using a specific software (ImageJ, US-MD). For each shape, recovery indices were calculated and recovery index (RI) *versus* time curves were built. RI were calculated as follows:

- for samples having original cylindrical helix shape (Figure 2a), which undergo supercoiling and extension in the programming of the temporary shape

$$RI_{\emptyset}(\%) = \frac{\emptyset_t - \emptyset_0}{\emptyset_i - \emptyset_0} \times 100 \qquad \text{(Eq. 1)}$$

where $RI_{\emptyset}$ is the diameter recovery index, being $\emptyset_i$ the diameter measured in the original configuration, $\emptyset_0$ the diameter measured in the temporary shape and $\emptyset_t$ the diameter measured during shape recovery;

$$RI_{\emptyset/h}(\%) = \frac{(\emptyset/h)_t - (\emptyset/h)_0}{(\emptyset/h)_i - (\emptyset/h)_0} \times 100 \qquad \text{(Eq. 2)}$$

where $RI_{\emptyset/h}$ is the diameter-to-height ratio recovery index, being $(\emptyset/h)_i$ the diameter-to-height ratio measured in the original configuration, $(\emptyset/h)_0$ the diameter-to-height ratio measured in the temporary shape and $(\emptyset/h)_t$ the diameter-to-height ratio measured during shape recovery;

- for samples having original conical helix shape (Figure 2b), which undergo supercoiling and extension in the programming of the temporary shape

$$RI_{\emptyset}(\%) = \frac{\emptyset_t - \emptyset_0}{\emptyset_i - \emptyset_0} \times 100 \qquad \text{(Eq. 3)}$$

where $RI_{\emptyset}$ is the base diameter recovery index being $\emptyset_i$ the base diameter measured in the original configuration, $\emptyset_0$ the base diameter measured in the temporary shape and $\emptyset_t$ the base diameter measured during shape recovery;

$$RI_{\emptyset/h}(\%) = \frac{(\emptyset/h)_t - (\emptyset/h)_0}{(\emptyset/h)_i - (\emptyset/h)_0} \times 100 \qquad \text{(Eq. 4)}$$

where $RI_{\emptyset/h}$ is the base diameter-to-height ratio recovery index, being $(\emptyset/h)_i$ the base diameter-to-height ratio measured in the original configuration, $(\emptyset/h)_0$ the base

diameter-to-height ratio measured in the temporary shape and $(\emptyset/h)_t$ the base diameter-to-height ratio measured during shape recovery;

- for samples having original S shape (Figure 2c), which undergo a complex deformation into a paper clip shape during the programming of the temporary shape

$$RI_{\alpha_{xy}}(\%) = \frac{\alpha_{xy_t} - \alpha_{xy_0}}{\alpha_{xy_i} - \alpha_{xy_0}} \times 100 \qquad \text{(Eq. 5)}$$

where $RI_{\alpha_{xy}}$ is the α_{xy} recovery index, being α_{xy_i} the angle measured in the original shape, α_{xy_0} the angle measured in the temporary shape and α_{xy_t} the angle measured during shape recovery;

$$RI_{\alpha_{yz}}(\%) = \frac{\alpha_{yz_t} - \alpha_{yz_0}}{\alpha_{yz_i} - \alpha_{yz_0}} \times 100 \qquad \text{(Eq. 6)}$$

where $RI_{\alpha_{yz}}$ is the α_{yz} recovery index, being α_{zy_i} the angle measured in the original shape, α_{yz_0} the angle measured in the temporary shape and α_{zy_t} the angle measured during shape recovery;

$$RI_{\alpha_{xz}}(\%) = \frac{\alpha_{xz_t} - \alpha_{xz_0}}{\alpha_{xz_i} - \alpha_{xz_0}} \times 100 \qquad \text{(Eq. 7)}$$

where $RI_{\alpha_{xz}}$ is the α_{xz} recovery index, being α_{xz_i} the angle measured in the original shape, α_{xz_0} the angle measured in the temporary shape and α_{xz_t} the angle measured during shape recovery.

Since the samples can lie on two different planes in the crystallization vessel once they are no longer inside the capsule, only two angles can be measured at a time during the recovery of the original S shape. Therefore, the experiments for S-shaped samples were replicated twice. In Figure 2c an example is shown where α_{xy} and α_{xz} were measured on the same specimen by the two cameras, and α_{yz} was evaluated on a different sample.

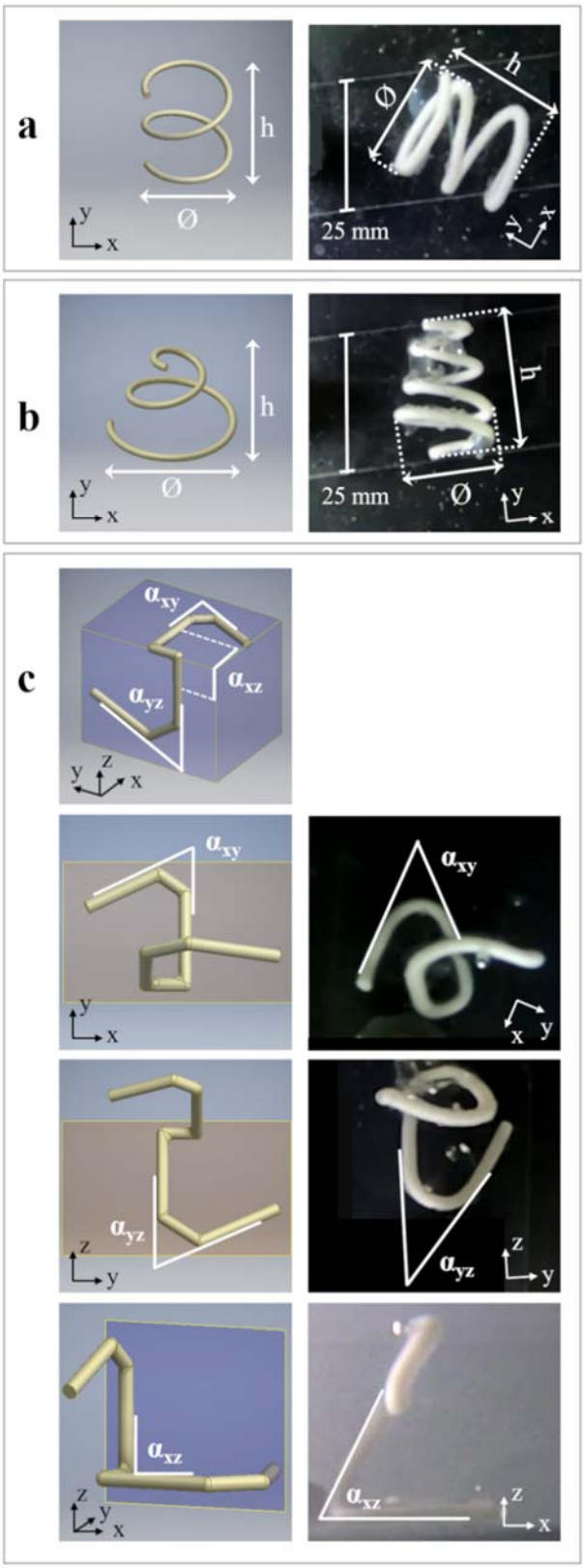

Figure 2: (left) Virtual models of (a) Cylindrical helix-, (b) Conical helix- and (c) S-shaped samples, and (right) Photographs of relevant specimens during shape recovery; parameters (*i.e.* diameter, height and angles) used to calculate RI are indicated.

2.2.3.2 Release performance

ALP-containing samples, either immediately after fabrication or following deformation into their temporary shape and insertion into a capsule, were tested for release using a USP38 dissolution apparatus 2 (50 rpm, 37 ± 0.5 °C, 900 mL HCl 0.1 N; Distek, CH; n = 6). Fluid samples were withdrawn at specific time points and assayed spectrophotometrically (λ = 251 nm). During the release test, photographs of samples were acquired every 5 s (GoPro Hero Session, US-CA).

2.2.4 Differential scanning calorimetry (DSC)

DSC analyses were performed by a DSC Q100 TA Instruments equipment (US-DE; n = 1), using nitrogen as a purge gas (70 mL/min). Indium was used as a calibration standard. Samples of about 10 mg were heated in aluminum pans from -50 °C to 240 °C, maintained at this temperature for 1 min, cooled down to -50 °C and reheated up to 240 °C. Both the heating and cooling steps were run at 10 °C/min.

3. Results and Discussion

Taking advantage of the experience previously gained in the development of indwelling PVA-based devices for intravesical administration of drugs, the main challenges to be faced were related to the peculiar characteristics of the new site for DDS retention.

3.1 Drug tracer selection

ALP, a xanthine oxidase inhibitor used as the first-line therapy for gout and hyperuricemia, was chosen as a model molecule in view of its greater absorption from the stomach, being in its non-ionized form in the acidic medium (pK_a 9.4), and from the duodenum as well as the upper jejunum [35-37]. Indeed, this drug has already been proposed as a candidate for being administered via a GRDDS combining floating and mucoadhesion strategies [37]. Moreover, its high melting point would make it in principle

suitable for processing under the temperature conditions required by the employed manufacturing techniques.

PVA-based formulations containing ALP, and GLY as the plasticizer, were subjected to a DSC cycle between -50 °C and 240 °C in order to assess the material T_g. Indeed, the temporary shape of a PVA-based SMX GRDDS has to be programmed by heating samples above T_g, and maintained by keeping them below T_g. Moreover, the recovery of the original shape would occur when the systems are exposed at a temperature above T_g, *i.e.* the body temperature. In Figure 3 DSC thermograms acquired are reported.

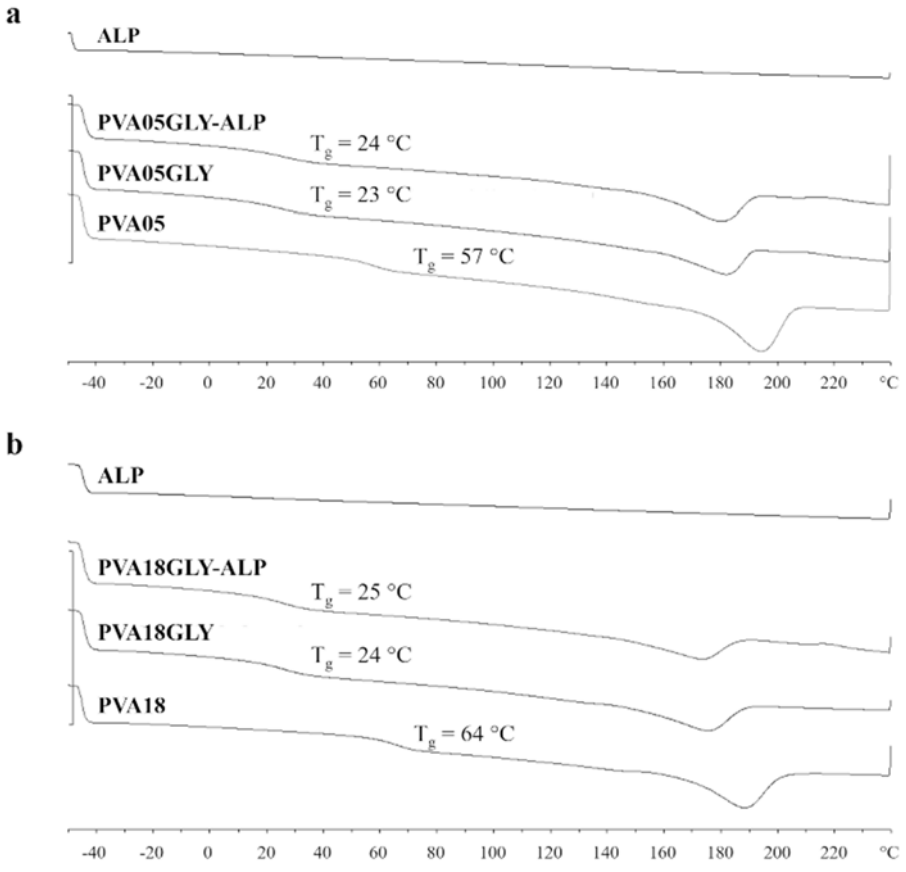

Figure 3: DSC thermograms (a) PVA05- and (b) PVA18-based materials. Thermograms relevant to ALP as such are also reported.

The plasticization effect of GLY on PVA, indicated by a decrease in T_g, was confirmed [1,38]. On the contrary, the presence of ALP was demonstrated not to affect the T_g of PVA05GLY and PVA18GLY.

3.2 Design concept

The original and the temporary shape of the SMX GRDDS under development should be compliant with the route of administration and the characteristics of the retentive organ. Accordingly, the original shape given on fabrication was conceived so as to provide the system with a spatial encumbrance that would prevent stomach emptying, *i.e.* at least 2 dimensions greater than 13 mm. Moreover, it would have to be endowed with large void volumes not to prevent passage of gastric fluids through the pyloric sphincter, should the device be positioned in its close proximity during residence in the stomach. On the other hand, the temporary shape to be imposed by subsequent deformation should be such as to allow conveyance of the device in a carrier system (*e.g.* a gelatin capsule) and easy swallowing. The shift from the latter to the former configuration should spontaneously take place after dissolution/breakup of the capsule in the gastric fluid, while elimination of the expanded system from the stomach would be ensured by the progressive dissolution of PVA.

3.3 4D printing of prototypes

FDM was first used for the manufacturing of SMX GRDDS prototypes, and a trial-and-error approach was adopted. This consisted in introducing progressing changes into the virtual model (*e.g.* diameter, height and number of windings of the helix as well as dimensions of the relevant cross-section) based on the evaluation of the printed prototypes. Helices based on PVA05GLY-ALP were printed at 190 °C requiring the use of raft and supports to avoid collapse of the incomplete item during deposition of successive layers. The printing speed was kept relatively low (23 mm/s) to avoid dragging of the latest layered material and reduce the vibrational stress undergone by the object

during fabrication, which could cause its detachment from the build plate. The temporary shape was obtained by manual supercoiling of the helices, thus decreasing their diameter and reducing the distance between the different windings. Virtual models of the original shape were developed starting from the helix design already proposed for the intravesical device. Having the average dimensions of the open pyloric sphincter as a reference, helices having diameter of 15 mm, height of 17 mm, number of windings of 1.5, thickness and height of the rectangular cross-section of 3 and 0.7 mm, respectively, were finally selected as a result of the trial-and-error design activity. Helix-shaped samples with these characteristics were identified as a satisfactory balance between encumbrance of the original configuration and mechanical resistance to undergo manual programming of a supercoiled temporary shape for insertion into capsules. In this respect, size AA DB capsules were selected as their internal diameter (approximately 9.4 mm) allowed the supercoiled helices to be housed. In Figure 4, virtual model and photographs of the selected 3D printed sample in the original and temporary shapes are reported. 4D printed systems had average weight of 571.70 mg (cv = 7.31) and drug load of 9.82% (cv = 4.06).

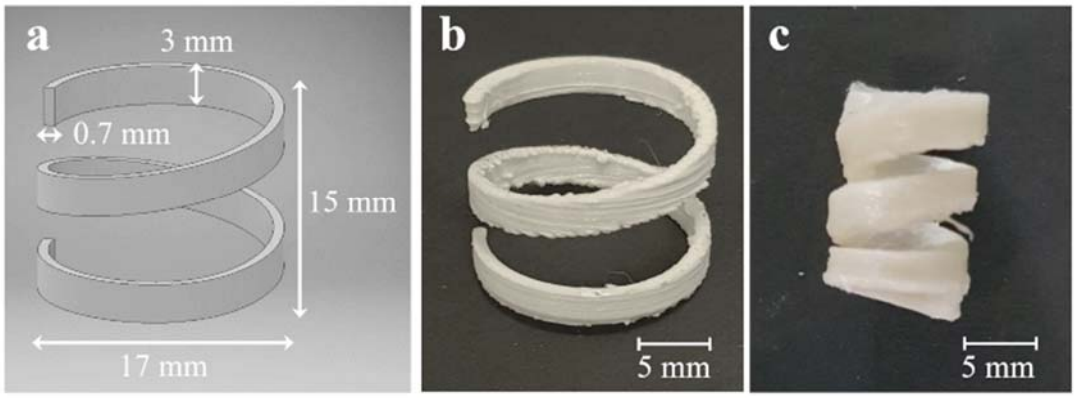

Figure 4: (a) Virtual model with dimensional details and photographs of a cylindrical helix-shaped sample printed from PVA05GLY-ALP in the (b) Original and (c) Temporary shape.

3.4 Performance of 4D printed prototypes

Evaluation of shape recovery and release testing of the printed items in the final configuration intended for oral intake (*i.e.* helices in their temporary shape, inserted into capsules) were carried out in acidic fluid. Photographs of a system maintained at 37 ± 0.5 °C time under unstirred conditions are reported in Table 2.

Immediately after immersion in HCl 0.1 N, the capsule began to soften. Breakup occurred on the capsule side and was complete in 3 min, in spite of a doubled wall thickness resulting from cap and body being overlapped. A major role of the pressure exerted by the helical device starting to expand was evident. In fact, analogous capsules filled with a blue powder tracer, tested under the same conditions, were shown to open in not less than 10 min, as highlighted by solvent staining. Moreover, when the capsule was ruptured and a wider exposure of the sample to the acidic medium was possible, shape modification occurred faster. This was expected due to the combined effect of temperature and water on the shape memory of PVA already investigated [1]. By visual inspection shape changes were no longer evident after 10 min, period of time during which extensive recovery of the original shape was achieved.

Table 2: Photographs acquired during shape recovery of a cylindrical helix-shaped sample printed from PVA05GLY-ALP, inserted into a DB capsule after programming of the temporary supercoiled shape.

				
t = 0	t = 90 s	t = 3 min	t = 5 min	t = 10 min

For release testing, systems conveyed within capsules were immersed free into the vessels, regardless their expected tendency to float, because the presence of any constraints (*e.g.* sinkers) might have impacted on shape recovery. Floating was indeed observed though helical devices were released from the capsules in a few minutes while expanding and sinking. Drug release from the 4D printed systems was sustained over 2 h (Figure 5).

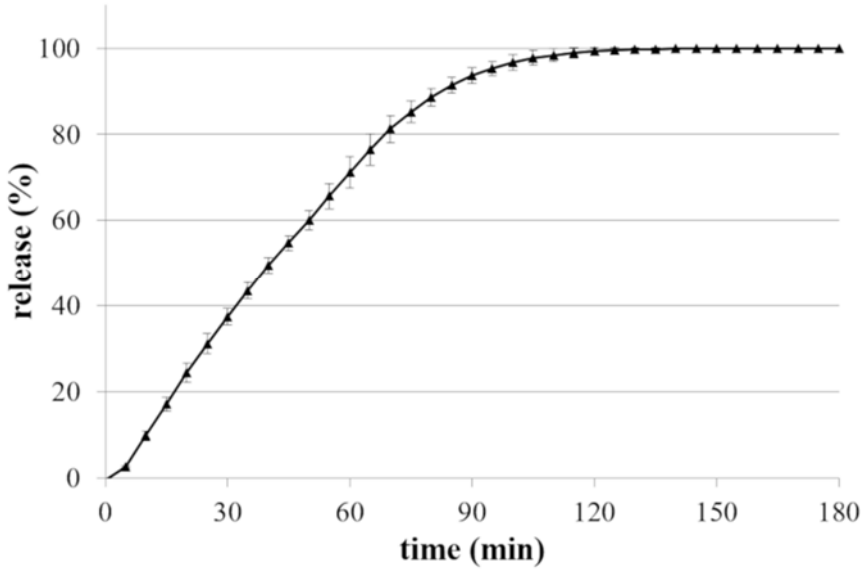

Figure 5: Average release profile from cylindrical helix-shaped samples printed from PVA05GLY-ALP, inserted into DB capsules after programming of the temporary supercoiled shape.

3.5 HME of prototypes

Given the promising results obtained using FDM, which is currently proposed for customization of delivery systems, SMX GRDDSs having different design, mechanical characteristics, duration of retention and release kinetics were worth investigating [39]. In this respect, a complete analysis of the thermo-mechanical behavior of PVA-based materials and devices through numerical simulations is ongoing. This approach would provide tools for the definition of the features of the system, reducing the number of experimental campaigns and the time as well as costs for testing. Starting from an empirical point of view, a simple approach was here adopted for the definition of further

shapes of the device. The production was based on HME as this technology can overcome limits observed when printing by FDM high-viscosity materials [1]. A higher molecular weight PVA, *i.e.* PVA18, was selected for the manufacturing of new prototypes, which would enable a better control of drug release rate.

The SMX GRDDS was conceived in different bulky original configurations, which could be achieved by post-processing of the extruded rod, *i.e.* by wrapping it around purposely-designed 3D printed templates of selected shapes. To simplify the experimental approach, all systems were obtained from a PVA18GLY-ALP rod of 1 mm in diameter. The method was inspired by that industrially used to produce corrugated breathing pipes *via* HME [40-43]. The designed templates involved different rod lengths to yield the original shapes, resulting in differing amounts of drug contained in samples of diverse shape. In this way, dose modification may also be pursued. Virtual models of templates and of items shaped by their use, *i.e.* cylindrical and conical helix-, S- and atom-shaped samples, are reported in Figure 6, together with photographs of the prototypes actually obtained. The design of templates was the challenging step. Templates were conceived to allow easy manual wrapping of the material coming out of the extruder. Accordingly, the dimensions of the groove were adjusted to enable effortless fitting of the rods. Moreover, when possible, a stem was included in the template to serve as a handle, thus facilitating wrapping operations. Size attributes imposed for the system were at least 2 dimensions > 20 mm and deformation to a temporary shape suitable for being contained in capsules not larger than the 00el ones (*i.e.* body external diameter = 8.18 mm and length of the closed capsule 25.3 mm). These were referred to as the standard size not to be exceeded for preserved patient acceptance and compliance [44,45].

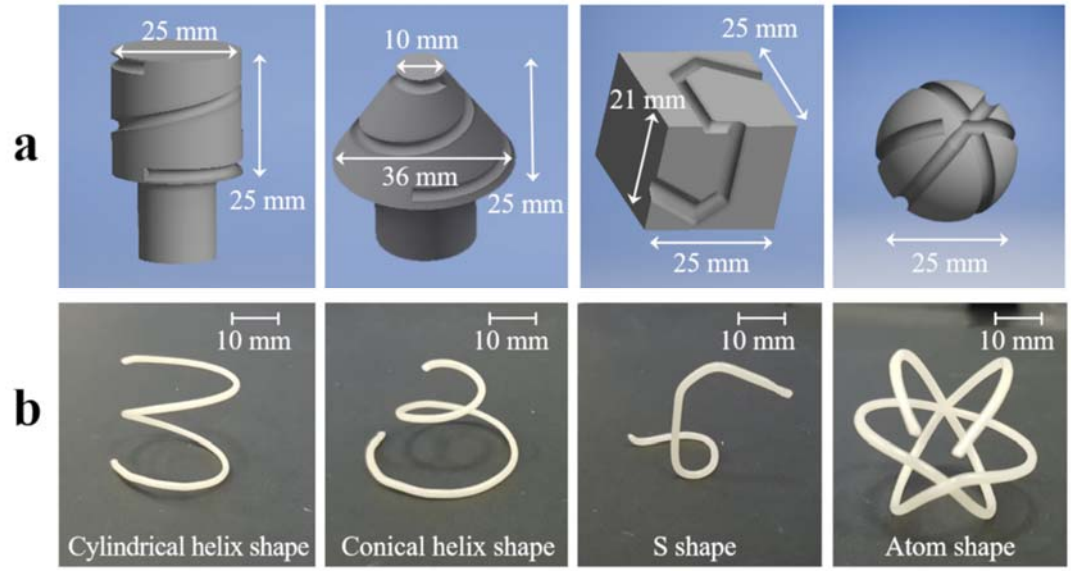

Figure 6: (a) Virtual models of templates and (b) Photographs of the samples obtained from cylindrical PVA18GLY-ALP rods of 1 mm in diameter.

In Table 3, the weight and ALP content data relevant to prototypes having different original configurations are reported. An amount of ALP consistent with the nominal one was measured from samples having different weights, thus confirming that no significant loss of drug occurred during HME. Moreover, weight variability of samples was reduced with respect to the printed items. This was partly attributed to the use of templates serving as a grid for wrapping and controlling the length of the rod.

Table 3: Weight and drug content of samples having different original shapes.

	weight mg (cv)	**ALP content** % on nominal (cv)
Cylindrical helix-shaped samples	300.07 (3.17)	98.8 (2.24)
Conical helix-shaped samples	298.62 (4.09)	99.3 (1.93)
S-shaped samples	140.87 (5.21)	99.1 (2.10)
Atom-shaped samples	401.87 (4.23)	99.6 (1.89)

Templates to be employed for programming the temporary shape of the prototypes under development were also designed and 3D printed. Virtual models of the latter and

photographs of samples deformed by their use are reported in Figure 7. With both conical and cylindrical helices, the same temporary shape, consisting in a supercoiled cylindrical helix, was used. On the other hand, S-shaped and atom-shaped samples were forced to take on paper clip and elliptical shapes, respectively. All these temporary shapes were demonstrated to fit into the 00el capsules (Figure 7c). Also in the programming step, the use of templates was proved useful to enhance the reproducibility of the process, making it less dependent on the operator.

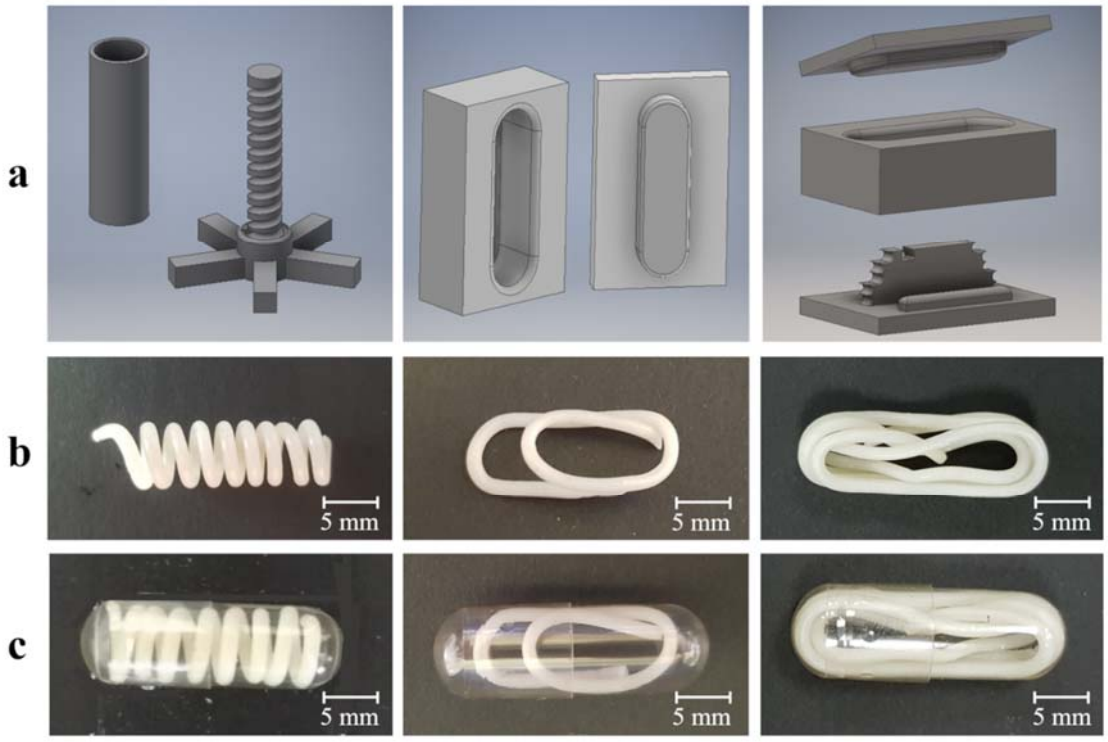

Figure 7: (a) Virtual models for templates used to program the temporary shape and (b) Photographs of the samples deformed by their use, obtained from PVA18GLY-ALP systems having different original shapes; (c) Photographs of the deformed samples inserted into size 00el Coni-Snap capsules.

3.6 Performance of extruded prototypes

Cylindrical and conical helix-, S- and atom-shaped samples in their original shape, along with cylindrical helix-shaped ones coated with Eudragit® RS/ Eudragit® RL 1/1, were evaluated for release (Figure 8).

From all the uncoated devices, similar release patterns were obtained, pointing out negligible role of the length. Drug release was prolonged for approximately 2 h. The release performance was not improved with respect to the printed PVA05-based specimens, despite the use of a higher molecular weight PVA. This was ascribed to the higher surface/volume ratio of the extruded systems (about 4 mm^{-1}) as compared with the printed ones (3.5 mm^{-1}). The selected die, resulting in relatively small size of the rod, was chosen in that it allowed a variety of temporary shapes to be easily obtained and compared.

The attempt to prolong the duration of release through application of an insoluble/permeable coating, such as resulting from the commonly used Eudragit® RS/ Eudragit® RL mixture, was proven effective, thus highlighting a possible formulation strategy worthy of further investigation.

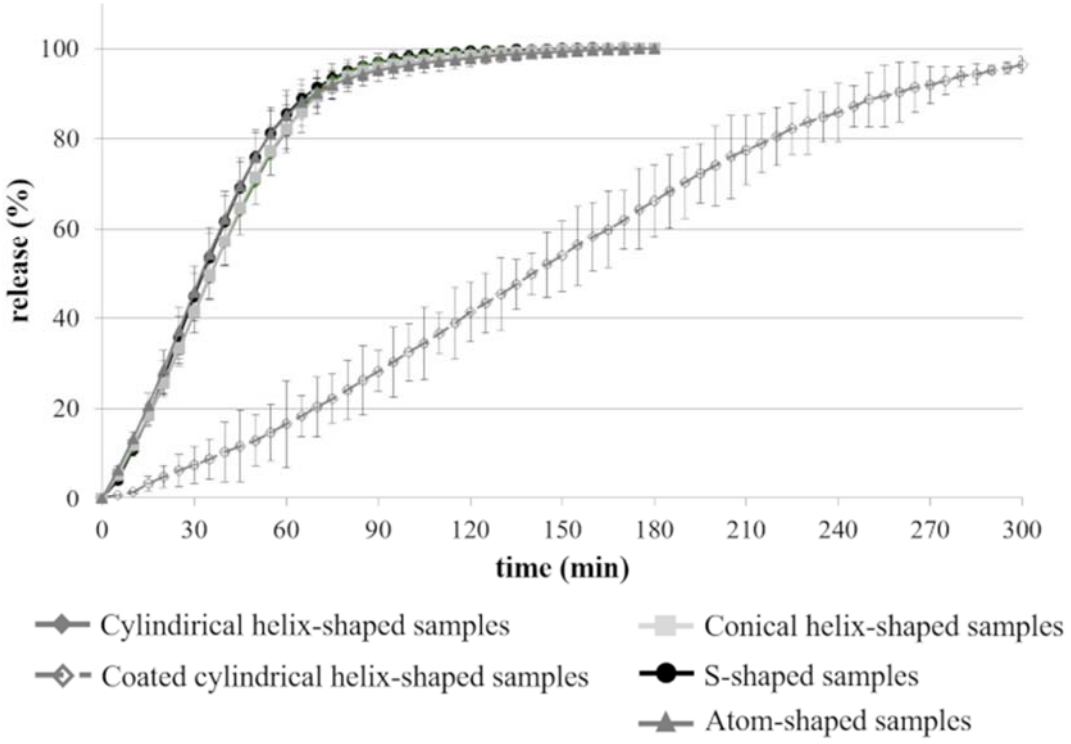

Figure 8: Average release profiles from coated and uncoated extruded PVA18GLY-ALP samples having different original shapes.

Further tests were performed with uncoated samples inserted into capsules. All the prototypes showed ability to recover the original shape except for the atom-shaped ones. This might be associated with the temporary shape imposed, characterized by many tight folds and thus involving longer lasting manual processing at the deformation temperature. As for the 4D printed prototypes, also the extruded systems showed the most marked changes in terms of shape recovery within the first minutes of testing. By way of example, photographs of a system having original conical helical shape, maintained at 37 ± 0.5 °C under unstirred conditions, are reported in Table 4. Breakup of the capsule occurred after 45 s. Also with extruded samples, the effect of the force exerted by the inner prototype while recovering its shape was evident. RI relevant to samples having conical and cylindrical helical shapes as well as S shape was also measured (Figure 9 and 10). In order to monitor increase in spatial encumbrance of the systems over time,

specific RIs were calculated for each shape. In all cases, exceeding dimensions of 13 mm was used as the criterion for acceptable shape recovery.

When dealing with conical and cylindrical helices, recovery of the initial diameter was considered the crucial step. In fact, the length of such items in the supercoiled temporary shape was already > 20 mm. A diameter greater than or equal to 13 mm, corresponding to a $RI_{Ø}$ of 41% and 23% for cylindrical and conical helices, respectively, was achieved in less than 2 min (Figure 9a and 9b). Moreover, the samples gained approximately 90% and 60% of their original diameter within 5 min of testing. The time for reaching the threshold dimension was relatively short, which could be attributed to the combined effect of temperature and fast water uptake of the systems. This was considered potentially suitable for addressing a major safety issue of expandable GRDDSs, connected with the time needed to achieve the bulky retentive configuration. Indeed, late expansion might result in small intestine location of the system with possible clogging of the canal, and also loss of the absorption window with consequent reduction of bioavailability.

To define the overall spatial encumbrance of the helices, $RI_{Ø/h}$ was also evaluated. Setting the diameter-to-height ratio of samples in their original shape equal to 100, cylindrical helices exhibited the ability to reach 77% of $RI_{Ø/h}$ in 5 min, while items with conical helical shape recovered about 60% in the same time frame.

Because recovery of S shape involved the opening of the temporary paper-clip configuration, it was evaluated by measuring three angles associated with xy, zx and yz planes, *i.e.* $\alpha_{xy,}$ $\alpha_{xz,}$ and α_{yz} (Figure 2c and Figure 10). For these systems, simultaneous widening of two angles would be sufficient to achieve size compatible with gastric retention. 43°, 33° and 32° were calculated to be the threshold limits for $\alpha_{xy,}$ $\alpha_{xz,}$ and α_{yz}, respectively. Such values were always reached within 5 min of testing and kept increasing. Evident changes were no longer recorded after 15 min. In this time frame, α_{xy} and α_{yz} achieved approximately 70% of recovery, while α_{xz} reached almost 90%. This could be associated with the possibility of the system to freely move in the xz plane, while the

opening of α_{xy} and α_{yz} might have been hindered by the sliding friction on the bottom surface of the crystallization vessel.

Evaluation of the shape memory performance was also carried out after storage of the prototype-containing capsules at ambient conditions for at least 1 month and no major changes were highlighted.

Release profiles of prototypes in their temporary shape, tested either free or inserted into capsules, were shown to be analogous to that of samples in their original shape, confirming the robustness of the SMX GRDDS under development.

As regards cylindrical helix-shaped samples provided with the Eudragit® RS/ Eudragit® RL coating, promising results were preliminary obtained demonstrating their capability of being programmed in the temporary supercoiled configuration, recovering the original shape upon contact with aqueous fluid at body temperature and slowly releasing the drug tracer over 6 h.

Table 4: Photographs acquired during shape recovery of a conical helix-shaped sample extruded from PVA05GLY-ALP, inserted into size 00el Coni-Snap capsule after programming of the temporary supercoiled shape.

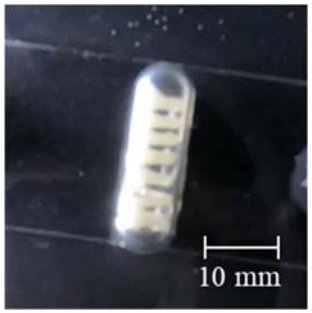				
t = 0	t = 45 s	t = 1 min and 30 s	t = 3 min	t = 5 min

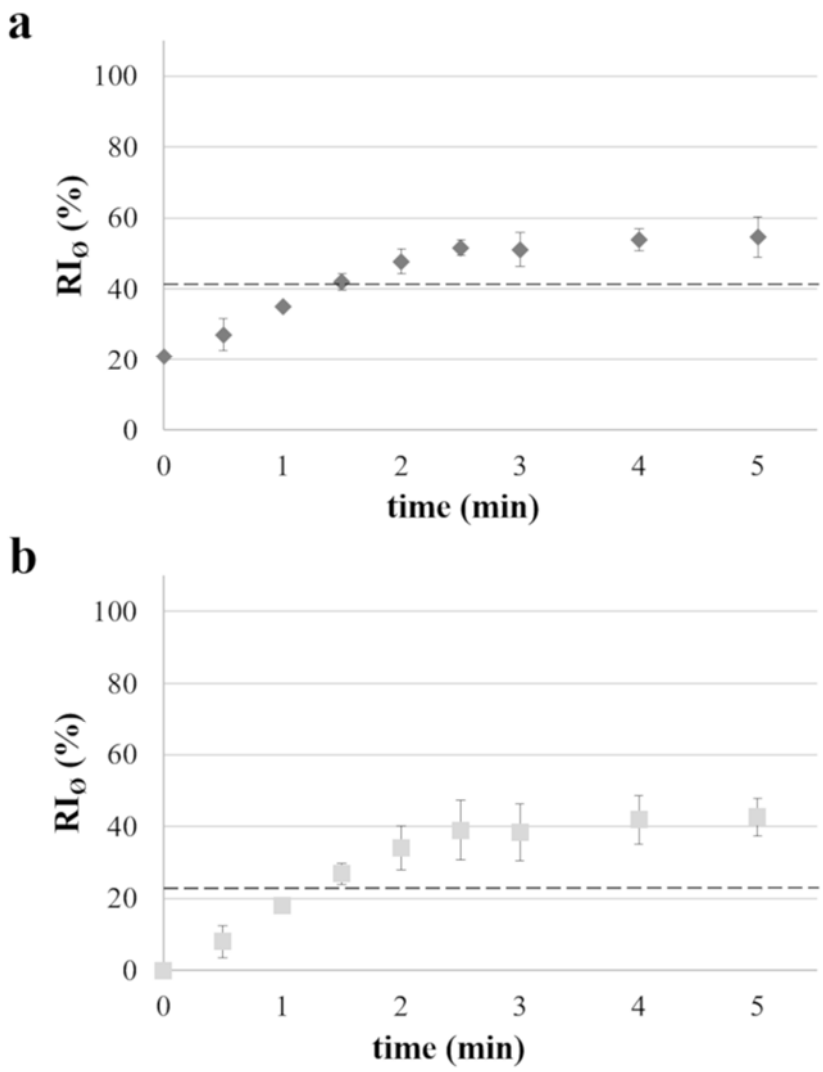

Figure 9: $RI_{Ø}$ versus time curves relevant to samples having original (a) Cylindrical and (b) Conical helical shapes. The dashed lines represent threshold $RI_{Ø}$.

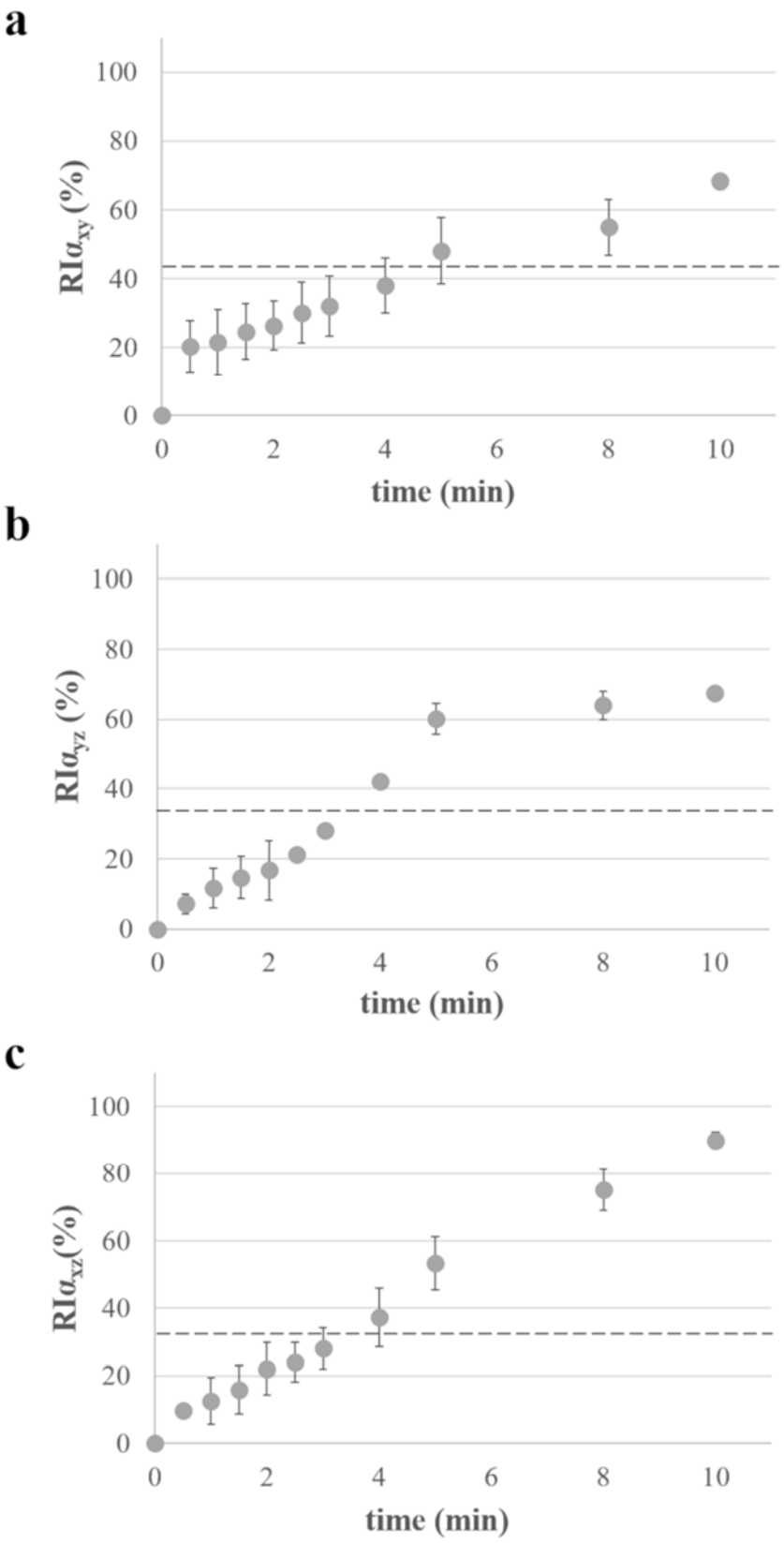

Figure 10: $RI_{\alpha(x,y,z)}$ *versus* time curves relevant to samples having original S shape. The dashed lines represent threshold $RI_{\alpha(x,y,z)}$.

4. Conclusions

In the present work, a novel expandable GRDDS was described. Gastric retention is of great interest in the case of drugs that are absorbed to a greater extent in the upper gastrointestinal tract or indicated for the therapy of widespread local diseases. Indeed, they would increase patient compliance because of reduced frequency of administration and enhance the therapy efficacy. The strategy here pursued was based on the use of pharmaceutical-grade PVA, which was already proved to be endowed with shape memory ability. This would allow the system to spontaneously shift from a temporary shape programmed by deformation, suitable for oral administration, to an expanded original one enabling gastric retention due to proper spatial encumbrance. The proposed device could thus be considered a shape-memory expandable GRDDS (SMX GRDDS). Because the relevant expansion mechanism is based on the combination of body temperature and contact with a minimum volume of fluids, the system may only poorly be susceptible to physiological variables of the gastric environment. Prototypes having different original shapes were successfully manufactured either directly by 4D printing or by manual processing of extruded rods. A quantitative method was set up to evaluate shape modifications undergone by extruded samples over time in unstirred acidic environment at 37 ± 0.5 °C. The temporary shape enabled, in all cases, insertion into commercial gelatin capsules of widely used sizes. A satisfactory extent of recovery of the original cylindrical and conical helix as well as S shapes was reached in a few minutes with respect to a previously set threshold value. Shape changes imposed through heating and mechanical deformation were demonstrated not to impact on the release performance of prototypes. However, the timescale of the release process was found to be an issue, in view of the longer-lasting performance that is known to be required for GRDDSs. In this respect, the application of a diffusive polymeric film onto cylindrical extruded helices was demonstrated a suitable formulation approach to prolong release over 6 h.

In future development studies, further improvement of the duration of release could be pursued primarily entailing selection of different release-controlling coating

formulations, of PVAs with higher molecular weights or else of different shape memory polymers. Moreover, modification in the overall surface/volume ratio of the device and changes in the length of extruded rods to increase the drug load will be taken into account. In this respect, the versatility that the manufacturing approach would provide could be advantageous. An in-depth evaluation of the mechanical behavior of the system and the contribution of temperature and amount of water on its expansion will also be performed.

References

1. A. Melocchi, N. Inverardi, M. Uboldi, F. Baldi, A. Maroni, S. Pandini, F. Briatico-Vangosa, L. Zema, A. Gazzaniga, Retentive device for intravesical drug delivery based on water-induced shape memory response of poly(vinyl alcohol): design concept and 4D printing feasibility, Int. J. Pharm. 559 (2019) 299-311.
2. D. H. Altreuter, A. R. Kirtane, T. Grant, C. Kruger, G. Traverso, A. M. Bellinger, Changing the pill: developments toward the promise of an ultra-long-acting gastroretentive dosage form, Expert Opin. Drug Deliv. 15 (2018) 1189-1198.
3. P. L. Bardonnet, V. Faivre, W. J. Pugh, J. C. Piffaretti, F. Falson, Gastroretentive dosage forms: overview and special case of Helicobacter pylori, J. Control Release 111 (2006) 1-18.
4. R. Gupta, P. Tripathi, P. Bhardwaj, A. Maho, Recent advances in gastro retentive drug delivery systems and its application on treatment of H. Pylori infections, J. Anal. Pharm. Res. 7 (2018) 404-410.
5. M. Kumar, D. Kaushik, An overview on various approaches and recent patents on gastroretentive drug delivery systems, Recent Pat. Drug Deliv. Formul. 12 (2018) 84-92.
6. C. M. Lopes, C. Bettencourt, A. Rossi, F. Buttini, P. Barata, Overview on gastroretentive drug delivery systems for improving drug bioavailability, Int. J. Pharm. 510 (2016) 144-158.
7. J. Chen, W. E. Blevins, H. Park, K. Park, Gastric retention properties of superporous hydrogel composites, J. Control Release 64 (2000) 39-51.
8. E. A. Klausner, E. Lavy, M. Borta, E. Cserepes, M. Friedman, A. Hoffman, Novel gastroretentive dosage forms: evaluation of gastroretentivity and its effect on levodopa absorption in humans, Pharm. Res. 20 (2003) 1466-1473.
9. E. A. Klausner, E. Lavy, M. Friedman, A. Hoffman, Expandable gastroretentive dosage forms, J. Control. Release 90 (2003) 143-162.

10. H. Omidian, J. G. Rocca, K. Park, Advances in superporous hydrogels, J. Control Release 102 (2005) 3-12.
11. S. Verma, K. Nagpal, S. K. Singh, D. N. Mishra, Unfolding type gastroretentive film of Cinnarizine based on ethyl cellulose and hydroxypropylmethyl cellulose, Int. J. Biol. Macromol. 64 (2015) 347-352.
12. A. M. Bellinger, M. Jafari, T. M Grant., S. Zhang, H. C. Slater, E. A. Wenger, S. Mo, Y. -A. L. Lee, H. Mazdiyasni, L. Kogan, R. Barman, C. Cleveland, L. Booth, T. Bensel, D. Minahan, H. M. Hurowitz, T. Tai, J. Daily, B. Nikolic, L. Wood, P. A. Eckhoff, R. Langer, G. Traverso, Oral, ultra-long-lasting drug delivery: application toward malaria elimination goals, Sci. Transl Med. 8 (2016) 1-12.
13. A. R. Kirtane, O. Abouzid, D. Minahan, T. Bensel, A. L. Hill, C. Selinger, A. Bershteyn, M. Craig, S. S. Mo, H. Mazdiyasni, C. Cleveland, J. Rogner, Y. -A. L. Lee, L. Booth, F. Javid, S. J. Wu, T. Grant, A. M. Bellinger, B. Nikolic, A. Hayward, L. Wood, P. A. Eckhoff, M. A. Nowak, R. Langer, G. Traverso, 2018, Development of an oral once-weekly drug delivery system for HIV antiretroviral therapy, Nat. Commun. 9 (2018) 2.
14. J. Liu, Y. Pang, S. Zhang, C. Cleveland, X. Yin, L. Booth, J. Lin, L. Y. -A. Lee, H. Mazdiyasni, S. Saxton, A. R. Kirtane, T. V. Erlach, J. Rogner, R. Langer, G. Traverso, Triggerable tough hydrogels for gastric resident dosage forms, Nat. Commun. 8 (2017) 124.
15. X. Liu, C. Steiger, S. Lin, G. A. Parada, J. Liu, H. F. Chan, H. Yuk, N. V. Phan, J. Collins, S. Tamang, G. Traverso, X. Zhao, Ingestible hydrogel device, Nat. Commun. 10 (2019) 493.
16. R. C. R. Beck, P. S. Chaves, A. Goyanes, B. Vukosavljevic, A. Buanz, M. Windbergs, A. W. Basit, S. Gaisford, 3D printed tablets loaded with polymeric nanocapsules: An innovative approach to produce customized drug delivery systems, Int. J. Pharm. 528 (2017) 268-279.

17. N. Genina, J. P. Boetker, S. Colombo, N. Harmankaya, J. Rantanen, A. Bohr, Anti-tuberculosis drug combination for controlled oral delivery using 3D printed compartmental dosage forms: From drug product design to in vivo testing, J. Control. Release 268 (2017) 40-48.
18. A. Goyanes, M. Kobayashi, R. Martínez-Pacheco, S. Gaisford, A. W. Basit, Fused-filament 3D printing of drug products: Microstructure analysis and drug release characteristics of PVA-based caplets, Int. J. Pharm. 514 (2016) 290-295.
19. G. Kollamaram, D. M. Croker, G. M. Walker, A. Goyanes, A. W. Basit, S. Gaisford, Low temperature fused deposition modeling (FDM) 3D printing of thermolabile drugs, Int. J. Pharm. 545 (2018) 144-152.
20. G. Loreti, A. Maroni, M. D. Del Curto, A. Melocchi, A. Gazzaniga, L. Zema, Evaluation of hot-melt extrusion technique in the preparation of HPC matrices for prolonged release, Eur. J. Pharm. Sci. 52 (2014) 77-85.
21. A. Maroni, A. Melocchi, F. Parietti, A. Foppoli, L. Zema, A Gazzaniga, 3D printed multi-compartment capsular devices for two-pulse oral drug delivery, J. Control. Release 268 (2017) 10-18.
22. G. Matijašić, M. Gretić, J. Vinčić, A. Poropat, L. Cuculić, T. Rahelić, Design and 3D printing of multi-compartmental PVA capsules for drug delivery, J. Drug Deliv. Sci. Technol. 52 (2019) 677-686.
23. A. Melocchi, F. Parietti, G. Loreti, A. Maroni, A. Gazzaniga, L. Zema, 3D printing by fused deposition modeling (FDM) of a swellable/erodible capsular device for oral pulsatile release of drugs, J. Drug Deliv. Sci. Technol. 30 Part B (2015) 360-367.
24. A. Melocchi, G. Loreti, M. D. Del Curto, A. Maroni, A. Gazzaniga, L. Zema, 2015, Evaluation of hot-melt extrusion and injection molding for continuous manufacturing of immediate-release tablets, J. Pharm. Sci. 104 (2015) 1971-1980.
25. A. Melocchi, F. Parietti, S. Maccagnan, M. A. Ortenzi, S. Antenucci, F. Briatico-Vangosa, A. Maroni, A. Gazzaniga, L. Zema, Industrial development of a 3D-

printed nutraceutical delivery platform in the form of a multicompartment HPC capsule, AAPS PharmSciTech. 19 (2018) 3343-3354.

26. B. Gao, Q. Yang, X. Zhao, G. Jin, Y. Ma, F. Xu, 4D bioprinting for biomedical applications, Trends Biotechnol. 34 (2016) 746-756.
27. A. Y. Lee, J. An, C. K. Chua, Two-way 4D printing: a review on the reversibility of 3D-printed shape memory materials, Eng. 3 (2017) 663-674.
28. M. Zarek, M. Layani, I. Cooperstein, E. Sachyani, D. Cohn, S. Magdassi, 3D printing of shape memory polymers for flexible electronic devices, Adv. Mater. 28 (2015) 4449-4454.
29. M. Zarek, N. Mansour, S. Shapira, D. Cohn, 4D Printing of shape memory-based personalized endoluminal medical devices, Macromol. Rapid Commun. 38 (2017) 1600628.
30. Z. Ding, C. Yuan, X. Peng, T. Wang, H. J. Qi, M. L. Dunn, Direct 4D printing via active composite materials, Sciences Adv. 3 (2017) e1602890-e1602896.
31. W. M. Huang, Z. Ding, C. C. Wang, J. Wei, Y. Zhao, H. Purnawali, Shape memory materials, Mater. Today 13 (2010) 54-61.
32. M. Maniruzzamann, 3D and 4D printing in biomedical applications: process engineering and additive manufacturing, Weinheim Ed., Wiley VCH (2018) Weinheim, D.
33. https://www.drugbank.ca/drugs/DB00437, last access on July 15, 2019.
34. A. Melocchi, F. Parietti, A. Maroni, A. Foppoli, A. Gazzaniga, L. Zema, Hot-melt extruded filaments based on pharma-grade polymers for 3D printing by fused deposition modeling, Int. J. Pharm. 509 (2016) 255-263.
35. H. Jaeger, D. Russmann, J. Rasper, J. Blome, Comparative study of the bioavailability and the pharmacodynamic effect of five allopurinol preparations, Arzneimittelforschung, 32 (2017) 438-443.
36. N. Rouge, P. Buri, E. Doelker, Drug absorption sites in the gastrointestinal tract and dosage forms for site-specific delivery, Int. J. Pharm. 136 (1996) 117-139.

37. O. P. Sharma, M. V. Shah, D. C. Parikh, T. A. Mehta, Formulation optimization of gastroretentive drug delivery system for allopurinol using experimental design, Expert Opin. Drug Deliv. 12 (2015) 513-524.

38. M. Mohsin, A. Hossin, Y. Haik, Thermal and mechanical properties of poly(vinyl alcohol) plasticized with glycerol, J. Appl. Polym. Sci. 122 (2011) 3102-3109.

39. L. Zema, A. Melocchi, A. Maroni, A. Gazzaniga, 3D printing of medicinal products and the challenge of personalized medicine, J. Pharm. Sci. 106 (2016) 1697-1705.

40. H. Chan, B. Yi, Pipe extrusion die with a cooled and vacuumed additional mandrel, 2019, Patent number: 4,808,098

41. A. E. Kolosov, A. S. Sakharov, D. E. Sidorov, V. I. Sivetskii, Aspects of profile shaping of corrugated tubular components. Part 3. Extrusion shaping of tubular polymeric blanks for manufacture of corrugated pipes, Chem. Pet. Eng. 48 (2012) 199-206.

42. D. E. Sidorov, V. I. Sivetskii, A. E. Kolosov, A. S. Sakharov, Shaping of corrugation profiles during production of corrugated tubular articles, Chem. Pet. Eng. 48 (2012) 384-390.

43. G. S. Sutton, D. J. Kelley, R. A. Kolbet, Systems and methods for making multi-wall corrugated pipe, (2010), Patent number: US 2010/022430.6 A1

44. https://www.fda.gov/downloads/drugs/guidances/ucm377938.pdf, last access on July 15, 2019.

45. https://unitaid.org/assets/Lyndra-NC-September-2018.pdf, last access on July 15, 2019.

Chapter II

The content of Chapter II has already been published in: J. Mech. Behav. Biomed. Mater. 124 (2021) 104814.

EXPERIMENTAL AND COMPUTATIONAL ANALYSIS OF A PHARMACEUTICAL-GRADE SHAPE MEMORY POLYMER APPLIED TO THE DEVELOPMENT OF GASTRORETENTIVE DRUG DELIVERY SYSTEMS

Abstract

The present paper aims at developing an integrated experimental/computational approach towards the design of shape memory devices fabricated by hot-processing with potential for use as gastroretentive drug delivery systems (DDSs) and for personalized therapy if 4D printing is involved. The approach was tested on a plasticized poly(vinyl alcohol) (PVA) of pharmaceutical grade, with a glass transition temperature close to that of the human body (*i.e.* 37 °C).

A comprehensive experimental analysis was conducted in order to fully characterize the PVA thermo-mechanical response as well as to provide the necessary data to calibrate and validate the numerical predictions, based on a thermo-viscoelastic constitutive model, implemented within a finite element framework. Particularly, a thorough thermal, mechanical, and shape memory characterization under different testing conditions and on different sample geometries was first performed. Then, a prototype consisting of an S-shaped device was fabricated, deformed in a temporary compact configuration and tested. Simulation results were compared with the results obtained from shape memory experiments carried out on the prototype. The proposed approach provided useful results and recommendations for the design of PVA-based shape memory DDSs.

Keywords: shape memory polymers, drug delivery systems, expandable gastroretentive drug delivery systems, constitutive modeling, poly(vinyl alcohol).

1. Introduction

Shape memory polymers (SMPs) have been widely employed in the biomedical field, due to their capability to be stored and delivered to the patient in a temporary compact shape and to revert, as a consequence of the application of a triggering stimulus, to a deployed permanent shape, which should be functional to a specific need [1]. They have been mainly proposed and patented for the development of medical devices for minimally-invasive surgery, *e.g.* self-tightening sutures [2,3], self-expandable biodegradable stents [4], thrombectomy devices [5] and embolization plugs [7-9]. More recently, SMPs have been exploited also in the fields of tissue engineering and biomanufacturing in order to obtain both self-deploying grafts [10,11] and to provide dynamic scaffolds for cell culture with a topological control based on the shape evolution of the substrate [12-14].

On the other hand, the use of SMPs for the development of drug delivery systems (DDSs) has been proposed only in few pioneering works [15-19]. In general, promising applications of shape memory materials in the drug delivery field are those for which a shape evolution is essential for different purposes, mainly to ensure retention of the DDS in a targeted organ so as to *i)* increase the bioavailability of the conveyed drug, *ii)* treat local diseases, and *iii)* prolong the drug release in order to reduce the dosing frequency and consequently increase patient adherence to the therapeutic regimen [20-23]. Thanks to the development of 4D printing concept, *i.e.* 3D printing of stimulus responsive materials (including SMPs), the use of SMPs has recently gained further attention in the pharmaceutical field [24], since it enables the fabrication of devices with complex design, capable of shape-shifting over time under the application of an external non mechanical stimulus. In this respect, also the shape memory effect exhibited by a commercially available poly(vinyl alcohol) (PVA) of pharmaceutical grade may be effective, especially in view of its safety and established use. PVA is a water-soluble synthetic polymer, commonly used as excipient in the preparation of cosmetics and medicines (JPE 2018, Ph. Eur. 10th Ed., USP-NF 2021). The production of high-purity pharmaceutical-grade PVA follows the rule of the current good manufacturing practices (cGMPs) and the

resulting product is compliant with the requirements of various official compendia (JPE 2018, Ph. Eur. 10th Ed., USP-NF 2021), thus being suitable for the formulation of pharmaceutical products [25].

In particular, PVA has a very low oral acute toxicity and, when orally administered, does not accumulate in the body, being also very poorly absorbed by the gastrointestinal tract [26,27]. Furthermore, due to its chemical composition, the shape memory behavior of PVA can be triggered by the exposure to direct heating [28], indirect heating (*e.g.* microwave [29,30], Joule heating [31]), water [32-37] and, in some cases, also light [38]. The multiple actuation stimuli suitable for PVA, in addition to its biocompatibility, make this polymer a promising candidate for shape memory applications in the biomedical and pharmaceutical field involving contact with human body, where heating of even few degrees above the body temperature may cause damages to surrounding tissues [39].

The great potential of PVA towards 4D printing technology has been recently proved in companion papers [40,41]. Here, the shape memory effect of a commercial PVA of pharmaceutical grade was first leveraged for the development of an intravesical retentive drug delivery platform [40]. Furthermore, prototypes of a PVA-based gastroretentive DDS were developed via hot melt extrusion and 3D printing [41], which needed to fulfil different constraints regarding the way of administration depending on the target organ (*i.e.* via the oral route with a gelatin capsule for the gastroretentive DDS *vs* through catheterization for the intravesical platform).

The gastroretentive DDS were conceived with *i)* a permanent shape with spatial encumbrance suitable for the retention in the stomach (*i.e.* cylindrical and conical helices and S-shape) and *ii)* a temporary shape compliant with oral administration in a size 00el hard-gelatin capsule (*i.e.* a supercoiled helix and a paper-clip shape). In particular, gastric retention would be ensured by designing a permanent shape with at least two dimensions bigger than 11-13 mm, which is considered the average dimension of the wide open pylorus [42,43]. Conversely, the dimensions of the commercially available size 00el capsule (*i.e.* diameter of about 8.18 mm and closed length of 25.3 mm) were used as

reference for the development of the temporary shape. Indeed, this capsule size is one of the biggest approved, which still provides a comfortable oral administration from the patient perspective [20,44]. The recovery of the permanent shape at body temperature was then studied in simulated gastric fluid. This study [41] was focused on pharmaceutical and technological issues. In fact, the selection of the proper formulation was not trivial as the choice of the active ingredient needed to fulfil different constraints related to *i)* the thermal stability of the drug for the high-temperature processing techniques employed and *ii)* its relevance for use in a gastroretentive system. Additionally, the manufacturing of the formulation was optimized and addressed with different techniques.

Despite the good results obtained in these companion papers [40,41], an effort still has to be made towards a comprehensive experimental and theoretical approach in order to conveniently make use of the shape memory response of pharmaceutical grade PVAs for the design of smart DDSs. More specifically, the availability of a theoretical and computational framework to speed up product development, thus avoiding costly experiments, would be highly useful.

The present work aims at exploring the possibility of supporting the design phase of DDSs relying on the shape memory response of PVA by means of a computer-aided modeling activity implemented within a finite element analysis framework. The prototype here investigated is the S-shaped device already presented in the companion paper by the same authors [41].

To date, several constitutive models have been proposed for the analysis and simulation of the shape memory effect of different polymers (see [45]), including thermo-viscoelastic [46-54] and phase transition [55-60] approaches.

The three-dimensional generalized Maxwell thermo-viscoelastic model was here adopted and applied to describe the behavior of the selected PVA. The choice of dealing with such a model is motivated by the fact that it is largely employed to describe the behavior of SMPs processed by means of either traditional techniques or 4D printing [52,61-64] and its parameters can be all identified based on experimental tests. In particular, the

calibration approach proposed by Diani and colleagues was here explored and discussed, which consisted in determining the time-temperature dependence of the viscoelastic properties of the polymer under investigation by using a dynamic mechanical analysis procedure without the need for shape memory cycling [62].

From the reviewed literature, it may be noted that most of the current works regarding SMPs focuses on one or more of the following topics: *i)* chemical synthesis to address peculiar shape memory effects [33,65-70], *ii)* processing and fabrication studies involving new fabrication routes (*e.g.* multi-material 3D printing, electrospinning) [72-75], *iii)* thermo-mechanical characterization and development of new constitutive models [45,53,55,76-78], iv) application of the shape memory effect to prototypes/functional devices [8,9,11,64,79,80]. In this paper, we focused on a new design concept related to a novel application identified in the drug delivery field. Therefore, a comprehensive set of experiments was carried out in order to gather the data required for the characterization of the thermo-mechanical behavior of the material and for the calibration and validation of the adopted model.

The paper is organized as follows: *i)* Section 2 covers all the details regarding the experimental activities and the basis of the modeling approach, *ii)* Section 3.1 contains the thermo-mechanical data required for the model, *iii)* Section 3.2 describes other thermo-mechanical data useful for understanding the shape memory response of the material, *iv)* Section 3.3 deals with the shape memory behavior of PVA-based specimens, *v)* Section 3.4 illustrates the model validation and its implementation on experimental data, and *vi)* Section 3.5 is focused on the behavior of the final prototype.

2. Experimental

2.1 Materials

A plasticized polymeric formulation was prepared by blending a PVA of a specific grade (PVA18; viscosity 18 mPas; Gohsenol™ EG 18P, Nippon Gohsei, J) with glycerol (GLY;

Pharmagel, I), followed by grinding of the mixture by a blade mill and recovering the powder fraction with dimension < 250 μm.

The specimens were obtained by hot melt extrusion with a twin-screw extruder (Haake™ MiniLab II, Thermo Scientific, US-WI) equipped with counter-rotating screws and different dies.

Bars and rods of 50 mm in length were obtained by cutting from samples extruded through a rectangular cross-section (5 x 2 mm2) die and a custom-made aluminum circular (ø = 1 mm) one, respectively. Further information concerning the formulation and process parameters can be found in companion papers (bars [40]; rods [41]).

2.2 Study design

The motivation for this research stems from the tremendous research efforts currently being pursued in the materials science and manufacturing fields towards the aim of designing active materials and structures capable of functional shape changes in an autonomous and untethered way, that is of utmost importance for several challenging applications in which external and non-mechanical actuation of a device is desirable. The relevance of this topic is of peculiar importance in the biomedical and drug delivery field, as highlighted in recent editorials, review papers and book chapters [23,24,81] which underline how programmable/active and untethered materials hold great promise for delivering drugs inside the human body in an autonomous fashion.

The goal of this study was to develop and characterize a self-expandable gastroretentive drug delivery device by taking into account the inherent shape-recovery capability of SMPs. In fact, the shape memory effect reveals to be useful to such an aim, by leveraging the possibility of programming a temporary shape, which can be fitted inside a commercially available capsule, and exploiting the recovery of the permanent shape upon exposure to the physiological conditions in the stomach to achieve a bulky configuration capable to be retained in the organ.

This objective was addressed by making use of an SMP of pharmaceutical grade and by applying *i)* a comprehensive thermo-mechanical characterization and *ii)* a computational activity based on a widely used constitutive model implemented in a commercial finite element modeling framework.

More in details, a pharmaceutical formulation was selected, composed of a semi-crystalline SMP (*i.e.* PVA of pharmaceutical grade) and a plasticizer (*i.e.* glycerol), with the possibility of loading also an active ingredient (*i.e.* allopurinol). Given the heterogeneous nature of this formulation, which does not represent the standard macromolecular architecture peculiar of SMPs, a comprehensive thermo-mechanical characterization was first performed, consisting of both *i)* preliminary and well-established testing protocols to identify the shape memory effect and *ii)* more complex experimental methods, purposely set up in order to characterize thermo-mechanical features relevant for this specific novel application. To the first aim and specifically to identify the not-a priori known properties for shape memory testing (such as the accessible temperature window), we used widely employed methods [82-84] based on differential scanning calorimetry and single-frequency dynamic mechanical analysis, mechanical testing under uniaxial conditions, and shape memory protocols involving programming of a temporary shape and thermally stimulated recovery of the permanent one. In addition, ad hoc testing protocols were set-up to characterize the material towards the novel application identified in the drug delivery field. We employed multi-frequency dynamic mechanical analysis to gain insight into the viscoelasticity of the material and its relaxation behavior as a function of frequency and time. Results were used to gain insight into the relaxation behavior as a function of time of the material prototype which will be constrained in the capsule in its temporary shape, for different storage temperatures (*i.e.* room temperature, 25 °C, and a temperature characteristic of cold storage, -15 °C). To complete the shape memory characterization, we designed specific testing protocols performed on material specimens to study the effect of a prolonged strain on the shape memory performances under different deformation conditions and triggered either by

thermally stimulated recovery or under isothermal conditions. This non-conventional testing method reveals useful to approximate the effect of the constraint exerted by the capsule on the prototype in its temporary shape on the final shape memory performances. Then, the results of the conducted thermo-mechanical characterization allowed us to generate input data useful for the calibration of the chosen model (the generalized Maxwell model) which approximates the material as composed by several Maxwell elements (a series of viscous dampers and elastic springs) arranged in parallel. We chose this model, instead of formulating new constitutive equations, due to its versatility in catching the shape memory effect in polymers with a limited number of physical parameters. However, a careful investigation concerning both the calibration and validation of this model still needs to be performed in the current literature for the specific material formulation (composed of a semi-crystalline SMP and a plasticizer). The conducted investigation is helpful in providing new insights concerning the application of the chosen constitutive model to this pharmaceutical formulation to support the design of new delivery systems in the near future.

2.3 Mechanical and thermal analysis

An extensive investigation of the mechanical and thermal behavior of PVA18 was performed in order to address the shape memory characterization of the material and understand its shape memory response, as well as to collect useful data for constitutive modeling and numerical simulations.

Dynamic mechanical thermal analyses (DMTA) were performed on extruded bars by using a DMA Q800 (TA Instruments) in tensile conditions under strain control (gauge length: 10-15 mm), according to single-frequency and multiple-frequency approaches. The former consists in applying an oscillating displacement (10 μm of amplitude) at 1 Hz scanning a region from -50 °C to 200 °C with a heating rate of 3 °C/min. The maximum heating temperature was chosen equal to the processing temperature and evaluated as safe because no signs of material degradation occurred neither in the differential scanning

calorimetry analysis later describer nor in preliminary thermogravimetric analysis additionally performed, which showed onset of degradation above 250 °C. In the latter, a displacement amplitude of 15 μm (*i.e.* within the linear viscoelasticity region) was applied scanning a region from -50 °C to 160 °C at 0.5 °C/min with a sweep at a discretized set of frequencies (100Hz, 60Hz, 40Hz, 30Hz, 20Hz, 10Hz, 6Hz, 4Hz, 3Hz, 2Hz, 1Hz, 0.6Hz, 0.4Hz). In both cases, a 0.01 N pre-load force was applied.

Quasi-static mechanical tests were carried out both under tensile and compressive conditions above the glass transition temperature (T_g), *i.e.* in the rubber-like region. Tensile tests were carried out on extruded bars (gauge length: 10 mm) at 60 °C by using a DMA Q800 (TA Instruments) at a ramp force of 1 N/min up to the maximum load allowed (18 N). Compression tests were carried out at 60 °C by means of an electromechanical dynamometer (Instron Mod. 3366) on samples cut from the bars and tested through their thickness (cross-section: 5x5 mm2), with a crosshead speed equal to 0.5 mm/min.

Differential Scanning Calorimetry (DSC) analyses were carried out by means of a DSC Q100 (TA Instruments) on specimen slices of about 10 mg. The tests were carried out with the use of nitrogen as purge gas and under the following thermal program: heating from -50 °C to 240 °C at 10 °C/min; cooling from 240 °C to -50 °C at 10 °C/min; second heating from -50 °C to 240 °C at 10 °C/min.

2.4 Shape memory tests

The shape memory characterization was carried out as a function of both temperature and time. The tests consisted of a two-step thermomechanical history: *i)* an initial so-called "programming" step by which a temporary shape was imposed, followed by *ii)* a subsequent recovery step. The thermo-mechanical histories were designed on the basis of DSC and DMTA results, which highlighted a T_g of the material close to 30 °C (see Section 3.2).

Programming of the temporary shape was carried out according to the thermomechanical history described in Section 2.4.1. The recovery performance was studied under heating ramps, according to the protocol of the so-called "Thermally stimulated recovery" (TSR) (see Section 2.4.2), and as a function of time in isothermal recovery tests (see Section 2.4.3). In addition to the conventional programming history, also a programming history including a stress relaxation step was explored (see Section 2.4.4).

The tests were performed both on extruded bars and rods, using the bars for the TSR tests, since they provided a more efficient grip with the DMA fixture, and rods for the isothermal tests, as they have the same cross-section adopted for the prototypal device (see Section 2.4.5), whose recovery occurred under isothermal conditions.

Moreover, the shape memory behavior was studied on the extruded prototypal device as described in Section 2.4.5.

2.4.1 Programming

The programming step was carried out under the following heating/cooling history, based on the T_g of the material: *i)* heating at 60 °C (*i.e.* approximately T_g + 30 °C), kept at least for 10 minutes to allow the sample to equilibrate, *ii)* application of a specific deformation, *iii)* cooling well below T_g (about -20 °C) while keeping the imposed temporary shape, *iv)* storage at -20 °C until the application of the recovery step.

Two main deformation conditions were applied in the programming step:

i) tensile deformation: a ramp force was applied at 1 N/min through the dynamic mechanical analyzer DMAQ800 at 60 °C up to the maximum load allowed (18N);

ii) U-folding: this was applied on the straight I-shaped specimens so as to obtain a U-shaped temporary shape by using a properly built fixture.

2.4.2 Thermally Stimulated Recovery tests

Thermally stimulated recovery (TSR) tests were carried out on previously programmed samples to investigate the shape memory behavior of the material as a function of

temperature. A recovery ratio index (RI) was defined to assess the shape recovery performance.

TSR tests consisted in a controlled heating ramp. Both the definition of RI and testing conditions depend on the deformation conditions applied during programming, as here outlined:

i) tensile deformation: the programmed bars were subjected to a heating ramp from -20 °C to 100 °C at 0.5 °C/min, under the application of a small load (0.005 N) to continuously monitor the specimen length. The test was carried out in the DMA Q800 under tensile conditions and the recovery index for tensile shape memory characterization ($RI_{tensile}$) was defined as follows:

$$RI_{tensile} = \frac{l - l_{prog}}{l_0 - l_{prog}} \quad \text{(Eq. 1)}$$

where l_0 is the original length of the specimen, l_{prog} is the length after the programming step, and l is the actual length of the specimen; all length measurements were acquired directly by the DMA optical encoder.

ii) U-folding: the folded bars were tested in a lab oven, by placing the U-shaped sample with one half fixed to the oven plate and leaving the other half free to move. The applied heating ramp ranged from 20 °C to 100 °C (with the preliminary test run up to 180 °C) at about 0.5 °C/min, measuring the temperature with a thermocouple placed near the sample and monitoring the recovery process with a camera (Nikon D700), acquiring 1 frame/20s (resolution of the pictures: 300 dpi x 300 dpi). The recovery index for this characterization ($RI_{folding}$) was defined as follows:

$$RI_{folding} = \frac{\alpha - \alpha_{prog}}{\alpha_0 - \alpha_{prog}} \quad \text{(Eq. 2)}$$

where the various angles α, all measured in rad, are defined as shown in Figure1. α_0 is the initial angle of the specimen, (α_0 = p), α_{prog} is the angle after the programming step (α_{prog} »0), and α is the actual angle.

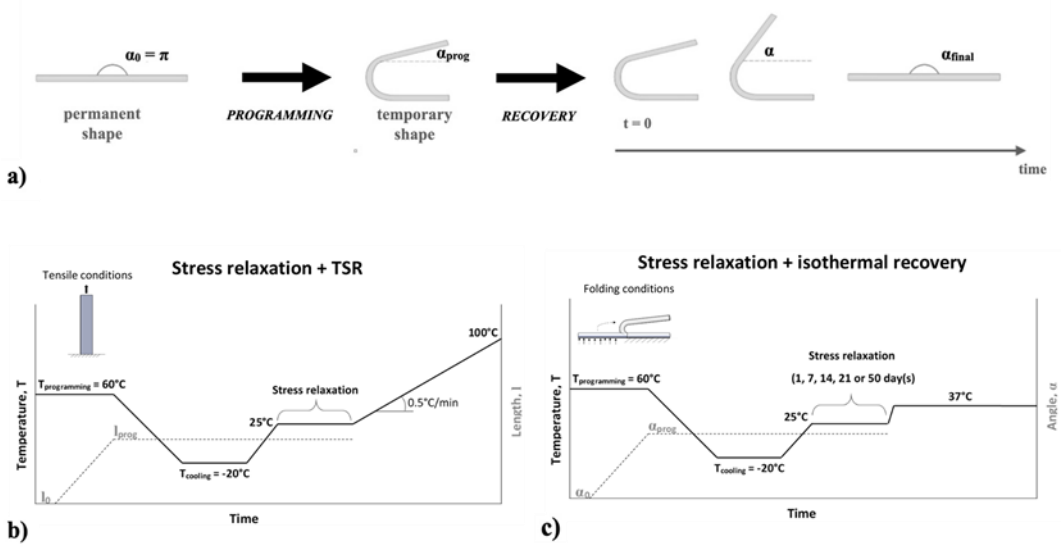

Figure 1: a) Sketch of the U-folding programming. Definition of the angles, α, by a schematic description of the bar shape changes from I-shaped to U-shaped within programming, and through recovery; b) Schematics for the experimental protocol for the TSR test following stress relaxation under tensile condition; c) Schematics for the experimental protocol for the isothermal recovery test following stress relaxation under folding condition.

2.4.3 Isothermal recovery tests

Samples subjected to U-folding were also subjected to isothermal recovery tests. Such tests were performed by placing programmed rod samples into a glass beaker, which was maintained at 37 ± 1 °C by immersing it in a temperature-controlled water bath. A thermocouple was placed near the sample and temperature values were recorded during the whole test. The space in the glass was enough to allow the sample to freely change its shape. Changes in the angle α were recorded by means of the camera (Nikon D700) placed above the beaker and recovery index values were calculated over time as reported in Eq. (2).

2.4.4 Recovery experiments on specimens subjected to prolonged constraint

An ad hoc shape memory cycle, involving the presence of a stress relaxation period, was specifically conceived with the aim of investigating whether a prolonged constraint may

affect the shape memory behavior of the specimens. In fact, the prototype will be stored in a gelatin capsule in its temporary shape before use (*i.e.* before the administration which will result in the dissolution of the capsule once in the stomach) and the impact of this constraint applied to the temporary shape to the shape memory performance cannot be a priori predicted. Therefore specific testing protocols were performed on material specimens comprising *i)* the achievement of a temporary shape under a given deformation; *ii)* the holding of the applied deformation for a given time span to simulate a stress relaxation step; *iii)* the promotion of the recovery following removal of the applied deformation and application of relevant temperature conditions, either under temperature ramp (TSR) or under isothermal conditions The testing protocol is sketched in Figure 1b and 1c for the two recovery conditions.

TSR tests were carried out under tensile conditions in the dynamic mechanical analyzer on programmed bar-shaped specimens subjected to various relaxation times. Samples programming consisted of applying a strain equal to 10% at 60 °C and cooling to -20 °C under fixed strain. Afterwards, while keeping the applied strain constant, a thermal equilibration at 25 °C was applied and the samples were held under this condition for increasing relaxation time (t_{rel} = 0 min (no relaxation), 9, 90 and 900 min). Finally, the quasi-stress-free TSR protocol for tensile deformation was applied setting up a heating ramp from 25 °C to 100 °C at 1 °C/min.

Isothermal tests were carried out only under bending conditions on rod specimens bent in a U-shape. The temporary U-shape in the fixture was equilibrated at room temperature (about 25 °C) and kept under static vacuum with silica gel for different relaxation periods (1, 7, 14, 21 and 50 days) prior to the isothermal recovery. Finally, isothermal recovery was performed at 37 ± 1 °C, monitoring the recovery as described in Section 2.4.3.

2.4.5 Shape memory tests on prototypal device

The prototype concept consisted in developing a DDS to be manufactured in an "original" permanent configuration, to be administered in a "programmed" collapsed

configuration, and able to self-expand in the patient stomach, recovering the "original" configuration upon interaction with gastric fluids at body temperature, thus preventing passage through the wide open pylorus. A schematic showing the desired working mechanism for the device is reported in Figure 2a. The design constraints concerning gastric retention and oral administration as well as their impact on the design phase of both permanent and temporary shapes were in-depth addressed in the companion paper [41].

Starting from the extruded rods, S-shaped samples extending in the three dimensions were manufactured. Each specimen was obtained by wrapping the extruded rod, while still hot, around a purposely developed template, as shown in Figure 2b, and removing it after 2 min cooling under pressurized air. The template was 3D-printed by a Kloner3D 240® Twin (Kloner3D, I) printer, from commercial carbonium nylon filament used as received. Further information concerning the sample and template preparation are reported in the companion paper [41]. The final shape of the specimen, along with the characteristic angles to evaluate its shape evolution, are also reported in Figure 2b. The resulting samples were packed in heat-sealed alufoil moisture barrier bags before being employed.

The S-shaped specimen were then programmed in a planar paper clip temporary shape, by heating them up to 60 °C. The deformed shape was achieved by inserting the specimen in a properly designed template. Deformed samples were finally cooled at -20 °C and maintained under this temperature for at least 1 h before testing. The template and the specimen temporary shape are depicted in Figure 2c.

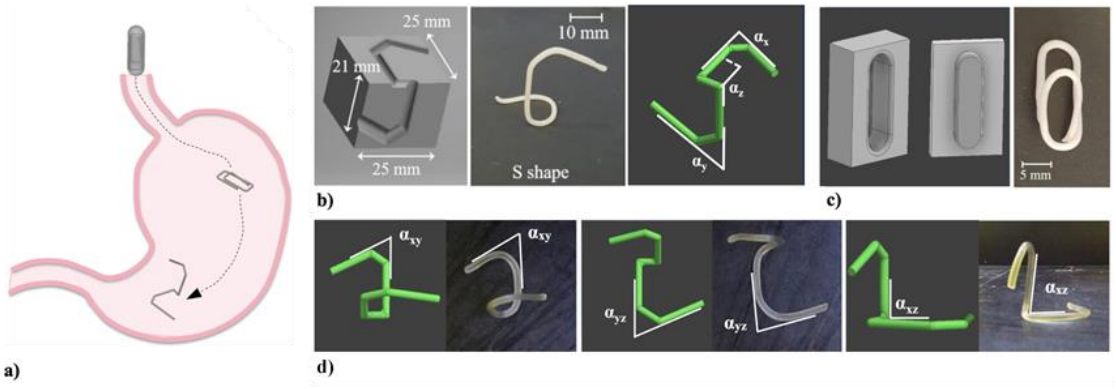

Figure 2: a) Sketch of the shape changes underwent by the S-shaped clip from oral administration inside a capsule to retention into the stomach; b) CAD model of the template for the preparation of the original S-shaped clip, along with a photograph of the resulting sample and the relevant CAD model in which the peculiar angles defining its shape were highlighted; c) CAD model of the template for programming the temporary paper-clip shape along with a photograph of the resulting sample; d) CAD models and photographs of the samples during shape recovery in which angles used to calculate the recovery indices were highlighted.

Recovery of the original shape was studied in a thermal chamber at 37 °C, placing the specimen inside a crystallization vessel and monitoring the process with two digital cameras positioned above and in front of the specimen (GoPro Hero Session, US-CA; n = 3). The photographs acquired were processed using a specific software (ImageJ, US-MD).

For each of the three α angles, as defined in Figure 2d, recovery indices (RIs) were calculated as follows:

i) $$RI_{\alpha xy} = \frac{\alpha_{xy} - a_{xy\,prog}}{a_{xy,0} - a_{xy\,prog}} \quad \text{(Eq. 3)}$$

ii) $$RI_{\alpha yz} = \frac{\alpha_{yz} - a_{yz\,prog}}{a_{yz,0} - a_{yz\,prog}} \quad \text{(Eq. 4)}$$

iii) $$RI_{\alpha xz} = \frac{\alpha_{xz} - a_{xz\,prog}}{a_{xz,0} - a_{xz\,prog}} \quad \text{(Eq. 5)}$$

with $\alpha_{ij,0}$ the angle measured in the original shape, $\alpha_{ij,prog}$ the angle measured in the temporary shape, and α_{ij} is the actual angle during recovery (ij corresponding to xy, yz and xz in Eq. 3, 4 and 5, respectively).

RIs were measured on triplicates. Indeed, a total of six tests was carried out, since the samples can lie on two different planes in the crystallization vessel and only two angles can be measured at a time during the recovery of the original S shape.

2.5 Modeling and simulation

The viscoelastic behavior of the material was captured using a three-dimensional generalized Maxwell model [62].

According to the Abaqus/Standard finite element code (Simulia, Providence, RI) nomenclature, the storage and loss modulus are defined, respectively, as follows:

$$G'(\omega) = G_0[1 - \sum_{i=1}^{N} \bar{g}_i^P] + G_0 \sum_{i=1}^{N} \frac{\bar{g}_i^P \tau_i^2 \omega^2}{1+\tau_i^2 \omega^2} \qquad \text{(Eq. 6)}$$

$$G''(\omega) = G_0 \sum_{i=1}^{N} \frac{\bar{g}_i^P \tau_i \omega}{1+\tau_i^2 \omega^2} \qquad \text{(Eq. 7)}$$

where $\bar{g}_i^P$ and τ_i are the Prony-parameters and G_0 represents the unrelaxed modulus (*i.e.* the modulus at time t = 0), calibrated on the storage and loss modulus master curves (see Section 2.3), as proposed by Diani et al. [62]. Here we derived the Prony parameters from DMA tests performed in tensile conditions, rather than in shear mode.

The Prony parameters, $\bar{g}_i^P$ and τ_i (I = 1,…,N), represent the 2N unknows defining the spring-damper elements of the adopted constitutive model and have to be determined from experimental data. In the present case, they were simultaneously determined from the storage and loss modulus master curves reported in Figure 3b and 3c, starting from the optimization procedure introduced by Kraus et al. [85].

Particularly, in order to reduce the number of unknowns, we adopted the same number N for the spring-damper elements and the examined frequency decays, since one Maxwell Element per measured frequency decade can be considered sufficient to map the

relaxation behavior [85]. Then, we assumed the relaxation times τi equal to certain positive values per decades, in order to reduce the number of unknowns from 2N to N. Accordingly, the problem was formulated as a least square optimization problem, where the target function was expressed as a function of the unknown N parameters $(\bar{g}_1^P, \dots, \bar{g}_N^P)$, as follows [85]:

$$f(\bar{g}_1^P, \dots, \bar{g}_N^P) = \sum_{i=1}^{N} \left[\left(logG^{'}(\omega_i) - logG^{'}_{exp}(\omega_i) \right)^2 + 10 \left(logG^{''}(\omega_i) - logG^{''}_{exp}(\omega_i) \right)^2 \right] \quad \text{(Eq. 8)}$$

subjected to thermodynamic constraints, *i.e.* $0 \leq \bar{g}_i^P < 1$, $\sum_{i=1}^{N} \bar{g}_i^P \leq 1$ and $\sum_{i=1}^{N} \bar{g}_i^P \leq 1$. In (Eq. 8) G'_{exp} and G''_{exp} represent, respectively, the storage and loss modulus obtained experimentally.

This problem was solved using a two-step procedure. In the first step, the problem was solved by a genetic algorithm; in the second step, the N parameters resulting from the first step were used as initial guess parameters in a global gradient based optimization tool in order to find the final fitting parameters.

The functional dependency of the time and temperature was expressed through the shift factors, $a_{T_0}^T$, obtained through the master curve construction and whose dependence on temperature was approximated by an Arrhenius-like approach, as follows:

$$\ln a_{T_0}^T = \frac{E_0}{R} \left(\frac{1}{T} - \frac{1}{T_0} \right) \quad \text{(Eq. 9)}$$

where E_0, typically representing the activation energy of the relaxation process, has to be determined experimentally on the shift factor values employed for the master curve construction [62], R is the universal gas constant, T is the actual temperature, and T_0 is the reference temperature, both expressed as absolute temperatures.

The model was used within a finite element framework. Particularly, the generalized Maxwell model, its finite strain extension [86], and the Arrhenius equation (Eq. 9) are available in Abaqus/Standard. The Prony parameters that define the master curve for small strains can be used for the finite strain model extension.

In addition, a description of the mechanical behavior of the materials in terms of an elastic response is required. In order to account for large deformation and according to experimental evidences reported in Section 3.4, the hyperelastic Yeoh model [87] was adopted under the hypothesis of incompressible material behavior, after comparison with other hyperleastic models available in the Abaqus library, which revealed to be worst-performing. The corresponding strain energy potential function U(ε) is defined as follows:

$$U = C_{10}(\bar{I}_1 - 3) + C_{20}(\bar{I}_1 - 3)^2 + C_{30}(\bar{I}_1 - 3)^3 \qquad \text{(Eq. 10)}$$

where C_{i0} are temperature-dependent material parameters and the first deviatoric strain invariant $\bar{I}_1$ is

$$\bar{I}_1 = \lambda_1^2 + \lambda_2^2 + \lambda_3^2 \qquad \text{(Eq. 11)}$$

being $\bar{\lambda}_i = J^{-1/3}\lambda_i$ the deviatoric stretches, λ_i the principal stretches, $J = det(\boldsymbol{F})$ is the total volume ratio with $\boldsymbol{F}$ the deformation gradient.

3. Results

3.1 Data generation for modeling the shape memory response

The constitutive model employed to describe the shape memory response of the specimens is based on the viscoelastic behavior of the investigated material. In fact, the shape memory response is associated with the increase in chain mobility occurring over time and promoted by temperature, and with the entropic elasticity of the material in the rubber state as well. For this reason, the data for the model were obtained from the full master curve of the mechanical dynamical response of the material, and from the measurements of its response in the rubbery region, well above T_g.

The viscoelastic behavior described by master curves was measured starting from the multifrequency dynamic-mechanical analysis described in Section 2.3. The results are

reported in Figure 3 for what regards the storage modulus, displayed as isothermal sweeps as a function of frequency (Figure 3a); then, the curves were mutually shifted until best superposition, by applying a frequency-temperature equivalence principle for a reference temperature, chosen as T_0 = 60 °C (Figure 3b). This approach was employed also for the loss modulus (Figure 3c) and tan δ master curves construction, and it allowed to obtain a full description of the temperature dependence in terms of the shift factor *versus* temperature correlation (Figure 3d). In fact, the introduction of the frequency (time) - temperature correlation through the shift factors allows to shift from the temperature to frequency domains, *i.e.* a change from T_0 to T can be considered as a change from ν_0 to a^T_{T0}* ν.

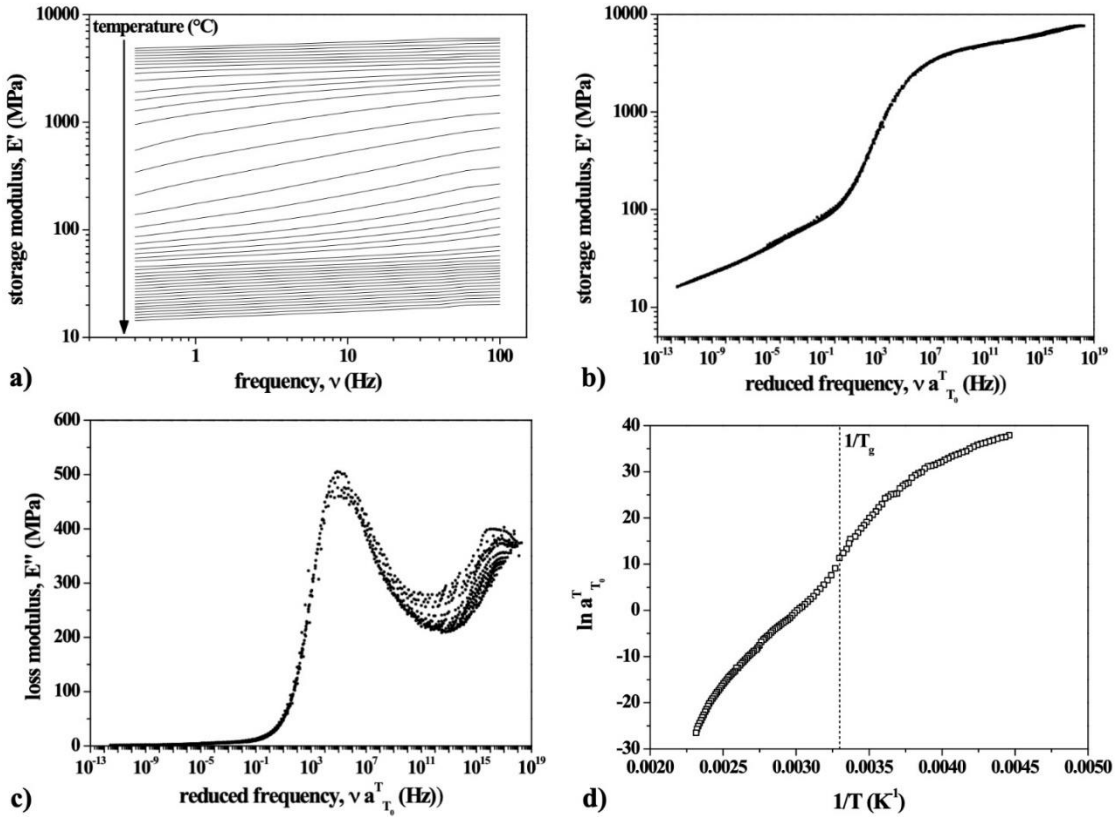

Figure 3: a) Storage modulus as a function of frequency in isothermal segments of the multifrequency DMA test; temperature increases downwards from -50 °C to 160 °C, temperature for each curve was not provided to improve readability; master curve b) Of the storage modulus and c) Of the loss modulus as a function of reduced frequency (T0 = 60 °C); d) Map of the shift factor - temperature correlation.

The storage modulus master curve showed a continuous decrease of modulus as frequency decreases. Indeed, it moved from high modulus values (about 3-7 GPa for frequency above 10^{10} Hz) to values between 100 and 10 MPa at frequencies below the relaxation one, along a continuous decreasing trend. The shift factors a^{T}_{T0}, plotted as a function of the inverse absolute temperature, highlighted the presence of a multiple Arrhenius dependence in the glassy region, and barely suggested a Williams-Landel-Ferry dependence across the glass transition (on a short region between 25 °C (1/T = 0.00335 K^{-1}) and 80 °C (1/T = 0.00283 K^{-1}); $1/T_g$ = 0.00327 K^{-1}).

Starting from these data, an attempt to describe the relaxation modulus as a function of time was made and reported in Figure 4 for a temperature T_0 = 25 °C, under the approximation that E ≃ E' and that the reduced time is $t/a^{T}_{T0} \simeq (\omega^{*}a^{T}_{T0})^{-1}$.

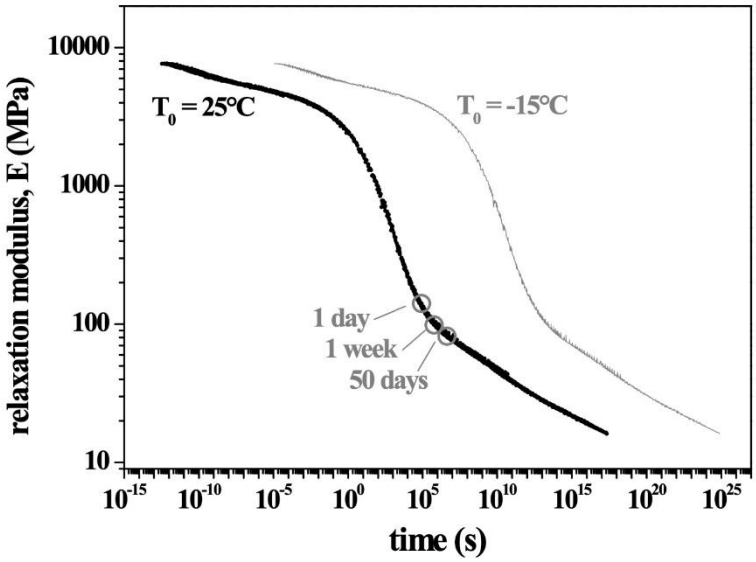

Figure 4: Approximate relaxation modulus master curve as a function of time for a temperature T_0 = 25 °C, with relevant instants for the relaxation process; in gray: master curve for a temperature T_0 = -15 °C.

This representation was useful in describing the stress relaxation occurring under a fixed strain condition. The curve for T_0 = 25 °C suggested that at room temperature a large portion of the relaxation process took place in short time, so that after 1 day the end of

the transition region was approached, and after 1 week the material entered its rubbery region. However, for longer times, although the material is in the relaxed state, its modulus value remained very high up to more than 50 days. Although calculated following an approximation, the results allowed to quantify the extent of the relaxation process as a function of time, and clearly suggested that, as expected, a significant decrease of modulus already occurred at relatively short times. In fact, after 1 day the modulus was reduced to about 2% of its "unrelaxed" value (*i.e.* the value measured at the shortest time), and after 50 days it got further reduced to about 1% of the same value. By contrast, the curve referred at T= -15 °C (*i.e.* a typical value for low temperature storage) suggested a significantly slower relaxation. The material was still in its glassy region at least up to 1 day, and approached the transition region at 50 days, with a modulus equal to about 2 GPa.

These findings may be important when dealing with the encapsulated gastroretentive device, pointing out that by simply storing it for very short times at room temperature, a large relaxation process may occur and this could affect the shape memory response by simultaneously better fixing the temporary folded shape and partially erasing the memory of the permanent, or undeformed, one. In fact, as the system may easily recover part of the deformation at room temperature, the presence of the constraint provided by the capsule could help prevent it. Due to its low T_g, PVA may undergo significant stress relaxation, whose effect on the achievement of shape recovery is not *a priori* known, especially following prolonged constrained conditions. For these reasons, the shape memory behavior after imposing a constraint was worthy of analysis and the results are reported in Section 3.3.

3.2 Characterization of the thermo-mechanical behavior

The thermal and thermo-mechanical behavior of the material was further investigated by DSC and DMTA experiments. The DSC thermograms and storage modulus (E') curves as a function of temperature are reported in Figure 5a and 5b, respectively.

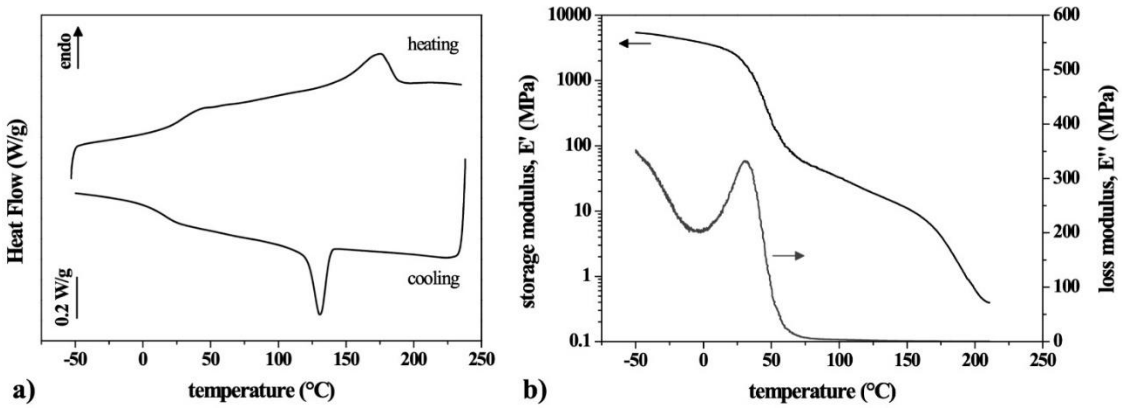

Figure 5: a) DSC thermograms showing the cooling and second heating scan; b) DMTA curves of the storage modulus and loss modulus as a function of temperature at 1 Hz.

In particular, in Figure 5a the cooling and second heating scans are reported, which allowed to identify the glass transition temperature (T_g), the melting temperature (T_m), the crystallization temperature (T_c), and the enthalpy at melting, from which it was possible to calculate the degree of crystallinity.

The T_g was identified slightly above room temperature, at about 27 °C, whereas T_m and T_c occurred at higher temperatures (T_m = 179 °C and T_c = 132 °C). This clearly confirmed that the material may manifest significant viscoelastic effects, such as stress relaxation or strain recovery, at room temperature. Conversely, its crystalline structure required temperatures well above 120 °C to be modified. By evaluating the area of the melting peak (ΔH_m = 25.9 J/g), the crystallinity content was quantified as about 18.7% (assuming the melting enthalpy of 100% crystalline PVA equal to 138.60 J/g [88]).

Analogous consideration can be drawn from the DMTA data, thanks to which the transition region was clearly identified slightly above room temperature, and extending up to 60 °C, and T_g, evaluated from the peak of the loss modulus curve, is equal to 33 °C.

In the thermo-mechanical characterization, also the inherent shrinkage ability, deriving from internal stresses, was taken into account. In fact, the presence of stresses, related to the extrusion processing history of the material, may lead to changes in the specimen geometry, such as axial shrinkage or flexural bending, which might disturb the

measurement of the shape memory response. For this reason, freshly extruded specimens were subjected to a heating ramp in the Dynamic Mechanical Analyzer under quasi-stress-free conditions in order to measure the presence of shape variation phenomena upon heating. The results obtained are displayed in Figure S1 (Supplementary material). Shrinkage seemed to become a relevant effect only at temperatures above 160 °C. Therefore, the shrinkage effect due to processing frozen stress was thus present but should not interfere with the shape recovery process, which is known to take place across the glass transition region [40].

3.3 Characterization of the shape memory response

The shape memory behavior was investigated through shape memory cycles, starting with the "programming" of extruded samples in a temporary shape, and continuing with recovery tests carried out in isothermal experiments or under a heating ramp, as described in Section 2.4. More in details, recovery tests triggered by a heating ramp (TSR tests) are widely used to evaluate the shape-memory performance of thermally-activated SMPs, since their activation mechanism relies on changes in macromolecular mobility occurring over a transformation temperature window (in this case, over the glass transition region). Results of the TSR tests were used to test the prediction capability of the calibrated model. Conversely, recovery tests under isothermal conditions were performed at 37 °C to simulate the intended actuation stimulus for the ultimate DDS and quantify its recovery capability in such conditions.

A sketch of the shape memory test carried out in tensile configuration is shown in the inset of Figure 6a for the standard programming history. The specimen was first heated up to 60 °C, then deformed up to the applied strain (ε_{appl} = 10%), cooled under fixed strain down to -20 °C, and then unloaded and subjected to a heating ramp at 0.5 °C/min, during which the shape recovery occurred.

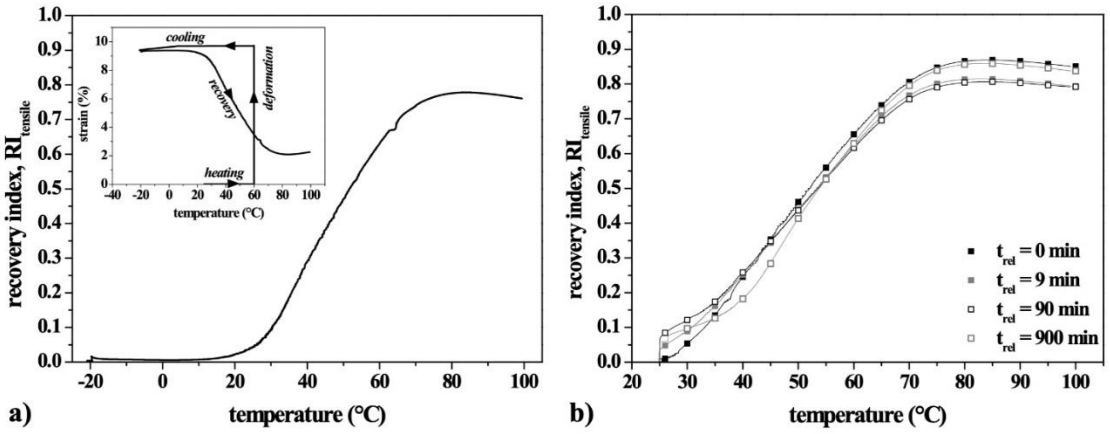

Figure 6: Recovery index, $RI_{tensile}$, curves as a function of temperature along a heating ramp for a specimen subjected to recovery a) Right after cooling under fixed strain and b) For various relaxation times t_{rel} under fixed strain (0, 9, 90 and 900 min). Inset of Figure 8a: Representation of the shape programming and recovery protocol in terms of strain *vs* temperature.

The curve reported in Figure 6a showed a continuous recovery of the applied strain from room temperature up to 100 °C: the recovery seemed to start at about 10 °C, but gained a significant rate only above 30 °C, finally leading to an almost complete (84%) recovery of the applied strain at 80 °C. The inversion of the recovery at high temperatures may be due to the concurrent thermal expansion of the sample, becoming the only dimensional change present once the recovery process is complete. The presence of an irreversible strain is often associated with the response of a semicrystalline polymer in the absence of a crosslinked structure and when heating is well below melting temperature.

The curves in Figure 6b refer to specimens subjected to stress relaxation at room temperature before recovery. For all the specimens tested, the recovery took place immediately after unloading, and for those subjected to relaxation it started with a first step increment of the recovery index, representing an elastic, or short-time viscoelastic, response. The extent of such instantaneous recovery became higher as the time under relaxation increased. This finding highlighted that, during the relaxation step, the specimen, trying to recover but being forced under fixed strain, increased its internal

energy, finally leading to such an early sharp recovery. After this early step, the subsequent recovery seemed to occur at an initial lower rate for samples that were kept under relaxation for longer times, but a similar increasing trend was found above 50 °C, and the maximum recovery slightly varied, with no dependence on relaxation history, between 81% and 87%. Based on the results obtained, the relaxation step at room temperature for a time scale in the order of one day seemed not to alter the shape memory capabilities but only the early recovery stage. Therefore, the memory of the system did not fade with relaxation time, but its elastic spring-back recovery increased.

The shape memory behavior under flexure was measured on specimens with an inherent I-shape, folded at 60 °C in a U-shaped configuration and cooled to -20 °C. Their recovery behavior was measured both as a function of temperature (TSR tests) and as a function of time (isothermal tests at 37 °C). The results are reported in Fig 7a and 7b, for the TSR and isothermal experiments.

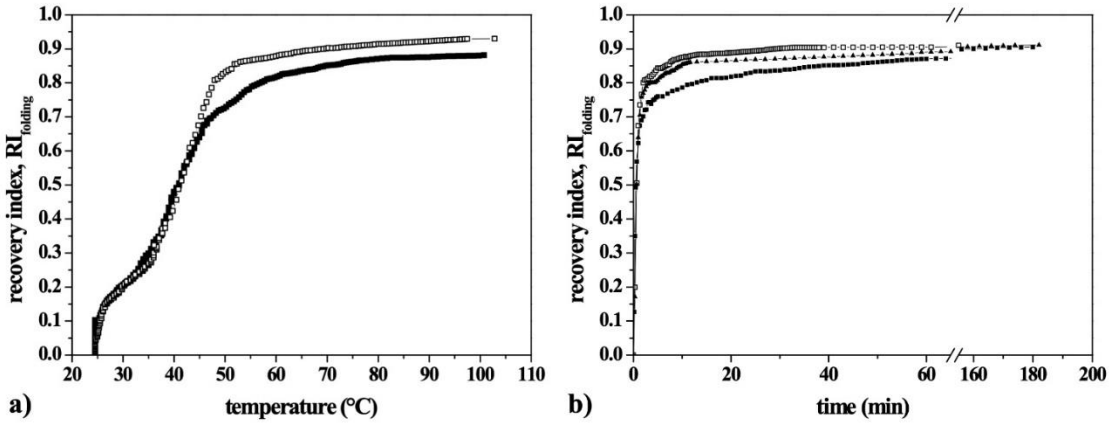

Figure 7: Recovery index, $RI_{folding}$, curves measured in replicates a) As a function of temperature in TSR tests and b) As a function of time in isothermal recovery tests at 37 °C, depicting their recovery from folded U-shape to the inherent I-shape as a function of temperature and time, respectively.

The results of the TSR tests were consistent with those obtained under tensile configuration, displaying a recovery process that is active already at room temperature

and achieves significant speed at about 45 °C, finally recovering around 90% of the applied angle. The maximum recovery was measured at 100 °C, but the process may be considered practically fully achieved already at 50-55 °C. Interestingly, isothermal recovery tests at 37 °C clearly showed that such recovery degrees may be reached also at human body temperature, requiring only few minutes to reach 70% of the permanent shape, and a time span that ranges between 10 to 40 minutes for the process to be completed.

A test concerning the effect of the relaxation step was also carried out for this type of geometry, by maintaining the specimens in the constrained U-shape at room temperature for times varying between 1 to 50 days. The corresponding $RI_{folding}$ curves are reported as a function of time in Figure 8 as average recovery index for a same recovery time among three replicates. Error bars were not reported to provide readability, but they can be found in Table 1 for given instants.

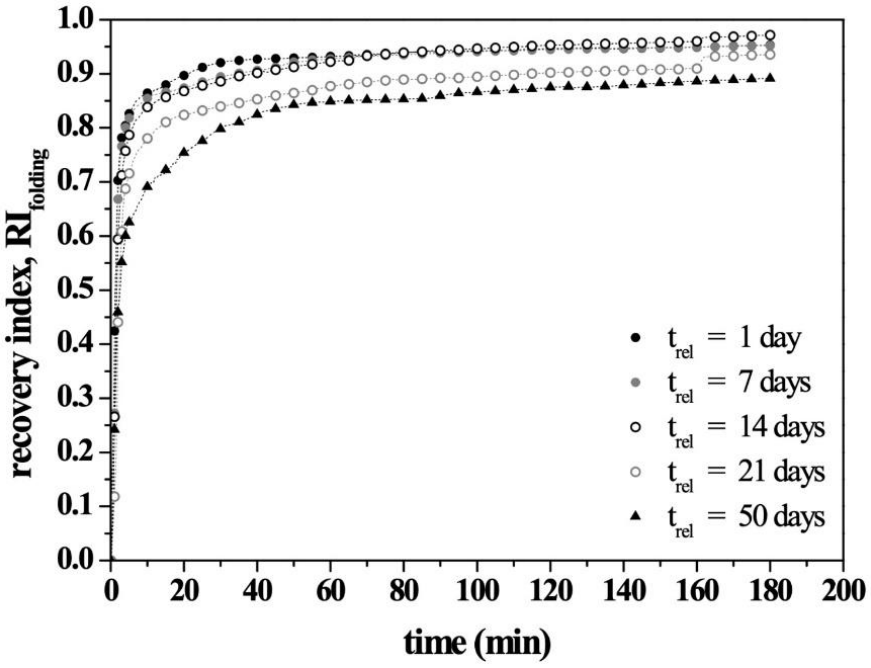

Figure 8: Recovery index, $RI_{folding}$, curves for isothermal experiments carried out at 37 °C on U-shaped folded specimen maintained in that shape at room temperature for various relaxation times t_{rel} (1, 7, 14, 21, 50 days) before the recovery experiment.

Table 1: Recovery index $RI_{folding}$ data, measured at various recovery times in isothermal experiments carried out at 37 °C on U-shaped folded specimens which were maintained in that shape at room temperature for various relaxation times (1, 7, 14, 21, 50 days) before activating recovery.

Relaxation time, t_{rel} (d)	**$RI_{folding}$ at 1 min**	**$RI_{folding}$ at 10 min**	**$RI_{folding}$ at 20 min**	**$RI_{folding}$ at 180 min**
1	0.42 ± 0.28	0.86 ± 0.05	0.90 ± 0.04	0.95 ± 0.02
7	0.27 ± 0.14	0.85 ± 0.01	0.87 ± 0.02	0.95 ± 0.03
14	0.26 ± 0.18	0.84 ± 0.08	0.87 ± 0.08	0.97 ± 0.04
21	0.12 ± 0.12	0.78 ± 0.05	0.82 ± 0.04	0.93 ± 0.01
50	0.24 ± 0.12	0.69 ± 0.10	0.75 ± 0.09	0.89 ± 0.03

The average curves of Figure 8 clearly showed a similar shape memory response over time, with a significant recovery (at least about 70%) in the first 10 minutes. It was then followed by a recovery of reduced rate, the latter being almost the same rate independent of the relaxation time, which led to a total recovery between 90 and 95% in the subsequent 3 hours. However, on the average, the specimens displayed lower recovery at any given instant as the relaxation time increased. In particular, this effect was evident for long relaxation times (21 and 50 days, respectively), whereas for relaxation up to 14 days the effect may be considered of minor importance. The results can be justified in light of the great relaxation occurring at room temperature, as suggested from Figure 4. From a micromechanical point of view, stress relaxation on polymer chains due to the achievement of a more stable configuration may reduce the tendency to recover as well as the overall memory of the pristine shape. If such an effect was dominant, the shape memory performances of the final device would have been greatly affected depending on prolonged permanence in folding conditions, resulting in a non-functional device. However, in our material this effect can be considered not so relevant. In fact, the significant extent of recovery reached in the first 10 minutes, independent of the

relaxation time, suggested that the presence of a relaxation period, potentially represented by the encapsulation of the DDS, did not cancel the shape memory performance of the DDS, even if it slightly affects final level of recovery. Considering the data reported in Table 1, the difference in the recovery index for a given time turned out to be less striking in light of the measurement scattering, although a slight divergence was maintained for the average recovery index.

3.4 Model validation

The shape memory response was modelled on the basis of the thermo-viscoelastic approach described in Section 2.5, in which the dependence of the mechanical behavior on time and temperature was based on the dynamic moduli master curves and on the shift factors dependence on temperature.

Accordingly, model parameters were all identified from the experimental curves presented in previous sections.

The optimization problem was implemented in Matlab, by choosing N=33 Maxwell elements. Table 2 reports the obtained parameters as $\bar{g}_i^P$ and τ_i couples.

Table 2: Prony parameters of the generalized Maxwell model: normalized moduli, $\bar{g}_i^P$ and relaxation times, τi, evaluated at T0 = 60 °C. Floating point notation with four significant digits has been adopted, but the computations have been done in double precision with all digits.

$\bar{g}_i^P$	τi (s)	$\bar{g}_i^P$	τi (s)	$\bar{g}_i^P$	τi (s)
0.3741E-02	1.00E-21	0.6076E-01	1.00E-10	0.1030E-02	10
0.3755E-02	1.00E-20	0.8027E-01	1.00E-09	0.9899E-03	100
0.3889E-02	1.00E-19	0.7426E-01	1.00E-08	0.6661E-03	1000
0.5769E-02	1.00E-18	0.9410E-01	1.00E-07	0.6938 E-03	10000
0.1261E0	1.00E-17	0.6122E-01	1.00E-06	0.6495E-03	100000
0.8581E-01	1.00E-16	0.5382E-01	1.00E-05	0.5313E-03	1.00E+06
0.6632E-01	1.00E-15	0.2378E-01	0.0001	0.5367E-03	1.00E+07
0.6756E-01	1.00E-14	0.1487E-01	0.001	0.3026E-03	1.00E+08
0.4612E-01	1.00E-13	0.6108E-02	0.01	0.3103 E-03	1.00E+09
0.5620E-01	1.00E-12	0.3251E-02	0.1	0.6797E-04	1.00E+10
0.5285E-01	1.00E-11	0.1979E-02	1	0.3229E-03	1.00E+11

These parameters allowed to obtain a good fit of the experimental behavior, as shown in Figure 9a and 9b, in which experimental and calibrated curves are shown for the storage and loss modulus, respectively.

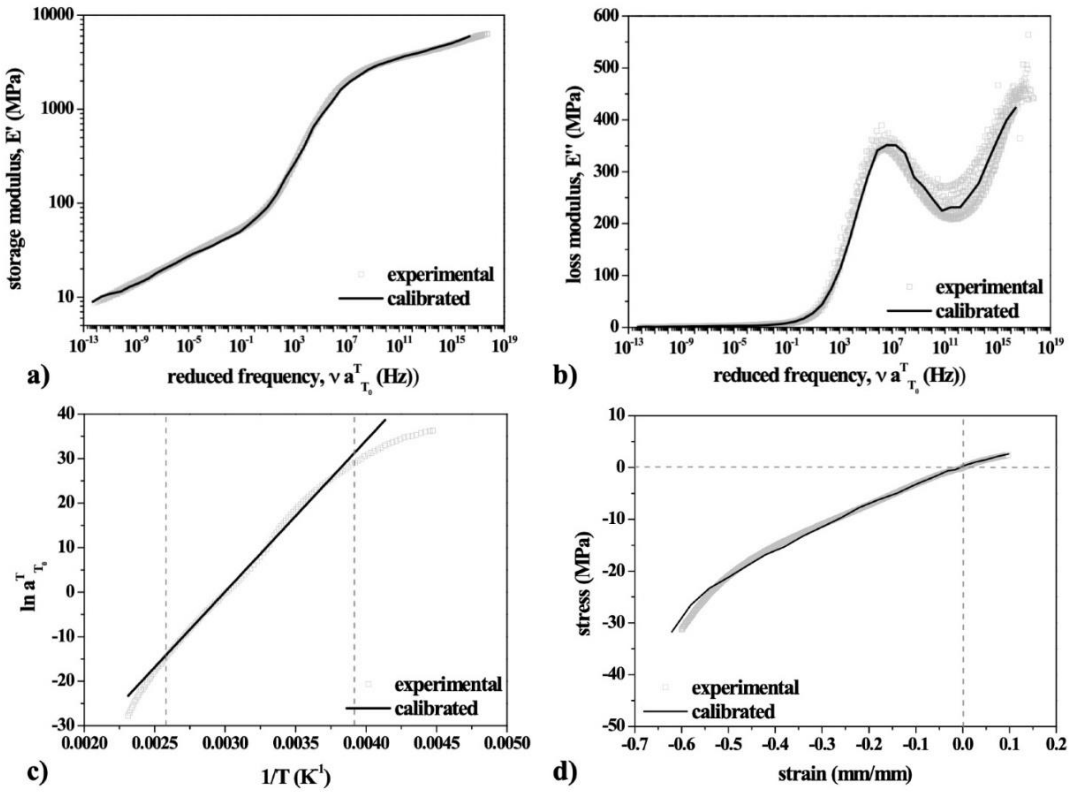

Figure 9: Experimental curves (grey dots) versus fitted (black solid line) for: a) The storage modulus; b) The loss modulus; c) Arrhenius approximation of the calculated horizontal shift factors and d) experimental stress-strain curve (both under tension and compression) versus fitted curve at 60 °C.

The shift factors employed for the master curve construction, allowing to describe the time-temperature dependence, were interpolated by the Arrhenius equation (Eq. 9), whose parameters were identified based on the experimental shift factor versus 1/T correlation represented in Figure 3d. The Arrhenius equation was chosen as easier to implement in the computational framework and still providing a good approximation over a large set of data. The parameter T_0 was assumed equal to the reference temperature, *i.e.* T_0 = 60 °C, while the parameter E_0 was fitted on a region of temperature between -20 °C (1/T = 0.0039 K^{-1}) and 115 °C (1/T = 0.0026 K^{-1}), *i.e.* the region where the curve in Figure 3d exhibits a fairly regular linear correlation. The interval between -20 °C and 115 °C was chosen since it offered a good coverage of the temperatures involved in the conducted shape memory tests. The parameter E_0 for the Arrhenius equation was taken

equal to 282.38 kJ/mole. The comparison between the calibrated and experimental curves is reported in Figure 9c and demonstrates a good matching for the temperature interval of interest.

The Yeoh model parameters, as introduced in Eq. (10), were identified on the stress versus strain curves of Figure S2 (Supplementary material), both for the tensile and compression behavior measured at 60 °C, obtaining the parameters C10 = 49.8E5 Pa, C20 = -10.6E5 Pa, and C30 = 1.48E5 Pa. The experimental and modelled curves are shown in Figure 9d and display a good matching for strains ranging from -0.6 to 0.1. The covered range matches the values achieved in the shape memory tests described below.

The model was then validated on the experimental results regarding the flexural configuration (*i.e.* bending the specimen between a straight I-shaped configuration to a folded U-shaped one as described in Section 3.3). Accordingly, the specimen geometry was meshed by using eight-node linear isoparametric hexahedral elements, reduced integration with hourglass control, hybrid with constant pressure. The experimental test was reproduced numerically by imposing appropriate boundary conditions and temperature history, as detailed in the following. Temperature was assumed uniform in the bar.

First, the TSR test was simulated. The geometry, the coordinate system, and the applied boundary conditions are provided in Figure 10b. A pressure, p = 3000 MPa, was imposed on the half bar at 60 °C to bend the bar from a straight I-shaped configuration to a folded U-shaped one. The pressure caused the bending of the bar of an angle α_{prog}. The deformed U-shaped bar was kept in position during cooling up to -20 °C to simulate the programming step. Particularly, the bar was first cooled down to 20 °C in 20 min and then to -20 °C in 5 min. Afterwards, the constrained bar was heated up to 25 °C in 5 min and the constraints were removed. The bar was kept at 25 °C for 5 min. Finally, the bar was heated up to 100 °C in 148 min to induce shape recovery.

Experimental and numerical results are compared in Figure 10a, where $RI_{folding}$ is represented as a function of temperature. The permanent shape, the programmed shape, and the recovered shapes at 50 °C and 70 °C are reported in Figure 10b.

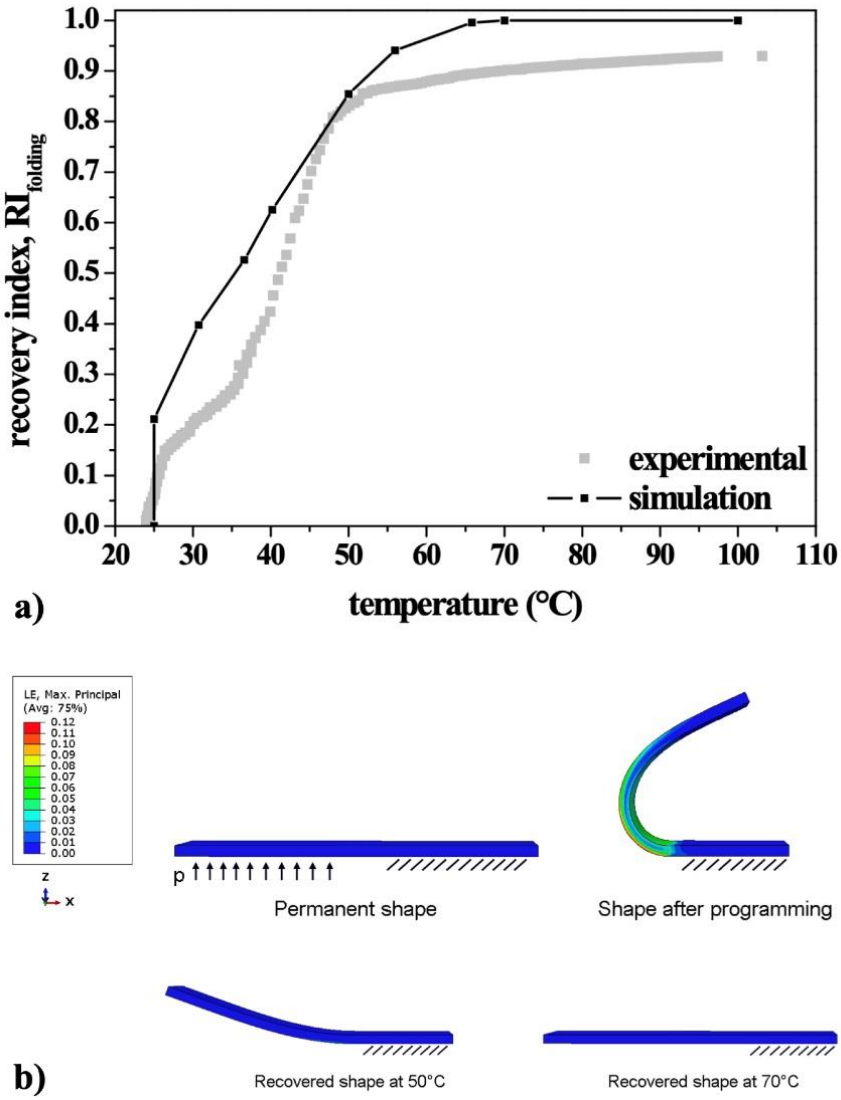

Figure 10. a) Comparison between experimental (grey open squares) and numerical (black full squares) recovery indexes, $RI_{folding}$, for the TSR test on bar; b) Results of numerical simulations showing the contour plot of the maximum principal logarithmic strain.

The predicted curve had a trend similar to the experimental one, suggesting that recovery takes place across similar region and with a similar dependence on temperature. This

trend is composed by a first almost vertical branch, that can be associated to an elastic recovery after unloading, followed by a sigmoidal-like branch, revealing an increasing recovery index with increasing temperature. However, the model slightly overpredicted the experimental response, so that at most temperatures the predicted recovery index turned out to be higher than that measured experimentally. This may be partly due to a thermal lag experienced by the specimens during the heating ramp, which is not taken into account by the model. Furthermore, the model reasonably did not consider the presence of an irreversible strain, predicting complete recovery, as it is shown in Figure 10b with the permanent straight I-shaped configuration fully recovered at 70 °C.

Then, the isothermal test was simulated on a rod-shapes sample. The coordinate system and the applied boundary conditions are the same provided in Figure 10b. Similarly to the previous simulation, a pressure, p = 3000 MPa, was imposed on half rod at 60 °C. The deformed U-shaped rod was then kept in position during cooling up to -20° C. Particularly, the bar was first cooled down to 20°C in 60 min and then to -20°C in 5 min. Finally, the constraints were removed from the deformed rod, which was then brought up to 37 °C in 5 min. The rod was kept at 37 °C for 180 min to induce shape recovery. In Figure 11, numerical results based on the aforementioned parameters (black open squares) were compared to experimental data (grey open squares) in terms of the recovery index $RI_{folding}$. The curves qualitatively showed a similar response, with a faster increase in the first 20 minutes followed by a relatively slower recovery. However, in this case, the model strongly underpredicted the recovery index measured at a certain instant. Indeed, a slower recovery process was predicted, and the poor agreement with the measured data is supposed to be related to a non-adequate description of the time-temperature correlation. As shown in Figure 11, the permanent straight I-shaped configuration was not fully recovered after 160 min.

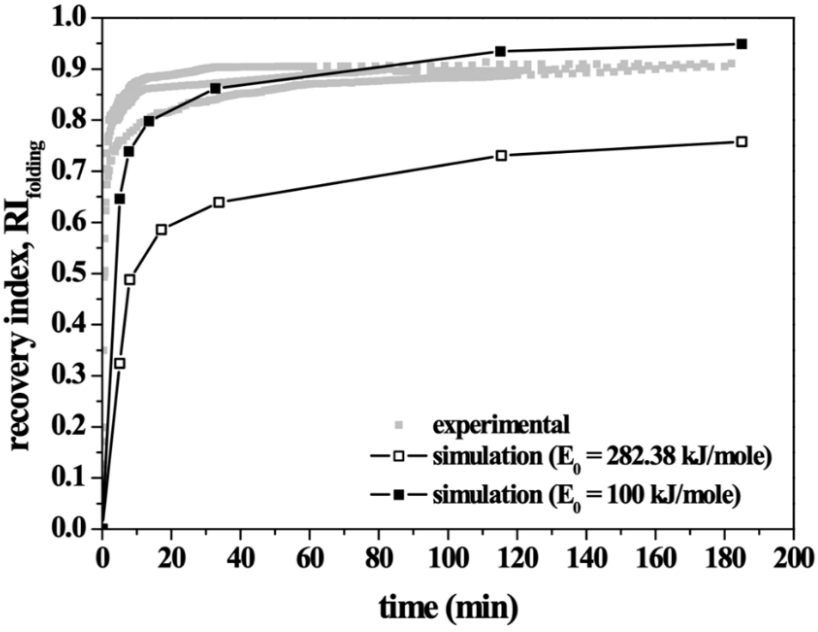

Figure 11: Comparison between experimental (grey open squares) and numerical (black open squares: E_0 = 282.38 kJ/mole; black full squares: E_0 = 100 kJ/mole) recovery indexes, $RI_{folding}$, for isothermal tests at 37 °C on rods.

Such a deviation between the simulation curve and the experimental recovery curve was not fully unexpected, since under isothermal conditions even slight differences between the material behavior and the one predicted by extrapolated parameters may determine important differences on the recovery time scales. Indeed, this is particularly likely to occur when the recovery process is happening in proximity of the glass transition.

For this reason, in order to improve the model prediction capability under isothermal conditions, without abandoning the Arrhenius equation that may be easily implemented in Abaqus, the value of the parameter E_0 was determined following a trial and error approach, until a good matching between the isothermal recovery curves was found. The numerical results under this latter modification (black full squares), obtained with an E_0 value equal to 100 kJ/mol, clearly demonstrated a better agreement.

Two considerations have to be remarked. First, for this specific material, a full description of the shape memory response on the basis of sole DMA results is not possible, probably due to the complex chains motion occurring in a semicrystalline material, as well as to the

fact that isothermal experiments and simulations were performed in condition strongly dominated by the viscoelastic behavior, since temperature was very close the material T_g. The improved response obtained following a change in E_0, which may be derived from the isothermal curves, suggested, as a potential strategy, to calibrate the Prony series parameters of the model based on the DMA results, and the E_0 value directly on an isothermal shape recovery curve. In addition, the new E_0 value for the Arrhenius-like equation is lower than that obtained from the shift factors employed for the master curve construction. This may also be reasonable, as the relaxation chain motion taking place during DMA regards small strain deformation and, in this case, E_0 represented the activation energy for relaxation motions. Conversely, the shape recovery phenomenon generally involves larger strains, proper of a non-linear viscoelastic response, whose recovery may be based on motions requiring lower activation energy, due to the stored internal energy and the larger free volume. A further possibility for a potential refinement of the numerical prediction that may be attempted regards the fitting of the time-temperature correlation on shift factor values obtained from the construction of a recovery index master curve. This approach consists in performing multiple isothermal recovery tests at different temperatures, followed by the tentative application of a time-temperature superposition scheme for rigidly shifting the curves with respect to the one related to the reference temperature until best superposition [89]. For this material, this approach would have increased the complexity of both the experimental and numerical parts. In fact, because of the T_g close to room temperature, the required sub-T_g isothermal testing would have been difficult to perform and the modeling activity would have lost its relatively simple implementation, by requiring additional data for the model calibration.

3.5 Shape memory performance of extruded prototypes and modelling the response

The shape recovery of S-shaped samples from the temporary planar paper-clip shape suitable for capsule administration was evaluated upon immersion of samples in aqueous medium kept at 37 °C and by monitoring three angles (*i.e.* α_{xy}, α_{yz} and α_{xz}) (Figure 2). This

way, it was possible to calculate three corresponding recovery indexes, whose evolution over time is reported in Figure 12. The specimens showed a very efficient recovery response. Interestingly after the first 30 s, all the angles increased enough to make the system reaching a size compatible with gastric retention, as detailed by Melocchi et al. [41]. Particularly, α_{xy} increases up to 52° ± 4°, well above the 43° required for retention. Similarly, α_{yz} opened up to 43° ± 22° (angle required: 32°), while α_{xz} reached 59° ± 4° (angle required: 33°). In this respect, the prototypes demonstrated the ability to recover the original shape, and although the tests lasted up to 20 min, 3-4 minutes were enough for the specimens to achieve a steady state in their shape recovery. Actually, some of them seemed to over-recover the applied strain, being characterized by a steady state recovery index close to 110%-120%. This may be associated with the presence of frozen-in stresses in the extruded bars or with inadequate fixing of the S shape.

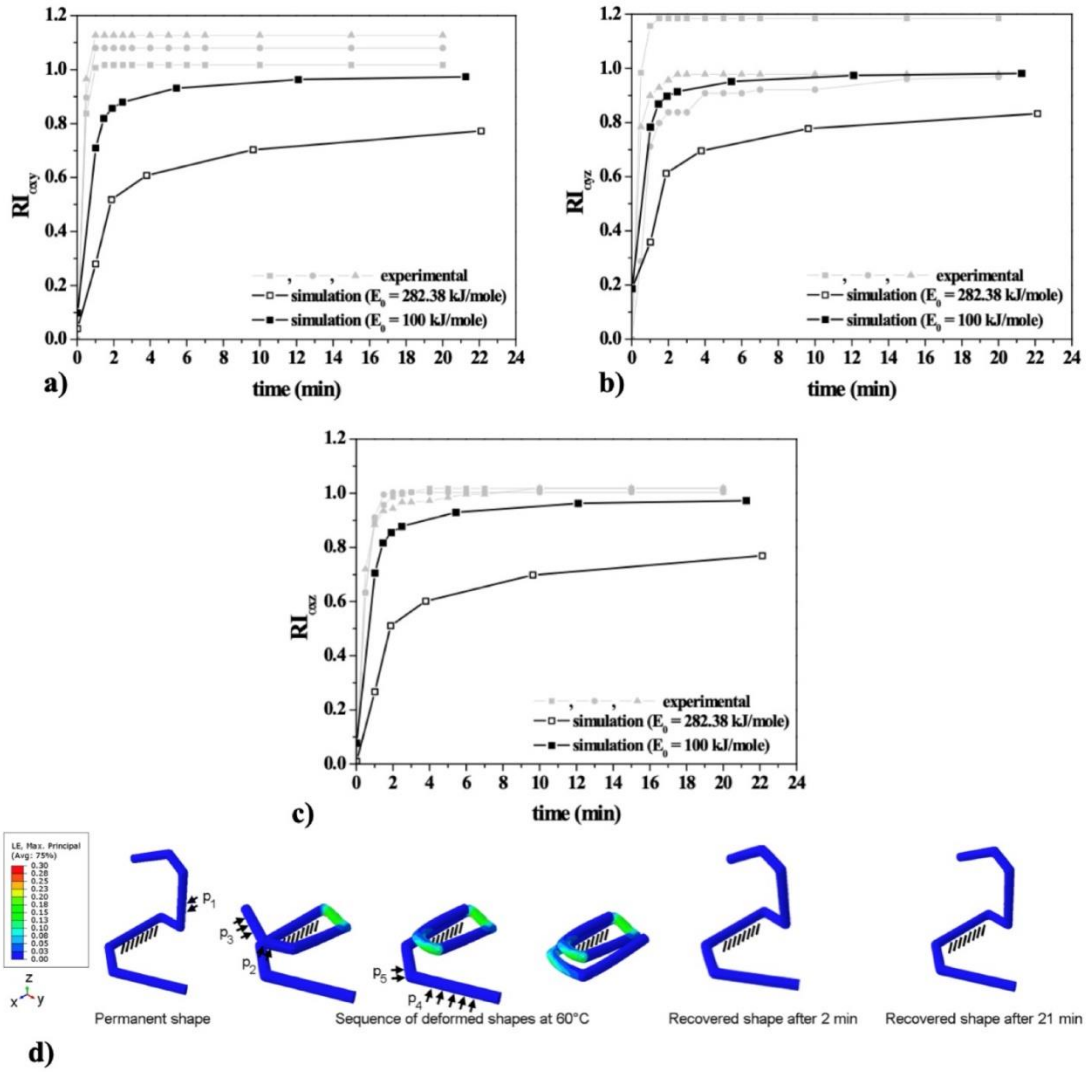

Figure 12: Comparison between experimental (grey full squares) and numerical (black open squares: E_0 = 282.38 kJ/mole; black full squares: E_0 = 100 kJ/mole) recovery indexes, RI, for isothermal tests at 37 °C on prototypes. Recovery Index curves: a) $RI_{\alpha,xy}$, b) $RI_{\alpha,yz}$, c) $RI_{\alpha,xz}$. d) Results of numerical simulations with E_0 = 100 kJ/mole, showing the contour plot of the maximum principal logarithmic strain. The following values were adopted: p1=2.5E6 Pa, p2=7.0E5 Pa, p3=7.9E4 Pa, p4=9.0E3 Pa, p5=6.5E5 Pa.

The model was checked also by performing a numerical simulation on S-shaped prototypes deformed to take on a paper-clip shape. Accordingly, the clip geometry was meshed by using four-node linear tetrahedron, hybrid with linear pressure. The experimental test was reproduced numerically by imposing appropriate boundary conditions and temperature history, as detailed below. The temperature field was

assumed to be uniform in the clip. The geometry, the coordinate system, and the applied boundary conditions are provided in Figure 12d. Different pressures were imposed sequentially to reproduce the experimental deformation of the prototype in a paper-clip configuration at 60 °C. To avoid penetration during the deformation, a surface-to-surface contact was activated on the model. In particular, a 0.03 friction contact was adopted, enforced by linear penalty method.

The prototype was kept in the deformed position during cooling down to -20 °C in 5 min. At that point, constraints were removed from the deformed clip to ensure any elastic recoil at -20 °C. Then, the clip was heated up to 37 °C in 1 min and maintained at this temperature for 21 min to observe shape recovery.

As evident from Figure 12, the original shape was not fully recovered after 21 min, suggesting also in this case that the predicted trend is slower than the real response, and the need for resorting to a change in E_0 to improve the model prediction ability. In this respect, a value of 100 kJ/mole was applied, as derived from the good matching between experiments and simulation in the case of the folded rods (see Figure 11). The adoption of this value, derived from relatively simple isothermal recovery experiments, allowed to obtain a significantly improved agreement between experiments and simulation. This is clear by observing the results of the numerical simulation in Figure 12 and particularly, the shapes attained after 2 min and 21 min of recovery. The results clearly highlight the importance of a correct model calibration, based on the studied application and, consequently, on the type of associated testing environment.

4. Conclusions

In this work, the possibility of describing by a comprehensive experimental characterization and computer-aided simulation modelling the shape-shifting response of DDSs made of a pharmaceutical formulation (*i.e.* a matrix-forming polymer, a plasticizer and the possibility of loading also an active ingredient) based on

pharmaceutical-grade shape memory polymers was investigated. In this respect, a specific prototype made of plasticized PVA was developed. It consisted in a three dimensional S-shaped item with a temporary planar shape (*i.e.* paper-clip shape). The recovery process under isothermal conditions exhibited a significantly high rate for temperature close to, or above, the human body temperature. In particular, at 37 °C about 70% of the original shape was recovered in only few minutes. The simulation activity was pursued within a finite element analysis framework. A 3D generalized Maxwell thermo-viscoelastic model, whose parameters were fitted from the data obtained through *i)* DMTA experiments (at small strains, in the linear viscoelastic region) and *ii)* tensile and compression tests in quasi-static conditions above the material T_g, were used. An Arrhenius-type dependence on temperature, driven by the value of a single parameter that is the activation energy E_0, was considered for the time-temperature shift factors.

The modeling approach here adopted turned out to be effective in simulating the shape memory behavior of the DDS prototype based on the specific pharmaceutical formulation under investigation, when using an appropriate value of E_0. In fact, due to the high complexity of the viscoelastic response of the material at the recovery temperature, which is quite close to the material T_g, the use of an E_0 value determined in the linear viscoelastic regime may be inadequate. The strategy here proposed for the selection of the proper E_0 for the simulation consisted in considering the latter as an adjustable parameter, whose value could be determined from shape recovery isothermal tests carried out on a sample based on the material of interest with a very simple shape. By pursuing this strategy, the modeling approach proposed in this paper could be easily exploited and used in support of the design of DDSs composed of shape memory polymers. In fact, by having validated our integrated approach, potential refinements and extensions of this work may regard changes in the material formulation, by loading and considering one or different active principles and characterize/optimize their release performances.

Supplementary information

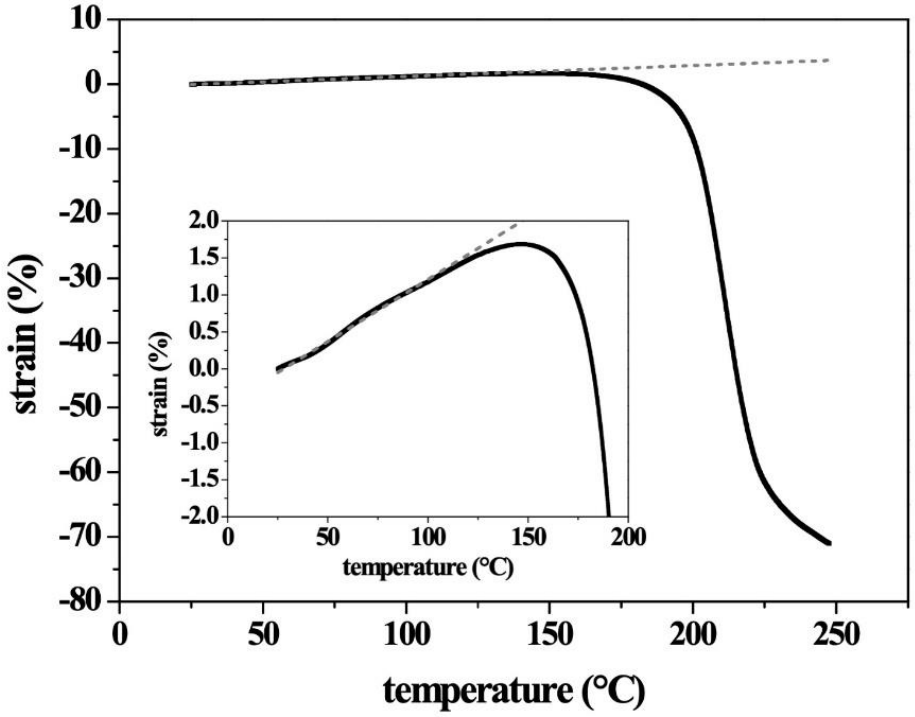

Figure S1: Quasi-stress-free strain change due to shrinkage of the specimen along a heating ramp. The dashed line is reported as baseline representing an ideally pure thermal expansion. Inset: magnification of the shrinkage curve and of the baseline for temperatures up to 180 °C.

In Figure S1 the shrinkage behavior is correlated with the deviation from an ideal baseline (dashed line in the graph), representing the thermal expansion of the specimen. This representation highlighted that a significant shrinkage process may take place, and the overall shrinkage, evaluated up to 250 °C, summed up to 75% of the specimen length after extrusion. However, shrinkage seemed to become a relevant effect only at temperatures above 160 °C, and the magnification of the traces reported in the picture inset showed that the curve deviation onsets at about 100 °C and summed up to only 1 % at about 150 °C.

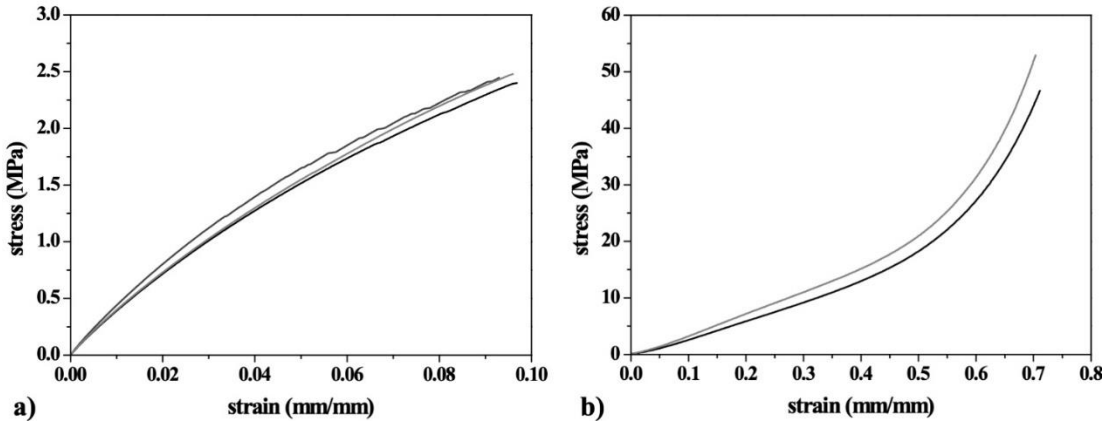

Figure S2: Nominal stress *vs* nominal strain curves at 60 °C measured in triplicate in a) tensile tests and b) Compression tests.

The material mechanical behavior above T_g was investigated at 60 °C and the results, obtained by experiments under tensile and compression conditions (see Section 2.3), are displayed as nominal stress versus nominal strain curves in Figure S2a and S2b, respectively. The tensile behavior was studied up to the maximum strain applied during the tensile programming of the temporary shape, due to a limited extension of the DMA crosshead. On the other hand, the compressive conditions were applied up to very high level of strain (about 70%). These curves were fitted with the Yeoh hyperelastic model in Figure 9d.

References

1. M. Behl, A. Lendlein. Shape-memory polymers. Mater. Today 10 (2007) 20-28.
2. A. Lendlein, R. Langer, Biodegradable, elastic shape-memory polymers for potential biomedical applications. Sci. 296 (2002) 1673-1676.
3. A. Lendlein, R. Langer, Biodegradable shape memory polymeric sutures. (2012) Patent number:. US 8,303,625 B2.
4. C. M. Yakacki, R. Shandas, C. Lanning, B. Rech, A. Eckstein, K. Gall, Unconstrained recovery characterization of shape-memory polymer networks for cardiovascular applications. Biomaterials 28 (2007) 2255-2263.
5. W. Small IV, T. S. Wilson, W. J.Benett, J. M. Loge, D. J. Maitland, Laser-activated shape memory polymer intravascular thrombectomy device. Opt. Express 13 (2005) 8204-8213.
6. J. P. Bearinger, D. J. Maitland, D. L Schumann, T. S. Wilson, System for closure of a physical anomaly. (2014) Patent number: US 8,882,786 B2.
7. A. J. Boyle, T. L. Landsman, M. A. Wierzbicki, L. D. Nash, W. Hwang, M. W. Miller, E. Tuzun, S. M. Hasan, D. J. Maitland. In vitro and in vivo evaluation of a shape memory polymer foam over -wire embolization device delivered in saccular aneurysm models. J. Biomed. Mater. Res. B 104 (2016), 1407-1415.
8. T. L. Landsman, R. L. Bush, A. Glowczwski, J. Horn, S. L. Jessen, E. Ungchusri, K. Diguette, H. R. Smith, S. M. Hasan, D. Nash, F. J. Jr. Clubb, D. J. Maitland, Design and verification of a shape memory polymer peripheral occlusion device. J. Mech. Behav. Biomed. 63 (2016) 195-206.
9. R. Kunkel, D. Laurence, J. Wang, D. Robinson, J. Scherrer, Y. Wu, B. Bohnstedt, A. Chien, Y. Liu, C.-H., Lee, Synthesis and characterization of bio-compatible shape memory polymers with potential applications to endovascular embolization of intracranial aneursyms. J. Mech. Behav. Biomed. 88 (2018) 422-430.

10. R. M. Baker, L.-F. Tseng, M. T. Iannolo, M. E. Oest, J.H. Henderson, Self-deploying shape memory polymer scaffolds for grafting and stabilizing complex bone defects: A mouse femoral segmental defect study. Biomaterials 76 (2016) 388-398.
11. A. Pandey, G. Singh, S. Singh, K. Jha, C. Prakash, 3D printed biodegradable functional temperature-stimuli shape memory polymer for customized scaffoldings J. Mech. Behav. Biomed. 108 (2020) 103781.
12. L.-F. Tseng, P. T. Mather, J. H. Henderson, Shape-memory-actuated change in scaffold fiber alignment directs stem cell morphology. Acta Biomater. 9 (2013) 8790-8801.
13. T. Gong, K. Zhao, G. Yang, J. Li, H. Chen, Y. Chen, S. Zhou, The control of mesenchymal stem cell differentiation using dynamically tunable surface microgrooves. Adv. Healthc. Mater. 3 (2014) 1608-1619.
14. J. Wang, A. Quach, M. E. Brasch, C. E. Turner, J. H. Henderson, On-command on/off switching of progenitor cell and cancer cell polarized motility and aligned morphology via a cytocompatible shape memory polymer scaffold. Biomaterials 140 (2017) 150-161.
15. C. Wischke, A. T. Neffe, S. Steuer, A. Lendlein, Evaluation of a degradable shape-memory polymer network as matrix for controlled drug release. J. Control. Release 138 (2009), 243-250.
16. C. Wischke, A. Lendlein, Shape-memory polymers as drug carriers - a multifunctional system. Pharm. Res. 27 (2010) 527-529.
17. Y. Xiao, S. Zhou, L. Wang, X. Zheng, T. Gong, Crosslinked poly(ε-caprolactone)/poly(sebacic anhydride) composites combining biodegradation, controlled drug release and shape memory effect. Compos. Part B-Eng. 41 (2010) 537-542.
18. M. Balk, M. Behl, C. Wischke, J. Zotzmann, A. Lendlein, Recent advances in degradable lactide-based shape-memory polymers. Adv. Drug Deliver. Rev. 107 (2016) 136-152.

19. A. Kirillova, L. Ionov, Shape-changing polymers for biomedical applications. J. Mater. Chem. B 7 (2019) 1597-1624.
20. A. M. Bellinger, M. Jafari, T. M. Grant, S. Zhang, H. C. Slater, E. A. Wenger, S. Mo, Y.-A.L. Lee, H. Mazdiyasni, L. Korgan, R. Barman, C. Cleveland, L. Booth, T. Bensel, D. Minahan, H.M. Hurowitz, T. Tai, J. Daily, B. Nikolic, L. Wood, P. A. Eckhoff, R. Langer, G. Traverso, Oral, ultra–long-lasting drug delivery: Application toward malaria elimination goals. Sci. Transl. Med. 8 (2016) 365ra157.
21. A. R. Kirtane, O. Abouzid, D. Minahan, T. Bensel, A. L. Hill, C., Selinger, A. Bershteyn, M. Craig, S. S. Mo, H. Mazdiyasni, C., Cleveland, J. Rogner, Y.-A. L. Lee, L. Booth, F. Javid, S. J. Wu, T. Grant, A. M. Bellinger, B. Nikolic, A. Hayward, L. Wood, P. A. Eckhoff, M. A. Nowark, R. Langer, G. Traverso, Development of an oral once-weekly drug delivery system for HIV antiretroviral therapy. Nat. Commun. 9 (2018) 2294.
22. S. Babaee, S. Pajovic, A. R. Kirtane, J. Shi, E. Caffarel-Salvador, K. Hess, J. E. Collins, S. Tamang, A. V. Wahane, A. M. Hayward, H. Mazdiyasni, R. Langer, G. Traverso, Temperature-responsive biometamaterials for gastrointestinal applications. Sci. Transl. Med. 11 (2019) eaau8581.
23. A. Maroni, A. Melocchi, L. Zema, A. Foppoli, A. Gazzaniga, Retentive drug delivery systems based on shape memory materials, J. Appl. Polym. Sci. 137 (2020) 48798.
24. J. Firth, S. Gaisford, A. W. Basit, A New Dimension: 4D printing opportunities in pharmaceutics. In: Basit A., Gaisford S. Eds., 3D Printing of Pharmaceuticals. AAPS Advances in the Pharmaceutical Sciences Series, vol 31, Springer (2018), Kent, UK.
25. https://www.gohsenol.com/doc_e/spcl/spcl_01/spcl_08.shtml Last access: April 2021
26. C. C. DeMerlis, D. R. Schoneker, Review of the oral toxicity of polyvinyl alcohol (PVA). Food Chem Toxicol. 41 (2003) 319-326
27. S. Muppalaneni, H. Omidian, Polyvinyl alcohol in medicine and pharmacy: a perspective. J Develop Drugs 2 (2013) 1000112.

28. H. Du, J. Zhang, Shape memory polymer based on chemically cross-linked poly(vinyl alcohol) containing a small number of water molecules. Colloid Polym. Sci. 288 (2010), 15-24.
29. H. Du, Y. Yu, G. Jiang, J. Zhang, J. Bao, Microwave-induced shape-memory effect of chemically crosslinked moist poly(vinyl alcohol) networks. Macromol. Chem. Phys. 212 (2011) 1460-1468.
30. H. Du, Z. Song, J. Wang, Z. Liang, Y. Shen, F. You, Microwave-induced shape-memory effect of silicon carbide/poly(vinyl alcohol) composite. Sensor. Actuat. A-Phys. 228 (2015) 1-8.
31. F.-P. Du, E.-Z. Ye, W. Yang, T.-H. Shen, C.-Y. Tang, X.-L. Xie, X.-P. Zhou, W.-C. Law, Electroactive shape memory polymer based on optimized multi-walled carbon nanotubes/polyvinyl alcohol nanocomposites. Compos. Part B-Eng. 68 (2015) 170-175.
32. H. Du, J. Zhang, Solvent induced shape recovery of shape memory polymer based on chemically cross-linked poly(vinyl alcohol). Soft Matter 6 (2010) 3370-3376.
33. L. Wang, X. Yang, H. Chen, G. Yang, T. Gong, W. Li, S. Zhou, Multi-stimuli sensitive shape memory poly(vinyl alcohol)-graft-polyurethane. Polym. Chem. 4 (2013) 4461-4468.
34. X. Qi, X. Yao, S. Deng, T. Zhou, Q. Fu, Water-induced shape memory effect of graphene oxide reinforced polyvinyl alcohol nanocomposites. J. Mater. Chem. A 2 (2014) 2240-2249.
35. H. Chen, Y. Li, G. Tao, L. Wang, S. Zhou, Thermo- and water-induced shape memory poly(vinyl alcohol) supramolecular networks crosslinked by self-complementary quadruple hydrogen bonding. Polym. Chem. 7 (2016) 6637-6644.
36. Z. Fang, Y. Kuang, P. Zhou, S. Ming, P. Zhu, Y. Liu, H. Ning, G. Chen, Programmable shape recovery process of water-responsive shape-memory poly(vinyl alcohol) by wettability contrast strategy. ACS Appl. Mater. Inter. 9 (2017) 5495-5502.

37. S. Paonessa, N. Barbani, E. C. Rocchietti, C. Giachino, C. Cristallini, Design and development of a hybrid bioartificial water-induced shape memory polymeric material as an integral component for the anastomosis of human hollow organs. Mater. Sci. Eng. C-Mater. 75 (2017) 1427-1434.

38. Y. Bai, J. Zhang, X. Chen. A thermal-, water-, and near-infrared light-induced shape memory composite based on polyvinyl alcohol and polyaniline fibers. ACS Appl. Mater. Inter. 10 (2018) 14017-14025.

39. K. Gall, C. M. Yakacki, Y. Liu, R. Shandas, N. Willett, K. S. Anseth, Thermomechanics of the shape memory effect in polymers for biomedical applications. J. Biomed. Mater. Res. A (2005) 339-348.

40. A. Melocchi, N. Inverardi, M. Uboldi, F. Baldi, A. Maroni, S. Pandini, F. Briatico-Vangosa, L. Zema, A. Gazzaniga, Retentive device for intravesical drug delivery based on water-induced shape memory response of poly(vinyl alcohol): design concept and 4D printing feasibility. Int. J. Pharm. 559 (2019) 299-311.

41. A. Melocchi, M. Uboldi, N. Inverardi, F. Briatico-Vangosa, F. Baldi, S. Pandini, G. Scalet, F. Auricchio, M. Cerea, A. Foppoli, A. Maroni, L. Zema, A. Gazzaniga, Expandable drug delivery system for gastric retention based on shape memory polymers: Development via 4D printing and extrusion. Int. J. Pharm. 571 (2019) 118700.

42. N. Salessiotis, Measurement of the diameter of the pylorus in man: Part I. Experimental project for clinical application. Am. J. Surg. 124 (1972) 331-333.

43. D. H. Altreuter, A. R. Kirtane, T. Grant, C. Kruger, G. Traverso, A. M. Bellinger, Changing the pill: developments towards the promise of an ultra-long-acting gastroretentive dosage form. Expert Opin. Drug. Del. 15 (2018) 1189-1198.

44. S. Zhang, A. M. Bellinger, D. L. Glettig, R. Barman, Y.-A.L. Lee, J. Zhu, C. Cleveland, V. A. Montgomery, L. Gu, L. D. Nash, D. J. Maitland, R. Langer, G. Traverso, A pH-responsive supramolecular polymer gel as an enteric elastomer for use in gastric devices Nat. Mater. 14 (2015) 1065-1071.

45. E. Yarali, A. Taheri, M. Baghani, A comprehensive review on thermomechanical constitutive models for shape memory polymers. J. Intel. Mat. Syst. Str. 31 (2020) 1243-1283.

46. H. Tobushi, T. Hashimoto, S. Hayashi, E. Yamada, Thermomechanical constitutive modeling in shape memory polymer of polyurethane series. J. Intel. Mater. Syst. Str. 8 (1997) 711–718.

47. J. R. Lin, L. W. Chen, Shape-memorized crosslinked ester-type polyurethane and its mechanical viscoelastic model. J. Appl. Polym. Sci. 73 (1999) 1305-1319.

48. J. Morshedian, H. A. Khonakdar, S. Rasouli, Modeling of shape memory induction and recovery in heat-shrinkable polymers. Macromol. Theory Simul. 14 (2005) 428-434.

49. J. Diani, Y. Liu, K. Gall, Finite strain 3D thermoviscoelastic constitutive model for shape memory polymers. Polym. Eng. Sci. 46 (2006) 484-492.

50. T. D. Nguyen, H. J. Qi, F. Castro, K. N. Long, A thermoviscoelastic model for amorphous shape memory polymers: incorporating structural and stress relaxation. J. Mech. Phys. Solids 56 (2008) 2792–2814.

51. T. D. Nguyen, C. M. Yakacki, P. D. Brahmbhatt, M. L. Chambers, Modeling the relaxation mechanisms of amorphous shape memory polymers. Adv. Mater. 22 (2010) 3411-3423.

52. V. Srivastava, S. A. Chester, L. Anand, Thermally actuated shape-memory polymers: experiments theory, and numerical simulations. J. Mech. Phys. Solids 58 (2010) 1100-1124.

53. S. Alexander, R. Xiao, T. D. Nguyen, Modeling the thermoviscoelastic properties and recovery behavior of shape memory polymer composites. J. Appl. Mech. 81 (2014) 041003.

54. R. Xiao, J. Guo, T. D. Nguyen, Modeling the multiple shape memory effect and temperature memory effect in amorphous polymers. RSC Adv. 5 (2015) 416-423.

55. Y. Liu, K. Gall, M. L. Dunn, A. R. Greenberg, J. Diani, Thermomechanics of shape memory polymers: uniaxial experiments and constitutive modeling. Int. J. Plasticity 22 (2006) 279-313.

56. Y.-C. Chen, D. C. Lagoudas, A constitutive theory for shape memory polymers. Part I. large deformations. J. Mech. Phys. Solids 56 (2008) 1752–1765.

57. Z. D. Wang, D. F. Li, Z. Y. Xiong, R. N. Chang, Modeling thermomechanical behaviors of shape memory polymer. J. Appl. Polym. Sci. 113 (2009) 651-656.

58. S. Reese, M. Böl, D. Christ, Finite element-based multi-phase modeling of shape memory polymer stents. Comput. Methods Appl. Mech. Eng. 199 (2010) 1276-1286.

59. P. Gilormini, J. Diani, On modeling shape memory polymers as elastic two phase composite materials. CR Mécanique 340 (2012) 338-348.

60. E. Boatti, G. Scalet, F. Auricchio, A three-dimensional finite-strain phenomenological model for shape-memory polymers: Formulation, numerical simulations, and comparison with experimental data. Int. J. Plasticity 83 (2016) 153-177.

61. S. J. Hong, W. R. Yu, J. H. Youk, Y. R. Cho, Polyurethane smart fiber with shape memory function: experimental characterization and constitutive modeling. Fiber. Polym. 8 (2007) 377-385.

62. J. Diani, P. Gilormini, C. Frédy, I. Rousseau, Predicting thermal shape memory of crosslinked polymer networks from linear viscoelasticity. Int. J. Solids Struct. 49 (2012) 793-799.

63. K. Yu, T. Xie, J. Leng, Y. Ding, H. J. Qi, Mechanisms of multi-shape memory effects and associated energy release in shape memory polymers. Soft Matter, 8 (2012) 5687.

64. T. Chen, O.R. Bilal, K. Shea, C. Daraio, Harnessing bistability for directional propulsion of soft, untethered robots. P. Natl. Acad. Sci. USA 115 (2018) 5698–5702.

65. K. Kratz, S. A. Madbouly, W. Wagermaier, A. Lendlein, Temperature-memory polymer networks with crystallizzable controlling units. Adv. Mater. 23 (2011) 4058-4062.

66. M. Behl, K. Kratz, U. Noechel, T. Sauter, A. Lendlein. Temperature-memory polymer actuators. Proc. Natl. Acad. Sci. USA 110 (2013) 12555-12559.

67. Z.-C. Jiang, Y.-Y. Xiao, Y. Kang, B.-J. Li, S. Zhang, Semi-IPNs with moisture-triggered shape memory and self-Hhealing properties. Macromol. Rapid. Comm. 38 (2017) 1700149.

68. K. Wang, Y.-G. Jia, X. X. Zhu, Two-way reversible shape memory polymers made of cross-linked cocrystallizable random copolymers with tunable actuation temperatures. Macromol. 50 (2017) 8570-8579.

69. W. Kuang, P. T. Mather, Tuning of reversible actuation via ROMP-based copolymerization semicrystalline polymers. Polymer 156 (2018) 228-239.

70. T. Li, Y. Li, X. Wang, X. Li, J. Sun, Thermally and near-infrared light-induced shape memory polymers capable of healing mechanical damage and fatigued shape memory function. ACS Appl. Mater. Interfaces 11 (2019) 9470-9477.

71. B. Peng, Y. Yang, K. Gu, E. J. Amis, K. A. Cavicchi, Digital light processing 3d printing of triple shape memory polymer for sequential shape shifting. ACS Materials Lett. 1 (2019), 410-417.

72. A. Andreu, P.-C. Su, J.-H. Kim, C. Siang, I. Kim, J. Lee, J. Noh, A. Suriya, Y.-J. Yoon, 4D printing materials for vat photopolymerization. Additive Manufacturing 44 (2021) 102024.

73. G. Ehrmann, A. Ehrmann, 3D printing of shape memory polymers. J. Appl. Polym. Sci. 138 (2021) 50847.

74. Y. Xia, F. Zhang, L. Wang, Y. Liu, J. Leng, Electrospun shape-memory polymer fibers and their applications. In Dong Y., Baji A., Ramakrishna S., (eds) Electrospun polymers and composites, ultrafine materials, high performance fibres and

wearables, Woodhead Publishing Series in Composites Science and Engineering (2021) 567-596, Cambridge (US-MA).

75. Q. Zhang, X. Kuang, S. Weng, L. Yue, D. J. Roach, D. Fang, H. J. Qi, Shape-Memory Balloon Structures by Pneumatic Multi-material 4D Printing. Adv. Funct. Mater. 31 (2021) 2010872.
76. K. K. Westbrook, V. Parakh, T. Chung, P. T. Mather, L. C. Wan, M. L. Dunn, H. J. Qi, Constitutive Modeling of Shape Memory Effects in Semicrystalline Polymers With Stretch Induced Crystallization. J. Eng. Mater. Technol. 132 (2010) 041010.
77. M. Baghani, R. Naghdabadi, J. Arghavani, S. Sohrabpour, A thermodynamically-consistent 3D constitutive model for shape memory polymers. Int. J. Plast. 35 (2012) 13-30.
78. G. Scalet, S. Pandini, M. Messori, M. Toselli, F. Auricchio, A one-dimensional phenomenolgical model for the two-way shape-memory effect in semi-crystalline networks. Polymer 158 (2018) 130-148.
79. D. Safranski, J. C. Griffis, Shape-memory polymer device design 1st edition (2017). A volume in Plastics Design Library.
80. T. Chen, K., Shea, An Autonomous Programmable Actuator and Shape Reconfigurable Structures Using Bistability and Shape Memory Polymers. 3D Printing and Additive Manufacturing 5 (2018) 91-101.
81. I. Lukin, S. Musquiz, I. Erezuma, T. H. Al-Tel, N. Golafshan, A. Dolatshahi-Pirouz, G. Orive, Can 4D bioprinting revolutionize drug development? Expert Opin. Drug Del. 14 (2019) 953-956.
82. G. Baer, T. S. Wilson, D. L. Matthews, D. J. Maitland, Shape-memory behavior of thermally stimulated polyurethane for medical applications. J. Appl. Polym. Sci. 103 (2007) 3882-3892.
83. W. Wagermaier, K. Kratz, M. Heuchel, A. Lendlein, Characterization methods for shape-memory polymers. In Lendlein, A. (Ed), (2010). Shape-memory polymers, Advances in Polymer Science, vol. 226, 97-145, Springer-Verlag.

84. B. Atli, F. Gandhi, G. Karst. Thermomechanical characterization of shape memory polymers. J. Intell. Mater. Syst. Struct. 20 (2009) 87-95.

85. M. A. Kraus, M. Schuster, J. Kuntsche, G. Siebert, J. Schneider, Parameter identification methods for visco- and hyperelastic material models. Glass Struct. Eng. 2 (2017) 147-167.

86. J. C. Simo, On a fully three-dimensional finite strain viscoelastic damage model: formulation and computational aspects. Comput. Methods Appl. Mech. Eng. 60 (1987) 153-173.

87. O. H. Yeoh, Some forms of the strain energy function for rubber. Rubber Chem. Technol. 66 (1993) 745-771.

88. N. A. Peppas, E. W. Merrill, Differential scanning calorimetry of crystallized PVA hydrogels. J. Appl. Polym. Sci. 20 (1976) 1457-1465.

89. N. Inverardi, S. Pandini, F. Bignotti, G. Scalet, S. Marconi, F. Auricchio, Sequential motion of 4D printed photopolymers with broad glass transition. Macromol. Mater. Eng. 305 (2020) 1900370.

Chapter III

The content of Part III, Chapter III has been submitted for publication to: Coatings (2021).

DATASET ON A SMALL-SCALE FILM-COATING PROCESS DEVELOPED FOR SELF-EXPANDING 4D PRINTED DRUG DELIVERY DEVICES

Abstract

Film-coating is widely performed in the pharmaceutical field to enhance aspect/taste and mechanical properties of dosage forms, to protect them from the environment and to modify their performance. In this respect, it was recently involved in the development of 4D printed prolonged-release systems intended for organ retention. During coating processes, liquid formulations are sprayed onto moving cores, whose shape, weight and surface characteristics are essential to attain a homogeneous film. Devices of complex shapes, composed of smart materials and fabricated by hot-processing techniques such as extrusion and fused deposition modeling 3D printing might be poorly compatible with the requirements of traditional coating methods. *e.g.* need for spherical substrates with smooth surface and stable to temperature. The present work was aimed at evaluating, at a small scale level, the feasibility of a versatile equipment for film-coating of rod-shaped extruded and printed prototypes with different section. Equipment design and set up of process parameters was performed starting from both polymeric solutions and suspensions and testing as cores 50 mm-long rod-shaped samples based on shape memory poly(vinyl alcohol). Integrity and thickness of the applied layer and its impact on shape memory and release performance of prototypes were evaluated.

Keywords: film-coating, controlled release, shape memory effect, hot melt extrusion, fused deposition modeling, 4D printing, poly(vinyl alcohol), methacrylic acid copolymers.

1. Introduction

Accessibility of manufacturing techniques based on hot-processing and availability of smart polymers (*e.g.* materials changing their shape/characteristics in response to an external stimulus) has open up new possibilities in pharmaceutics, the most charming regarding 4D printing [1-5]. The accomplishment of challenging therapeutic goals hitherto considered unattainable and the development of personalized drug products through small-scale production processes might become a viable reality [6].

In previous works, self-expanding systems based on pharmaceutical-grade poly(vinyl alcohol) (PVA) and prepared by hot melt extrusion and fused deposition modeling (FDM), thus involving 4D printing, were proposed for intravesical and intragastric applications [7-9]. Prototypes were conceived in an original shape (*e.g.* U-, S- and helix like) with such a spatial encumbrance that their rapid emptying from the target organ could be avoided, thus ensuring long-lasting residence and release. Moreover, being composed of shape memory polymers, they were able to take on a temporary shape suitable for administration inside a catheter or a capsule, and to recover the original one upon contact with water at body temperature. In the development of the organ-retentive PVA-based systems, film-coating was considered in order to improve mechanical properties and prolong release duration, without affecting the shape memory effect.

In the drug delivery field, film-coating of solid dosage forms is often performed to improve aspect, mechanical properties, swallowability as well as taste of the product, to protect it from the outer environment (*e.g.* humidity, light) and to control the release of the conveyed drug [10-12]. The process generally consists in spraying polymeric solutions/suspensions onto tumbling or fluidized substrates (*e.g.* granules/pellets, tablets) depending on the equipment employed (*i.e.* rotating pans or fluid beds). In order to achieve a continuous film of uniform thickness over the cores, formulation and process parameters need to be adjusted. In particular, drying conditions defined by the air temperature and relevant flow rate, and the ability to expose continuously or alternately the whole surface of the substrates may turn out critical. In this respect, the proper

exposure of the cores during the process mainly depends on their shape, weight as well as surface characteristics, and the best results are obtained with spherical smooth ones. Substrates characterized by complex shape (*e.g.* with edges and folds) as well as particular thermal and mechanical properties, thus involved in thermal programming of a temporary shape, could be an issue and will require the development of dedicated processes.

In the present manuscript the feasibility of a lab-scale, versatile and easy to set up film-coating process for self-expanding rod-shaped PVA-based devices fabricated by hot melt extrusion (HME) and FDM 3D printing was demonstrated. A dedicated equipment was designed and a new coating process was developed. In view of the desired performance and based on preliminary trials performed by casting, two coating formulations based on methacrylic acid copolymers were selected. Data on equipment and process set up, relevant robustness and reproducibility as well as impact of the applied coating on shape memory and release performance of the prototypes were collected.

2. Materials and Methods

2.1 Materials

PVA05 and PVA48 (Gohsenol™ EG 05P and 48P, Nippon Gohsei, J); glycerol (GLY; Pharmagel, I); allopurinol (ALP; FarmaQuimica sur S.L., ES); methacrylic acid copolymers, Eudragit® RS 100 and RL 100 (Evonik, D); ready-to-use dispersion of methacrylic acid copolymers, Eudragit® NE (Evonik, D); triethyl citrate (TEC; Sigma Aldrich, D); ethanol (Sigma Aldrich, D).

2.2. Methods

2.2.1 Fabrication of prototypes and equipment parts

PVA48 and PVA05 were kept in an oven at 40 °C for 24 h prior to use. Plasticized PVA formulations were prepared by mixing PVAs with 15% GLY in a mortar. The amount of

plasticizer was expressed as % by weight on the dry polymer. 10% of ALP, calculated as % by weight on the plasticized polymeric formulation, was added by mixing in a mortar. Starting from the PVA48 based formulation rod-shape prototypes with a circular cross-section were prepared by HME. A twin-screw extruder (Haake™ MiniLab II, Thermo Scientific, US-WI) equipped with counter-rotating screws and a circular die of 1.50 mm in diameter was employed and the extruded rods were cut into 50 mm long samples. Starting from the PVA05-based formulation filaments with circular cross section of nominal 1.75 ± 0.05 mm in diameter were prepared by HME for feeding the FDM printer. A custom-made aluminum circular die of 1.80 mm in diameter was employed. Extruded rods were manually pulled and forced to pass through a caliper connected with the extruder and set at 1.80 mm as previously described [13]. After cooling, the filament diameter was verified every 5 cm in length, and portions out of specifications were discarded. In Table 1 HME parameters for the PVA-based formulations are reported.

Table 1: HME process parameters

Polymeric formulation	T (°C)	Screw speed (rpm)	Torque (N·cm)
(PVA05 + 15% GLY) +10% ALP	170	80	100
(PVA48 + 15% GLY) + 10% ALP	175	80	120

FDM 3D printing was performed by a dual arm 3D printer (Kloner3D 240® Twin, Kloner3D, I) equipped with 0.5 mm nozzles. It was employed to fabricate both rod-shaped prototypes with squared cross section (side = 1.5 mm) and parts of the rotating mechanism of the coating equipment showed in Figure 2. They were designed by means of Autodesk® Autocad® 2016 (software version 14.0 Autodesk Inc., US-CA) and the CAD files were saved in stl format and imported to the equipment software (Simplify 3D, I). Rod-shaped samples were fabricated starting from the in-house prepared filaments based on PVA05 (printing conditions: nozzle temperature = 180 °C, build plate temperature = 70 °C, infill = 100%, layer height = 0.10 mm, printing speed = 23 mm/s); the equipment

parts were printed from commercial poly (lactic acid) (PLA) filament used as received (printing default conditions provided by the software for high-resolution PLA-based prints: nozzle temperature = 220 °C, infill = 100%, layer height = 0.10 mm, printing speed = 50 mm/s).

Extruded and printed rod-shaped prototypes were coated with: *i)* an ethanolic solution (final concentration 30% weight/volume) containing Eudragit® RS and RL (mixed in a 3:1 ratio by weight) and TEC as a plasticizer (15% by weight on the dry polymeric blend) and *ii)* a 30% ready-to-use aqueous suspension of Eudragit® NE. Description of the equipment and coating process developed is the main topic of the manuscript. Coating processes were carried out at ambient conditions (21 ± 0.5 °C and 55% RH).

2.2.2 Characterization of prototypes

Uncoated and coated prototypes were characterized for weight (n = 6; Sartorius, D) and dimensions. The diameter of the extruded specimens was checked using a caliper in 3 different positions to rule out possible ovalization phenomena. The caliper was also used to check the width and height of FDM prototypes in 3 different points along their length. To evaluate thickness of the coated prototypes, samples (n = 6) were cut and photographs of the cross section were acquired using a digital microscope (Digital Microscope AM-413T, Dino-Lite, I). The latter were processed (ImageJ, US-MD) to take the measure of the coat thickness in at least 6 different points along the circumference as highlighted in Figure 1.

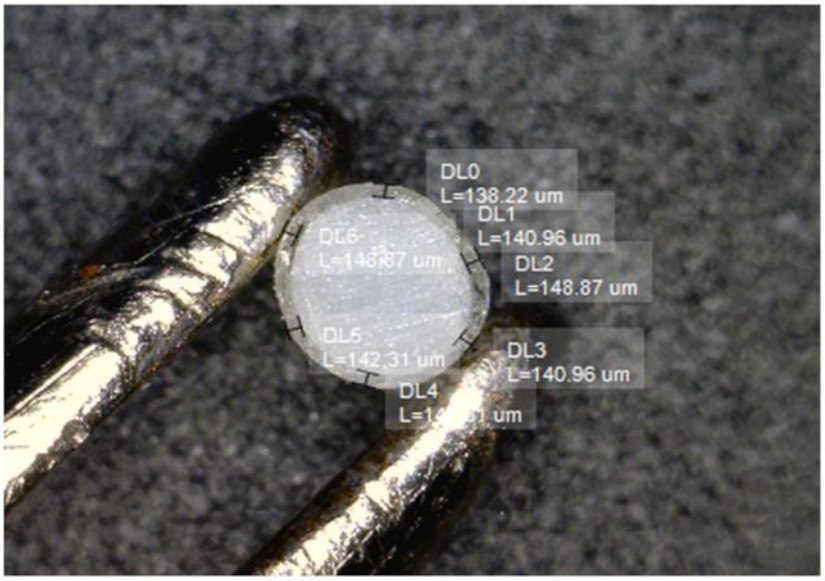

Figure 1: Digital photograph of the cross-section of an extruded rod coated for 16 min with the Eudragit® NE aqueous suspension with thickness measurements taken into 7 different positions (DL0 –DL6).

Uncoated and coated prototypes were tested for shape memory effect according to [7]. Samples were heated at 35 °C above their glass transition temperature (T_g) and forced to take on a temporary U-shape. Then they were cooled below T_g in the deformed shape. Shape recovery was studied upon immersion of the deformed samples into a crystallization vessel, filled with 250 mL of HCl 0.1N and kept at 37 ± 0.5 °C by means of a thermoregulated bath. The recovery process was monitored using a digital camera positioned above (distance 13 cm) the specimen (GoPro Hero Session, US-CA; n = 3). The photographs acquired were processed using a specific software (ImageJ, US-MD) to calculate the recovery index (RI) as follows.

$$RI = \frac{\alpha - \alpha_p}{\pi - \alpha_p} \qquad \text{(Eq. 1)}$$

where α_p is the angle obtained in the programming phase (angles in rad).

By linear interpolation of the recovery data immediately before and after the time point of interest time to 50% ($t_{50\%RI}$) and 80% ($t_{80\%RI}$) recovery, respectively, were calculated.

T_g of the rod-shaped prototypes was determined by means of DSC analysis (DSC Q100, TA Instruments, US-DE; n = 1) using nitrogen as a purge gas (70 mL/min). Indium was used as a calibration standard. Samples of about 10 mg were heated in aluminum crucibles from -50 °C to 240 °C, maintained at this temperature for 1 min, cooled down to -50 °C and reheated up to 240 °C. Both heating and cooling steps were run at 10 °C/min.

Uncoated and coated prototypes in their original shape were tested for release using a USP38 dissolution apparatus 2 (50 rpm, 37 ± 0.5 °C, 900 mL HCl 0.1 N; Distek, CH; n = 6). Fluid samples were withdrawn at specific time points (0.5, 2 and 6h) and assayed spectrophotometrically (λ = 251 nm) to calculate the percentage of ALP released.

3. Results and Discussion

3.1 Equipment setup

A lab-scale equipment comprising two assemblies for both spraying the coating formulation and implementing the rotation of rod-shaped samples was conceived and in-house assembled. An outline of the equipment developed is reported in Figure 2.

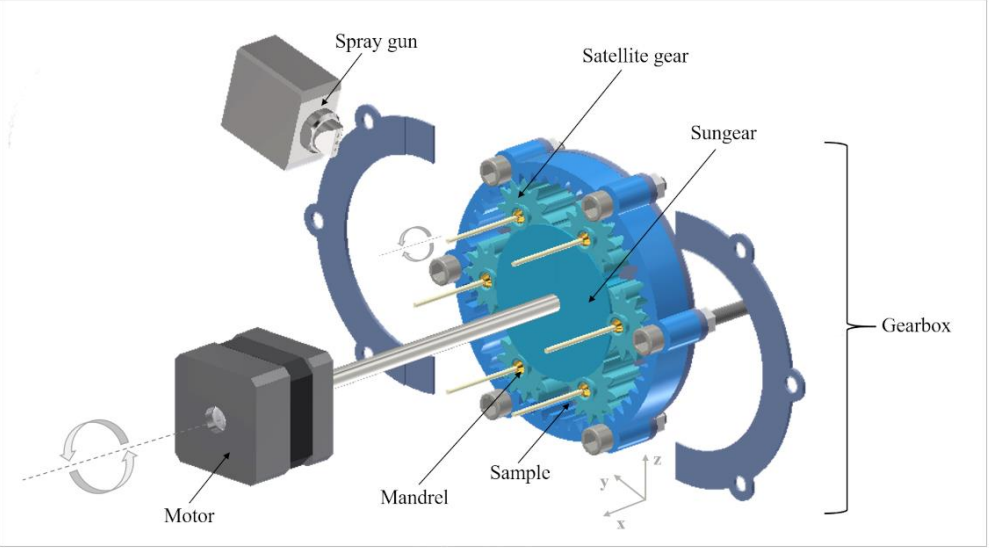

Figure 2: Outline of the assembled coating equipment.

The spraying system was derived from a pan coating setup. It comprised a low-pressure spray gun entailing a 3-ways (*i.e.* control, atomizer and pattern) nozzle, which was maintained in a fixed position by means of a stand provided with different clamps connecting the latter to the chassis of the rotating assembly. The positioning of the spray gun - *i.e.* 20 cm, distance from the gearbox in the x axis; 30 cm, distance from the base of the gearbox in the z axis; 10 cm, distance from the nearest sample in y axis; 30° inclination with respect to the xy plane (Figure 2) - was selected to assess the desired spray width and the actual coverage area relevant to all the samples during rotation. The spray gun was connected to a peristaltic pump and to an air inlet, the rotation rate and pressure of which could be fine-tuned by the operator. Spraying rate and pattern of either solutions and suspensions could be customized. While the control port of the gun just opened and closed the access for liquid, the atomizer allowed to adjust the drop dimensions and the geometry of the spray pattern. For instance, the ability to direct the spray cone towards samples was improved by changing the pattern pressure parameter, thus ovalizing the spray pattern. In the case of the 50mm-long rod-shaped prototypes with one dimension bigger than the others, this led to a more targeted spraying over the entire length of the sample.

The rotating mechanism relied on an epicyclic planetary gearbox. Each part of the latter was designed and printed in-house (Figure 3).

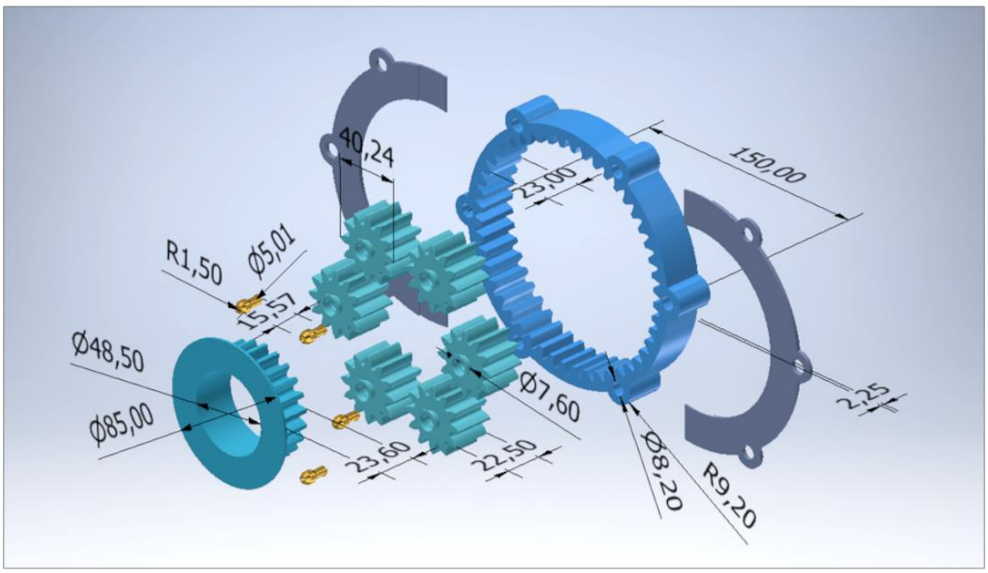

Figure 3: Virtual models with dimensional details of the 3D printed parts of the equipment.

More into detail, the gearbox consisted of two different sets of gears (*i.e.* the sungear and the satellite gears) purposely assembled. The sungear was directly kept in motion by a rotor and transmitted combined movements to the six satellite gears attached to it. These were in-built with the sungear and were devised with a central hole containing mandrels, which were included to enable precise arrangement and secure fixing of samples. The presence of mandrels increased the equipment versatility, by allowing samples with different shape and dimensions to be housed. While the sungear moved around its own axis only, the satellites also rotated around the sun (*i.e.* revolution movement). This way, the samples could periodically face the spray pattern, being able to dry during the rest of the rotation/revolution movement.

During coating processes, the equipment was placed into an isolated chamber, provided with aspiration, control of temperature as well as relative humidity and a device for hot-air circulation to be activated when needed.

3.2 Process setup

Liquid formulations of methacrylic copolymers - *i.e.* plasticized ethanolic solution of Eudragit® RS and RL and ready-to-use aqueous suspension of Eudragit® NE - were selected for the coating process. Preliminary tests based on a trial and error approach were carried out in order to identify suitable process parameters for coating PVA-based rod-shaped prototypes of 50 mm in length fabricated by HME and FDM having circular or squared cross-section, respectively. This step was particularly challenging with the aqueous suspension in view of the high PVA water solubility, which might compromise the device integrity during the process. In Table 2 the final coating conditions identified are reported.

When dealing with the aqueous suspension, the early formation of a gel layer on the sample surface was observed by increasing the spraying rate. Therefore, this parameter was maintained lower compared to the ethanolic solution, and the drying conditions were consistently adapted, *i.e.* by increasing the air temperature and its flow. Moreover, in order to attain a comparable spraying cone with either the solution and suspension, the pattern pressure needed to be reduced as well. Overall, the selected spraying and drying conditions gave rise to alternating spraying passages occurring at constant intervals. Therefore, the rotation speed of the rod-shaped specimens needed to be adjusted, also taking spacing among the samples into account, in order to lead to an effective coating, *i.e.* passage of samples inside the spray cone exactly at each spraying occurrence.

Table 2: Coating process conditions.

Coating formulation	Spraying rate (mL/min)	Pressure of the nebulized air (bar)	Pattern pressure (bar)	Drying air temperature (°C)	Drying air flow (m^3/h)	Sample rotation speed (rpm)
Eudragit® RS/RL ethanolic solution	7	0.75	1	40	50	2.3
Eudragit® NE aqueous suspension	2.1	0.5	0.75	60	65	1.5

3.3 Evaluation of coated prototypes

Samples with increasing weight gain and coating thickness were obtained at successive time points of the coating processes (*i.e.* 4, 8 and 16 min) (Table 3). All samples underwent a curing process (*i.e.* 2 h in a ventilated oven set at 40 °C), which turned out essential to attain a continuous smooth film. By way of example, photographs of extruded cylindrical prototypes and printed squared once coated with the Eudragit® RS/RL ethanolic solution at the different process times are reported in Figure 4.

Table 3: Weight gain and coating thickness of HME and FDM 3D printed samples coated for different times.

		Eudragit® RS/RL ethanolic solution		**Eudragit® NE aqueous suspension**	
	Coating time (min)	**Weight gain, mg (CV)**	**Thickness, µm (CV)**	**Weight gain, mg (CV)**	**Thickness, µm (CV)**
HME	**4**	38.43 (5.02)	113.06 (3.63)	7.73 (3.48)	55.86 (7.64)
	8	61.22 (6.34)	202.95 (4.28)	21.33 (4.84)	84.03 (7.88)
	16	133.58 (3.44)	445.48 (2.36)	39.33 (7.31)	140.59 (3.35)
FDM	**4**	37.50 (4.99)	105.04 (7.69)	6.53 (4.62)	50.97 (8.12)
	8	59.67 (6.51)	199.63 (6.92)	18.75 (5.98)	78.33 (9.58)
	16	130.03 (3.07)	440.09 (8.06)	37.66 (3.65)	135.64 (5.23)

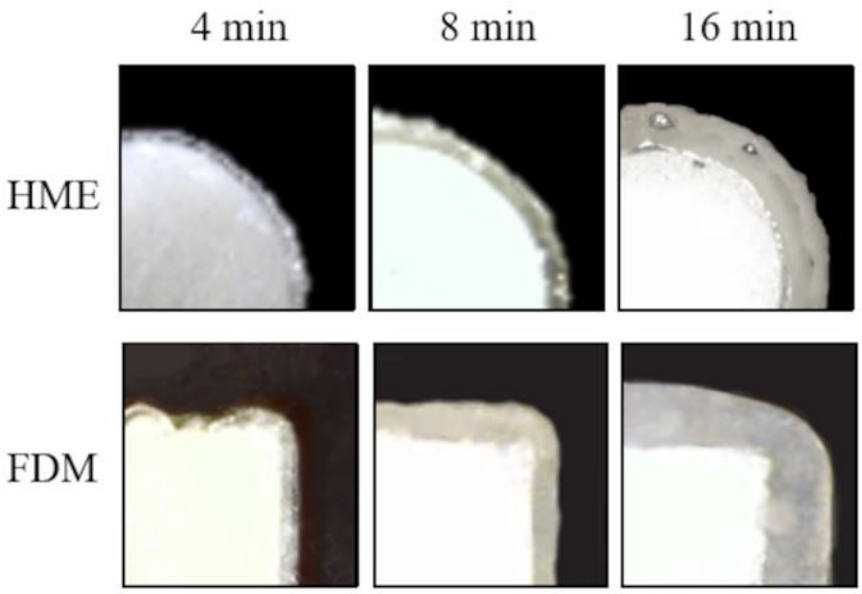

Figure 4: Photographs of the cross section of HME and FDM 3D printed samples coated with the Eudragit® RS/RL ethanolic solution for different times.

The coating thickness was shown to increase with the process time, and turned out uniform in all the positions over the different samples. At any process time considered, a lower thick film was found on Eudragit® NE-coated prototypes with respect to Eudragit® RS/RL-coated ones. This was consistent with the lower amount of water-based suspension sprayed for the same time interval.

In order to confirm the suitability of the coating process developed, the reproducibility of the performance of coated rod-shaped prototypes in terms of shape memory effect and drug release was evaluated. Shape memory behavior was tested according to a method previously developed involving the programming of samples in a temporary U-shape [7]. The integrity of the film after the programming step was visually checked. No cracking phenomena were observed regardless of the coating formulation and thickness. Recovery of the original rod-shape of the prototypes was tested following immersion in aqueous fluids at 37 °C. Calculated recovery parameters, *i.e.* time to attain a recovery index equal to 50 and 80%, relevant to coated prototypes and to uncoated ones used as reference, are

reported in Table 4. The percentage of drug released after 0.5, 2, 6 and 12 h from uncoated and coated rod-shaped prototypes are reported in Table 5. The variability of data relevant to both shape recovery and release performance of coated samples, highlighted by the CV parameters, was shown analogous to that of the uncoated ones.

Overall, the data obtained confirmed the hypothesis that the application of polymeric coatings is a suitable strategy to control the release rate of shape-memory drug delivery systems without affecting their smart performance. The coating process developed was successful for the attainment of drug delivery systems intended for organ retention and based on pharmaceutical-grade hydrophilic swellable/soluble shape-memory polymers. In addition, the equipment proposed, aside from being scalable, would be useful to pharmaceutical scientists who need to implement film-coating processes for non-traditional solid substrates (*e.g.* non-spherical or complex shape with edges and folds, critical thermal and mechanical properties) at a small scale level.

Table 4: Recovery parameters ($t_{50\%RI}$ and $t_{80\%RI}$) relevant to uncoated and coated samples.

		Uncoated	Eudragit® RS/RL ethanolic solution			Eudragit® NE aqueous suspension		
			Coating time (min)			Coating time (min)		
			4	8	16	4	8	16
$t_{50\%RI}$ (CV)	HME	20 s (8)	19 s (7)	29 s (3)	27 s (3)	21 s (5)	20 s (2)	18 s (5)
	FDM	52 s (10)	1 min 21 s (11)	2 min 41 s (10)	3 min 05 s (13)	1 min 58 s (9)	1 min 2 s (12)	50 s (11)
$t_{80\%RI}$ (CV)	HME	54 s (5)	55 s (4)	4 min 19 s (4)	12 min 14 s (5)	1 min 46 s (3)	51 s (4)	21 s (4)
	FDM	4 min 42 s (10)	8 min 50 s (11)	14 min 22 s (11)	16 min 55 s (13)	5 min 38 s (10)	4 min 15 s (12)	4 min 3 s (9)

Table 5: Percentage of drug released at different time points relevant to uncoated and coated samples.

		Uncoated	Coated					
			Eudragit® RS/RL ethanolic solution			Eudragit® NE aqueous suspension		
			Coating time (min)			Coating time (min)		
			4	8	16	4	8	16
0.5h (CV)	HME	21.15 (5.34)	1.54 (1.00)	0.69 (5.20)	0.00 (0.00)	1.88 (7.64)	1.02 (8.69)	0.62 (10.55)
	FDM	78.94 (12.67)	8.37 (15.89)	4.06 (17.24)	3.25 (4.80)	8.64 (8.36)	3.89 (9.44)	1.97 (11.22)
2h (CV)	HME	68.55 (15.11)	17.44 (5.04)	4.87 (13.54)	4.79 (6.68)	9.44 (13.73)	4.55 (14.83)	4.49 (15.28)
	FDM	100.00 (0.00)	33.38 (6.99)	17.44 (18.02)	10.57 (4.39)	15.03 (12.88)	6.79 (13.97)	6.22 (18.55)
6h (CV)	HME	97.90 (1.04)	59.26 (7.09)	16.96 (10.44)	12.14 (3.62)	19.70 (1.42)	7.66 (15.86)	8.66 (13.74)
	FDM	100.00 (0.00)	74.56 (3.46)	35.32 (19.05)	20.30 (12.76)	25.71 (3.47)	18.99 (13.82)	14.16 (11.69)

References

1. A. Melocchi, M. Uboldi, M. Cerea, A. Foppoli, A. Maroni, S. Moutaharrik, L. Palugan, L. Zema, A. Gazzaniga, A graphical review on the escalation of fused deposition modeling (FDM) 3D printing in the pharmaceutical field. J. Pharm. Sci. 109 (2020) 2943-2957.
2. R. V. Tiwari, H. Patil, M. A. Repka, Contribution of hot-melt extrusion technology to advance drug delivery in the 21st century. Expert Opin. Drug Deliv. 13 (2016) 451-464.
3. L. Zema, G. Loreti, A. Melocchi, A. Maroni, A. Gazzaniga, Injection Molding and its application to drug delivery. J. Control. Release 159 (2012) 324-331.
4. A. Maroni, A. Melocchi, L. Zema, A. Foppoli, A. Gazzaniga, Retentive drug delivery systems based on shape memory materials. J. Appl. Polym. Sci. 137 (2020) 48798.
5. A. Melocchi, M. Uboldi, M. Cerea, A. Foppoli, A. Maroni, S. Moutaharrik, L. Palugan, L. Zema, A. Gazzaniga, Shape memory materials and 4D printing in pharmaceutics. Adv. Drug Deliv. Review. 173 (2021) 216-237.
6. L. Zema, A. Melocchi, A. Maroni, A. Gazzaniga, Three-dimensional printing of medicinal products and the challenge of personalized therapy. J. Pharm. Sci. 106 (2017) 1697-1705.
7. A. Melocchi, N. Inverardi, M. Uboldi, F. Baldi, A. Maroni, S. Pandini, F. Briatico-Vangosa, L. Zema, A. Gazzaniga, Retentive device for intravesical drug delivery based on water-induced shape memory response of poly(vinyl alcohol): design concept and 4D printing feasibility. Int. J. Pharm. 559 (2019) 299-311.
8. A. Melocchi, M. Uboldi, N. Inverardi, F. Briatico-Vangosa, F. Baldi, S. Pandini, G. Scalet, F. Auricchio, M. Cerea, A. Foppoli, A. Maroni, L. Zema, A. Gazzaniga, Expandable drug delivery system for gastric retention based on shape memory polymers: Development via 4D printing and extrusion. Int. J. Pharm. 571 (2019) 118700.

9. N. Inverardi, G. Scalet, A. Melocchi, M. Uboldi, A. Maroni, L. Zema, A. Gazzaniga, F. Auricchio, F. Briatico-Vangosa, F. Baldi, S. Pandini, Experimental and computational analysis of a pharmaceutical-grade shape memory polymer applied to the development of gastroretentive drug delivery systems. J. Mech. Behav.. Biomed Mater. 124 (2021) 104814.
10. L. A. Felton, Characterization of coating systems, AAPS PharmSciTech. 8 (2007) 258-266.
11. L. A. Felton, S. C. Porter, An update on pharmaceutical film coating for drug delivery. Expert Opin. Drug Deliv. 10 (2013) 421-435.
12. S. C. Porter, L. A. Felton, Techniques to assess film coatings and evaluate film-coated products. Drug Dev. Ind. Pharm. 36 (2010) 128-142.
13. A. Melocchi, F. Parietti, A. Maroni, A. Foppoli, A. Gazzaniga, L. Zema, Hot-melt extruded filaments based on pharmaceutical grade polymers for 3D printing by fused deposition modeling. Int. J. Pharm. 509 (2016) 255-263.

Conclusions

The Ph.D. research project undertaken was born in the context of identifying pharmaceutical applications of smart materials such as shape memory polymers. In particular, it was aimed at evaluating the possibility of developing drug delivery systems (DDSs) intended for prolonged retention into hollow muscular organs. Bladder and stomach were selected as the main target areas, in view of the still pending challenges relevant to administration and release of drugs in these specific sites.

A comprehensive review of the literature available was carried out, considering shape memory alloys, shape memory polymers and their pharmaceutical applications. Hence, prototypes of organ-retentive DDSs based on pharmaceutical-grade shape memory polymers were designed and successfully developed, taking advantage of hot melt extrusion and 3D printing by fused deposition modeling. In the latter case, the work done laid the basis for the implementation of 4D printing in pharmaceutics. Moreover, film-coating of the prototypes attained was demonstrated a viable strategy to improve mechanical properties and extend release duration without impacting on their shape memory behavior.

In view of the promising results obtained during the preliminary studies, the experimental campaign was also coupled with computer-aided simulation modeling. This way, the design step of new organ-retentive DDSs could be eased, for instance by reducing relevant time and costs of development and limiting the number of samples to be fabricated.

Overall, the work performed highlighted the need for developing a multidisciplinary approach, entailing complete thermo-mechanical and shape-memory characterization of the starting materials, engineering of the design phase as well as of the set-up of processes parameters and evaluation of the resulting prototypes in terms of release performance, stability and modeling of their behavior. In this respect, various scientific collaborations have been prompted, involving experts working in mechanical engineering, polymer science and simulation modeling areas.

At the same time, to push the current boundaries relevant to organ retentive systems, especially when targeting the so-called ultra-long performance, a broader perspective turned out to be essential. This would potentially mean:

- implementation of a range of manufacturing processes, and particularly of different 3D printing techniques, also to be applied in combination (*e.g.* gel and thermoplastic extrusion, binder jetting);
- use of smart materials poorly known in pharmaceutics, even resorting to polymers specifically devised and engineered for the targeted therapeutic objective;
- working on systems with innovative and hybrid design, in which different parts of the device have complementary purposes (*e.g.* retention, controlled release, non-invasive elimination).